

**CONTROL AND REDUCTION OF FRICTION-INDUCED VIBRATION
IN
SOME INDUSTRIAL APPLICATIONS**

By

Marie-Claude Taponat

Diplôme d'Ingénieur Génie Mécanique - INSA Lyon

A THESIS SUBMITTED IN PARTIAL FULFILLMENT OF
THE REQUIREMENTS FOR THE DEGREE OF
MASTERS OF APPLIED SCIENCE

in

THE FACULTY OF GRADUATE STUDIES
DEPARTMENT OF
MECHANICAL ENGINEERING

We accept this thesis as conforming
to the ~~required~~ standard

THE UNIVERSITY OF BRITISH COLUMBIA

October 1996

© Marie-Claude Taponat, 1996

In presenting this thesis in partial fulfilment of the requirements for an advanced degree at the University of British Columbia, I agree that the Library shall make it freely available for reference and study. I further agree that permission for extensive copying of this thesis for scholarly purposes may be granted by the head of my department or by his or her representatives. It is understood that copying or publication of this thesis for financial gain shall not be allowed without my written permission.

Department of Mechanical Engineering.

The University of British Columbia
Vancouver, Canada

Date 8/10/96

ABSTRACT

The frictional behaviour of several combinations of industrial friction materials that are related to two specific applications was investigated experimentally and analytically. The objective is to gain knowledge on how to better control and eliminate, if necessary, friction-induced vibrations in industrial applications. The materials studied exhibited either stick-slip or quasi-harmonic vibration. The friction-velocity characteristic has been proved to be a useful tool to predict the vibrational behaviour of a friction pair. In the quasi-harmonic case, a non-linear analytical friction model based on an approximation technique, can predict the occurrence and the amplitude of friction-induced vibration when the system is submitted to a static normal load. The effect of dynamic normal loading on the frictional behaviour and on the occurrence of chaos has also been investigated. No chaotic motion was detected. Stick-slip vibrations can be extinguished by a normal loading with a small amplitude and a frequency close to the natural frequency of the system. In the case of quasi-harmonic vibration, it can be quenched and is replaced by a vibration with the excitation frequency and usually with a smaller amplitude than that of the quasi-harmonic vibration. Experimental, analytical and numerical results were all in good agreement for the quasi-harmonic type of vibration.

Table of contents

ABSTRACT	ii
Table of contents	iii
List of tables	v
List of figures	vi
ACKNOWLEDGEMENTS	xi
INTRODUCTION	1
LITERATURE REVIEW	4
2.1 <i>Historical background</i>	4
2.2 <i>The significance of the friction-velocity curve</i>	5
2.3 <i>The influence of normal stiffness</i>	6
2.4 <i>Applications</i>	8
2.5 <i>Elimination and control of friction-induced vibration</i>	10
2.6 <i>Chaotic oscillation</i>	14
FRICION MODEL	16
3.1 <i>Equation of motion</i>	16
3.2 <i>Friction-velocity (f-v) characteristic modeling</i>	17
3.3 <i>Dynamic friction models</i>	18
3.3.1. Stick-slip vibration	19
3.3.2. Quasi-harmonic vibration	20
INDUSTRIAL FRICTION MATERIALS AND ASSOCIATED FRICTION PROBLEMS	26
4.1 <i>Specimen description</i>	27
4.1.1. "Paper-to-metal" contact	27
4.1.2. "Paper-to-paper" contact	29
4.2 <i>Other media and parameters</i>	29
4.2.1. Normal load	30
4.2.2. Sliding velocity	30
4.2.3. Type of lubricant	30

EXPERIMENTAL TECHNIQUES OF FRICTION MEASUREMENT	31
5.1 <i>Description of the apparatus</i>	31
5.2 <i>Measurement techniques and instrumentation</i>	33
5.2.1. Static measurement method	33
5.2.2. Direct measurement method	34
5.3 <i>Testing procedure</i>	36
5.3.1. Paper-to-metal combination	36
5.3.2. Paper-on-paper combination	39
EXPERIMENTAL RESULTS	40
6.1. <i>Blotting paper on cast iron</i>	41
6.2. <i>Friction (clutch) plate on steel</i>	45
6.3. <i>Paper-on-paper</i>	46
6.4. <i>Curve fitting F-V equations</i>	48
THEORETICAL AND NUMERICAL ANALYSES OF AN AUTONOMOUS SYSTEM	50
7.1. <i>Analytical study</i>	50
7.1.1. Combinations showing stick-slip vibrations	50
7.1.2. Combinations showing quasi-harmonic vibrations	51
7.2. <i>Numerical study</i>	51
7.2.1. Combinations showing stick-slip vibrations	51
7.2.2. Combinations showing quasi-harmonic vibrations	52
7.3. <i>Discussion</i>	53
FRICTION-INDUCED VIBRATIONS WITH PERIODIC NORMAL EXCITATION	56
8.1 <i>Numerical analysis</i>	57
8.1.1. Combinations showing stick-slip vibrations	58
8.1.2. Combinations showing quasi-harmonic vibrations	59
8.1.3. Discussion	63
8.2. <i>Experimental results</i>	63
8.2.1. Combinations showing stick-slip	64
8.2.2. Combinations showing quasi-harmonic vibrations	66
8.3. <i>Discussion</i>	68
DISCUSSION	70
CONCLUSIONS	76
REFERENCES	78
Appendix 1	83
Appendix 2	88

List of tables

5.1.	Testing conditions for the Ford friction plate	38
6.1.	Material and lubricant combinations tested	40

List of figures

3.1	Autonomous system	91
3.2	System with an external dynamic force	91
3.3	Different types of friction-velocity curves	92
	(a) Coulomb friction	
	(b) Continuously decreasing curve	
	(c) Humped curve	
4.1	Photomicrographs of Ford friction plate surface	93
4.2	Photomicrographs of blotting paper surface	93
4.3	Photomicrographs of Dexron friction plate surface	94
4.4	Photomicrographs of type F friction plate surface	94
4.5	Photomicrographs of newsprint surfaces	95
	(a) Surface A1	
	(b) Surface A2	
5.1	General view of the pin-on-disk machine	96
5.2	View of the slider	97
	(a) for blotting paper combination	
	(b) for friction plate combination	
5.3	View of the lower disc	98
	(a) for blotting paper combination	
	(b) for friction plate combination	
5.4	Steppar motor arrangement for dynamic loading	99
5.5	Electromagnetic shaker arrangement for dynamic loading	99
5.6	View of the load transducer for static measurement method	100
6.1	Comparison of friction-velocity curves obtained by the direct and static measurement methods	101
6.2	Effect of normal load on the f-v curve	102
6.3	f-v characteristics for 4 fluids under a 8.9 N normal load	103
6.4	f-v characteristics for 3 fluids under a 17.8 N normal load	104
6.5	F-V curve, amplitude and frequency of experimental vibrations for #1 ATF	105
6.6	Friction vs. time plots at different velocities for #1 ATF	106
6.7	f-v curve, amplitude and frequency of experimental vibrations for semi-synthetic Dexron/Mercon IIE	107

6.8	Friction vs. time plots at different velocities for semi-synthetic Dexron/Mercon IIE (a) Static normal load of 17.8 N (b) Static normal load of 8.9 N	108
6.9	F-V curve, amplitude and frequency of experimental vibrations for Dexron/Mercon III	110
6.10	Friction vs. time plots at different velocities for Dexron/Mercon III	111
6.11	F-V curve, amplitude and frequency of experimental vibrations for type F lubricant	112
6.12	Friction vs. time plots at different velocities for type F lubricant	113
6.13	F-V curve, amplitude and frequency of experimental vibrations for slideway lubricant	114
6.14	Friction vs. time plots at different velocities for slideway lubricant	115
6.15	F-V curve, amplitude and frequency of experimental vibrations for friction plate combination	116
6.16	Friction vs. time plots at different velocities for friction plate combination Static normal load of 8.9 N	117
6.17	Effect of the normal load on the vibration amplitude for the paper-on-paper combinations	118
6.18	Effect of the normal load on the vibration amplitude for the paper-on-paper combinations	119
6.19	Friction vs. time plots at different velocities for same paper-on-paper combination (a) A1 vs. A1 (b) A2 vs. A2	120
6.20	Friction vs. time plots at different velocities for different paper-on-paper combination (a) A2 vs. A1 (b) A1 vs. A2	122
6.21	Experimental and polynomial fitted F-V curves for type F lubricant	124
6.22	Experimental and polynomial fitted F-V curves for blotting paper combination with semi-synthetic Dexron/Mercon IIE lubricant	125
6.23	Experimental and polynomial fitted F-V curves for slideway lubricant	126
6.24	Experimental and polynomial fitted F-V curves for friction plate combination with semi-synthetic Dexron/Mercon IIE lubricant	127
6.25	Experimental and polynomial fitted F-V curves for A1 vs. A1 paper-on-paper combination	128
6.26	Experimental and polynomial fitted F-V curves for A2 vs. A1 paper-on-paper combination	129

7.1	Experimental, analytical and numerical vibration amplitudes for blotting paper combination with semi-synthetic Dexron/Mercon IIE lubricant	130
7.2	Experimental, analytical and numerical vibration amplitudes for blotting paper combination with slideway lubricant	131
7.3	Experimental, analytical and numerical vibration amplitudes for friction plate combination with semi-synthetic Dexron/Mercon IIE lubricant	132
7.4	Experimental, analytical and numerical vibration amplitudes for blotting paper combination with type F lubricant	133
8.1	Effect of the load and frequency ratios on numerical vibration amplitude. Blotting paper combination with type F lubricant	134
8.2	Bifurcation diagrams for type F combination	135
	(a) Parameter α	
	(b) Parameter V	
	(c) Parameter β	
8.3	Multiperiodic motion of order 2 for type F combination	136
	(a) Phase-plane plot	
	(b) Time series	
	(c) Frequency spectrum	
8.4	Multiperiodic motion of order 3 for type F combination	137
	(a) Phase-plane plot	
	(b) Time series	
	(c) Frequency spectrum	
8.5	Multiperiodic motion of order 4 for type F combination	138
	(a) Phase-plane plot	
	(b) Time series	
	(c) Frequency spectrum	
8.6	Chaotic motion for type F combination	139
	(a) Phase-plane plot	
	(b) Poincaré map	
	(c) Time series	
	(d) Frequency spectrum	
8.7	Chaotic motion for type F combination	140
	(a) Phase-plane plot	
	(b) Poincaré map	
	(c) Time series	
	(d) Frequency spectrum	
8.8	Bifurcation diagrams for parameter V	141
	(a) Blotting paper with semi-synthetic Dexron/Mercon IIE lubricant	
	(b) Blotting paper with slideway lubricant	
	(c) Friction plate with semi-synthetic Dexron/Mercon IIE lubricant	

8.9	Bifurcation diagrams for parameter α	142
	(a) Blotting paper with semi-synthetic Dexron/Mercon IIE lubricant	
	(b) Blotting paper with slideway lubricant	
	(c) Friction plate with semi-synthetic Dexron/Mercon IIE lubricant	
8.10	Subharmonic entrainment of order 2. Blotting paper with slideway lubricant	143
	(a) Phase-plane plot	
	(b) Time series	
	(c) Frequency spectrum	
8.11	Subharmonic entrainment of order 3. Blotting paper with slideway lubricant	144
	(a) Phase-plane plot	
	(b) Time series	
	(c) Frequency spectrum	
8.12	Subharmonic entrainment of order 4. Blotting paper with slideway lubricant	145
	(a) Phase-plane plot	
	(b) Time series	
	(c) Frequency spectrum	
8.13	Subharmonic entrainment. Blotting paper with slideway lubricant	146
	(a) Phase-plane plot. $\alpha = 1.5$	
	(b) Phase-plane plot. $\alpha = 2.5$	
	(c) Phase-plane plot. $\alpha = 3.5$	
8.14	Subharmonic entrainment. Blotting paper with slideway lubricant	147
	(a) Phase-plane plot. $\alpha = 4/3$	
	(b) Phase-plane plot. $\alpha = 5/3$	
	(c) Phase-plane plot. $\alpha = 7/3$	
8.15	Multiperiodic motion. $\alpha = 2.15$. Blotting paper with slideway lubricant	148
	(a) Phase-plane plot	
	(b) Poincaré map	
	(c) Time series	
	(d) Frequency spectrum	
8.16	Effect of load and frequency ratios on numerical vibration amplitude Blotting paper combination with semi-synthetic Dexron/Mercon IIE lubricant	149
8.17	Effect of load and frequency ratios on numerical vibration amplitude Blotting paper combination with slideway lubricant	150
8.18	Effect of load and frequency ratios on numerical vibration amplitude Friction plate with semi-synthetic Dexron/Mercon IIE lubricant	151
8.19	Bifurcation diagrams for parameter β	152
	(a) Blotting paper with semi-synthetic Dexron/Mercon IIE lubricant	
	(b) Blotting paper with slideway lubricant	
	(c) Friction plate with semi-synthetic Dexron/Mercon IIE lubricant	
8.20	Effect of load and frequency ratios on experimental vibration amplitude	153

	Blotting paper with type F lubricant. $v = 0.52$ mm/s	
8.21	Effect of load and frequency ratios on experimental vibration amplitude and frequency - Blotting paper with type F lubricant. $v = 2.25$ mm/s	154
8.22	Effect of load and frequency ratios on experimental vibration amplitude and frequency - Blotting paper with type F lubricant. $v = 9.8$ mm/s	155
8.23	Vibration vs. time plots with dynamic loading Blotting paper with type F lubricant. $v = 0.52$ mm/s	156
8.24	Vibration vs. time plots with dynamic loading. Blotting paper with type F lubricant. $v = 0.2$ mm/s	157
8.25	Vibration vs. time plots with dynamic loading. Blotting paper with type F lubricant. $v = 2.25$ mm/s	158
8.26	Influence of dynamic loading on the static friction Blotting paper with type F lubricant. $v = 2.25$ mm/s	159
8.27	Subharmonic entrainment for slideway lubricant combination	160
8.28	Multiperiodic motion for slideway lubricant combination	161
8.29	Effect of load and frequency ratios on experimental vibration amplitude and frequency - Friction plate with semi-synthetic Dexron/Mercon IIE - $v = 10.5$ mm/s	162
8.30	Effect of load and frequency ratios on experimental vibration amplitude and frequency - Friction plate with semi-synthetic Dexron/Mercon IIE - $v = 31.4$ mm/s	163
8.31	Vibration vs. time plots with dynamic loading. Friction plate with semi-synthetic Dexron/Mercon IIE lubricant. (a) $v = 10.5$ mm/s (b) $v = 31.4$ mm/s	164

ACKNOWLEDGEMENTS

This study was made possible by the support of Natural Sciences and Engineering Research Council (NSERC). I would like to thank my supervisor Dr. Pak Ko, for his valued guidance, his encouragements and his boundless patience. All the experimental work was carried out in the Tribology Laboratory at the National Research Council of Canada and I thank everybody at NRC in Vancouver for their support throughout this research program. In particular, I am grateful to Mark Robertson for his help in all technical aspects of the study and to Tom Vanderhoek and Milos Simunek for their help in modifying the experimental equipment.

CHAPTER 1

INTRODUCTION

Many physical systems involve surfaces in relative motion and consequently, their behaviour is strongly influenced by the frictional characteristics of these sliding surfaces. At high velocities (usually 1 mm/s and above depending on the operating system considered) pure sliding can usually be observed and the friction coefficient between the two surfaces can be assumed as constant. However, when lower sliding velocities (usually less than 1 mm/s) are considered, smooth sliding is often replaced by an oscillatory sliding motion of one surface over the other. The occurrence of this motion is attributed to the frictional forces at the contacting surfaces and has thus been called "friction-induced vibration". This kind of vibration has been observed widely in industry. Automatic transmissions, machining processes, brake systems and robot manipulators are but a few applications where this phenomenon occurs. About 40 % of the friction-related problems in industry are due to vibration induced by friction. These forms of vibration are undesirable because of their detrimental effects on the operation and performance of mechanical systems. Specific problems include surface damage, wear of components, fatigue failure, noise, positioning errors in servomechanisms, and poorly finished surfaces in machining processes.

The subject of friction-induced vibration has been studied extensively over the last fifty years, bringing knowledge about the factors and parameters controlling the motion and identifying three types of friction-induced vibration. The first is stick-slip and it has been the most extensively covered and studied. Stick-slip vibration occurs at very low sliding velocities

of alternating stick and slip regimes. During the stick phase, the relative velocity between the two surfaces is zero and static friction forces are prominent. Sudden relaxation then occurs, during which the system is governed by dynamic friction forces. The second type is quasi-harmonic oscillation that usually occurs at higher sliding speeds and higher normal loads and has a characteristic sinusoidal waveform. This motion is governed by dynamic friction forces only. Comparatively, little work has been devoted to this type of friction-induced vibration. Although it has been reported by many researchers, only Brockley and Ko presented an experimental and theoretical investigation of the phenomenon. The last type is vibration induced by random surface irregularities. This usually occurs at relatively low normal loads and high speeds. Despite much research efforts, the whole phenomenon of friction-induced vibration is far from being fully understood and predictable, the friction itself being a very uncertain parameter.

The effect of normal movement and the application of a dynamic force to the frictional system, either transversally or normally have been investigated by some researchers, particularly in the case of stick-slip vibrations. A normal dynamic force has proven efficient in decreasing significantly stick-slip vibrations. However, apart from some early work by Ko, the effect of dynamic loading on the quasi-harmonic type of vibration has not been studied.

In recent years, demands for high quality products combined with fierce competition in industries require significant advances in machinery production with much improved efficiency and performance. Machines are often required to operate at higher loading and speed conditions. Control of friction and friction-induced vibration becomes an important factor for improving product quality and machine performance.

This study is concerned with the dynamics of friction-induced vibrations, particularly the quasi-harmonic type, in the presence of an external periodic excitation in the form of a dynamic normal force. Two industrial applications will be investigated experimentally and analytically. The first involves a paper-to-paper contact to illustrate different problems encountered in the pulp and paper industry and more specifically in paper processing like supercalendering or winding as in paper converting, handling or storing. The second type of contact concerns with sliding contacts between wet paper-based friction materials used in clutch assemblies and a steel and a cast iron counterpart to illustrate specific problems encountered in automatic transmissions. Quasi-harmonic type of friction-induced vibration can exist at high velocities and can affect the performance of automatic transmissions, brakes and clutches. This phenomenon has been widely reported and referred to as squeal. The objective is to gain better control and to eliminate, if necessary, friction-induced vibrations in industrial applications.

This thesis will first review literature concerning friction and friction-induced vibration. The development of a friction-induced vibration model will be followed by examination and investigation of the industrial friction materials and associated problems. These will be experimentally studied and theoretically and numerically analyzed, including chaotic analyses. A separate chapter is devoted to the study of the effect of dynamic normal loading on friction and friction-induced vibration.

CHAPTER 2

LITERATURE REVIEW

2.1 Historical background

The first names that come to mind when the subject of friction is mentioned are Amontons and Coulomb. Amontons [1], in the late seventeenth century was the first to rediscover Leonardo da Vinci's laws of friction, namely, that the frictional force is proportional to the normal load and that friction is independent of the size and the shape of the bodies in contact. In the late eighteenth century, Coulomb [2] went further and defined two types of friction: static friction force and kinetic friction force. Static friction force is equal to the force required to start the sliding of an initially motionless object. Kinetic friction is the force required to maintain the motion of the sliding body. Generally, static friction is greater than kinetic friction.

Nevertheless, it is only in the twentieth century that the subject of friction and in particular, friction-induced vibration began to gain greater attention. Wells in 1929 [3], was the first to publish a report on friction-induced vibration. While trying to measure kinetic friction coefficients at low speeds to find out how friction would be affected by velocity, he observed that the upper surface of the slider oscillated back and forth rather than smoothly sliding.

A few years later, Thomas [4] studied and solved the frictional vibration differential equations by using graphical and analytical techniques. He was the first to demonstrate the possibility of self-excited vibrations in frictional systems and stated the importance of the

difference between the static and kinetic dynamic friction in obtaining those vibrations.

Although he was not able to observe it experimentally, he also stated that a negatively sloped friction-velocity curve must exist in order for those vibrations to occur. He observed that stable oscillations could be obtained, depending on the value of the kinetic friction. Furthermore, he stated that simple harmonic oscillations could not be sustained in the presence of viscous damping, but stick-slip could if the damping was small. A few years later, Blok [5] treated the problem analytically and suggested that a sufficient increase in damping could eliminate totally the stick-slip vibrations. In 1940, he proved that the essential condition for the occurrence of self-excited oscillations is a decreasing friction-velocity relationship.

2.2 *The significance of the friction-velocity curve*

Since the '40s, many researchers have observed and stated the importance of the shape of the friction-velocity curve in affecting friction-induced vibrations, as well as its importance in defining the shape and amplitude of these oscillations.

Swift and Dudley [6] used Lienard graphical method for determining the vibration cycles from a friction-velocity curve. They found that the oscillation amplitude increases as the speed increases, result that did not agree with the findings of some other researchers. Brockley, Cameron and Potter [7] determined the existence of a critical velocity of the driven surface at which the stick-slip vibration died out. Its value is related to the system damping and to the velocity-dependent friction characteristics of the surfaces. They developed an expression relating the vibration amplitude and surface velocity in which vibration amplitude decreases

with increasing surface velocity. They also found that increasing the level of damping decreases the amplitude of the vibrations as well as the critical velocity.

While friction forces in stick-slip oscillations are alternatively time-dependent and velocity-dependent, friction forces in quasi-harmonic oscillations are exclusively velocity-dependent. Their existence is then critically dependent on the particular shape of the dynamic friction curve. The only researchers to really look into quasi-harmonic vibrations were Brockley and Ko in 1969 [8]. They first used Lienard graphical method to show that a hump at the beginning of the friction-velocity curve is one of the necessary conditions for the existence of this form of oscillation. They then used Krylov-Bogoliubov method to study the stability of the oscillations and determined that the vibrations start at a lower velocity boundary and their amplitude increases up to an upper velocity boundary determined by the amount of system damping. Their experimental results were in good agreement with the theoretical results. Bell and Burdekin [41] had observed this humped friction-velocity curve for polar lubricants earlier.

2.3 *The influence of normal stiffness*

Other factors influencing friction-induced vibration have been the subject of an extended literature review. One of them is the normal stiffness. Dweib and D'Souza [9] studied self-excited vibrations induced by dry friction and found that several mechanisms are in play. The main parameters are the effective coefficient of friction and the contact forces. In their experiments, as they increased the load, they noticed four different regions: a zone of linear increase of the coefficient of friction with the load, a zone of non-linear increase, a transient zone during which some random vibrations would occur and finally the zone of self-excited

vibrations. The ranges of normal forces for these four zones depend on system characteristics such as stiffness and damping. They developed a mathematical model where stiffness and damping are both non-linear. They found that there is a critical value of the normal force above which the steady-state sliding becomes unstable. This value is related to the natural frequency of the system. According to them, the mechanism that causes self-excited vibrations is the coupling between the different degrees of freedom.

Aronov et al. [10-11] presented a comprehensive experimental study of the interaction between friction, wear, friction-induced vibrations and system rigidity. They carried out their experiments on a pin-on-disk machine with steel specimens and water lubrication. They also found, for a set velocity, a critical value for the normal load above which high frequency self-excited vibrations are generated. This value of the critical load depends on the system rigidity. Their conclusion was the same as Dweib and D'Souza's [9], i.e. that self-excited oscillations are caused by a coupling between frictional and normal degrees of freedom. Later, Aronov et al. [10-11] studied the vibrational behaviour more specifically with an experimental setup that used a steel pin sliding over a cast iron disk without lubrication. They encountered the same four friction regimes as observed by Dweib and D'Souza. During the last phase where self-excited vibrations occur, the observed wear rate is several orders of magnitude higher than anywhere else. They also observed that the vibration frequency is the torsional frequency of the system and consequently, the energy needed to maintain the oscillations is supplied through the torsional mode. However, they recognized that in order to explain these vibrations accurately, a non-linear analysis is necessary.

Kato in 1985 [12-13] studied the effect of normal stiffness in the loading system. He especially stressed the importance of the test machine in the interpretation of experimental results. His conclusion was that wear is very sensitive to changes of normal stiffness in the loading system, which might be interpreted as the change of effective wear rate caused by the change of mean dynamic normal load. He noticed that the sliding-velocity curve shifts with a change of normal stiffness in the same way it would change with a variation of normal load. The review of many of these papers shows that, in the majority of cases, the occurrence of self-induced vibration is attributed to either the coupling between the different degrees of freedom or the negative slope of the friction-velocity relationship.

2.4 Applications

The subject of friction-induced vibration has gained much interest over the past fifty years. Numerous researchers have devoted a lot of time studying them as their presence has been identified in a lot of mechanical systems and assemblies with moving parts. Depending on the frequencies they occur at, they are referred to as squeal, chatter, shudder or groan and have often been linked to detrimental problems like excessive wear, severe damage, fatigue failure and objectionable noise levels. Different kinds of friction-induced vibrations can be observed in many practical situations, stick-slip, vibrations caused by random surface irregularities for relatively small values of the normal load and quasi-harmonic vibrations. Together, they account for 40 % of the frictional problems encountered in industry.

An example of these phenomena can be found in the research conducted by Bhushan [14]. He reported stick-slip induced noise in water-lubricated compliant rubber bearings.

Krauter [15] also reported the presence, under certain operating conditions, of chatter and squeal resulting in undesirable audible noise in the same type of water-lubricated bearings that are used to support ship propeller shafts. The onset of squeal and chatter is due to the growth of unstable vibration modes. One of the factors that mostly affects the onset of these vibrations is the negative slope of the friction-velocity curve. Rorrer and Eiss in 1995 [16] did some testing of frictional oscillations in wet and dry elastomeric materials used in automotive applications and found also that the friction-velocity relationship is the parameter governing the occurrence of friction-induced vibration and the oscillation magnitude. Kiryu, et al. [17] studied the ringing phenomenon occurring in automobile water pumps. They found that the shaft rotation induces a temperature change of the sealed liquid which results in a ringing sound. At low frequencies, stick-slip was observed and it transformed into quasi-harmonic oscillations at higher frequencies. They also found that the vibrations are related to the torsional, bending and axial vibration modes. Connel et al. [18] observed and identified stick-slip and quasi-harmonic in V-ribbed belts used to transmit power from engine crankshaft to automotive accessories. Nibert and Watts [19] mentioned that the potential for the widespread use of a slipping torque converter clutch is being prevented because of problems of shudder at low speeds, despite this clutches' ability to increase the fuel efficiency of the automobile.

In recent years, with the development of robotics and control systems, the subject of friction-induced vibrations gained renewed interest again. Applications like robot arms operate at very small amplitudes and low velocities and place a great importance on accuracy, sensitivity of motion and position, especially in medical applications. Sharma et al. [20] reviewed in their

paper the tribological failure problems encountered in robot components. Stick-slip is reported at joints when loading, lifting, or positioning, as well as at concentric columns and arms, chain drives, slideways, actuators and lead screws. Other dynamic friction problems are observed in elbow bends. Stick-slip is definitely one of the factors responsible for reduced performance and lifetime of manipulators. Comparatively, quasi-harmonic oscillations occur at higher velocities and consequently can be detrimental in the operation of automatic transmissions, brakes and clutches. Ibrahim [21], in a comprehensive literature review of all the problems related to friction-induced vibration, described different types of noise and vibrations associated with disc brake systems. The noise can be characterized by a generation of harmonics and limit cycles indicating a non-linear behaviour. Several mechanisms have been proposed to explain this phenomenon, among them, stick-slip, the negative friction-velocity slope and modal coupling. Moreover, the experimental results of Aronov et al. [11], mentioned above, undoubtedly relate friction-induced vibrations to wear and Aronov concluded that it should be expected that appearance of vibrations would cause the transition from mild wear to severe wear in moving components.

2.5 Elimination and control of friction-induced vibration

The above examples show that the presence of friction-induced vibrations in numerous engineering applications is a source of problems and many researchers are therefore investigating these phenomena in order to find ways to reduce or control these vibrations. The friction-velocity relationship between two contacting surfaces depends on various factors, including some chemical properties of the media. Therefore, research is being carried out on the

mechanical side of the problem as well as on the chemical side. Efforts are being made by chemical oil companies to develop automatic transmission fluids with additives to alter the negative slope of the friction-velocity characteristic. With the same objectives, a lot of research is also being done in the area of paper-based friction materials. Matsumoto [22] reported that paper-based friction materials, i.e. wet friction materials, are now the most common in automatic transmissions, in brake systems and in clutches and are being diversified to respond to an expanding range of applications, especially heavy-duty ones. These paper-based friction materials are composed of special raw papers, as well as synthetic fibers, fillers and resins. Filler contents do have the capacity to change the shape of the friction-velocity curve, therefore modifying the negative slope into a positive one. Moreover, paper based products absorb some of the additives contained in ATF, which can also affect the friction characteristics.

From a mechanical point of view, in the area of machine tools, it has been proven that a careful design of the tools and all moving components dramatically decreased the amount of vibration observed. Tolstoy [23] was the first to notice the importance of the normal degree of freedom in the behaviour of friction-induced vibrations. In experiments with a mass-spring-damper system sliding on a belt, he observed that the forward movements of a slider occur simultaneously with upward normal jumps. Simultaneously, there is a decrease in electrical conductance in the interface during the slip phase. He concluded that the decrease in friction observed during the sliding phase of stick-slip is a direct consequence of the jumping. Moreover, he noticed that external damping of these normal free microvibrations could eliminate friction force fluctuations so that static and kinetic friction were no longer

distinguishable. Tolstói's conclusion was that all apparent variations in friction could be reduced or eliminated by restraining the normal degree of freedom. He, with Derjaguin and Push in 1957 [24], established the conditions for stick-slip disappearance by using the equation of motion of a slider on a horizontal plane, but he assumed a linear friction-velocity relationship in the model. Later he, with Borisova and Grigorova [25], studied the friction reduction obtained when perpendicular oscillations were forced onto the system. He explained that, during sliding, the normal vibration increased the distance between the two surfaces, resulting in a decrease in the average contact area and consequently decreased the friction. Their theoretical and experimental results were in good agreement. Tolstói was the first to investigate friction reduction resulting when a normal vibrational force is applied to a friction pair.

Ko [26] applied transverse vibrations to a frictional system and found that a high frequency external excitation with a small vibration amplitude may be used as means of extinguishing unwanted quasi-harmonic vibration. His results were confirmed theoretically. He also simulated dynamic loading in his experiment and showed that stick-slip could be extinguished by a small dynamic-to-static normal load ratio. Quasi-harmonic oscillation needed a higher external force magnitude in order to be extinguished. However, in the dynamic loading case, the agreement between theory and experiment for the quasi-harmonic oscillation was not as good as for the stick-slip type.

Hunt [27] proposed to improve positioning accuracy in machine tool slideways by using an excitation normal to the contact without any other machine modification. He made an attempt to measure the minimum oscillatory force necessary to break the sticking part of the

stick-slip cycle, thus ensuring a smooth motion of the slider. Using a modified lathe-bed apparatus, with an electromagnetic shaker acting in a vertical plane over the moving steel block, he obtained a nearly-smooth motion at frequencies close to the resonant frequency of the system. He found that the load oscillating at one of the frequency of the system needed to be only a very low percentage of the static load in order to have a dramatic effect on vibration reduction.

Soom and Kim [28] and later with Hess [29-30] studied interactions between normal vibrations and friction during sliding. The normal vibrations they considered could be due to random external excitations or from internal excitations due to surface roughness. They examined the dynamic behaviour of steady-sliding Hertzian contacts under either external or internal random excitation. They also found that normal vibration caused a reduction of contact area and consequently some friction reduction.

Sakamoto [31] performed experiments similar to Tolstoi's. He applied a sinusoidal oscillatory normal load to a contact and observed that the friction force could be reduced and stick-slip suppressed. Once again, he found that the friction reduction at the resonance frequency of the system was strong. In two later papers, Sakamoto et al. [32-33] tried to corroborate these experimental findings with a theoretical analysis. They also stressed the importance of the testing apparatus as the extent of friction reduction depends on the vibration characteristics of the system in the loading direction and on the frequency of the vibratory load. It would appear that, without a good knowledge of the system used, it is hard to know how much of the vibratory input is actually acting on the contact, and therefore hard to determine the

extent of friction reduction. The insertion of mechanical damping in the vibration direction is also a useful method to prevent vibratory contact.

Skaere and Staelh [34] also looked into the influence of external vibration on the frictional force, varying frequencies and amplitudes of the vibration as well as normal loads and material combinations. Their experimental setup allowed them to apply vibration across or along the direction of motion. The materials studied were two types of steel. Skaere and Staelh found that it is possible to increase, reduce or not change the frictional forces through the application of external vibration. An increase in friction could be obtained through viscous damping of the friction surface which increased adhesion between the materials. Their results lead them to the conclusion that the friction change is the result of a tendency to separation or pick-up of the materials.

2.6 *Chaotic oscillation*

More recently, researchers' interest has also been aroused by some other aspects of friction-induced vibration like chaotic behaviour. Awrejcewicz [35] reported chaotic motion in a frictional system. His theoretical study used Coulomb friction to model the friction between the two surfaces. Popp and Stelzer [36-37] studied chaotic oscillation in frictional systems both experimentally and theoretically. Theoretically, they used a decreasing friction-velocity relationship along with an external transversal excitation. They found chaotic motion experimentally and numerically as well as p-periodic motion. Chaos has been shown to occur in certain frequency bands separated by bands with p-periodic solutions. Narayanan and Jayaraman [38] carried out the same kind of study for which they just considered Coulomb

friction instead of a varying friction-velocity relationship. Hess and Wagh [39] reported chaotic normal oscillation and friction at mechanical joints with nonlinear elastic properties. Their theoretical study considered a constant relative sliding velocity of the components to avoid the added complexity of the variation of friction with velocity.

Ibrahim [21] in his literature survey reported some more cases of chaotic oscillation in diverse frictional systems like chatter in machine tool systems, disc brake squeal and noise as well as wheel/rail squeal. Because of the importance of controlling friction-induced vibration in many engineering applications, he stressed the need for further work on modeling of friction-induced vibration, especially those encompassing the non-linearities of the friction characteristics.

CHAPTER 3

FRICTION MODEL

The friction characteristics resulting from the motion of one surface over another form an important facet of the behavior of many physical systems. The simplest form of a frictional system is often represented by a block sliding on a flat surface.

3.1 *Equation of motion*

Figure 3.1 shows a friction model which consists of a single degree of freedom mass m with displacement x sliding on a lower surface moving at constant velocity v . The slider mass is restrained by a spring of linear stiffness k and a damper of coefficient r . The coefficient of friction between the slider and the lower surface is μ_k , which may be constant or, as in a majority of cases, considered as a non-linear function of sliding velocity $(v - \dot{x})$.

The equation of motion for an autonomous system as that shown in figure 3.1 can be written as

$$m\ddot{x} + r\dot{x} + kx = w_s \mu_k = f_{\mu k} \quad (1)$$

where w_s is the normal force acting on the slider and $f_{\mu k}$ is the dynamic friction force

In the case of a system that combines a constant normal force w_s with a varying (dynamic) normal force w_d as shown in figure 3.2, the equation may be written as:

$$m\ddot{x} + r\dot{x} + kx = w_s \mu_k + (w_d \sin \delta) \mu_k \quad (2-a)$$

$$m\ddot{x} + r\dot{x} + kx = w_s \mu_k (1 + \beta \sin \delta t) \quad (2-b)$$

where β is the load ratio $\frac{W_{dynamic}}{W_{static}}$ and δ is the external excitation frequency, and the friction-velocity relationship of μ_k is assumed to remain unchanged during the dynamic loading situation.

In the case of an autonomous system, depending on the friction-velocity relationship taken by the coefficient of friction μ_k , different situations can occur. If μ_k takes on a constant value, as given by the Coulomb friction model, equation (1) is reduced to a linear differential equation which exhibits damped vibration during the transient state but does not show any during the steady state. The solution for the steady state is $x = \frac{w_s \mu_k}{k}$, the physical displacement of the slider. The scope of this thesis is concerned with situations where μ_k does not take on a constant value but has a non-linear characteristic instead. Under these conditions, the slider can be made to oscillate back and forth.

3.2 Friction-velocity (f-v) characteristic modeling

The expression for the coefficient of friction μ_k can take on different forms which lead to different vibrational behaviors. Some of the most common occurrences for these friction-velocity characteristics are presented in figure 3.3. Figure 3.3-a shows the case when μ_k is a constant i.e., Coulomb friction, which does not cause any vibration. A large part of early

research studies concentrated on this constant friction model, which is still used in many practical engineering applications. Figure 3.3-b shows an idealized version of the f-v characteristic where the static friction is higher than the dynamic friction. There are different variations to that idealized form. The main characteristic exhibited by this type of purely decreasing f-v relationship is the occurrence of “saw-tooth” shaped stick-slip oscillation owing to the higher static coefficient of friction. Figure 3.3-c illustrates yet another idealized example of f-v curves, the “humped curve” where the coefficient of friction increases initially. Brockley and Ko [3,4] showed that a hump in the f-v curve is a necessary condition for the existence of quasi-harmonic vibration.

There are various mathematical expressions to model these f-v relationships. Exponential, polynomial as well as hyperbolic functions have all been used in former studies. In the present investigation, the friction force function was expressed in the form of a n-th order polynomial.

$$f_{\mu k} = C_n(v - \dot{x})^n + \dots + C_2(v - \dot{x})^2 + C_1(v - \dot{x}) + C_0 \quad (3)$$

where $(v - \dot{x})$ is the relative sliding velocity and $v > \dot{x}$ (when $\dot{x} = v$, the situation becomes that of stick-slip), ω is the natural frequency of the system and $C_0, C_1, C_2, \dots, C_n$, are constants that may be adjusted to fit the equation to measured friction values.

3.3 *Dynamic friction models*

The two types of vibrational behaviour studied have inherent differences. Therefore, each requires a different model.

3.3.1. Stick-slip vibration

For f - v curves of the type shown in figure 3.3-b, i.e., with a static coefficient of friction higher than the dynamic one, equation (1) is applicable only during the slip part of the stick-slip oscillation. A discontinuity exists in the transition from slip to stick. During the stick phase, the two surfaces move together, $(v - \dot{x}) = 0$, i.e. $\dot{x} = v$ and $\ddot{x} = 0$. The equation of motion then reduces to

$$rv + kx = w_s \mu = f_{static}$$

$$\mu \rightarrow \mu_{static}$$

or

$$x = \frac{f_{static} - rv}{k} \quad (4)$$

The static friction force f_{static} has an undetermined value. Based on experimental evidence, f_{static} is sometimes considered to be a function of the time of stationary contact [47]. Others have argued that, even during the so-called stationary contact, application of a tangential force could cause micro-slip. The onset of gross slip (or break-away of static friction) is primarily dependent on the rate of application of the tangential force [48]. In either case, f_{static} is not a constant but a function involving other parameters.

Therefore, under this circumstance, a simple solution can not be obtained from equation (1) alone. Both equation (1) for modeling the slip phase, and equation (4) for the stick phase have to be considered. Solutions for this kind of problem can be obtained by graphical methods such as Lienard phase-plane technique. Alternately, a piecewise computational method can be used to link the equations, such as equations (1) and (4), or numerically to deal with the

mathematical discontinuity condition. Several analytical techniques have been developed for treating the stick-slip problem by considering a linearized f - v relationship and assigning a constant value for the static friction, reducing the dynamic frictional system to an ordinary differential equation [49].

3.3.2. Quasi-harmonic vibration

For f - v curves of the “humped” type, as presented in figure 3.3-c, the problem can be addressed analytically by solving equation (1) alone. These characteristics can be fitted with a n -th order polynomial as in equation (3). This polynomial is incorporated into the equation of motion. Depending on whether an autonomous or a dynamically loaded system is considered, two different equations of motion are obtained and different methods of solution are needed.

Autonomous system

For the autonomous case, substituting equation (3) into (1) yields:

$$\ddot{x} = -\omega^2 x - \frac{r}{m} \dot{x} + \frac{1}{m} [C_0 + C_1(v - \dot{x}) - C_2(v - \dot{x})^2 + \dots + C_n(v - \dot{x})^n] \quad (5)$$

This equation can be solved analytically by a technique which uses the method of first approximation by Krylov-Bogoliubov (K-B method), developed by Ko [26]. This technique applies only to situations where $(v - \dot{x}) > 0$. If $(v - \dot{x}) = 0$, a discontinuity occurs. The details of the development of this method can be found in Appendix 1.

For simplification, this equation can be normalized and rewritten as follows (the details of the normalization can also be found in Appendix 1).

$$\ddot{X} + R\dot{X} + X = \frac{1}{E} F(V - \dot{X}) \quad (6)$$

where the normalized friction-velocity function $F(V - \dot{X})$ may be re-arranged to give

$$F(V - \dot{X}) = B_0 - B_1\dot{X} + B_2\dot{X}^2 - B_3\dot{X}^3 + \dots + (-1)^n B_n\dot{X}^n$$

Subsequently, equation (6) can be further re-arranged to give

$$\ddot{X} + X + \gamma G(\dot{X}) = 0 \quad (7)$$

where $G(\dot{X})$ is a non-linear function of \dot{X} including the system damping term “R”, thus

$$\gamma G(\dot{X}) = Q_1 \left[\dot{X} - \beta_2 \dot{X}^2 + \dots - (-1)^n \beta_n \dot{X}^n \right] / E$$

where $Q_1 = c\omega h + B_1$, $\beta_1 = Q_1/Q_1 = 1$, $\beta_2 = B_2/Q_1$ and $\beta_n = B_n/Q_1$; $E = m\omega^2 h$ and $\omega^2 = k/m$, and where h is an arbitrary linear constant for the normalization procedure (Appendix 1).

The approximate solution for equation (7) is

$$X = A(\tau) \sin(\tau + \varphi(\tau)) \quad \text{for } \gamma G(\dot{X}) \ll 1$$

where both $A(\tau)$ and $\varphi(\tau)$ are functions varying with time.

The application of a polynomial friction function (Appendix 1) yields

$$\dot{A} = -\frac{Q_1}{2E} \sum_{k=1}^{k \leq (n+1)/2} \frac{{}^{(2k-1)}P_k}{2^{(2k-2)}} \beta_{(2k-1)} A^{(2k-1)} = \Phi(A) \quad (8)$$

where ${}_n P_k = \frac{n!}{(n-k)!k!}$ is the expression for the binomial coefficients in the equation above.

The condition for a steady-state amplitude A of quasi-harmonic vibration is when $\dot{A} = \frac{dA}{dt} = 0$.

Thus, by setting equation (8) to zero, $\Phi(A)=0$, one can solve for A to obtain the steady-state amplitudes.

For a non-linear system, the amplitudes A_i need to be further tested for stability. To that effect, a slightly perturbed amplitude ($A_i + \delta A$) is considered, where δA is an absolute value of departure from the amplitude A_i . The development of the variational equations to the first order shows that

$$\frac{d(\delta A)}{dt} \cong \frac{d(\Phi(A_i))}{dA} \delta A$$

Thus, if $\frac{d(\Phi(A_i))}{dA} < 0$, since δA is an absolute value, then $\frac{d(\delta A)}{dt} < 0$, which means that the

initial departure δA tends to disappear for $\frac{d(\Phi(A_i))}{dA} < 0$, bringing the system back to a stable

limit cycle.

For stability,
$$\frac{d(\Phi(A_i))}{dA} < 0 \quad (9)$$

The above expression (9) is therefore the condition for obtaining a stable vibration amplitude.

On the other hand, if the result of expression (9) is positive, the vibration amplitude is unstable and there is no sustained vibration with that amplitude.

Dynamically loaded system

For the dynamically loaded system, substituting equation (3) into (2) yields:

$$\ddot{x} = -\omega^2 x - \frac{r}{m} \dot{x} + \frac{1}{m} [C_0 + C_1(v - \dot{x}) - C_2(v - \dot{x})^2 + \dots + C_n(v - \dot{x})^n] (1 + \beta \sin \alpha \omega t) \quad (10)$$

where δ becomes $\alpha \cdot \omega$, α being the frequency ratio and ω being the natural frequency of the system, i.e. $\omega^2 = k/m$.

The equation of motion for this dynamic system can be rewritten in the same fashion as equation (7) of the autonomous system.

$$\ddot{x} + \gamma(1 + \beta \sin \alpha \omega t)G(\dot{x}) + x = C_0(1 + \beta \sin \alpha \omega t)$$

where $G(\dot{x})$ is a non-linear function in \dot{x} . This equation is a non-linear differential equation that includes coefficients varying with time. In theory, equations with varying coefficients are solvable with the WKBJ method [42] which gives an approximation of the solution, assuming that the varying coefficient executes only relatively small changes about a large mean value.

However, this type of analysis involves tedious algebraic manipulations for a linear system, let alone a non-linear system. Moreover, the number of algebraic manipulations increases tremendously with the number of non-linear terms having varying coefficients. Therefore, since

the cases in the present study include as many as nine nonlinear terms, it was decided that a numerical analysis would be used instead.

The numerical analysis was performed using a software package called INSITE (Nonlinear Systems Investigative Toolkits for Everyone). This software package is made of a collection of programs used for the simulation and characterization of dynamical systems, with an emphasis on chaotic systems. It was chosen due to the possibility of chaotic behavior arising from the dynamically loaded system considered in the present study. In the course of the numerical study, diverse techniques are used; these include phase-plane plots, Poincaré maps, bifurcation diagrams and Lyapounov exponents. A brief explanation of these terms is given below in order to clarify them.

- **Phase-plane plots**

A phase-plane plot describes the variations of \dot{x} versus x . It shows the type of steady-state conditions the system reaches if it is stable like a focus point or a limit cycle. It is similar to the plots obtained experimentally on the x-y channel of the oscilloscope representing the variation of displacement with velocity.

- **Poincaré maps**

A Poincaré map is also known as a stroboscopic phase plane. It is the result of sampling the phase-plane at specific times, instead of continuously. A stable fundamental solution is then translated as a single point. A stable subharmonic of order n is seen as n fixed separate points on a Poincaré map. A chaotic motion, which is non-periodic does not show any repetition of points but shows instead a pattern with a layered structure.

- **Bifurcation diagrams**

A bifurcation diagram shows how changes in one parameter affect the behavior of the system. Values of the bifurcation parameter are represented from left to right. The final value reached by the system is plotted on the vertical axis. A steady-state situation whatever the value of the parameter, is visualized as a single line. If the line splits in two, the system frequency oscillates between two values (subharmonic $n = 2$). If the bifurcations occur at an increasing rate, the system turns chaotic i.e., the system reaches infinitely many different values.

- **Lyapounov exponents**

Lyapounov exponents are the ultimate method for making sure that a system is chaotic. They are numbers which measure the conflicting effects of stretching, contracting and folding in the phase-space of an attractor. A positive exponent means stretching while a negative means contracting. For a fixed-point attractor, all the Lyapounov exponents are negative, meaning an inward pull towards a steady-state. A periodic orbit attractor (limit cycle) has one exponent equal to zero and the other negative. A strange attractor has to have at least one positive exponent.

CHAPTER 4

INDUSTRIAL FRICTION MATERIALS AND ASSOCIATED FRICTION PROBLEMS

In the literature review in chapter 2, it has been mentioned that friction-induced vibration is a widespread problem in industry. Applications such as water-lubricated bearings, V-ribbed belts used for transmission, brakes in cars, bikes and washing machines, joints or linear feed drives in robotics, clutches in automatic transmissions, rail/wheel contacts, as well as paper during making and handling, all exhibit some kind of friction-induced vibration. Friction-induced vibrations can manifest themselves acoustically, like in squeal or chatter, creating undesirable high noise levels. They can cause inaccurate positioning or jerky motion, like in robotics and machine tools applications. Moreover, their presence can increase the wear rate of moving surfaces and cause early fatigue failure. In most cases, their presence is undesirable.

In this thesis, frictional problems in two specific areas have been studied and analyzed. In an automobile, friction is present at all levels and in particular, in clutches and brakes. Generally, clutches and brakes use friction plates that are faced with a lining made of cellulosic, synthetic or asbestos fibers. Metallic wires can be added to improve the mechanical strength of these plates, along with diverse fillers. The fabric then constituted is impregnated with resin to improve compressive strength and wear resistance [43]. In wet clutches, these friction plates slide against steel surfaces. During the engagement process, the oil film between them is first squeezed, then the relative motion between them decreases and static friction occurs. For an efficient operation of wet clutches during this process, friction-induced vibration should be avoided; the knowledge of the frictional characteristics of this pair is needed to control the

Friction also plays an important role in the paper processing industry. The friction characteristics between paper/paper and paper/metal combinations affect the performance of paper processing and paper handling machinery. The requirements in friction performance often differ widely [44]. For example, a high friction coefficient is desirable for good roll formation and easy handling, to prevent roll deformation when braking in a newsprint pressroom, in shipping or in packaging, whereas a low friction coefficient is needed between the flute and steel corrugator or in converting machines. Paper friction and paper vibrational behavior depend on numerous factors such as paper roughness, paper strength as well as surface chemistry, filler contents and relative humidity.

To relate the present study to the industrial problems described above, several combinations of materials were studied. They generally fall into two groups of combinations: the “paper-to-metal” contact is primarily for clutch applications, and the “paper-to-paper” contact for paper processing applications. In this chapter, the physical characteristics of these combinations are described first; they are followed by studies of their frictional and vibrational characteristics and the influence of several parameters, such as the normal load and the type of lubricant.

4.1 Specimen description

4.1.1. “Paper-to-metal” contact

For the first group of friction materials, one type of friction plates used in automotive clutch assemblies was supplied by Ford Motors Corporation. As the supply of these specimens was limited, experimental tests were first carried out between a cast iron disk and a blotting paper slider with automatic transmission fluid (ATF) as lubricant, as it will be shown later that the

blotting paper has a very similar fibre construction as the friction plates. This combination was used in a previous study [26] to simulate the behavior of clutch assemblies. It was used here for preliminary testing.

A preliminary examination of the surfaces under an optical microscope revealed some interesting characteristics of the friction materials. The Ford friction plate appears to be composed of some kind of fibers that intertwine to form an intricate network impregnated with resin (figure 4.1). No other particles or metallic wires can be observed anywhere on the plate surface. The whole plate surface appears very porous, with cavities and gaps between the fibers, such that the underlying layers can be seen. Some areas show a slightly higher density of fibers while some others look more resinous. The blotting paper surface shown in figure 4.2 appears to have a similar structure. It clearly is a good candidate as a substitute for simulating friction plate behavior; the fiber size, arrangement and apparent density of the paper look similar to those of the Ford friction plate and the paper does not appear to contain any other additives, like metallic particles or other kinds of fibers. The main difference between the two materials is that blotting paper is not solidified in resin. Without the resin, the blotting paper has less compressive strength than the friction plate.

In addition to the Ford friction plate, two other plate materials, Dexron and type F, were also examined with an optical microscope. At first sight, the Dexron friction plate, which is shown on figure 4.3 appears also very porous with big gaps between fibers revealing the underlying layers. Paper fibers intertwine with another type of rigid black fibers. A few metallic particles are trapped randomly across the surface. The whole fabric is also solidified in resin. This plate is on the whole rather similar to the Ford plate and its compacity seems about the same. On the

other hand, the type F friction plate presented in figure 4.4 looks quite different from the former one. The density of fibers seems higher even though it is still rather porous. Some large black particles are embedded in the matrix.

4.1.2. “Paper-to-paper” contact

For the second type of contact, a type of recycled newsprint was supplied by a paper company. The two sides of this paper are referred to in the subsequent paragraphs as A_1 and A_2 . When observed under an optical microscope, this newsprint presents a rather different picture from those given earlier by the friction plates. The fibers appear more undone and flattened (figure 4.5). Other components, such as multicolor specks, are also present, which show that recycled pulp enters the composition of this paper. Some other fillers such as calcium carbonates appear as fluffy particles in between the fibers. Both sides of the paper were examined, the only noticeable difference being that side A_2 shows somewhat less colored specks than side A_1 . Otherwise, both surfaces appeared very similar.

4.2 Other media and parameters

The frictional and vibrational behaviours of sliding surfaces can be affected by many external parameters, in addition to their material and structural properties. In the present study, the influences on F-V characteristics of normal load, and of the type of lubricant for the paper-to-metal combination, were examined.

4.2.1. Normal load

In metallic friction, friction force is normally considered as being proportional to the applied

normal force. However, fiber products such as friction plates and paper products that are studied here can be significantly affected by the normal load as it controls the pressure on the surfaces. The normal load can alter the fiber structure. In the case of friction plates for transmission clutches, this change in fiber structure could affect the presence of transmission fluid or lubricant at the interface, e.g., either trapping or squeezing out the fluid.

4.2.2. Sliding velocity

Although Coulomb friction assumes that coefficients of friction are independent of sliding velocities, many material combinations, particularly non-metallic combinations in lubricated sliding, often exhibit friction characteristics that vary with sliding velocities. The present study applies the friction-velocity characteristics to the friction-induced vibration behaviours of the industrial materials described in the previous section.

4.2.3. Type of lubricant

The type of lubricant used with a tribological pair can have a dramatic effect on its frictional characteristics and vibrational behavior. Each lubricant has different properties, such as its viscosity and additives contents that can act as friction modifiers. They are chosen to provide a wide range of characteristics for specific applications. Several types of automatic transmission fluids (ATF), as well as one slideway oil, were used in this study with the friction material combinations involving the friction plate and the blotting paper.

CHAPTER 5

EXPERIMENTAL TECHNIQUES OF FRICTION MEASUREMENT

Experimental equipment and measurement techniques are critical in all frictional studies. The measurement of friction involves relative motion of the surfaces and is often related to some form of displacement measurement that can easily be disturbed by external, internal or environmental conditions. For example, measurements can be subjected to vibrations coming from the drive of the test rig. These extraneous vibrations can cause variations in the friction forces and should be minimized for greater accuracy. If self-excited oscillations occur, such as stick-slip or quasi-harmonic vibration, the displacement of the slider can fluctuate widely; in these cases, a simple average of the displacements can give erroneous values for the friction and other measurement methods that will be described below need to be used. Finally, the state of surfaces, lubrication conditions and other environmental factors can also cause fluctuations in friction levels by changing the contact properties. A careful monitoring of these conditions should ensure their consistency and improve measurement reproducibility.

5.1 Description of the apparatus

The experimental test rig used in this study was a pin-on-disk machine (figure 5.1). Originally built in the Mechanical Engineering Department's former Tribology Laboratory, it was designed for the study of friction-induced vibrations and associated static and dynamic friction forces [40]. This test rig consists of a lower specimen in the shape of a flat disk driven by a succession of rubber "O" rings and toothed belts mounted on speed-reduction pulleys and toothed wheels and an upper specimen assembly which is attached to a cantilever beam mounted

on pivots at its fixed end. The upper specimen is pressed against the disk by a static normal force applied through a second cantilever beam mounted at the same pivot point as the former one. For the present study, the upper specimen (figure 5.2) is a rectangular slider inserted into a hemispherical specimen holder which allows self-alignment of the contacting specimens. The lower specimen is a metal disc, 12.5 cm in diameter, housed and secured in a circular trough by three set screws (figure 5.3).

The full velocity range of the apparatus is from 1 $\mu\text{m}/\text{sec}$ to 20 cm/sec, although the commonly used range is from 5 $\mu\text{m}/\text{sec}$ to 10 cm/s. The number of belts and pulleys used provides a specific range of rotational speeds and a smooth motion, even at very slow speeds.

The test rig was modified for the studies of the effect of normal loading. Two different approaches were chosen. The first one involved the use of two stepper motors driving two out-of-balance masses and rotating in phase to create a sinusoidal normal force. The second approach uses an electromagnetic shaker to obtain the same effects.

In the first case, a new cantilever beam was attached to the opposite end of the original loading arm. The two stepper motors were mounted side-by-side at the end of the beam, each driving an eccentric lead mass (figure 5.4). When these eccentric masses are set in phase, an oscillating normal force is created and transmitted to the loading arm where the static load is applied. The normal force transmitted to the slider is then a combination of a static and dynamic normal load. By changing the weight of the eccentric masses, different normal loads can be obtained, but to avoid an horizontal component, the weights should have identical masses. In the second case, a small electromagnetic shaker (figure 5.5) was attached to the loading arm and located above the slider, where the static normal load is applied in the autonomous case. In

this arrangement, the shaker itself constitutes the static normal load and can be balanced by weights at the other end of the loading arm to obtain the desired normal load. A small mass is attached to the shaker. When the shaker is excited, this small mass combines with the internal dynamic mass of the shaker to provide an oscillating normal inertia force. This inertia force is monitored by a load cell fixed between the shaker and the loading arm.

5.2 Measurement techniques and instrumentation

Experimentally, friction and friction-velocity characteristics can be obtained by either one of the two techniques described below.

5.2.1. Static measurement method

The standard method for measuring friction and obtaining friction-velocity characteristics is by a static measurement using either strain gauges or a load cell. In this case, a load cell is mounted on the test rig and pressed perpendicularly against one side of the upper specimen assembly (figure 5.6). As the disc rotates, the friction causes the slider to move firmly against the load cell which monitors the instantaneous static force and the subsequent kinetic force developed by the slider. Measurements are taken for different disc velocities and plotted to construct the friction-velocity curve.

Alternately, for pure sliding motion, i.e., when there is no friction-induced vibration, the constant displacement of the slider coupled with the stiffness of an elastic that holds the slider restraining device can also provide the friction force measurement needed. For example, in the present set-up, the displacement of the slider is monitored by strain gauges mounted at the base of the slider-arm assembly. These gauges are connected to a bridge amplifier which is in turn

connected to an oscilloscope where the signal is acquired. Calibration of the strain gauges allows the reading of the signal as a displacement or as a friction force.

On the other hand, if the measuring system is subjected to friction-induced vibration, the assessment of the dynamic friction force becomes difficult as the slider velocity is not constant and therefore, ignoring inertia forces and simply averaging the displacements could lead to erroneous results.

5.2.2. Direct measurement method

Friction force measurement

An experimental technique making use of all the dynamic signals obtained during friction-induced vibration was first developed by Bell and Burdekin in 1966 [41]. They determined that monitoring both displacement x and acceleration \ddot{x} signals of the oscillating slider and plotting $(m\ddot{x} + kx)$ versus the dynamic velocity signal \dot{x} would represent a dynamic friction-velocity characteristic (i.e., $m\ddot{x} + kx = f_{\mu k} - r\dot{x}$) that would have included the viscous damping force of the system. Practically, the displacement and the acceleration signals are appropriately scaled and ought to be in 180° phase, i.e. when there is no friction, a straight line will be obtained, the slope of which represents the value of the damping coefficient, r). They are then fed to the differential amplifier of an oscilloscope and displayed on the y-axis against the velocity signal in a x-y plot. In this fashion, only one vibration cycle can provide a trace of the friction-velocity curve over an extended range of velocities. This experimental method was employed with success by several other researchers including Brockley and Ko in 1969 [42]. It was also used

in the present study to monitor friction and obtain friction-velocity curves for the different surface combinations.

Acceleration measurement

The acceleration in the sliding direction is monitored by a piezoelectric accelerometer mounted on the top of the slider-arm assembly. The accelerometer is then connected to a charge amplifier where the amplification is adjusted to match that of the displacement signal from the strain gauges, and is fed to the same channel of the oscilloscope, where the two signals are added as previously described. To calibrate the amplification, the slider is made to vibrate freely, i.e., it is separated from the lower specimen, and the gain control is adjusted until the two signals are equal and opposite.

Velocity measurement

The velocity of the vibrating slider-arm assembly is measured by an electromagnetic type transducer fixed on the arm in front of the slider. The signal is fed to the x-channel of the oscilloscope.

Displacement measurement

The displacement of the slider-arm assembly is monitored by the strain gauges, whose displacement calibration is obtained by deflecting the beam with a micrometer. The beam stiffness is deduced from the displacement signals and the forces that are used to deflect the beam. The calculations of the system parameters are presented in appendix 2.

5.3 Testing procedure

Testing procedures are critical to the friction measurement process, as changes in the physical state of material surfaces like roughness, or in lubrication conditions and other chemical and environmental factors can cause fluctuations of the friction level. Consistency in the testing procedure is of utmost importance to obtain meaningful and repeatable measurements. Therefore, several testing procedures were developed to suit each type of material combination and test conditions. The material combinations studied in this thesis are divided into two groups, namely, the paper-to-metal and the paper-to-paper combination. They require very different testing procedures which are reviewed in this section.

5.3.1. Paper-to-metal combination

For paper-to-metal contacts, two types of combinations are studied; one involves the contact between a cast iron disk and a blotting paper slider, the other one involves the contact between a clutch plate and a steel slider. Both cases involve the use of a lubricant or transmission fluid between the two samples. Nevertheless, the testing procedures present some similarities.

Blotting paper-on-cast iron with lubricant

To ensure similar contact conditions between the paper sample and the cast iron disk for all test, the following steps were carried out:

- The disk surface was repolished with 15 microns diamond powder between each test or with 1000 grit SIC paper followed by 15 microns diamond powder if scratches created by the paper surface were noticeable on the disk surface.

- The disk surface was carefully cleaned between each test by ultrasounds and ethanol to remove all the oil and residues that could contaminate the conditions for the subsequent test. It was also cleaned in the same fashion after each repolishing phase.

- Data acquisition was triggered by an optical sensor at the same position on the disk surface for each test, which minimized surface effects on the results. For example, a minor surface undulation around the disk perimeter may induce some periodic variations in friction that could be misinterpreted as friction-induced vibrations during tests with high disc velocities.

Since friction materials like blotting paper and friction plates used in this study are porous, some kind of running-in is necessary to reach stable friction and sliding conditions. The blotting paper slider, once put in place is run on the disk surface for 5 full rotations of the disk at 9.8 mm/s, which is sufficient to bring stable sliding and lubricating conditions for the slider. For the static measurement method, the measurements were carried out from the lowest to the highest sliding velocity, then repeated for decreasing velocities. If the results were not similar, the measurement series was repeated with a new slider. For both static and direct methods, all results presented proved reproducible.

With repeated sliding, wear of the surfaces occurs. As the test proceeds, the paper slider is slowly covered by a layer of compacted metallic particles detached from the cast iron disk surface. They are located mainly on the leading edge of the slider. These particles, embedded in the paper lining, consequently abrade the disk surface, causing scratches on the cast iron. When this phenomenon occurs, testing is suspended and the disk is repolished.

Steel slider-on-friction plate with lubricant

This combination has sturdier surface properties than the previous one. A longer break-in period is required to reach stable surface conditions. The testing conditions are kept as close as possible from the testing conditions used by Ford to keep the results realistic. The semi-synthetic Dexron/Mercon IIE automatic transmission fluid is used for the testing. Both sets of testing conditions for the break-in phase and the real testing phase are given in table 5.1. To follow Ford specified conditions for the run-in period, our contact slider-friction plate would have to be run for 30 min at 539 mm/s under a normal load of 6.62 N. As our contact area is only a small portion of the whole plate surface and as the velocity they are using can not be respected because of the test rig velocity range, the break-in duration for our study was increased to 5 hours at a velocity of 50 mm/s. For the friction-velocity data collection, the Ford testing conditions can be respected. For our purpose, only the first 4 velocities that they used are tested. As the friction plate is impregnated with resin, its surface remains virtually unchanged for a long time under the test conditions used, and the same friction plate can be used for a whole series of measurements. The slider, on the other hand, is repolished frequently to maintain similar contact conditions.

Break-in period**Ford conditions**

Pressure	Surface	Velocity	Duration
104 kPa	whole disk surface	100 rpm	30 min.

Equivalent conditions for our system

Pressure	Slider surface	Velocity	Duration
6.62 N	63.62 mm ²	539 mm/s	5 hours

F-V data collection

Ford conditions				Equivalent conditions for our system			
Pressure	Surface	Velocity	Duration	Pressure	Slider surface	Velocity	Duration
345 kPa	whole disk surface	2 rpm	2 sec.	21.95 N	63.62 mm ²	10.5 mm/s	2 to 8 sec.
		6 rpm				31.4 mm/s	
		10 rpm				52.3 mm/s	
		14 rpm				73.3 mm/s	
		20 rpm				104.7 mm/s	
						

Table 5.1. Testing conditions for the Ford friction plates**5.3.2. Paper-on-paper combination**

This combination is a lot more fragile than the former two and needs special care. A different set of test procedures is followed. The slider and the disc portion are changed for each test as the paper surface does not have a very long life span. As the surfaces slide against each other, they deteriorate very rapidly. Fibers become undone, changing the surface and the friction characteristics. The deterioration occurs even faster with heavier loads. For example, testing with a 1.82 kg (4 lb) normal load caused the paper disk or the slider to be torn on several occasions. Consequently, the majority of tests was carried out for a 0.91 kg (2 lb) normal load. Overall, the paper-on-paper combination is more sensitive to minor surface changes due to repeated sliding. The paper-on-metal combination was therefore used initially for preliminary tests checking out the measurements methods.

CHAPTER 6

EXPERIMENTAL RESULTS

Tests were carried out for all the material combinations and lubricants listed in table 6.1. For each combination, friction measurement was taken for a range of disc velocities. For some combinations, the effect of normal load was studied. Friction-velocity characteristics were constructed using the static measurement technique described in section 5. For a majority of combinations, a dynamic friction-velocity characteristic was also obtained using the direct measurement technique described in the previous section. In general, the experimental F-V curves may be divided into three groups, each with a distinctive behavior. Several of the F-V curves were chosen to illustrate these different types of behaviors. These chosen F-V characteristics were computer-fitted with a polynomial function for subsequent use in the analyses using the friction models described in chapter 3.

Slider	Disk	Lubricant
Blotting paper	Cast iron	#1 ATF
Blotting paper	Cast iron	Type F ATF
Blotting paper	Cast iron	Dexron/Mercon III
Blotting paper	Cast iron	semi-synthetic Dexron/Mercon IIE
Blotting paper	Cast iron	slideway oil
Steel	Friction (clutch) plate	semi-synthetic Dexron/Mercon IIE
Newsprint A1	Newsprint A1	dry sliding
Newsprint A1	Newsprint A2	dry sliding
Newsprint A2	Newsprint A1	dry sliding
Newsprint A2	Newsprint A2	dry sliding

Table 6.1. Material combinations and lubricants tested

6.1. Blotting paper on cast iron

As described before, a slider with a blotting paper sample was run on a polished cast iron disk covered with a thin layer of transmission fluid. This configuration has the advantage of creating oscillations of fairly large amplitude and extreme regularity and allows steady-state oscillatory regimes to take place. All f-v characteristics were obtained with either the direct A-V-D method or the static measurement method. Figure 6.1 illustrates an example of a f-v curve obtained by using both static and direct measurement methods. The two friction-velocity characteristics obtained by the two methods are plotted for the same materials combination. The curves are parallel and their overall shape is the same. The small difference between the two friction levels is likely due to an offset error or a slight discrepancy between the calibration of both sensors. In spite of this, both methods show a good agreement in this example. Figure 6.2 shows the effect the normal load has on f-v characteristics by displaying them for one type of automatic transmission fluid and 4 normal loads. Increasing the normal load shifts the f-v curve up and, at high speeds, the ratio between the different curves is approximately the ratio between the normal loads, as in Coulomb's friction law. On the other hand, at low velocities, increasing the load seems to have increased the non-linear effects. The effect of sliding velocity is revealed at low speeds. In the present case, the friction is not constant anymore and a small hump can be noticed. The variations in friction and the hump observed at low speeds are enhanced with a higher normal load. The f-v curve is also smoother at higher loads and the results are more reproducible.

The effect of normal load on the paper physical aspect is also important. At 0.45 kg (1 lb) and 0.91 kg (2 lb) normal load, the paper aspect does not change much. On the other hand, at

1.37 kg (3 lb) and 1.92 kg (4 lb), the paper was compressed and flattened. This would decrease the oil absorption and reduce the effects due to an irregular smoothness of the paper surface. As a consequence, the general behavior is a lot smoother for heavier loads.

Figure 6.3 presents the f - v characteristics obtained with 4 different fluids subjected to the same static normal load of 0.91 kg (2 lb). Different types of characteristics can be observed. The #1 transmission fluid displays a decreasing type. The Dexron/Mercon IIE shows a very small localized hump at very low velocities and then the friction decreases. The type F ATF and the semi-synthetic Dexron/Mercon III both show a bigger hump for low velocities, then the latter starts decreasing and stabilizes at an approximately constant friction level while the former stays at the higher friction level after the peak of the hump. They all reach a fairly constant friction level at around 20 mm/s. Figure 6.4 presents the f - v characteristics for 3 types of fluid under a static normal load of 1.8 kg (4 lb). The type F ATF exhibits for this load a similar decreasing type of f - v curve while the semi-synthetic fluid and the slideway lubricant exhibit a well-defined hump. Different f - v characteristics lead to different vibrational behaviors, which are now reviewed for each lubricant.

- **Blotting paper vs. cast iron with ATF 1**

This fluid presents a decreasing type of f - v curve (figure 6.4). Its general behavior is characterized by the presence of stick-slip vibrations that occurred at different velocities starting from as low as $v = 0.28$ mm/s. In the very low velocity range, the vibrations are irregular. As can be seen in figure 6.5, the amplitude of the stick-slip vibration increases with the velocity for the lower velocities and the vibration frequency gets closer to the natural frequency of the

system at higher velocities. The friction vs. time plots of the vibrations can be seen on the graph sequence on figure 6.6. As the velocity increases, the stick-slip oscillation deviates from the standard saw-toothed shape. A certain amount of slipping occurs during the sticking phase and the relaxation is more progressive than in pure stick-slip. Eventually, for velocities at the upper end of the tested range, the vibrations turn into irregular quasi-harmonic vibration and the vibration amplitude drops, coinciding at where the friction-velocity curve levels off or increases slightly.

It is to be noted that a fair amount of wear was generated with this combination. After a test, the paper sample shows a fairly large quantity of metallic debris adhered on its surface. Scratches can be seen on the surface of the cast iron disk.

- **Blotting paper vs. cast iron with semi-synthetic Dexron IIE/Mercon lubricant**

This combination showed significantly less wear than the former one. For a static load of 17.8 N (4 lbs), its f-v curve exhibits a slight hump at the very beginning of the velocity range (figure 6.7). The friction vs. time plots for increasing sliding speeds can be seen in figure 6.8.(a). The hump is confirmed by the fact that oscillations do not start before a velocity of 2.25 mm/s is reached. The shape of the stick-slip vibration also degrades very rapidly to become more rounded, already hinting towards quasi-harmonic vibration. At 46.2 mm/s and above, the combination shows regular quasi-harmonic oscillation, seemingly stable. For a smaller static load of 8.9 N (2 lbs), regular stick-slip never occurs and stable quasi-harmonic vibration occurs around 13 mm/s after a transient state. For higher velocities, the vibration amplitude becomes irregular (figure 6.8.(b)).

- **Blotting paper vs. cast iron with Dexron III/Mercon ATF**

This lubricant exhibits what might be called a hump at low velocities, but it is so small that it is impossible to model with a non-linear function (figure 6.9). Under a static load of 8.9 N, vibrations do not start before 2.25 mm/s (figure 6.10). The stick-slip vibrations increase in amplitude and change to quasi-harmonic at 28.5 mm/s. As the velocity increases further, the amplitude of the quasi-harmonic vibration becomes irregular and decays.

- **Blotting paper vs. cast iron with type F ATF**

This lubricant does exhibit an even smaller hump in its F-V characteristic than the previous lubricant (figure 6.11) and vibrations of the stick-slip type start for smaller velocities around 0.5 mm/s (figure 6.12). The saw-toothed shape is purer than with any other combinations, more typical of the stick-slip vibration. The vibration amplitude increases with the velocity for all measurements. No decaying is observed. Around 18.3 mm/s, the vibration shape becomes less triangular and becomes increasingly quasi-harmonic-like as the velocity is increased.

Nevertheless, the velocity signal still shows some amount of sticking. The F-V characteristic of this combination was later assumed to be a continuously decreasing type.

- **Blotting paper vs. cast iron with slideway oil**

This combination exhibits a bigger hump than the other combinations. The F-V curve exhibits a fairly large hump at the beginning, then decreases for most of the velocity range and increases slightly at the end of the velocity range (figure 6.13). The vibrations generated by this combination are quasi-harmonic and start at 5 mm/s. Their amplitude increases continuously with the velocity and reaches a plateau for the upper velocities (figure 6.14). The frequency

ratio does not follow the same tendency as all the other combinations studied before. The frequency of the oscillations never vary much; the ratio is at first more than 1, it then decreases down to 0.9 to increase again and stabilize around 1. No decaying of the vibrations was observed.

6.2. Friction (clutch) plate on steel

The steel slider on friction plate combination was tested with semi-synthetic Dexron/Mercon IIE for lubricant and for two loads, 0.91 kg (1 lb) and 2.27 kg (5 lb). As described in chapter 5.3.1, 2.27 kg (5 lb) in our configuration is equivalent to the loading conditions used by Ford for collecting data for the friction-velocity characteristics. The normal load is an extremely important factor as it controls the pressure on the surfaces during the transition from a squeezed oil film formation to the static friction state when the clutch is acting. Both F-V curves were obtained with the static measurement method and can be seen on figure 6.15. They both present the same general shape. They exhibit a small hump at lower velocities and as the velocity increases, the friction level decreases slightly and then stabilizes at a fairly constant level for higher velocities. The main difference between the two loads is that the general level of friction, which is directly related to the normal load, changes. With the higher normal load, the amplitude of the hump is also slightly bigger. The plots of the vibration vs. time can be seen on figures 6.16 (a) and (b). In both load cases, small irregular friction-induced vibration can be observed for velocities as low as 5 mm/s, and rapidly transform into quasi-harmonic vibrations as the velocity increases. For velocities up to 31.4 mm/s, these quasi-harmonic vibrations appear irregular but stable. Their amplitude decreases and grows in an almost periodic fashion

but they never decay or disappear totally. An investigation of the phenomenon revealed that the amplitude variation is linked to the surface irregularities of the plate, i.e., the variations were observed to occur at roughly the same frequency in distance along the disc circumference. For higher velocities, the quasi-harmonic vibrations display higher amplitudes that are slightly irregular, but less so than at smaller velocities. Both F-V curves obtained with this combination are strikingly similar to the ones obtained with the same fluid on the blotting paper on cast iron combination. The friction-velocity plots obtained for this combination are very similar to the one obtained with the blotting paper on cast iron combination with the same lubricant, although the friction level obtained with the friction plate combination is slightly lower than with the blotting paper combination. The shape of the hump at low loads is strikingly similar. On the other hand, at higher loads, the amplitude of the hump remains small for the friction plate whereas it increases for the blotting paper combination. The main difference lies in the fact that the amplitude of the hump is smaller in the case of the friction plate and the overall friction level is also slightly smaller.

6.3. Paper-on-paper

In this series, both sides of a newsprint specimen were tested, first with sliding between same sides, i.e., A_1 vs. A_1 and A_2 vs. A_2 , then sliding between opposite sides, i.e., A_1 vs A_2 and A_2 vs. A_1 . In the second set, the two sides were alternating between the slider and the rotating disc. These combinations were tested for different velocities ranging from 0.02 mm/sec to 15 mm/sec. Most tests were carried out at 0.91 kg (2 lb), with a few carried out at 1.37 kg (3 lb) and 1.8 kg (4 lb). Paper-on-paper combinations are more sensitive to the environment than the

paper-on-metal combinations. The paper pair is fragile and very sensitive to wear, therefore heavier loads can break the fibers and cause them to become undone much faster than smaller loads. In some cases, for slow velocities, the high normal load actually caused the lower paper disk to be torn. Normal load has a very strong influence on the frictional behavior of this combination. For all paper combinations, the static friction force, as well as the friction coefficient, increase with the normal load. Normal load has also an effect on other parameters of the vibrational behavior, such as the vibration amplitude and the vibration frequency. For same paper combinations, vibration amplitude increases with the normal load while the vibration frequency decreases (figures 6.17 & 6.18). For different paper combinations, on the other hand, vibration amplitudes increase at first then decrease for the highest load. The vibration frequency follows the opposite trend. The change obtained for the highest load is likely a sign that the surfaces were irremediably damaged by the normal load, causing a change in their frictional properties. Their friction-time curves presenting the vibrational behavior are shown respectively in figures 6.19 and 6.20. At low velocities, most paper combinations exhibit stick-slip vibration. As observed in the results for "paper-on-metal" combinations, the frequency of the oscillations increases with the driving velocity to reach a maximum close to the natural frequency of the assembly. For higher speeds, the amplitudes of stick-slip oscillations decrease and are tentatively replaced by quasi-harmonic oscillations which, however, do not appear stable. Some tests were repeated for the 1.37 kg (3 lb) and 1.8 kg (4 lb) normal loads. Increasing the normal load increases the limit velocity at which stick-slip stops and decreases the frictional oscillations' frequency. One of the problems of the dry paper-to-paper contact is that, especially at high speeds, the paper surfaces deteriorate rapidly and no steady-state

oscillatory regime has time to take place. Pure sliding conditions can prevail rapidly. In those conditions, it is difficult to take accurate measurements as they have to be taken over a fairly short time and forces and displacements are very small. However, in practical applications in the paper industry, it is the first few sliding cycles that are of significance.

Obtaining “usable” F-V curves with these combinations was, as discussed earlier, somewhat difficult. The direct A-V-D measurement method, where the F-V curve is described by a full vibration cycle, had to be discarded because of a very high signal-to-noise ratio. The assessment of the F-V curve then had to be done with the static measurement method. The vibrational results presented earlier hinted at the fact that the F-V relationship for the paper combinations was of the purely decreasing type as stick-slip vibration was recorded for the smallest velocities. Nevertheless, quasi-harmonic vibrations were observed for higher velocities. These results seem to suggest that the F-V curve might encompass a decreasing characteristic followed by a humped one. The other explanation for this phenomenon is that these small quasi-harmonic vibrations might not be real but rather induced by some external vibrations of the test rig.

6.4. Curve fitting F-V equations

Several of the above characteristics were chosen for the analytical study. The chosen F-V curves from each group were curve-fitted with Matlab software for a n-th order polynomial function. For the “paper-to-metal” contact, the combinations involving blotting paper with type F, Dexron/Mercon IIE semi-synthetic, and slideway lubricants were selected, along with the friction plate and the A_2 vs. A_1 paper-on-paper combination. Figures 6.21 to 6.25 show the respective F-V curve with their corresponding polynomial fit. Usually, polynomials of order 9

or 11 fit the experimental curves best. Nevertheless, some of the characteristics displayed a small hump fairly close to the y-axis and the polynomials might not reflect perfectly the shape of the hump in such cases. The polynomials might also have a restricted range of validity. To perform the polynomial fit, the F-V curves were artificially extended to a higher range of velocities by adding values which would maintain the general tendency of the curve. In all cases, they were fitted in such a way that their validity range would at least coincide with the velocity range obtainable with the test rigs. Theoretical and experimental results should be comparable within that range.

The F-V characteristic of type F ATF was fitted with a 9th order polynomial that describes its decreasing tendency.

In the case of the Dexron/Mercon III friction-velocity characteristic (figure 5.10), the hump at the beginning of the velocity range is very small and very close to the y-axis. The polynomial fit obtained did not reflect the experimental curve satisfactorily. Consequently, the theoretical study of this combination was not pursued.

The combinations involving blotting paper and friction plate with semi-synthetic Dexron/Mercon IIE were both fitted with 10th order polynomials. In the first case, the resulting polynomial exhibits a hump slightly shifted from the experimental one.

A 9th order polynomial was sufficient to model the F-V characteristic of the slideway oil combination.

CHAPTER 7

THEORETICAL AND NUMERICAL ANALYSES OF AN AUTONOMOUS SYSTEM

This chapter presents theoretical analyses of the friction-induced vibration characteristics of the friction materials described in chapter 4. Each selected friction-velocity characteristic is studied analytically and numerically for an autonomous system, and the results are compared with the experimental ones.

7.1. Analytical study

The friction-velocity characteristics obtained in 6.4 were analyzed using the analytical method described in chapter 3.

7.1.1. Combinations showing stick-slip vibrations

It was seen in chapter 6 that three combinations exhibited stick-slip vibrations, the blotting paper combination with the type F lubricant and the paper-on-paper combinations. All have continuously decreasing F-V characteristics at lower velocities, which lead to stick-slip vibration. It has been discussed in section 3.3 that the analytical technique based on K-B method could only solve quasi-harmonic vibrational problems for F-V curves of the humped form. There is no provision for analysis of the stick period and hence no discontinuity when solving the differential equation. As a result, the analytical method revealed in these three cases that self-excitation occurs but a stable quasi-harmonic vibration is never reached. No vibration amplitude is then given by the analysis.

7.1.2. Combinations showing quasi-harmonic vibrations

Three material combinations are considered in this part: the combinations involving blotting paper with the semi-synthetic Dexron/Mercon IIE and slideway lubricants and the combination involving the friction plate. The plots on figures 7.1, 7.2 and 7.3 display experimental and theoretical F-V curves as well as the experimental, analytical and numerical amplitudes of stable vibration for the three aforementioned combinations. The analytical results for these three combinations are similar. All indicate the occurrence of stable quasi-harmonic vibration at velocities shortly after the hump in the friction-velocity characteristics. As the actual shapes of the F-V curve are not known past the experimental velocity range, and although the polynomial fits follow the curve tendency for a certain range, they still diverge from the experimental F-V curves at higher velocities. Therefore, their application is limited to the lower velocity range. Consequently, the analytical result shows that the quasi-harmonic vibrations decay quickly as velocity increases, whereas experimentally, vibration amplitudes continue to increase for some time.

7.2. Numerical study

The above cases were also numerically analyzed using the INSITE software package described in chapter 3.

7.2.1. Combinations showing stick-slip vibrations

For the blotting paper with type F lubricant combination, a 9th order polynomial was initially used to curve-fit the decreasing experimental F-V relationship of this combination. The numerical analysis showed that, for each of the velocities considered in this study, the vibration

amplitude kept on increasing without bounds, despite the fact that the polynomial was such that the slope of the F-V characteristic became positive at higher velocities. When absolute values of the relative velocities are used in the friction-velocity polynomial expression, i.e, creating a singularity on the zero axis and allowing the numerical analysis to continue to the other side of the zero sliding velocity axis, then numerical calculations can proceed without further problems for a wide range of velocities. For the autonomous system, vibrations begin at very low velocities. Their amplitudes increase steadily up to $v = 40$ mm/s, then the amplitude starts decreasing again as they are limited by the increasing part of the F-V curve. The amplitude continues to decrease until the vibration totally disappear when $v = 115$ mm/s. The results are plotted in figure 7.4.

For the paper-on-paper combinations, both curves obtained in chapter 6 were fitted with a 6th order polynomial. However, the problems encountered for the numerical simulation were the same as for the blotting paper with type F lubricant combination, i.e., the vibration amplitude grows without limits. In these two cases, even the introduction of the absolute value of the relative velocity as an artificial boundary condition did not allow the calculations to proceed. No numerical simulation was then obtainable for these two examples.

7.2.2. Combinations showing quasi-harmonic vibrations

Once again, the three combinations considered exhibit the same kind of behaviour. The results are included in figures 7.1. to 7.3. for comparison. Two types of motion can be observed. For a relative velocity less than the one at which the maximum of the hump is reached, which corresponds to the ascending part of the friction-velocity curve, the system evolves towards a

steady-state. The focus point is reached more or less fast depending on the initial conditions. After the humped part of the curves, stable limit cycles can be observed. The vibration amplitude increases with the velocity until it reaches a maximum different for each combination, after which the vibration amplitude starts decreasing again, being limited by an ascending part of the fitted curve for higher velocities. Eventually steady-state conditions prevail once again. The friction plate combination presents one slight variation to this scenario. The vibration amplitude decays around 38 mm/s to increase again a little later and finally disappears at $v = 60$ mm/s. This discontinuity in the results is due to the fact that both the analytical and numerical method are fairly sensitive to variations in the polynomial fitted curve and the presence of a small hump in this curve is sufficient to damp the vibration.

7.3. Discussion

Six material combinations were studied for an autonomous system analytically and numerically. When these results are compared with the experimental results described in chapter 6, two distinctive behaviors are recognized; one is exhibited by combinations with a continuously decreasing F-V characteristic that starts from the zero sliding velocity axis, represented by the paper-on-paper combinations and the combination with the type F transmission fluid; the other one is exhibited by combinations with a humped F-V characteristic represented by the combinations involving semi-synthetic Dexron/Mercon IIE transmission fluid and the slideway lubricant.

For the first type, the analytical method, which is valid for quasi-harmonic vibrations only, cannot deal with a continuously decreasing F-V characteristic. This type of F-V curve

inevitably lead to stick-slip vibrations which require separate consideration during the stick phase, when $V - \dot{X} = 0$. Experimentally, the paper-on-paper combinations exhibit stick-slip vibrations for low velocities, but the vibrations decay rapidly as the friction-velocity curve takes on a positive slope. The numerical method does not provide any results for these combinations, because of a lack of appropriate boundary conditions. For the combination involving the type F lubricant, numerical vibration amplitudes were obtained after introduction of an artificial boundary condition. Nevertheless, these amplitudes are not in very good agreement with the experimental values. Experimentally, the type F ATF combination shows stick-slip vibrations for the whole velocity range. For low velocities, the numerical values increase with the velocity at a much faster rate than their experimental counterparts. This is due to the use of absolute values instead of real values for the sliding velocities which is, in effect, allowing the numerical analysis to bypass the stick regime. For higher velocities, the numerical amplitudes start decreasing again because of the limitation exerted by the fitted curve, while the experimental amplitudes continue to increase. These examples show that, without a proper model for the stick phase, neither the analytical nor the numerical analysis can give a good representation of the phenomenon in the case of a decreasing friction-velocity relationship.

For the type exhibiting quasi-harmonic vibrations, the analytical, numerical and experimental vibration amplitudes are in good agreement for all three combinations studied. Experimentally, those combinations show different behaviours, depending on the velocity. For lower velocities, no vibrations are observed. As the velocity gets higher, quasi-harmonic vibration occurs, whose amplitude increases with the velocity. In all cases, the numerical amplitude is slightly bigger than the experimental one whereas the analytical one is slightly

smaller. In the low velocity range, the predicted amplitudes start slightly later than the experimental ones, as the hump of the polynomial fitted curve peaks a little later than the actual curve. At the high velocity end, both numerical and analytical vibrations die off quickly as the velocity increases whereas the experimental ones continue to increase again, because the fitted curve is limited to the velocity range considered.

The results clearly revealed that the analytical model works well with a humped friction-velocity characteristic, provided that the characteristic can be modeled accurately with a curve-fitting routine. A 9-th order polynomial, as used in the present study, is usually sufficient to describe the near-linear F-V curve with a relatively flat single hump in the low velocity range. For F-V characteristics with a continuously decreasing pattern, a stick-slip phenomenon will occur. A complex model to describe the conditions during the stick period is needed to add to the current analytical and numerical models which both analyze the slip period only.

CHAPTER 8

FRICITION-INDUCED VIBRATIONS WITH PERIODIC NORMAL EXCITATION

Friction-induced vibration is undesirable in a majority of cases. Many studies have attempted to find means to reduce or control this phenomenon. Adding a periodic normal loading to the static normal force has been shown to be effective in damping stick-slip vibrations [24-25-26]. On the other hand, the effect of dynamic loading on the quasi-harmonic type of friction-induced vibration has rarely been considered. Ko [26] studied the effect of a transverse periodic loading on this kind of vibration. He found that the external excitation force could extinguish the autoperiodic oscillation, and that harmonic and sub-harmonic entrainment were observed. His theoretical and experimental results were in good agreement. He also studied the influence of a dynamic loading such as the one used here. His experimental results showed no reduction in the friction level, but showed that the quasi-harmonic type of vibration could still be extinguished, if the dynamic force magnitude was high enough. Nevertheless, his numerical and experimental results were not in very good agreement.

It was mentioned in chapter 3 that, because the modeling equation for a system such as the one considered here included non-linearities coupled with time-varying coefficients, no analytical approach would be considered. A numerical approach using a software package called INSITE described in chapter 3 is used instead. This system is also studied experimentally for the different material combinations used in the previous chapter. Both numerical and experimental results for the different material combinations will be presented and compared.

8.1 Numerical analysis

Each combination was studied numerically using the same polynomial model obtained earlier. This polynomial fit gave for each combination the set of C_n constants needed by the program. The equation for the dynamically loaded system, eq. (10) is reprinted here.

$$\ddot{x} = -\omega^2 x - \frac{r}{m} \dot{x} + \frac{1}{m} [C_0 + C_1(v - \dot{x}) - C_2(v - \dot{x})^2 + \dots + C_n(v - \dot{x})^n] (1 + \beta \sin \alpha \omega t) \quad (10)$$

The damping coefficient r , the slider mass m and the natural frequency of the system ω are characteristics of the test rig and can be readily determined. In addition, the polynomial coefficients C_n are constants for each F-V characteristic. The values for the velocity V , the ratio of the dynamic force magnitude to the static load β , and the ratio of the external oscillation frequency to the system natural frequency α are parameters to be investigated. Random executions of the program can be done by giving any value to these parameters, but a more systematic study has to be carried out to understand thoroughly the system behaviour and the influence of each parameter. Therefore, for each material, the executions were carried out for a predetermined range of disc velocities, frequency ratios, and load ratios. For each frequency ratio and a chosen velocity, the load ratio β was incremented from 0 to 0.9. In the same objective, bifurcation diagrams where one parameter is varied while the others remain constant, were performed for these three parameters. Velocity v was varied between 0 and 60 or 80 mm/s, depending on the material combination studied. The load ratio β was varied between 0 and 1. The frequency ratio α was usually varied between 0.6 and 4. Depending on the type of behaviour observed on the bifurcation diagrams, specific executions could then be carried out, to

provide more information through friction vs. time plots, phase-plane plots or frequency spectra. In particular, time series and phase-plane plots were executed for cases studied experimentally for comparison purposes.

Similarly to the sequence carried out in the previous chapter, the results for the combinations showing stick-slip and the ones exhibiting quasi-harmonic vibration are treated separately.

8.1.1. Combinations showing stick-slip vibrations

The blotting paper combination with type F lubricant was studied. For this configuration, the addition of a dynamic normal load does not induce any decrease in vibration amplitude, whatever the velocity, the load ratio or the frequency ratio considered (figure 8.1). A closer look reveals the presence of different behaviours depending on the value of the frequency ratio. When the frequency ratio α takes on values equal or close to 1, even small values of the load ratio cause a significant increase in vibration amplitude and increasing the load ratio further quickly causes the calculations to go out of bounds. This resonance phenomenon is strongest for α equal to 1. Other values of α cause either a smaller increase or small variations of vibration amplitude around the static value. They combine their influence with the influence of β to have an effect mostly on the shape of the vibration, i.e., its frequency content, rather than on its amplitude.

The bifurcation diagram for α in figure 8.2(a) is a classical chaotic bifurcation diagram with periodic windows. It shows that, whenever the value of α is close to an integer, quasi-harmonic entrainment of order α is observed, the motion is multiperiodic. The displacement-velocity phase-plane plots obtained in such cases are presented in figures 8.3, 4 and 5, along with the

corresponding displacement vs.time plots and the frequency spectra. The load ratio β influences the spectral densities of the frequencies present. When α is different from an integer, the motion in general remains multiperiodic, but the number of frequencies present in the motion is much higher. In some cases, the motion can become slightly chaotic, as shown in the two cases in figures 8.6 and 8.7. In these two cases, the frequency spectra (figures 8.6(d) and 8.7(d)) show that all frequencies have the same weight and the phase-plane plots look chaotic. However, the Poincaré sections exhibit closed curves normally typical of multiperiodic motion, but where some slight folding, characteristic of chaotic motion, is present. The Lyapounov exponents are of different signs and the Lyapounov dimension is slightly different from an integer, which confirm the chaotic nature of this particular case.

8.1.2. Combinations showing quasi-harmonic vibrations

It has been shown in the study of the autonomous system that all the combinations exhibiting a humped characteristic produced similar responses. In the study of dynamic loading, the numerical results for these combinations also appear very similar. The general behaviour is first presented, then illustrated by some examples from the different test cases.

Just as in the previous case, bifurcation diagrams were performed for the parameters α , β and v .

- **Varying the velocity v**

Bifurcation diagrams were drawn for the velocity parameter, α and β being fixed (figures 8.8 a-b-c) for the three different material combinations. Figures a and c were drawn for $\alpha = 2.15$ and $\beta = 0.3$. Figure b was drawn for $\alpha = 2$ and $\beta = 0.3$. It has been shown in chapter 6 that the

velocity is an important parameter for the occurrence of quasi-harmonic vibration. It remains so in the case of an applied dynamic normal force. In the low velocity range where no friction-induced vibration occurs in the autonomous case, the application of a dynamic normal force causes some vibration of small amplitude to occur. The amplitudes of these vibrations depend on the parameters α and β . Their frequency is the excitation frequency. As the velocity is increased for a set of α and β , the vibration amplitude increases and multiperiodicity occurs, of order α if α is an integer (figure 8.8-b), or higher order if α is different from an integer (figures(8.8-a and c). When the velocity is increased beyond the limit at which quasi-harmonic vibration ceases in the autonomous case, the dynamic normal load continues to cause vibration in the system. Their amplitude decreases as the velocity moves farther away from the critical velocity for cessation of quasi-harmonic vibration. In all cases, amplitudes and frequencies of the obtained vibration depend on the values of α and β .

- **Varying the frequency ratio α**

In figure 8.9, the parameter varied in the bifurcation diagram is the external excitation frequency $\delta = \alpha\omega_n$, α being the frequency ratio and ω_n the natural frequency. Two main tendencies are revealed on the bifurcation diagrams plotted in figures 8.9 a-b-c, i.e., the behaviour of the system changes depending on whether α is close to an integer or not. If α is close to an integer, subharmonic entrainment of order α occurs, as shown on the phase-plane plots and their corresponding frequency plots in figures 8.10, 11 and 12. The limit cycle reached by the system then exhibits 1, 2, 3 or 4 frequencies depending on the case.

On the other hand, in between integer values of α , although the bifurcation diagram looks chaotic, multiperiodic motion with a high number of frequencies occurs. For $\alpha = 0.5, 1.5, 2.5\dots$,

some clear multiperiodic with convoluted limit cycles can be noticed in figure 8.13 a-b-c. The same type of phenomenon can also be observed for $\alpha = 2/3, 4/3, 5/3, 7/3, \dots$ in figure 8.14 a-b-c. If α is different from these values, subharmonic entrainment is still observed but as the frequency entrainment is out-of-phase with the natural frequency, the resulting number of frequencies present in the system is much higher than before. This is shown by the frequency spectra in figure 8.15-c. Phase-plane plots now become convoluted figures. The vibration vs. time plots show the superposition of all out of phase frequencies. Poincaré sections were plotted for different cases. All showed the presence of many harmonics but no folding of the sections was ever observed. Moreover, Lyapounov exponents calculated for these examples were of the same sign, which proved these were cases of p-periodic motions and not chaotic ones.

A fairly different behaviour is obtained for the specific case of α being close to 1. In figure 8.16, 17 and 18 are plotted the vibration amplitudes versus the load ratio β with the frequency ratio α being a parameter. This plots show that, whatever the material combination, the velocity considered or the load ratio, the addition of a dynamic normal load of frequency close to the natural frequency of the system tend to increase the original vibration amplitude rather than decreasing it. The effect is the strongest for a value of α slightly smaller than 1.

- **Varying the load ratio β**

The influence of β is more subtle than the influence of the previous parameters. From the bifurcation diagrams in figure 8.19 a-b-c, it appears that small values of β do not impede the multiperiodicity mentioned earlier, but that β can be increased up to a certain level where this multiperiodicity disappears. However, a more thorough study reveals that the influence of β is dependent on the values taken by α , as shown in figures 8.16, 17 and 18. When α is close to 1,

i.e., the frequency of the dynamic normal force is close to the natural frequency of the test rig, very small values of β can give a vibration with a beat frequency and in a few cases a decrease of the vibration amplitude. On the other hand, as β increases, the vibration amplitude starts increasing with it to reach amplitudes much higher than the original one; a resonance phenomenon is observed.

When α takes on different values, however, the influence of β changes. If α is an integer equal to 2, 3 or 4, an increase in β changes the shape of the phase-plane plot. Small values of β barely change the shape given by the original quasi-harmonic vibration, as the main frequency of the vibration is still the natural frequency of the system. Higher values of β give a shape with sharp indents showing that more frequencies now enter the spectrum, the excitation frequency being one of them. The amplitude of the vibrations usually decreases slightly as β increases, but not very significantly. When α is different from an integer, i.e., when a high order multiperiodicity is observed, the load ratio β has a stronger influence on the phase-plane plot. Small values of β cause the vibration amplitude to vary around the autonomous vibration amplitude with a beat frequency and the phenomenon becomes more pronounced as β is increased. Eventually, for higher values of β , the motion stops being multiperiodic and becomes periodic with the normal excitation frequency. The vibration amplitude is then at its smallest. The autonomous vibration has been quenched. From then on, the vibration amplitude grows again as β is further increased. The vibration is now being fed by the excitation. The level of load ratio necessary to have the stronger damping influence is found to be dependent on α as seen in figures 8.16, 17 and 18.

8.1.3. Discussion

For the combinations displaying a humped friction-velocity curve, the application of a dynamic loading can lead to a decrease in vibration amplitude. For the three combinations considered, the numerical results are mostly similar and their bifurcation diagrams performed for α , β and v all show the same trends. In all cases, the most noticeable effect was the one due to frequency alteration. Imposing a dynamic normal force has a strong effect on the frequency pattern of the vibrations, changing them from quasi-harmonic to multiperiodic vibrations. The influence of α and β is on the whole the same for each combination. However, the different material combinations are found to respond differently quantitatively. More significant decreases are obtained with the friction plate combination than with the blotting paper combination with the same lubricant. The vibration of the latter appeared more robust. In the later case, vibration amplitudes vary but stay globally around the same value as the one obtained for the static case. The fact that they respond differently may have different causes. The size and expansion of the hump in the F-V curve might have an influence on the robustness of the quasi-harmonic vibration obtained, making them likely to be influenced by a dynamic external force. Another explanation would be that some other characteristic of the polynomial might induce these effects.

8.2. *Experimental results*

Experimentally, tests with an external normal load were first carried out for the type F lubricant combination which produced stick-slip vibration under a static load. These tests can be related to previous work from other researchers and provide a comparison for the tests

involving quasi-harmonic vibration. Later, tests were carried out with the other lubricant combinations. For all combinations, several frequency ratios α were tested, from α being close to 1, i.e., the excitation frequency is close to the natural frequency of the system, to values of α close to 4. For each frequency setting, different load ratios β were applied. After each measurement series for a specific frequency ratio, a measurement for the static configuration was performed to make sure that the friction conditions under static loading remained unchanged. If they were found to have changed, the paper slider was changed to a new one to limit the influence due to changes in surface properties.

All tests were performed with the electromagnetic shaker arrangement described in chapter 4. A few tests were performed using the stepper motor assembly. However, it was found to produce too many extraneous vibrations to the whole system and was consequently not used.

8.2.1. Combinations showing stick-slip

Tests with a dynamic normal load were conducted for the blotting paper combination with type F lubricant.

The plots of vibration amplitude vs. the load ratio summarizing the results are presented in figures 8.20-21 & 22. Four velocities were tested: 0.2 mm/s, 0.52 mm/s, 2.25 mm/s and 9.8 mm/s. The static normal load for all tests was 4 lbs. Figure 8.20 presents the results for a disc velocity of 0.52 mm/s. It can be seen that, in all cases, the vibration amplitudes from tests with an external force were smaller than the one obtained under static load alone. Moreover, for a given frequency ratio α , the vibration amplitude decreases as β is increased. The frequency ratio seems to have a mild influence on the efficiency of the procedure. For certain values of α ,

for example 1.62, even a low value of β will cause a drastic drop in vibration amplitude. On the other hand, other values of α need a much higher value of β to create the same amount of vibration amplitude decrease. These results can be visualized more clearly on the plots on figure 8.23 representing the vibration amplitudes vs. time for different values of frequency and load ratios. Figure 8.24 displays the same kind of plots for a velocity of 0.2 mm/s. The results obtained for a disc velocity of 2.25 mm/s are fairly similar to the former ones and virtually all combinations of load and frequency ratios cause a decrease in vibration amplitude, and in a few cases, the vibration almost disappear (figures 8.21 and 8.25).

On the other hand, for a disc velocity of 9.8 mm/s, the dampening of the vibration is less efficient, the rate of decrease is lower than in the previous cases, higher values of β are necessary for the same amount of amplitude reduction (figure 8.22). In two cases where the value of α is close to 1, the vibration amplitude is in fact increased instead of being decreased; in this case, it seems that the vibration are entering into resonance. For this velocity, the influence of α does not appear as strong as with the other test cases. It can also be noticed that none of the tests performed in that series lead to vibration extinction.

The results clearly show that the influence of the load ratio β is strongly tied to the frequency ratio α . Vibration amplitude and vibration frequency appear totally interdependent, the first one decreasing while the second one increases. Figure 8.26.(a) shows that the maximum static friction force decreases slightly up to 0.5 with the load ratio for a disc velocity of 2.25 mm/s. Similarly, for a disc velocity of 0.52 mm/s, all measurements carried out with an external dynamic force show a 0.7 reduction in static friction force. However, at 9.8 mm/s, no visible decrease can be observed; the static friction force remains the same throughout the

experiments (figure 8.26.(b)). Then, whatever the load or frequency ratio, the level of friction force remains approximately the same.

The case of extremely low velocities is also worth mentioning. Tests carried out at these velocities under static loading did not present any vibration but only pure sliding with a constant friction force at a specific displacement. The addition of an external normal excitation at 20 Hz, just slightly over the natural frequency, gives rise to some irregular instantaneous stick-slip vibration which does not last. Different load ratios incurred the same behaviour. The addition of an external excitation at higher frequencies such as 40 or 75 Hz has a small influence on the position and the friction force the slider is at; it tends to increase the friction level a little bit but the effect is rather small.

8.2.2. Combinations showing quasi-harmonic vibrations

Several tests were done with the combination of blotting paper vs. cast iron with slideway oil, varying either the frequency ratio or the load ratio. These tests were carried out at a velocity of 46.2 mm/s. At this velocity for the autonomous system, a regime of stable quasi-harmonic vibration would have been reached. However, results with a dynamic loading are varied. Depending on the ratio combination, either little effect or an important influence have been noticed. The main result is that, depending on the frequency ratio, the effects on the vibration amplitude are diverse but whatever the ratios combination, all tests under a dynamic load exhibit a vibration amplitude higher than under static conditions. No vibration damping was ever observed. For frequency ratios around 1, increasing the load ratio increases the vibration amplitude. For others like $\alpha = 2.7$ or 2.97 , the vibration amplitude remains more or less the

same. For $\alpha = 3.24$, the vibration amplitude tends to increase with the load ratio. The shapes of the phase-plane plots offer more variety. They show indents typical of subharmonic entrainment for $\alpha = 2, 3$ or 4 . The results for $\alpha = 4$ are presented on the set of plots in figure 8.27. On the other hand, the plot for $\alpha = 2.15$ (figure 8.28) exhibits a complex pattern showing multiperiodicity.

The same type of tests was done with the combination of steel slider vs. friction plate with semi-synthetic Dexron/Mercon IIE lubricant as with the former ones. The load ratio and the frequency ratio were varied for two velocities, $v = 10.5$ mm/s and $v = 31.4$ mm/s. For the first velocity, as mentioned in chapter 6, the quasi-harmonic vibrations appeared not totally stable when subjected to a static normal load. When subjected to dynamic vibrations with a frequency ratio close to 1, no quenching of vibration was observed. On the contrary, heavy harmonic entrainment was observed and the vibration amplitude kept increasing with the load ratio β (figures 8.29 and 8.31.(a)). Frequency ratios equal to 1.62, 2.16 or 2.7 appeared to have a strong effect on the shape of the vibration and lead to entrainment at the excitation frequency for sufficiently high load ratios. However, the amplitudes of the vibration remained approximately the same. Higher frequency ratios did not show much effect.

For the second velocity, the quasi-harmonic vibrations under static loading were a lot bigger than in the first case if not quite regular (figures 8.30 and 8.31.(b)). However, the same trends were observed for all values of frequency and load ratios. Quantitatively, the effect of the dynamic normal loading is higher for lower disc velocities. Effectively, higher disc velocities are closer to the end of the velocity range deliverable by the test rig, thus getting closer to the

point where the whole test rig can enter in resonance, making it impossible to damp out the quasi-harmonic vibration caused by friction.

8.3. Discussion

Results from the numerical analysis of the combination exhibiting stick-slip confirm that the numerical technique, as in the analytical technique, in their present form, cannot provide proper analyses to dynamic models where a discontinuity, such as in the case of a continuously decreasing F-V characteristic, exists. The experimental results, on the other hand, show that it is possible to decrease the amplitude of stick-slip vibrations with the addition of a normal dynamic load. A carefully chosen combination of load and frequency ratio can lead to a dramatic decrease in vibration amplitude and can even extinguish the vibration. This finding is in agreement with results presented in earlier works [25-26-27].

The agreement between numerical and experimental results is good for combinations exhibiting quasi-harmonic vibration. For the slideway lubricant and the friction plate combination, a good agreement is found in the general trends, such as the role of the frequency ratio α . Subharmonic entrainment occurs as predicted by the numerical results. A fairly good agreement is also found in the amplitude of the vibrations obtained. The different figures presenting phase-plane plots and vibration vs. time plots for the slideway lubricant and the friction plate combinations show this agreement in both shape and amplitude. Both experimental and numerical results show that the quasi-harmonic vibration cannot be extinguished. Some decreases were observed in a few cases in the numerical results for the friction plate combination. However, these results were not confirmed experimentally,

indicating that the decrease observed in the numerical results was likely due to some local characteristic deviation of the polynomial fitted F-V curve.

Experimentally, the behaviour of combinations exhibiting quasi-harmonic vibrations is very different from the one exhibiting stick-slip vibration when a normal dynamic load is applied to the system. For the latter, the application of a dynamic normal load at a frequency close to the natural frequency is seen here as one of the most efficient ways of quenching the vibrations and the same conclusion has been reported before by many researchers. However, the application of the same kind of loading to a combination exhibiting quasi-harmonic vibrations leads to opposite results. Instead of being quenched, the quasi-harmonic vibrations are fed by this external excitation and increase in amplitude. The application of normal loading at other frequencies still tends to cause some amount of decrease in the stick-slip vibrations while it only causes some minor amplitude variations in the quasi-harmonic vibrations. The main effect it has in the latter type is the modification of the frequency content of the vibration.

CHAPTER 9

DISCUSSION

The frictional behaviour of several combinations of industrial friction materials that are related to two specific applications, namely: paper handling machinery and automotive transmission clutches, has been investigated both experimentally and analytically. The latter used dynamic friction models and numerical computational tools. In the course of this investigation, both stick-slip and quasi-harmonic types of friction-induced vibration were studied, with an emphasis on the latter. The effects of dynamic normal loading on friction-induced vibration were also studied. The aim is to gain better understanding of the sliding friction characteristics of these materials under static and dynamic loading conditions so that better control and improved performance of the related machinery components can be realized.

One of the first results that is interesting to note is that all the paper-to-paper combinations studied exhibited stick-slip vibrations, whereas among the paper-to-metal combinations, either stick-slip or quasi-harmonic vibrations were observed, depending on the lubricant used. In lubricated sliding contacts, the two surfaces are partially or fully separated by a thin film of the lubricant and therefore, in the short term at least, the friction-velocity characteristics at the contact will mainly depend on the lubricant's characteristics. The surface state of both counterparts are less important, as long as they present an even surface.

The shape of the friction-velocity curves determined experimentally provided a useful mean to characterize the different material combinations. It was confirmed that continuously decreasing F-V characteristics would lead to stick-slip oscillation while the so-called "humped"

curves were also obtained by a direct measurement method in addition to the standard static measurement method. The two curves appeared to be in fairly good agreement. The former, making use of a second order oscillation system, presented a powerful tool for obtaining a friction-velocity characteristic in one cycle of vibration, provided that the amplifications of the dynamic units, x , \dot{x} , \ddot{x} , were properly and precisely calibrated. The analytical and numerical results of stable vibration amplitudes obtained in the case of the autonomous system for the quasi-harmonic type of friction-induced vibration were in good agreement with the experimental results for all material combinations. No difference was observed between the results that were obtained either with the directly measured f-v curve or the statically measured f-v curve. It further proves that both methods are equally good for carrying out experimental measurements of the f-v curves under quasi-harmonic vibration.

For the polynomial fitting of the experimental f-v curves, the results show that, in most cases, a 9-th order polynomial is usually sufficient. Polynomial fits present the advantage of being fairly easy to handle analytically or numerically, however, some precautions are needed in order to obtain a good fit. As some experimental f-v curves are almost linear with only a very small hump at the beginning, they would require a higher order polynomial for proper fitting. It is also necessary to perform the curve fitting over a velocity range that is higher than the one considered for study as a polynomially fitted curve can diverge drastically once it is outside the fitted range, thus giving erroneous results for velocities that are near the limit of the velocity range.

The addition of a normal dynamic loading to quasi-harmonic vibration caused diverse behaviours: resonance for frequency ratios α close to 1 and sub-harmonic entrainments of order 2, 3 or 4 for α taking those values. Different types of multiperiodic motions were also observed for non-integer values of the frequency ratio. Beat frequencies were occasionally present, causing the vibration amplitude to alternately decrease and increase but in all cases, the main effect of the loading was the variation of the frequency content of the vibration. The agreement between the experimental and the numerical results was good, qualitatively as the same types of behaviour were observed and quantitatively as the vibration amplitudes followed closely the experimental results. This suggests that the present non-linear model with time-varying coefficients, based on the friction-velocity characteristic, can give satisfactory predictions of the behaviour of this kind of system.

One of the objectives of this study was to show that dynamic loading could be used as a mean to control or extinguish friction-induced vibration of the quasi-harmonic type. Both numerical and experimental results show cases where the autoperiodic vibration can be quenched if the load ratio is sufficiently high, it is then replaced by a vibration at the excitation frequency and, in most cases, with a smaller amplitude. In the numerical results, the load ratio value necessary to quench the autoperiodic vibration increases with the frequency ratio. Experimentally, this stage could not always be found. However, no total quenching of the vibration leading to a pure sliding motion was ever observed. These results can be compared to results of an earlier study by Ko [26]. His results showed that, although subharmonic entrainment was observed for lower values of the load ratio, an extinction of the quasi-harmonic vibration could be observed if the load ratio was sufficiently high. In his study, the extinction of

the autoperiodic vibration seemed to occur more readily than in the present one. The discrepancy between these two sets of results may be explained by the difference between the two experimental setups. Ko also used a pin-on-disk machine, but a motor equipped with rotating disks supporting out-of-balance masses was used to provide the dynamic normal loading. This dynamic loading system is similar in principle to the stepper motor assembly that was intended at first for the present study. It was discarded because the vibrations created by this type of loading system were not purely normal. Instead of a purely normal force, the resulting force often comprised some other component, such as a transversal one. Ko's other results had shown that the autoperiodic oscillation could be extinguished by a transversal excitation. In the normal dynamic loading case, it is possible that a transversal component of the excitation force became high enough as the load ratio was increased to damp out the quasi-harmonic vibration. Another possibility is that the transversal component acted in synergy with the normal one to damp the friction-induced vibration. These results stress the importance of testing equipment and procedures when studying friction.

Although it was not possible in this study to totally eliminate all vibrations at the contact surfaces, a vibrational normal loading could still be used to control the type of frictional vibration present in the system. Well chosen characteristics of periodic normal loading could change the frequency content of the frictional vibration and limit the vibration amplitude to certain bounds. The frictional vibration would then be replaced by a known type of vibration. Random excitation regimes would be less likely to take place and the known motion would consequently be easier to control and the frictional effects could be more easily overcome. The problem often encountered in the control of systems with friction is the unpredictability of the

friction phenomenon. The dynamic loading could remove to some extent the unpredictable part of the friction.

In the case of stick-slip vibration, the experimental results were in good agreement with results from earlier works [25-26-27]. A low load ratio at a frequency close to the natural frequency of the system is usually sufficient to damp out the stick-slip vibration. Other combinations of load and frequency ratios can also be efficient. However, it is interesting to note that, as the disc velocity was increased until the stick-slip frequency approached that of the natural frequency of the system, the vibration became more difficult to be quenched. At these high velocities, the stick-slip vibration transformed to the quasi-harmonic type of vibration. In this case, a normal dynamic loading still provides some damping, but to a much smaller extent than at smaller velocities.

In the numerical analysis, chaotic motion had been expected to arise in some situations from the addition of a normal dynamic loading to the frictional system. However, chaotic motion was found only in the numerical analysis of the blotting paper combination with the type F lubricant. As the analytical model was not prepared to handle stick-slip vibration, the study of the occurrence of this chaotic motion was not further pursued. In the numerical analysis for the material combinations presenting quasi-harmonic vibration, multiperiodic motions with a large number of frequencies were observed but chaotic motion was never recorded. Chaotic motion was also not observed experimentally but in order to make a proper analysis, at least a frequency analyzer would be necessary to detect the occurrence of chaotic motion.

In the autonomous case, the friction model can provide a useful tool for predicting the velocity range at which friction-induced vibration will occur. Effectively, the "humped" curve

exhibits two zones with different behaviours. The ascending zone, i.e., before the hump, where usually no vibration occurs as the damping is positive. On the other hand, the decreasing zone, i.e. after the hump, is akin to negative damping, therefore allowing the growth of friction-induced vibration. Thus a system can be designed to avoid operating in the velocity range within the decreasing zone or to modify the f-v characteristics with additives to extend the range of the increasing zone.

On the whole, the study of the paper-on-metal combination gave more satisfactory results than the paper-on-paper combinations. The latter all exhibited stick-slip vibration, which, as mentioned earlier, could not be addressed adequately with the present type of analytical model. All paper-on-paper combinations were studied only experimentally for a static loading. The fragility of this material combination increased the challenge of the experimental work, limiting the load and the test duration as the vibration would deteriorate the paper surface rapidly. Both sides of two types of newsprint were combined and studied. Each paper combination had a different friction-velocity curve and therefore produced a different set of stick-slip vibration, with variations in amplitude or frequency. These results suggest that the friction-induced vibrational behaviour could be a useful way of characterizing a paper surface.

CHAPTER 10

CONCLUSIONS

The frictional behaviour of several combinations of industrial friction materials that are related to two specific applications was investigated experimentally, numerically and in the autonomous case, analytically. In overall summary of the research, the following conclusions may be made:

1. Either stick-slip or quasi-harmonic vibration were exhibited by material combinations involving lubricants. On the other hand, paper-on-paper combinations in dry sliding exhibited only stick-slip vibration.
2. The friction-velocity characteristic is a useful tool to predict the vibrational behaviour of a friction pair. Its shape is related to the type of oscillation susceptible to occur. Moreover, in the quasi-harmonic case, a polynomial fitting of the humped F-V curve can be done and incorporated successfully in a friction model to predict the occurrence and the amplitude of friction-induced vibration when the system is submitted to a static normal load.
3. Experimentally, the friction-velocity characteristics can be acquired by two methods, a static measurement method and a direct measurement method that proves to be a fast and powerful way of acquiring the curve in only one vibratory cycle, providing that the equipment is properly calibrated. The results from both methods were in good agreement.
4. The application of a normal dynamic loading to a frictional system resulted in different responses, depending on the shape of the friction-velocity curve.

For the material combinations exhibiting a purely decreasing f-v curve, the experimental results showed that stick-slip vibration may be extinguished or dramatically decreased with a small dynamic-to-static load ratio. For the combinations displaying a humped curve, the quasi-harmonic vibration could be quenched with a higher load ratio, and replaced by an oscillation at the excitation frequency, in most cases, with a smaller amplitude. This result was confirmed numerically, which indicates that the assumption made in the dynamic loading model regarding the f-v relationship of μ_k is reasonable. In most cases, however, beat frequencies or subharmonic entrainment were observed as a result of dynamic loading.

5. The experimental and analytical techniques used in this thesis provide excellent tools for characterizing and evaluating paper and friction plate materials and their performances.

REFERENCES

- [1] Amontons, G., "De la Résistance Causée dans les Machines", Mémoires de l'Académie Royale A, 1699, pp.275-282.
- [2] Coulomb, C.A., "Théorie des Machines Simples", Mémoire de Mathématique et de Physique de l'Académie Royale, 1785, pp. 161-342.
- [3] Wells, J.H., "Kinetic Boundary Friction", The Engineer (London), Vol. 147, 1929, p.454.
- [4] Thomas, S., "Vibrations Damped by Solid Friction", "The Philosophical Magazine, London, 1930, Series 7, Vol. 9, p. 329.
- [5] Blok, H., "Fundamental Aspects of Boundary Friction", Journal of Automotive Engineers, 1940, Vol. 46, p. 275.
- [6] Swift, H.W., Dudley, B.R., "Frictional Relaxation Oscillations", The Philosophical Magazine, 1949, London, Series 7, Vol. 40, p.849.
- [7] Brockley, C.A., Cameron, R., Potter, A.F., "Friction-Induced Vibration", Journal of Lubrication Technology, Transactions of the ASME, April 1967, pp. 101-108.
- [8] Brockley, C.A., Ko, P.L., "Quasi-Harmonic Friction-Induced Vibration", Journal of Lubrication Technology, Transactions of the ASME, Vol. 92, 1970, pp. 550-556.
- [9] Dweib, A.H., D'Souza, A.F., "Self-Excited Vibration Induced by Dry Friction, Part 1: Experimental Study and Part 2: Stability and Limit Cycle Analysis", Journal of Sound and Vibration, 1990, Vol. 137, No. 2, pp.163-190.
- [10] Aronov, V., D'Souza, A.F., Kalpakjian, S., Shareef, I., "Experimental Investigation of the Effect of System Rigidity on Wear and Friction-Induced Vibrations", Journal of Lubrication Technology, Transactions of the ASME, Vol.105, April 1983, pp.206-211.
- [11] Aronov, V., D'Souza, A.F., Kalpakjian, S., Shareef, I., "Interactions among Friction, Wear and System Stiffness-Part 1: Effect of Normal Load and System Stiffness"-Part 2: Vibrations Induced by Dry Friction", Transactions of ASME, Vol 106, January 1984, pp.54-69.
- [12] Kato, K., Chiou, Y.C., Kayaba, T., "Effect of Normal Stiffness in Loading System on Wear of Carbon Steel- Part 1: Severe-Mild Wear Transition.", Journal of Tribology, Transactions of the ASME, October 1985, Vol. 107, pp. 491-495.

- [13] Kato, K., Chiou, Y.C., "Effect of Normal Stiffness in Loading System on Wear of Carbon Steel- Part 2: Dynamic Normal Load and Effective Sliding Distance.", *Journal of Tribology, Transactions of the ASME*, October 1985, Vol. 107, pp. 491-495.
- [14] Bhushan, B., "Stick-Slip Induced Noise Generation in Water-Lubricated Compliant Rubber Bearings", *Journal of Lubrication Technology, Transactions of the ASME*, April 1980, Vol. 102, No. 2, pp. 201-211.
- [15] Krauter, A.I., "Generation of Squeal/Chatter in Water-Lubricated Elastomeric Bearings", vol.103, *Journal of Lubrication Technology, Transactions of the ASME*, July 1981, pp.406-412.
- [16] Rorrer, R.A.L., Eiss, N.S., "Frictional Oscillations in Wet and Dry Elastomeric Sliding", *Tribology Transactions, STLE*, Vol. 38, No.2, 1995, pp. 323-328.
- [17] Kiryu, K., Yanai, T., Matsumoto, S., Koga, T., "An Analysis of "Ringing" Phenomena on a Water Pump Mechanical Seal, Part 1&2", *ASLE Transactions*, Vol. 28, No. 2, pp.261-267, 1985.
- [18] Connell, J.E., Rorrer, R.A.L., "Friction-Induced Vibrations in V-Ribbed Belt Applications", *DE* vol. 49, "Friction-Induced Vibration, Chatter, Squeal and Chaos", *ASME* 1992.
- [19] Nibert, R.K., Watts, R.F., "Evaluation of Anti-Shudder Characteristics and Anti-Shudder Durability of Automatic Transmission Fluids", *Synopses of the International Tribology Conference, Yokohama 1995*, p.437.
- [20] Sharma, J.P., Dwivedi, S.N., "Tribo-System in Robot Design", *Proceedings of the Conference "Robotics and Factories of the Future"*, North Carolina, USA, December 4-7, 1984, Springer-Verlag edition, pp.345-355.
- [21] Ibrahim, R.A., "Friction-Induced Vibration, Chatter, Squeal, and Chaos. Part 1: Mechanics of Contact and Friction. Part 2: Dynamics and Modeling.", *Applied Mechanics Review*, Vol. 47, No. 7, July 1994, pp. 209-252.
- [22] Matsumoto, T., "The Present and Future Trends of Wet Friction Materials", *Proceedings of the ITC Yokohama 1995 Satellite Forum "Tribology of Wet Friction Materials"*, pp.13-22.
- [23] Tolstoi, D., "Significance of Normal-Degree of Freedom and Natural Normal Vibrations in Contact Friction", *Wear*, Vol. 10, 1967, pp. 199-213.
- [24] Derjaguin, B.C., Tolstoi, D., Push, V.E., "A Theory of Stick-Slip Sliding of Solids", *Proceedings of the Conference on Lubrication and Wear, London, 1957*.

- [25] Tolstoj, D., Borisova, G.A., Grigorova, S.R., "Friction Reduction by Perpendicular Oscillation", Soviet Physics-Doklady, Vol. 17, No. 9, march 1973, pp. 907-909.
- [26] Ko, P.L., "Autonomous Quasi-Harmonic and Forced Vibrations of Frictional Systems", Ph.D. thesis, Department of Mechanical Engineering, University of British Columbia, october 1969.
- [27] Hunt, J.B., "Research note: Reduction in Relaxation Oscillation (Stick-Slip) Amplitudes by Normal Excitation", Journal of Mechanical Engineering Science, Vol. 19, No.1, 1977, pp.42-44.
- [28] Soom, A., Kim, C., "Interaction between Dynamic Normal and Frictional Forces during Unlubricated Sliding", Journal of Lubrication Technology, Transactions of the ASME, april 1983, vol. 105, pp.221-229.
- [29] Hess, D.P., Soom, A., Kim, C., "Normal Vibrations and Friction at a Hertzian Contact under Random Excitation: Theory and Experiments", Journal of Sound and Vibration, 1992, Vol. 153, No.3, pp.491-508.
- [30] Hess, D.P., Soom, A., "Normal Vibrations and Friction at a Hertzian Contact under Random Excitation: Perturbation Solution", Journal of Sound and Vibration, 1993, Vol. 164, No.2, pp.317-326.
- [31] Sakamoto, T., "Normal Displacement and Dynamic Friction Characteristics in a Stick-Slip Process", Tribology International, Vol.20, No. 1, February 1987, pp.25-31.
- [32] Abo, M., Sakamoto, T., Kakunai, S., "The Effect of Oscillatory Load on Sliding Friction", Proceedings of the Japan International Tribology Conference, Nagoya, 1990, pp.887-892.
- [33] Sakamoto, T. Abo, M., Kakunai, S. "Friction Reduction in a Stick-Slip Process under Vibratory Load", Japanese Journal of Tribology, Vol. 36, Number 1, 1991, pp.71-82.
- [34] Skaere, T., Staehl, J.E., "Static and Dynamic Friction Processes under the Influence of External Vibration", Wear, Vol. 154, No. 2, 1992, pp. 177-192.
- [35] Awrejcewicz, J., "Chaos in Simple Mechanical Systems with Friction", Journal of Sound and Vibration, Vol. 109, No. 1, 1986, pp. 178-180.
- [36] Popp, K., "Some Model Problems Showing Stick-Slip Motion and Chaos", ASME WAM, Proceedings of the Symposium on Friction-Induced Vibration, Chatter, Squeal and Chaos, 1992, Editors R.A. Ibrahim and A. Soom, DE-Vol. 49, pp.1-12.

- [37] Popp, K., Stelter, P., "Nonlinear Oscillations of Structures Induced by Dry Friction", Proceedings of IUTAM Symposium on Nonlinear Dynamics in Engineering Systems, Springer-Verlag, Berlin, 1990, pp. 233-240.
- [38] Narayanan, S., Jayaraman, K., "Chaotic Vibration in a Nonlinear Oscillator with Coulomb Damping", Journal of Sound and Vibration, Vol. 146, No. 1, 1991, pp. 17-31.
- [39] Hess, D.P., Wagh, N.J., "Chaotic Vibrations and Friction at Mechanical Joints", Proceedings of the Symposium on Friction-Induced Vibration, Chatter, Squeal and Chaos, 1992, Editors R.A. Ibrahim and A. Soom, DE- Vol. 49, pp.149-156.
- [40] Ko, P.L., Lowe, J.T., "A Low-Velocity Friction Machine for the Studies of Static and Dynamic Frictions with Special References to the Evaluation of Slide and Way oils", National Research Council, Controlled technical report CTR-WE-47, 1985.
- [41] Bell, R., Burdekin, M., "Dynamic Behaviour of Plain Slideways", Proceedings of the Institution of Mechanical Engineers, 1966, Vol. 181, Part 1, No. 8, pp.169-184.
- [42] Brockley, C.A., Ko, P.L., "The Measurement of Friction and Friction-Induced Vibration", Journal of Lubrication Technology, Transactions of the ASME, June 1970, No. 70-LubS-15.
- [43] The Tribology Handbook, Ed. M.J. Neale, Butterworths, London, 1973.
- [44] Jones, N., Peel, J.D., "Frictional properties of paper and their importance in supercalendering", Paper Technology, 1967, vol.8, no.1, pp.43-50
- [44] Cleveland, W.K.S., "Tractor Wet Brake and Wet Clutch Friction Properties", Journal of the National Lubricating Grease Institute, July 1987, Vol. 11, No. 4, pp. 135-138.
- [45] Eguchi, M., Takesue, M., Yamamoto, T., "Friction Characteristic of a Paper-Base Facing for a Wet Clutch: Experimental Results and Analysis Using Stribeck Curve", Japanese journal of Tribology, 1991, Vol. 36, No. 4, pp. 741-753.
- [46] Finkin, E.F., "The Consequences of Spline Friction in Multiple Disk Brake and Clutch Packs", Journal of Lubrication Technology, Transactions of The ASME, January 1968, pp. 65-71.
- [46] Evans, E.M., Whittle, J., "Friction in Wet Clutches", Proceedings of the Institution of Mechanical Engineers, 1967, Vol. 182, Pt. 3N, pp. 132-138.
- [47] Brockley, C.A., Davis, H.R., "The Time-Dependence of Static Friction", Journal of Lubrication Technology, Transactions of the ASME, January 1968, pp. 35-41.

[48] Johannes, V.I., Green, M.A., Brockley, C.A., "The role of the rate of application of the tangential force in determining the static friction coefficient.", short communication, Wear, Vol. 24, 1973, pp.381-385.

[49] McLachlan, N.W., "Theory of Vibrations", Dover Publication Inc., p.12, 1951.

Appendix 1
Application of the Krylov-Bogoliubov method to the quasi-harmonic friction-induced vibration problem

1. Normalization of the system's equations

Equations (1) and (2) from, respectively, the autonomous system and the system subjected to a normal dynamic loading are reprinted here.

$$m\ddot{x} + r\dot{x} + kx = w_s \mu_k \quad (1)$$

$$m\ddot{x} + r\dot{x} + kx = w_s \mu_k (1 + \beta \sin \delta t) \quad (2)$$

They can both be made dimensionless by the introduction of a displacement parameter h as

follows: $X = \frac{x}{h}$; $V = \frac{v}{\omega h}$ and using $\omega^2 = k/m$ and $\tau = \omega t$

Consequently, we have $\dot{X} = \frac{dX}{dt} \frac{dt}{d\tau}$ and $\ddot{X} = \frac{\ddot{x}}{\omega^2 h}$

Dimensionless equations for the two systems can be obtained by further multiplying equations

(1) and (2) by $1/(m\omega^2 h)$ and substituting the above expressions for X , \dot{X} , \ddot{X} .

$$\ddot{X} + R\dot{X} + X = \frac{1}{E} F(V - \dot{X}) \quad (3)$$

$$\ddot{X} + R\dot{X} + X = \frac{1}{E} F(V - \dot{X}) [1 + \beta \sin \alpha \tau] \quad (4)$$

where $R = r/(m\omega)$ and $E = (m\omega^2 h)$.

The friction force function $f_{\mu k} = w_s \mu_k$ has been converted into a function of the dimensionless sliding velocity $F(V - \dot{X})$.

2. Method of first approximation by Krylov-Bogoliubov

For an autonomous system, equation (3) can be rewritten in the form

$$\ddot{X} + X + \gamma G(\dot{X}) = 0 \quad (5)$$

If $\gamma = 0$, this equation reduces to a simple linear differential equation with a sinusoidal solution

$$X = a \sin(\tau + \phi) \quad (6)$$

where a and ϕ are constants.

For γ slightly different from 0 but remaining small, equation (6) can be used as a generating solution for the first approximation, provided the quantities a and ϕ are considered, not as constants, but as slightly varying functions of time. Thus equation (6) can be rewritten as:

$$X = a(\tau) \sin(\tau + \phi(\tau)) \quad (7)$$

This constitutes the basic idea of the method for the first approximation of the solution of the differential equation by K-B method. An additional condition is that \dot{X} should be of the form

$$\dot{X} = a \cos(\tau + \phi) \quad (8)$$

These two equations (7) and (8) cause the following constraint to be obtained.

$$\dot{a} \sin(\tau + \phi) + a \dot{\phi} \cos(\tau + \phi) = 0 \quad (9)$$

A second constraint is obtained by substituting these expressions for X and \dot{X} (differentiating with respect to a and ϕ) in equation (5). The solution of these two constraints gives expressions for \dot{a} and $\dot{\phi}$ as periodic functions of time. As γ is small, a and ϕ can be considered as slowly

varying functions of τ . Therefore a and ϕ can be assumed to remain constants over the interval τ to $\tau + 2\pi$.

Integration of the equations for \dot{a} and $\dot{\phi}$ between the limits τ to $\tau + 2\pi$, shows that all trigonometric terms drop out and only the constant terms $K_0(a)$ and $H_0(a)$ remain. We have

$$\frac{da}{d\tau} = -\gamma K_0(a) \quad \frac{d\phi}{d\tau} = \frac{\gamma}{a} H_0(a) \quad (10)$$

Since those expressions are periodic, they can be expanded in Fourier series to give the usual form of the first approximation by K-B.

$$\frac{da}{d\tau} = -\frac{\gamma}{2\pi} \int_0^{2\pi} G(a \cos \psi) \cos \psi d\psi = \phi(a) \quad (11)$$

$$\frac{d\psi}{d\tau} = 1 + \frac{\gamma}{2a\pi} \int_0^{2\pi} G(a \cos \psi) \sin \psi d\psi = \Omega(a) \quad (12)$$

The condition for a stationary oscillation or a limit cycle is $\phi(a) = 0$, that is $\phi(a_1) = 0$ is the condition for a limit cycle with amplitude a_1 .

To investigate the stability of the first approximation, a slightly perturbed amplitude ($a_1 + \delta a$) where δa is an absolute value of departure, is considered. It can be shown by the variational equations that, to the first order:

$$\frac{d}{d\tau}(\delta a) = \phi_a(a_1) \delta a \quad (13)$$

Then, if $\phi_a(a_1) < 0$, we have $\frac{d}{d\tau}(\delta a) < 0$, in other words, the initial departure δa has a tendency to disappear for $\phi_a(a_1) < 0$. Thus $\phi_a(a_1) < 0$ is the condition for a stable limit cycle and the condition $\phi_a(0) > 0$ is equivalent to the existence of an unstable singularity.

3. Application of the polynomial expression to the K-B method

The substitution of the polynomial expression of the F-V curve into the system's autonomous dimensionless equation (3) gives, after some manipulation,

$$\ddot{X} + \frac{1}{E} [(r\omega h + P_1)\dot{X} - P_2\dot{X}^2 + \dots - (-1)^n P_n \dot{X}^n] + X = \frac{P_0}{E} \quad (14)$$

where

$$P_0 = C_0 + C_1 V + \dots + C_n V^n$$

.....

$$P_k = C_k + \dots + {}_n J_k C_n V^{n-k} \quad \text{for } k = 0, 1, 2, 3, \dots, n$$

and where the binomial coefficients are given by ${}_n J_k = n!/(n-k)!k!$

The constant term on the right hand side of equation(14) is the static displacement and can be omitted in the amplitude analysis. Equation (14) can be further simplified by letting:

$$Q_1 = r\omega h + P_1 \quad \text{and} \quad Q_k = \frac{P_k}{Q_1}, \quad k = 2, 3, \dots, n.$$

$$\ddot{X} + \frac{Q_1}{E} [\dot{X} - Q_2 \dot{X}^2 + \dots - (-1)^n Q_n \dot{X}^n] + X = 0$$

The application of the K-B method obtained in part 2 leads to the following condition for the stationary amplitude:

$$\phi_a(a) = -\frac{Q_1}{2E} \sum_{k=1}^{\frac{n+1}{2}} \frac{(2k-1) {}_{2k-1} J_k}{2^{(2k-2)}} R_{2k-1} a^{2k-2} = 0$$

This equation is a polynomial in ' a ' which can be easily solved with the help of a computer.

The polynomial coefficients are formed by some series of n and are related to the power of the variable \dot{X} and can be explicitly expressed. This allows the setup of a generalized expression that a computer program can solve with the friction force function represented by a n -th order polynomial.

Appendix 2

System parameters

1. Natural frequency and system stiffness

If we assume, to simplify the problem, the slider assembly to be represented by a cantilever beam supporting a mass m , as shown on figure A.2.

Beam characteristics:

$$E = 2.10^{11} \text{ Pa}$$

$$I = 67.446.10^{-12} \text{ m}^4$$

$$L_1 = 0.06 \text{ m}$$

$$L_2 = 0.18 \text{ m}$$

$$M = 0.483 \text{ kg}$$

$$m_b = 0.049 \text{ kg}$$

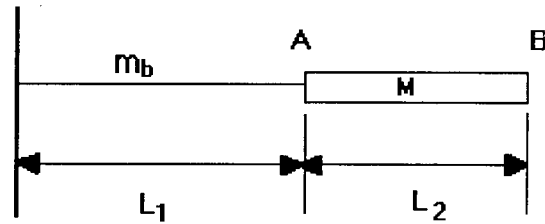


Figure A.2.

It is assumed that the vibration takes on a static deflection vibration form.

The deflection and the slope at at point A due to a force P acting at point B are

$$\delta_A = \frac{PL_1^3}{3EI} + \frac{PL_1^2 L_2}{2EI} = \delta_A \left(1 + \frac{3L_2}{2L_1}\right)$$

$$\theta_A = \frac{PL_1^2}{2EI} + \frac{PL_1 L_2}{EI} = \delta_A \left(\frac{3}{2L_1} + \frac{3L_2}{L_1}\right)$$

$$\delta_B = \delta_A + \theta_A L_2 = \delta_A \left(1 + \frac{3L_2}{L_1} + 3\left(\frac{L_2}{L_1}\right)^2\right)$$

The estimated equivalent stiffness of the system is $K = P/\delta_B = 5063.5 \text{ N/m}$

The natural frequency can then be deduced from the equation given in [49].

$$\omega_n \approx \sqrt{\frac{K}{M}} * \left(1 - \frac{33m_b}{280M}\right) = 101 \text{ rad/s}$$

The experimentally measured stiffness and damped natural frequency of the system are respectively:

$$k = 5200 \text{ N/m}$$

$$\omega = 116.2 \text{ rad/s}$$

2. System damping coefficient

The logarithmic decrement method was used to determine experimentally the system damping coefficient. The free vibrations of the beam, as it is clear of the lower surface, are recorded. The equation of motion is then:

$$m\ddot{x} + c\dot{x} + kx = 0$$

for which the solution is $x = e^{-\delta t} (A_1 \cos \omega t + A_2 \sin \omega t)$

The logarithm of the ratio of two successive maxima x_p and x_{p+1} or the ratio of two maxima x_p and x_{p+q} , when the damping is small, is measured.

$$\text{Ln} \frac{x_p}{x_{p+q}} = \text{Ln} \frac{e^{-\delta t} (A_1 \cos \omega t + A_2 \sin \omega t)}{e^{-\delta(t+q2\pi/\omega)} (A_1 \cos(\omega t + 2q\pi) + A_2 \sin(\omega t + 2q\pi))}$$

which simplifies into

$$\text{Ln} \frac{x_p}{x_{p+q}} = \text{Ln} \frac{e^{-\delta t}}{e^{-\delta(t+2\pi q/\omega)}} = \text{Ln} e^{\delta 2\pi q/\omega} = 2\pi q \delta / \omega$$

Consequently,

$$\delta = \frac{\omega}{2\pi q} \operatorname{Ln} \frac{x_p}{x_{p+q}}$$

Moreover,

$$\omega_n^2 = \omega^2 + \delta^2$$

From experimental results, we have $\frac{x_p}{x_{p+10}} = 2.34$ and $\omega = 116.2$ rad/s

$$\therefore \delta = 1.577 \quad \text{and} \quad \omega_n = 116.21 \text{ rad/s}$$

The damping coefficient of the system is $r = 2m\delta = 1.7$ kg/s

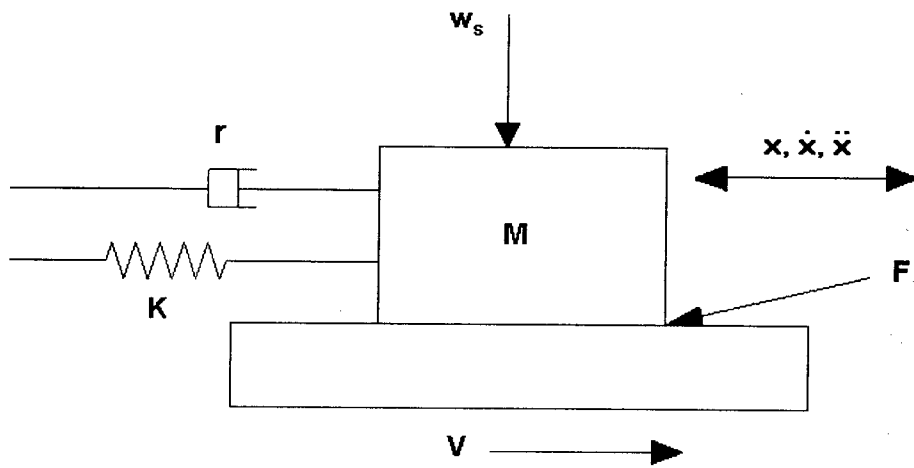


Figure 3.1. Autonomous system

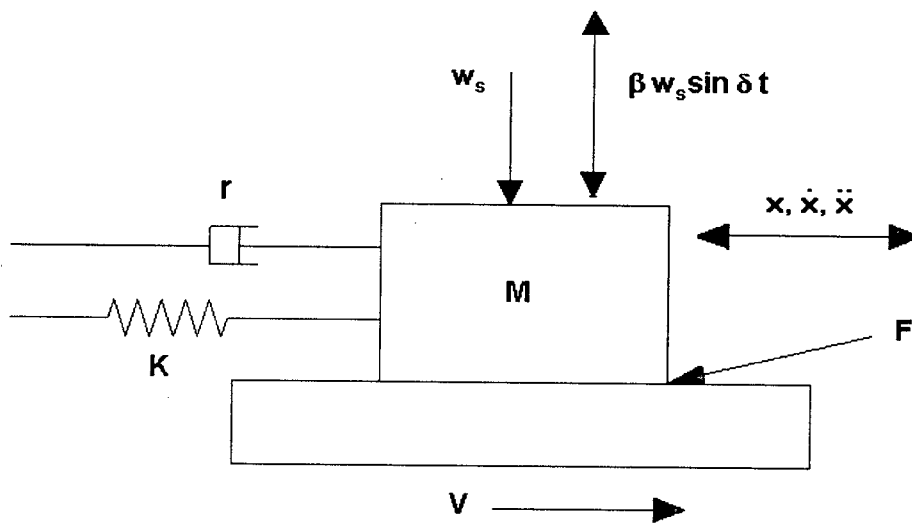
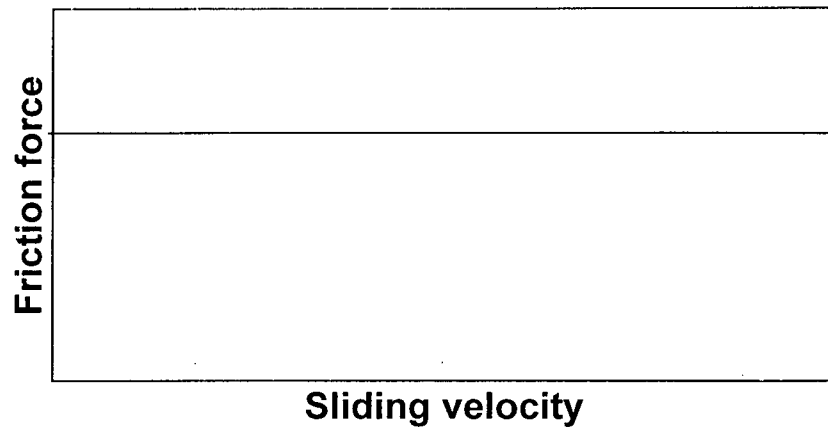
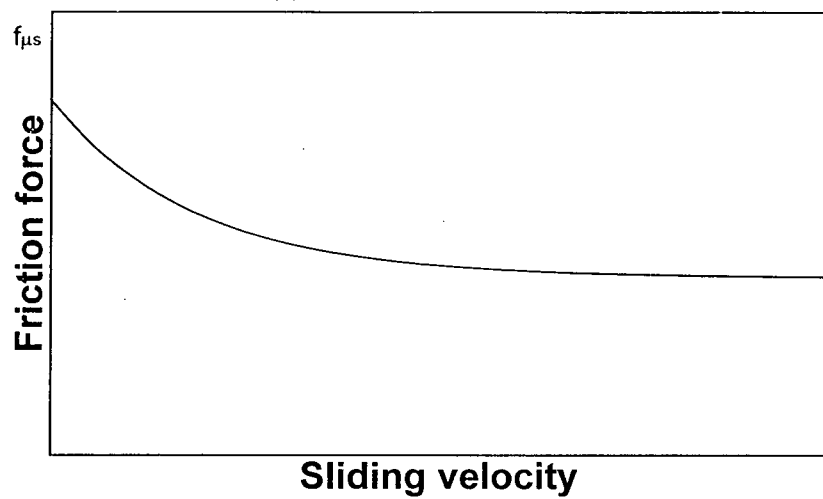


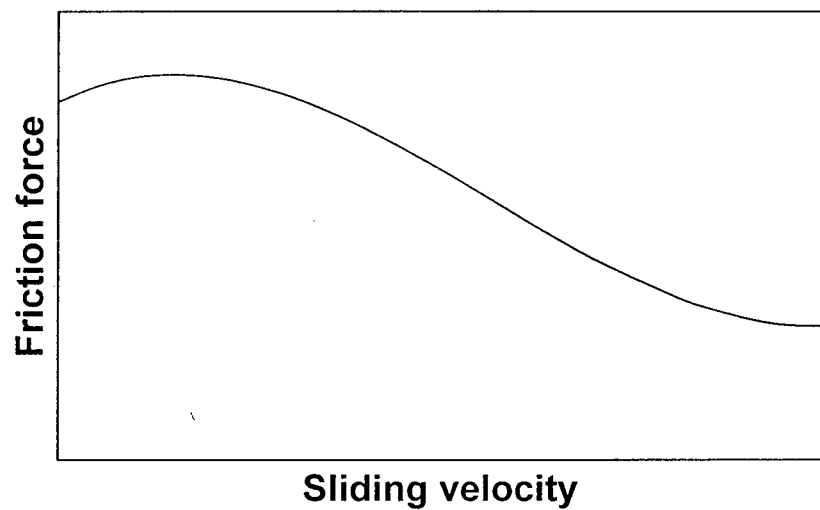
Figure 3.2. System with an external dynamic normal force



(a) Coulomb friction



(b) Continuously decreasing curve



(c) Humped curve

Figure 3.3. Different types of dynamic friction-velocity curves
The static friction has an undetermined value along the zero-axis depending on other parameters.

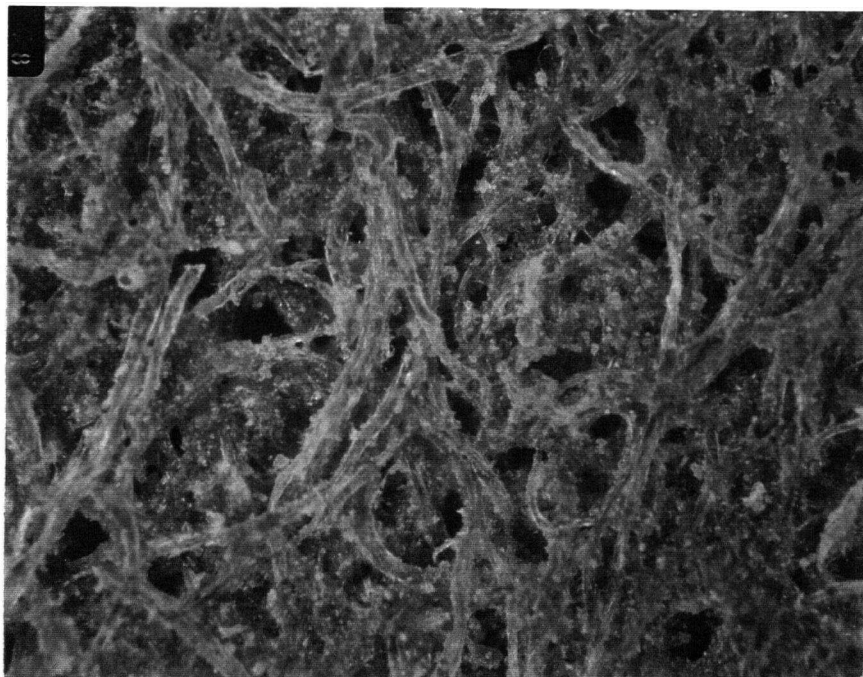


Figure 4.1. Photomicrograph of the Ford friction plate surface

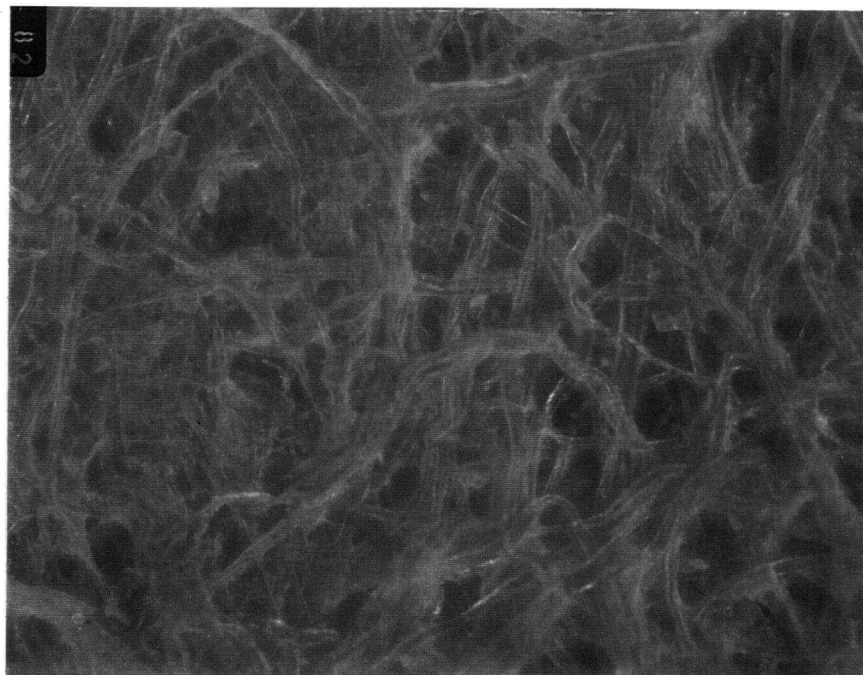


Figure 4.2. Photomicrograph of the blotting paper surface

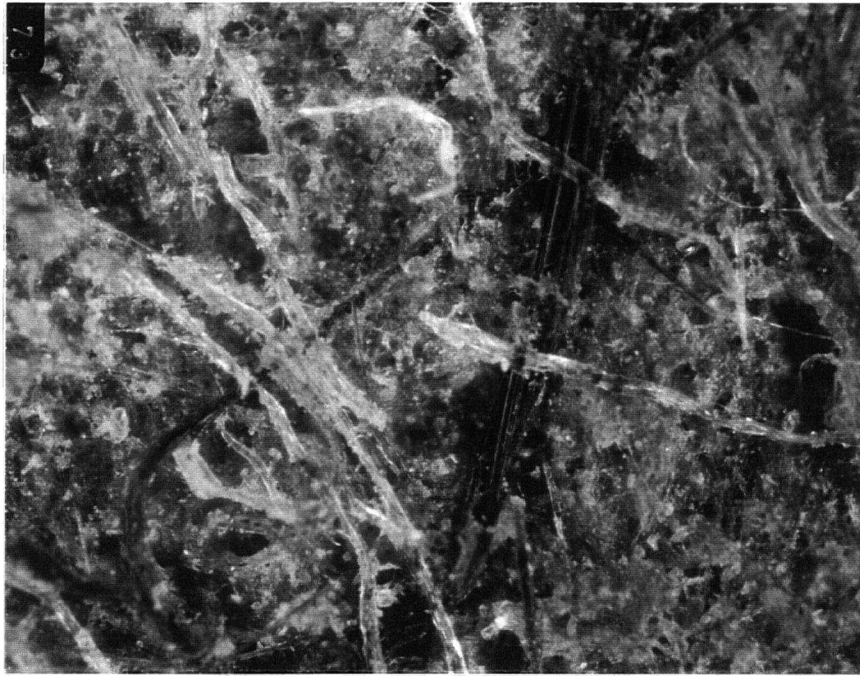


Figure 4.3. Photomicrograph of the Dexron friction plate surface

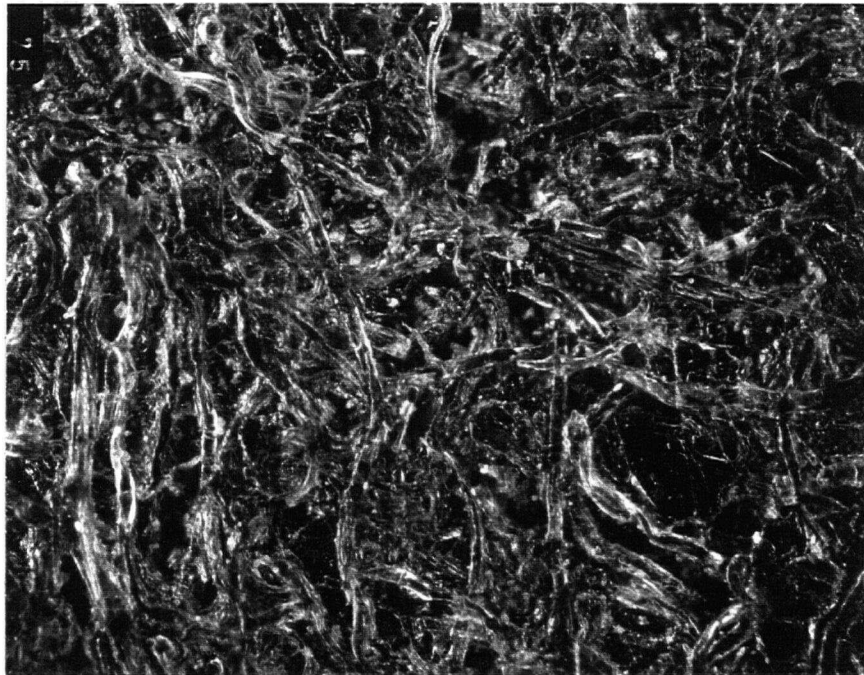
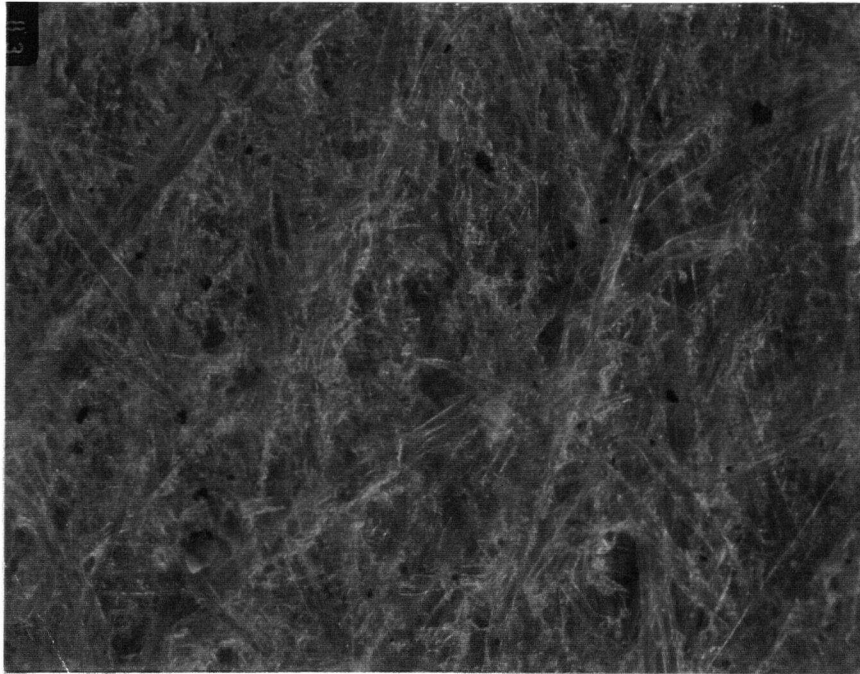
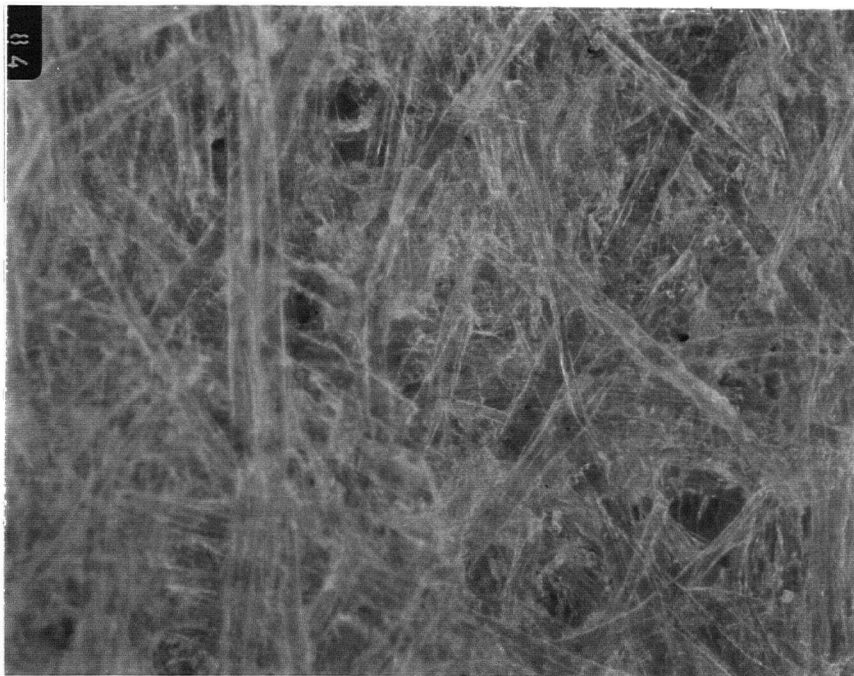


Figure 4.4 Photomicrograph of the type F friction plate surface



(a) Surface A_1



(b) Surface A_2

Figure 4.5 Photomicrographs of the newsprint surfaces

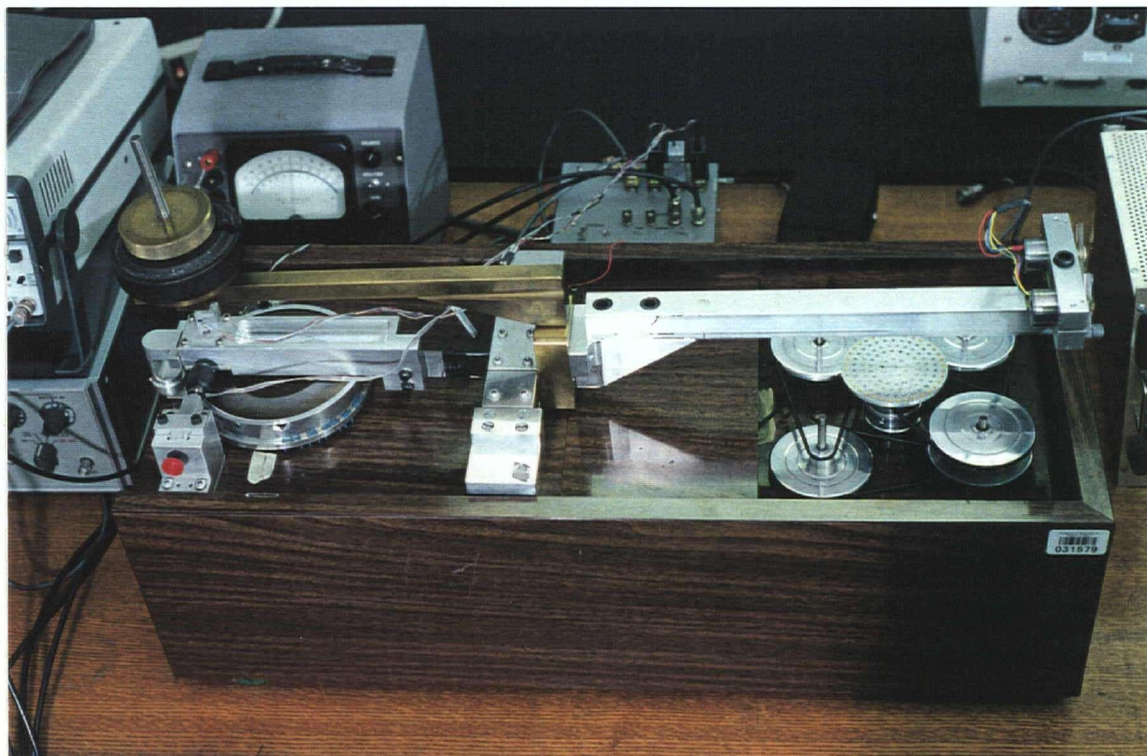


Figure 5.1 General view of the pin-on-disk machine



Figure 5.2 (a) View of the rectangular slider for blotting paper combination

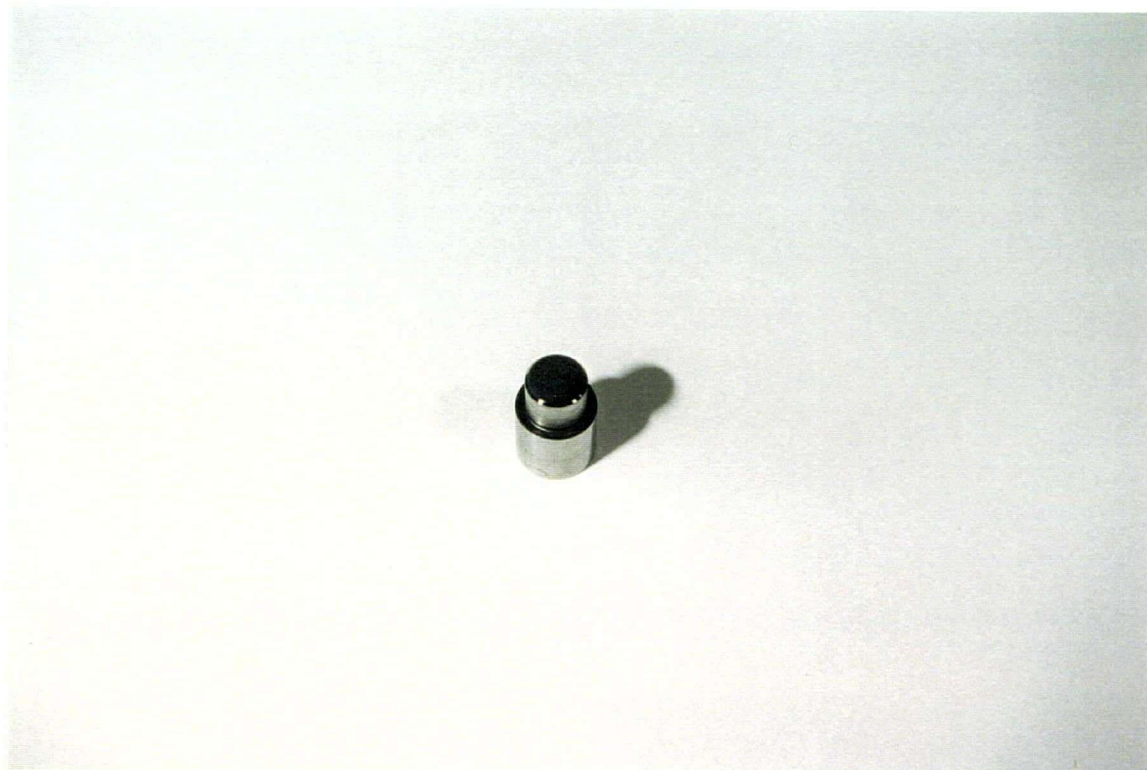


Figure 5.2 (b) View of the circular metal slider for friction plate combination



Figure 5.3.(a) View of the lower disc for blotting paper combination



Figure 5.3.(b) View of the lower disc for friction plate combination



Figure 5.4 Stepper motor arrangement for dynamic loading

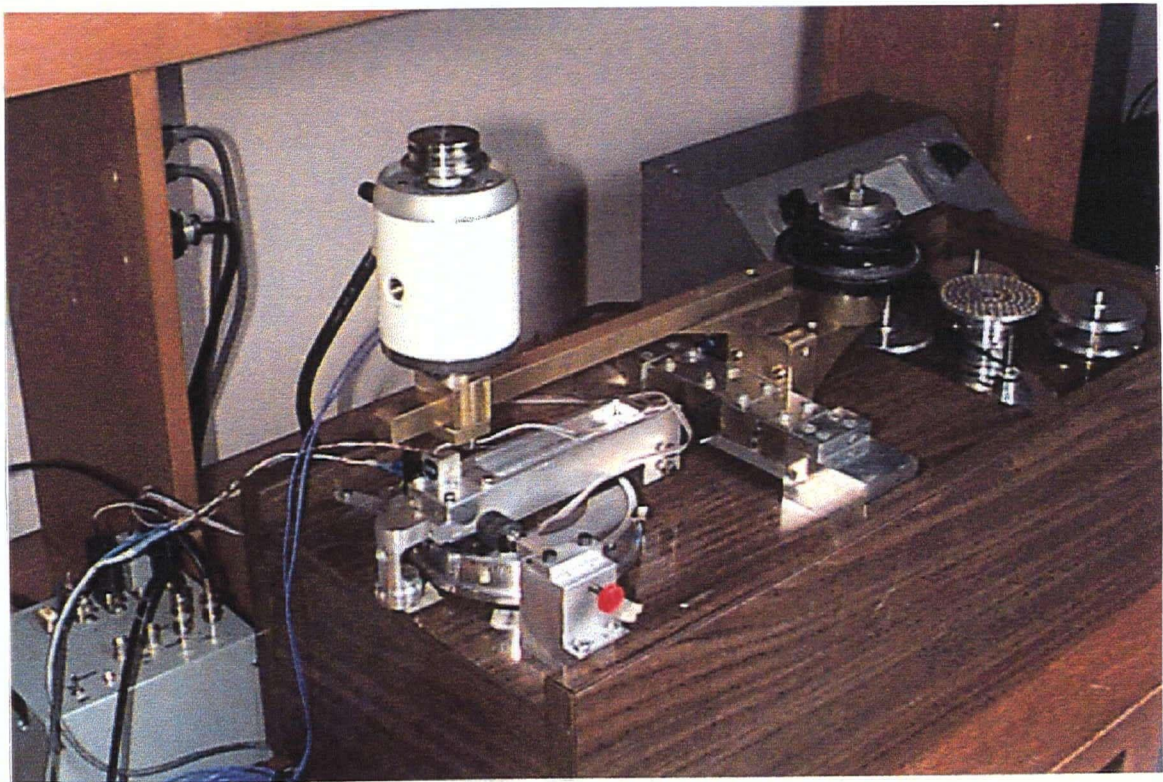


Figure 5.5 Electromagnetic shaker arrangement for dynamic loading

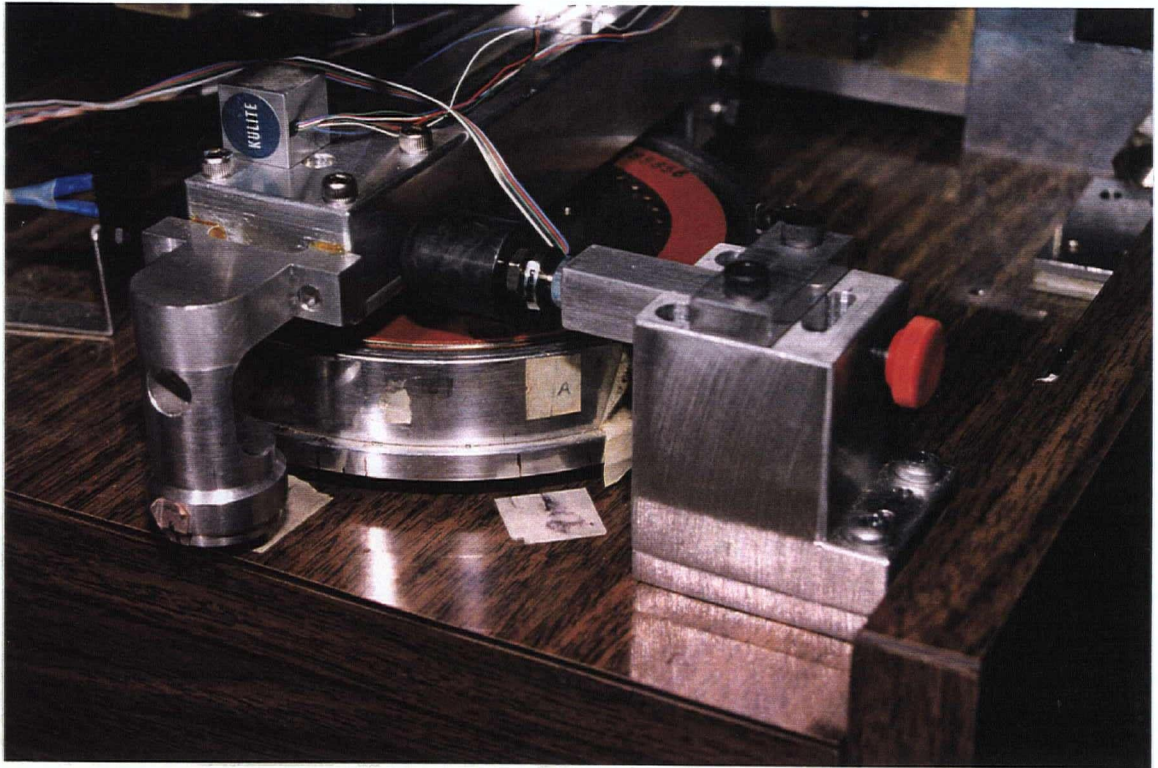


Figure 5.6 View of the load transducer for static measurement method

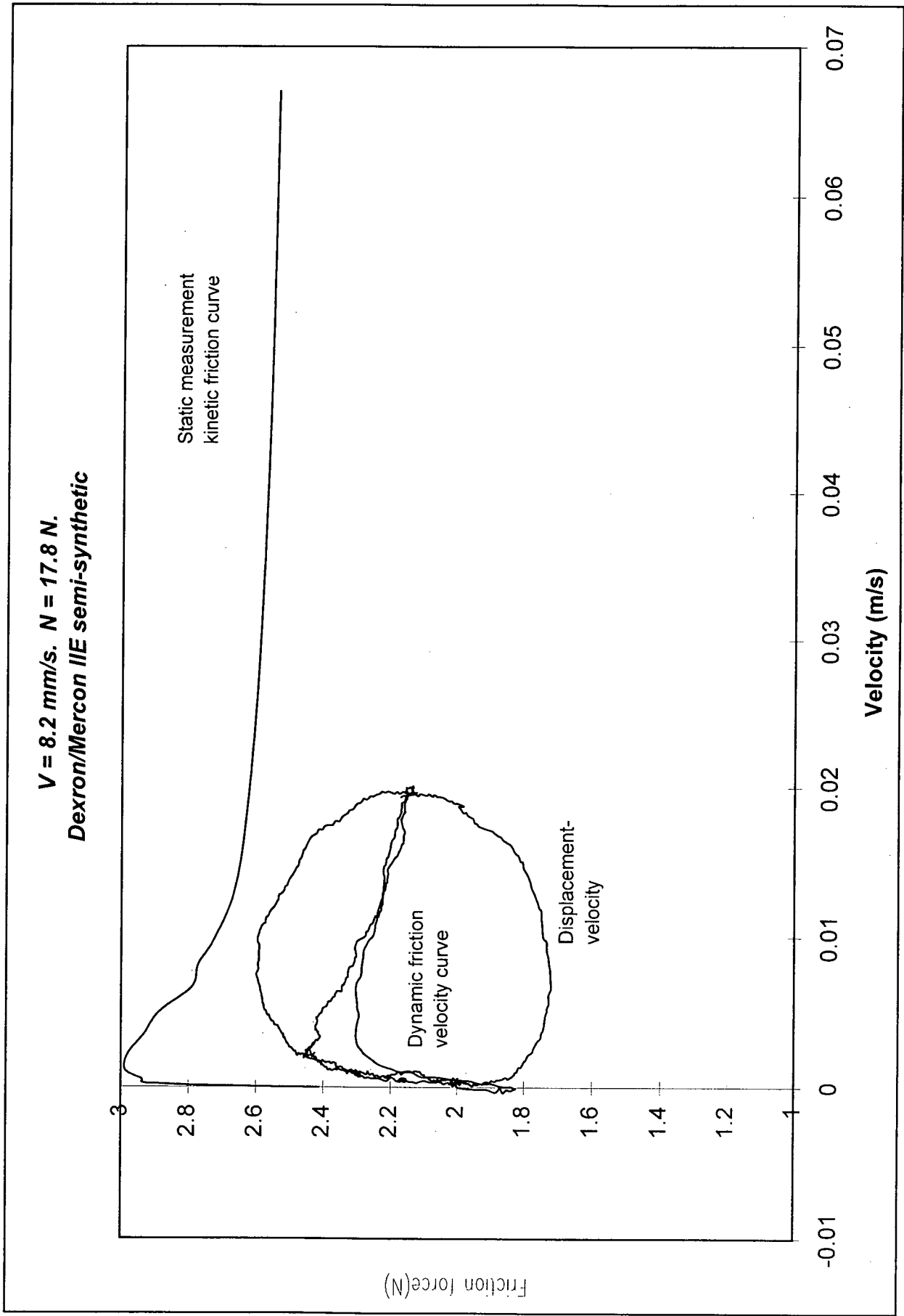


Figure 6.1. Comparison of friction-velocity curves obtained by direct and static measurement methods

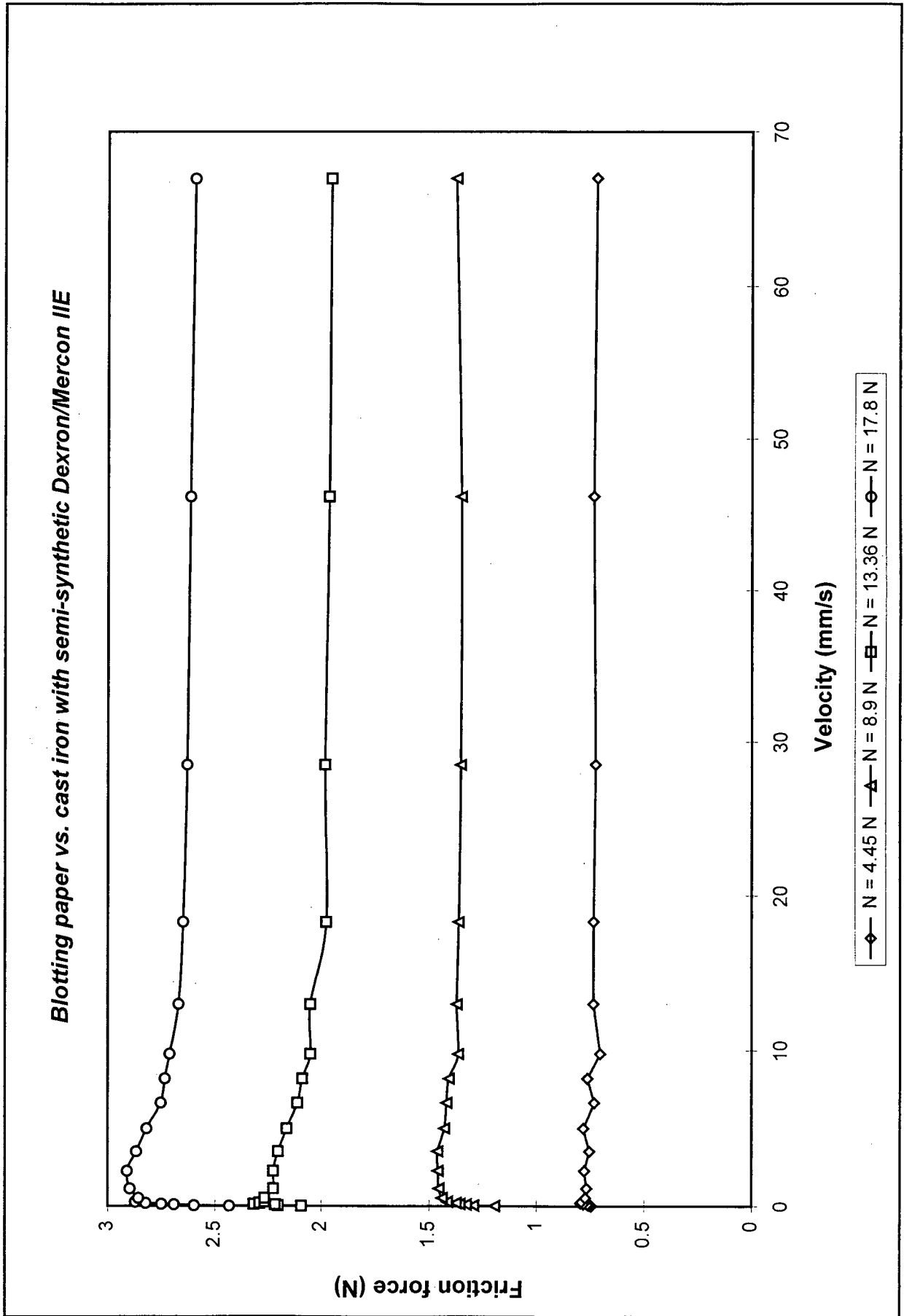


Figure 6.2. Effect of normal load on the f-v curve

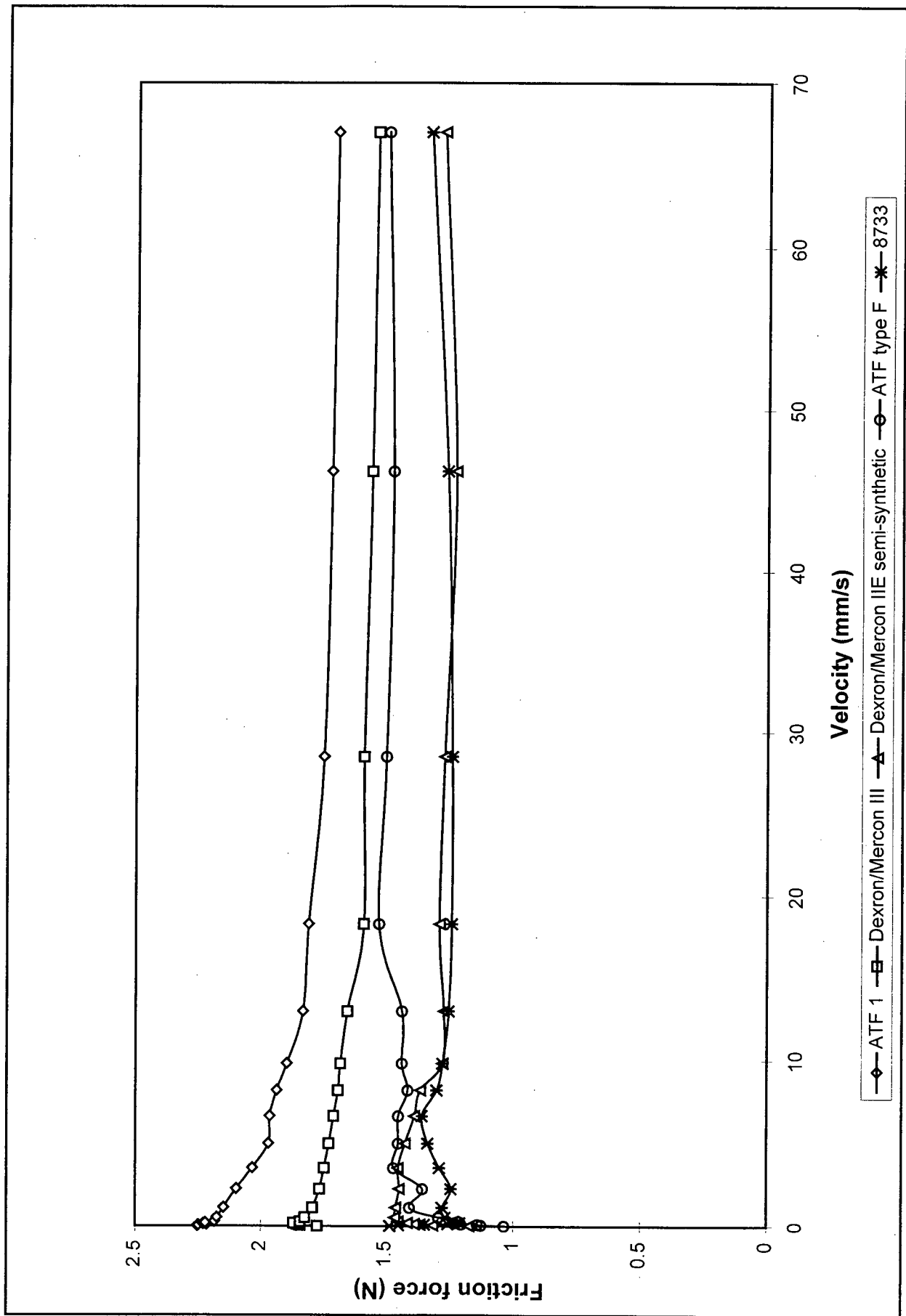


Figure 6.3. f-v characteristics for 4 fluids under a 8.9 N normal load

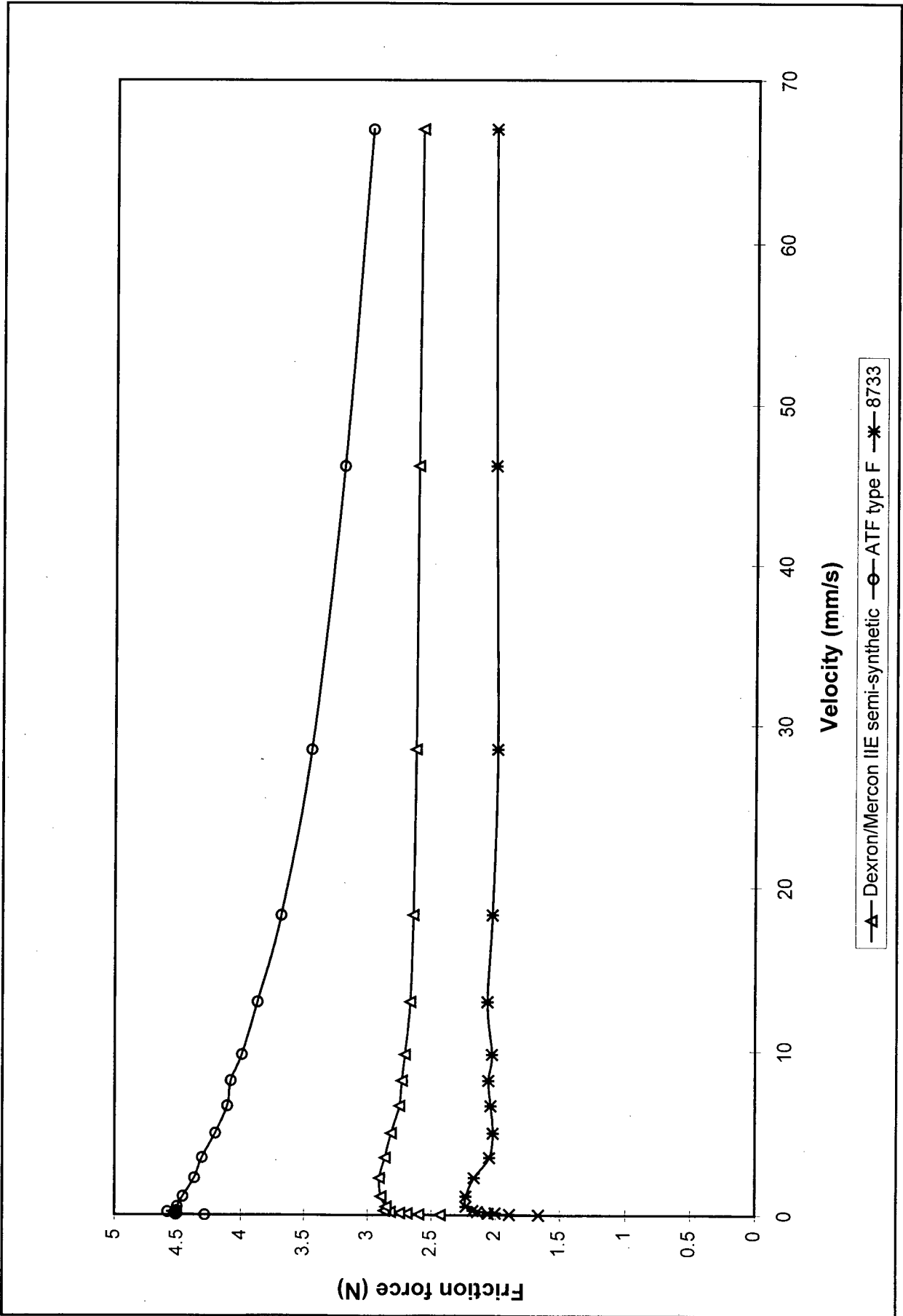


Figure 6.4. f-v characteristics for 3 fluids under a 17.8 N normal load

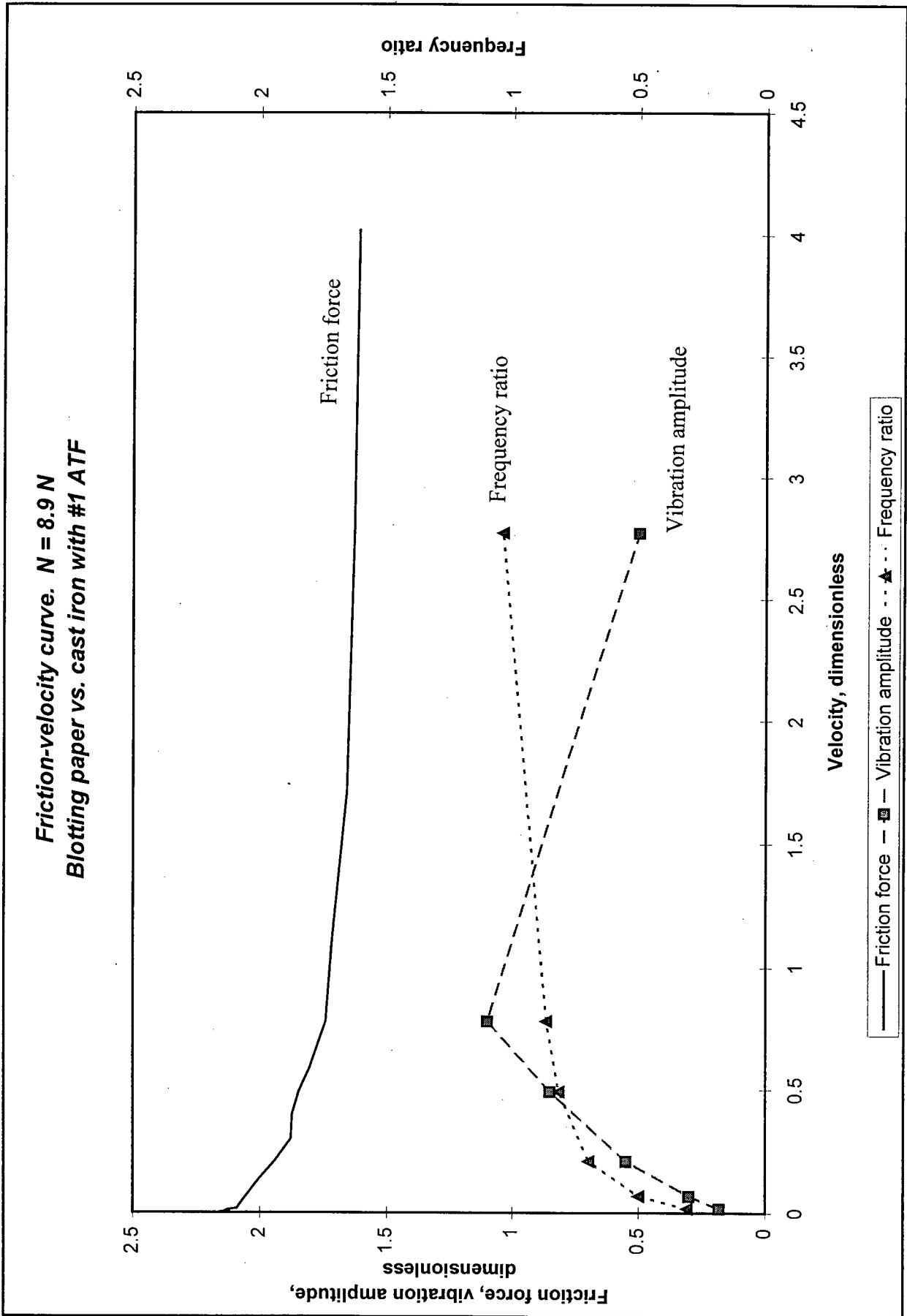


Figure 6.5. F-V curve, amplitude and frequency of experimental vibrations for #1 ATF

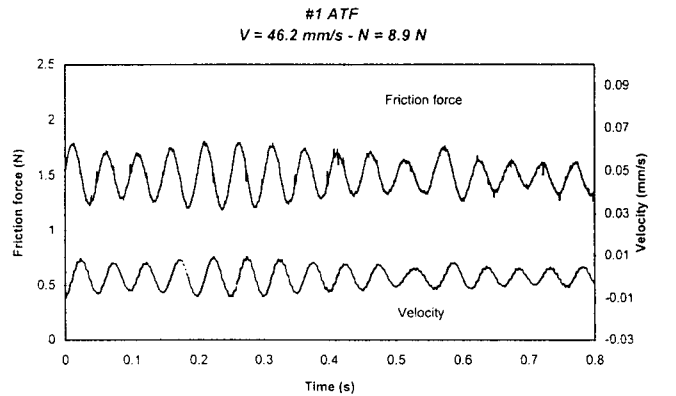
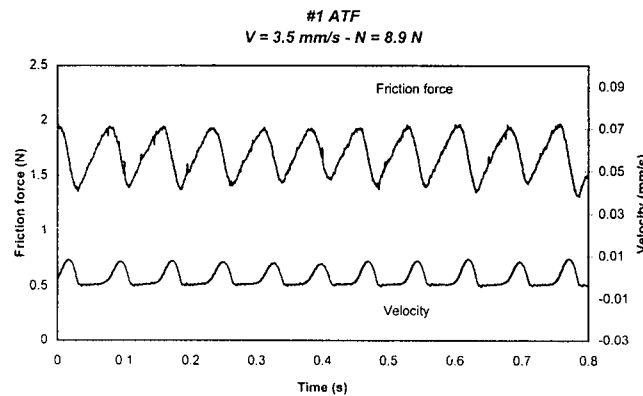
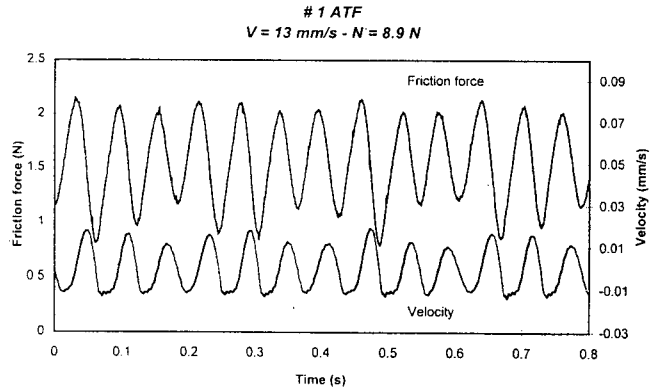
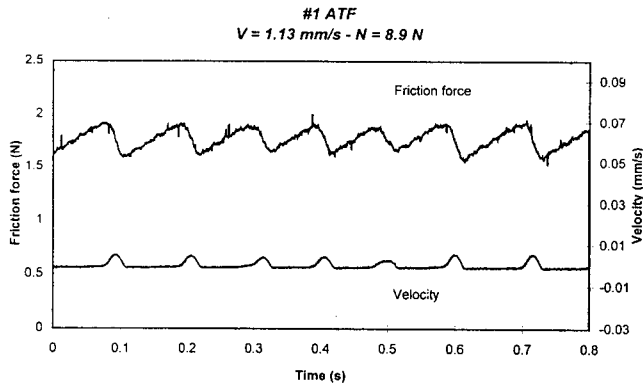
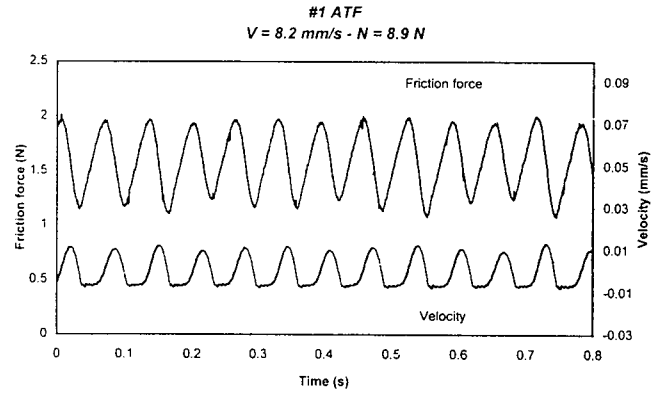
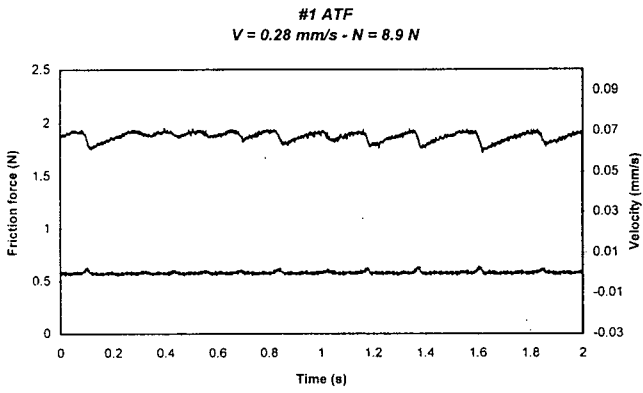


Figure 6.6 Friction vs. time plots at different velocities for #1 ATF

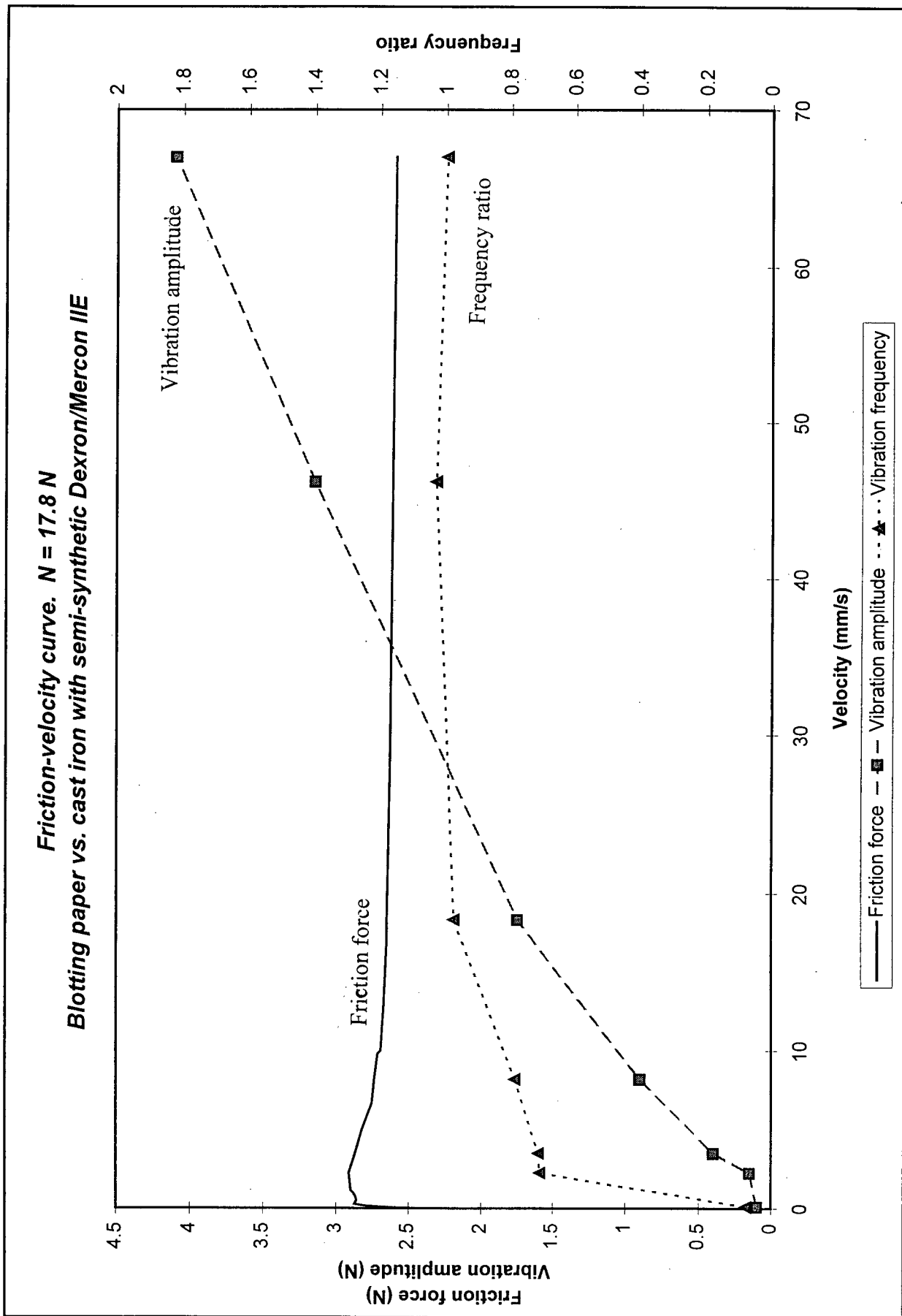


Figure 6.7. $f-v$ curve, amplitude and frequency of experimental vibrations for semi-synthetic Dexron/Mercon IIE

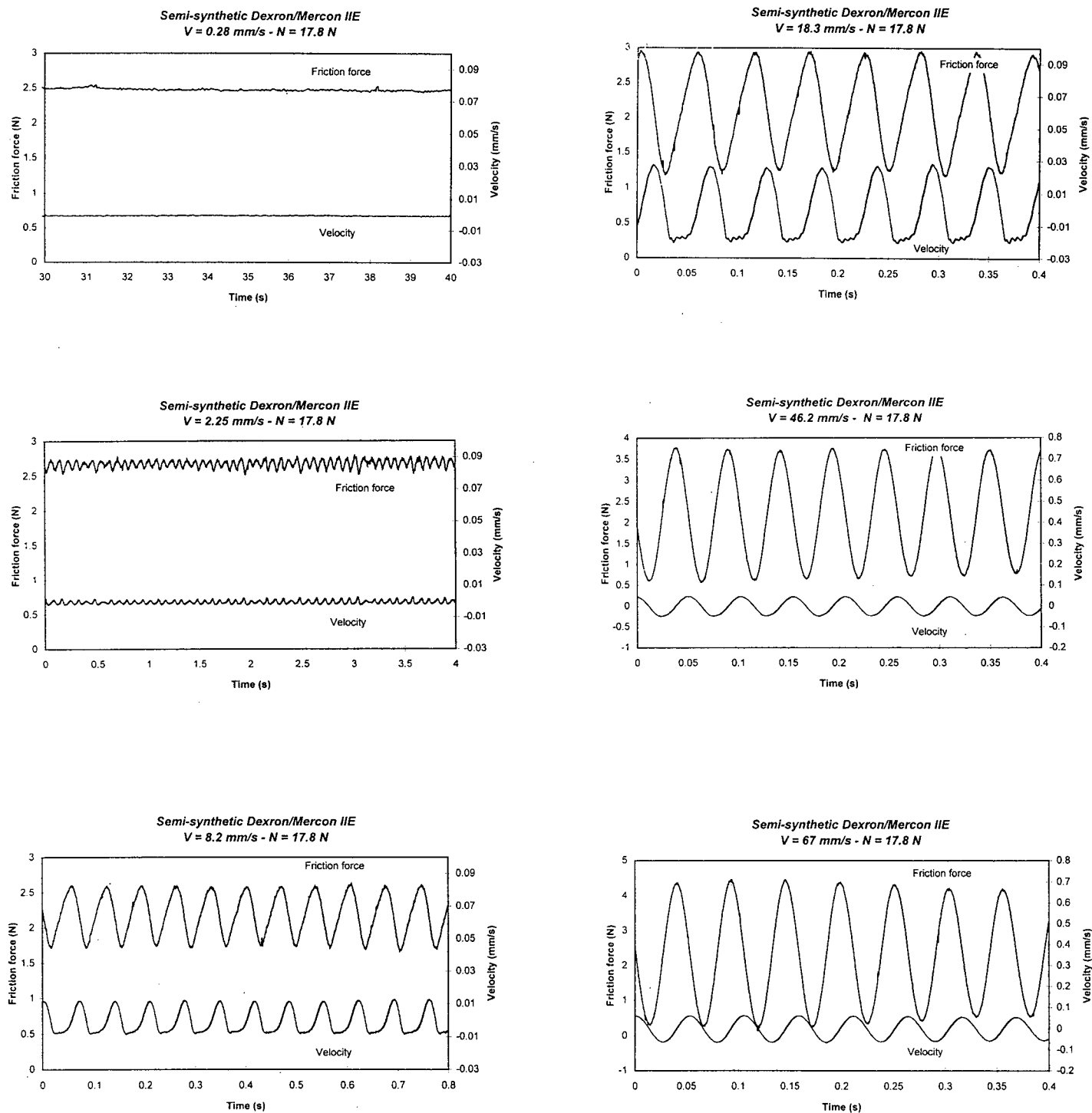


Figure 6.8 (a) Friction vs. time plots at different velocities for semi-synthetic Dexron/Mercon IIE. Static normal load of 17.8 N

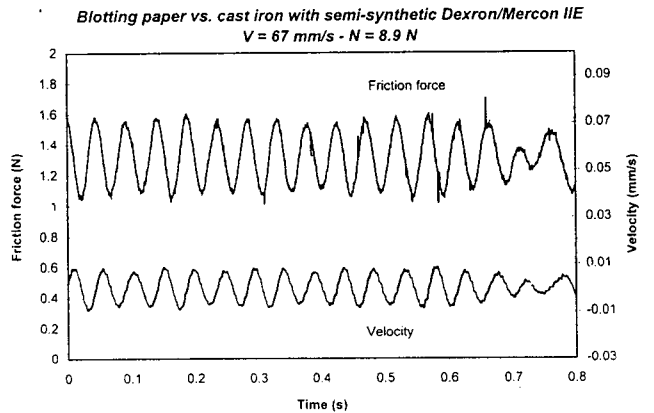
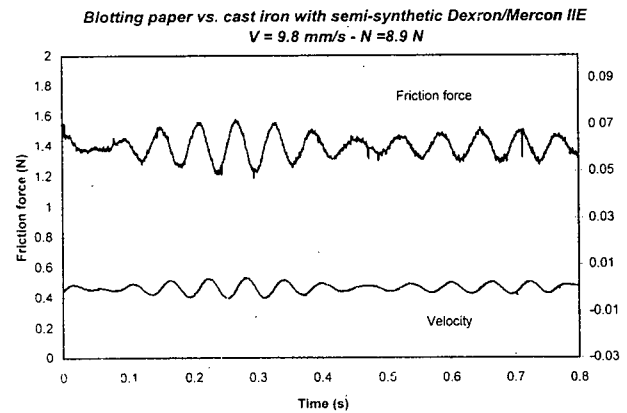
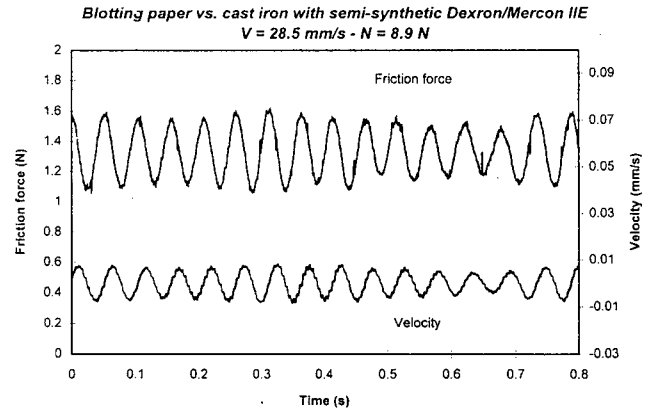
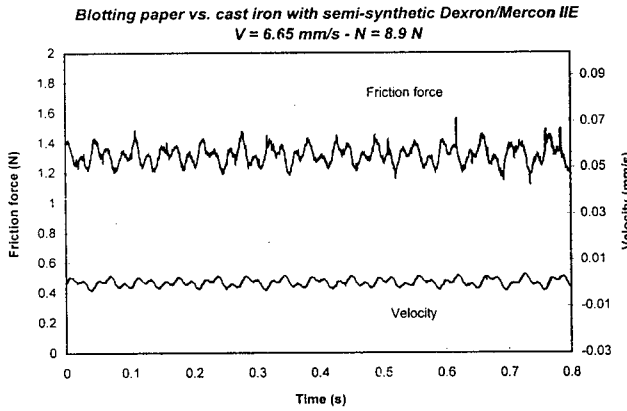
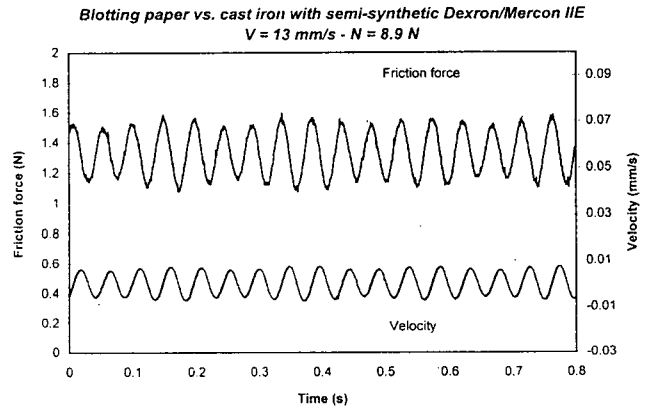
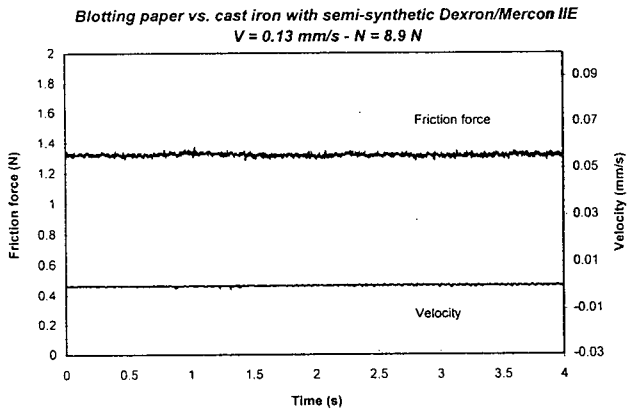


Figure 6.8 (b) Friction vs. time plots at different velocities for semi-synthetic Dexron/Mercon IIE. Static normal load of 8.9 N

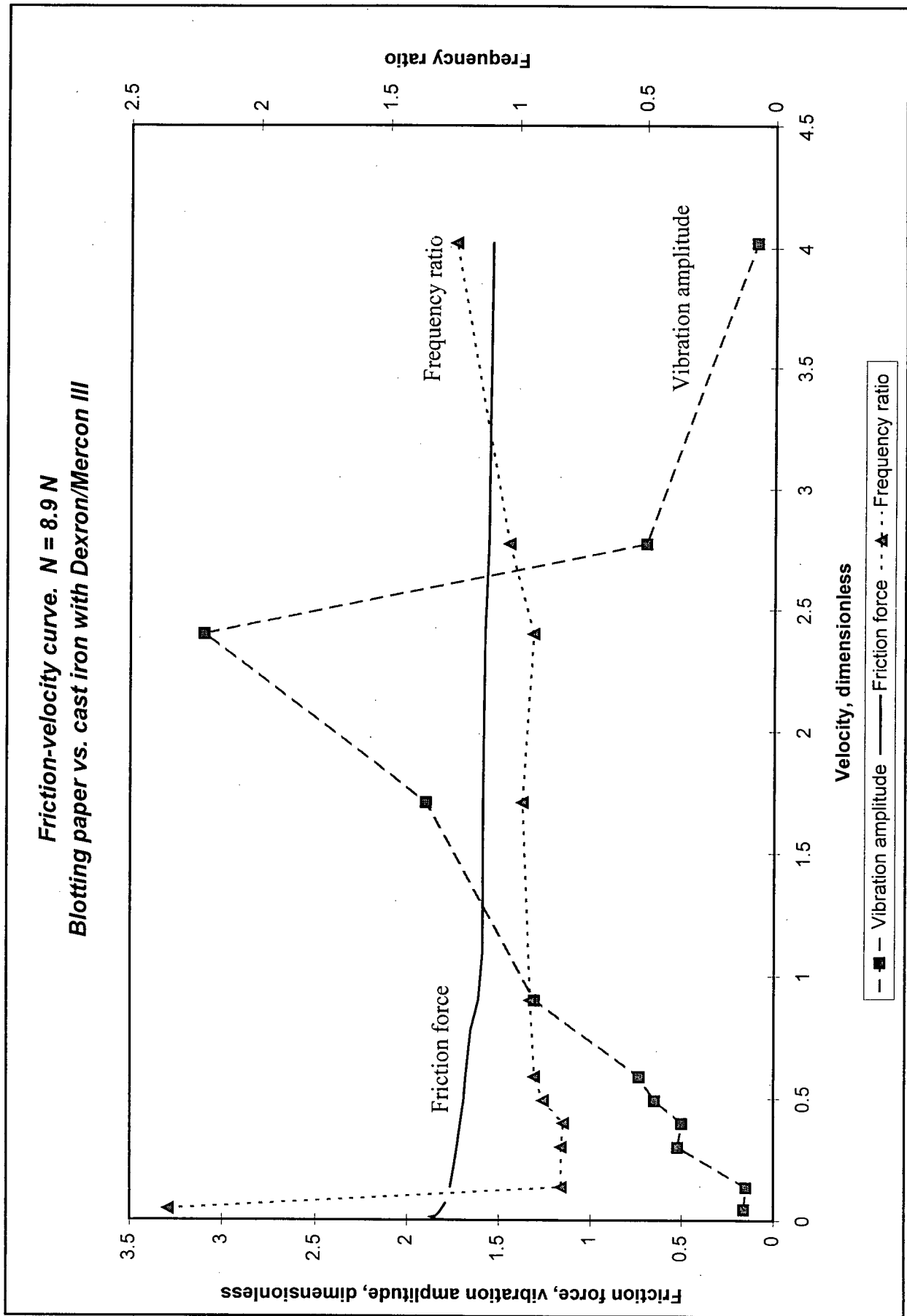


Figure 6.9. F-V curve, amplitude and frequency of experimental vibrations for Dexron/Mercon III

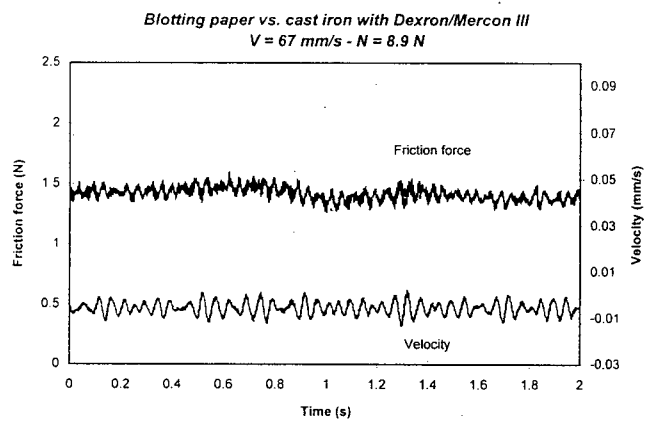
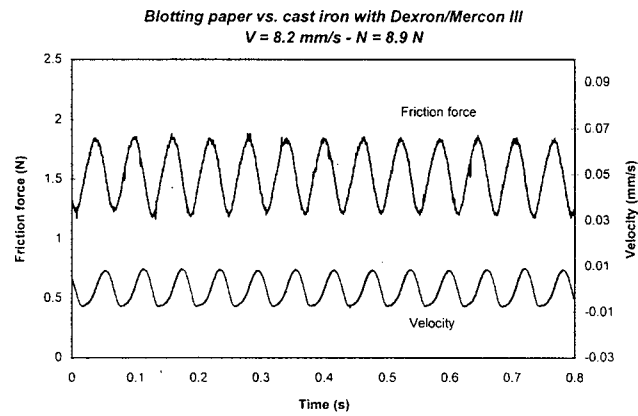
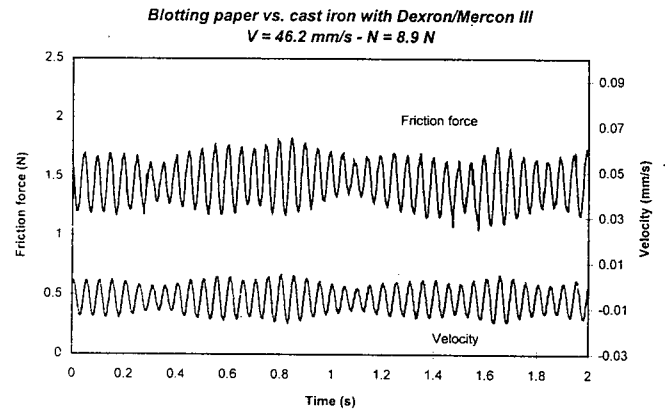
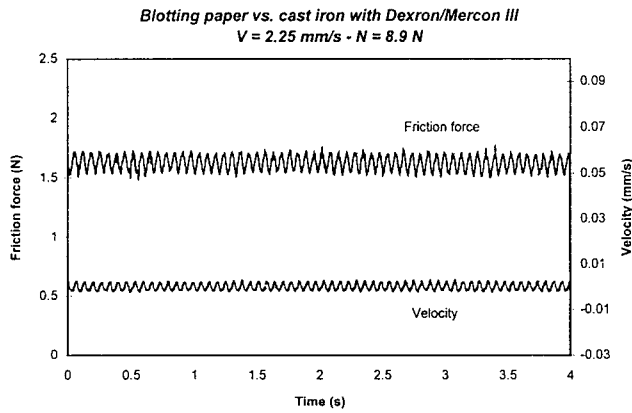
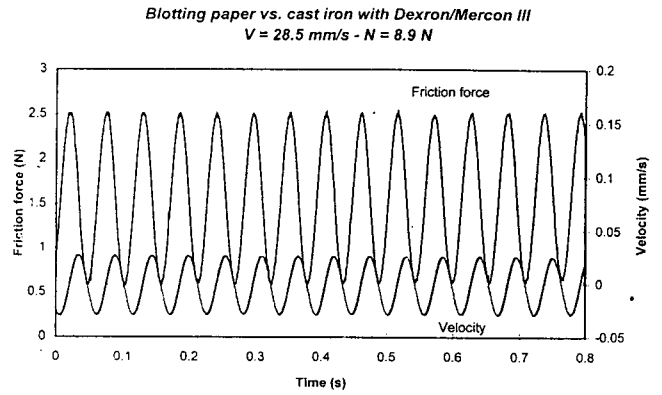
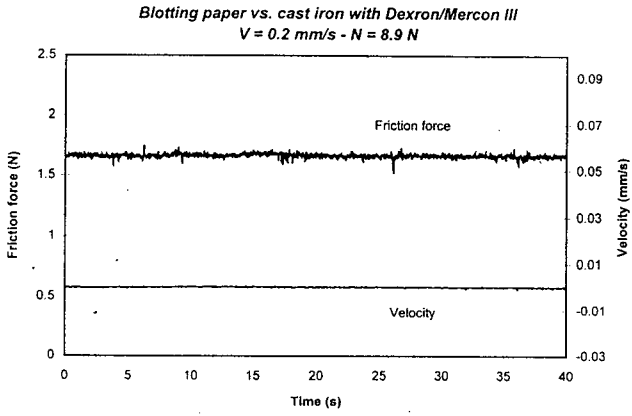


Figure 6.10 Friction vs. time plots at different velocities for Dexron/Mercon III

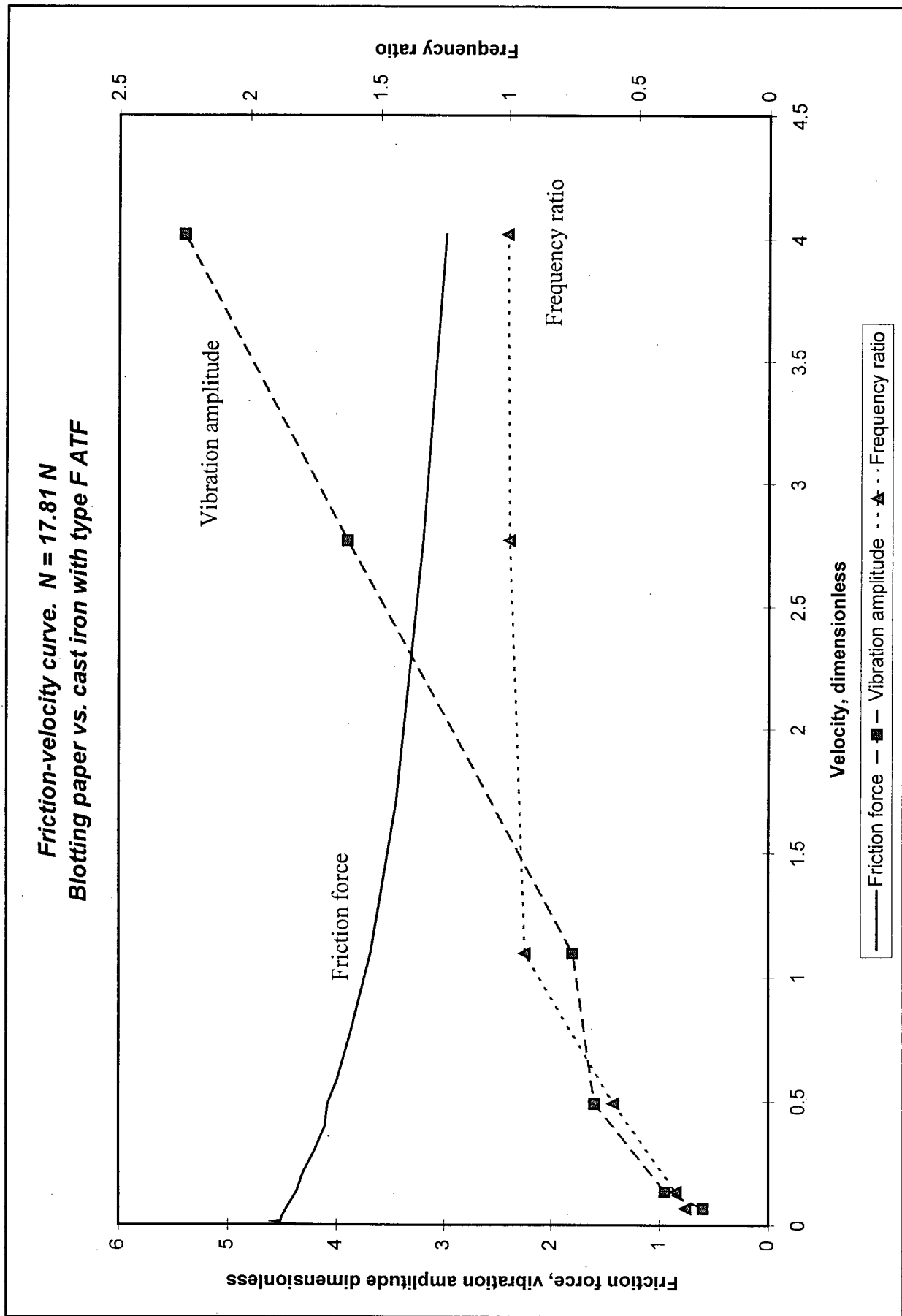


Figure 6.11. F-V curve, amplitude and frequency of experimental vibrations for type F lubricant

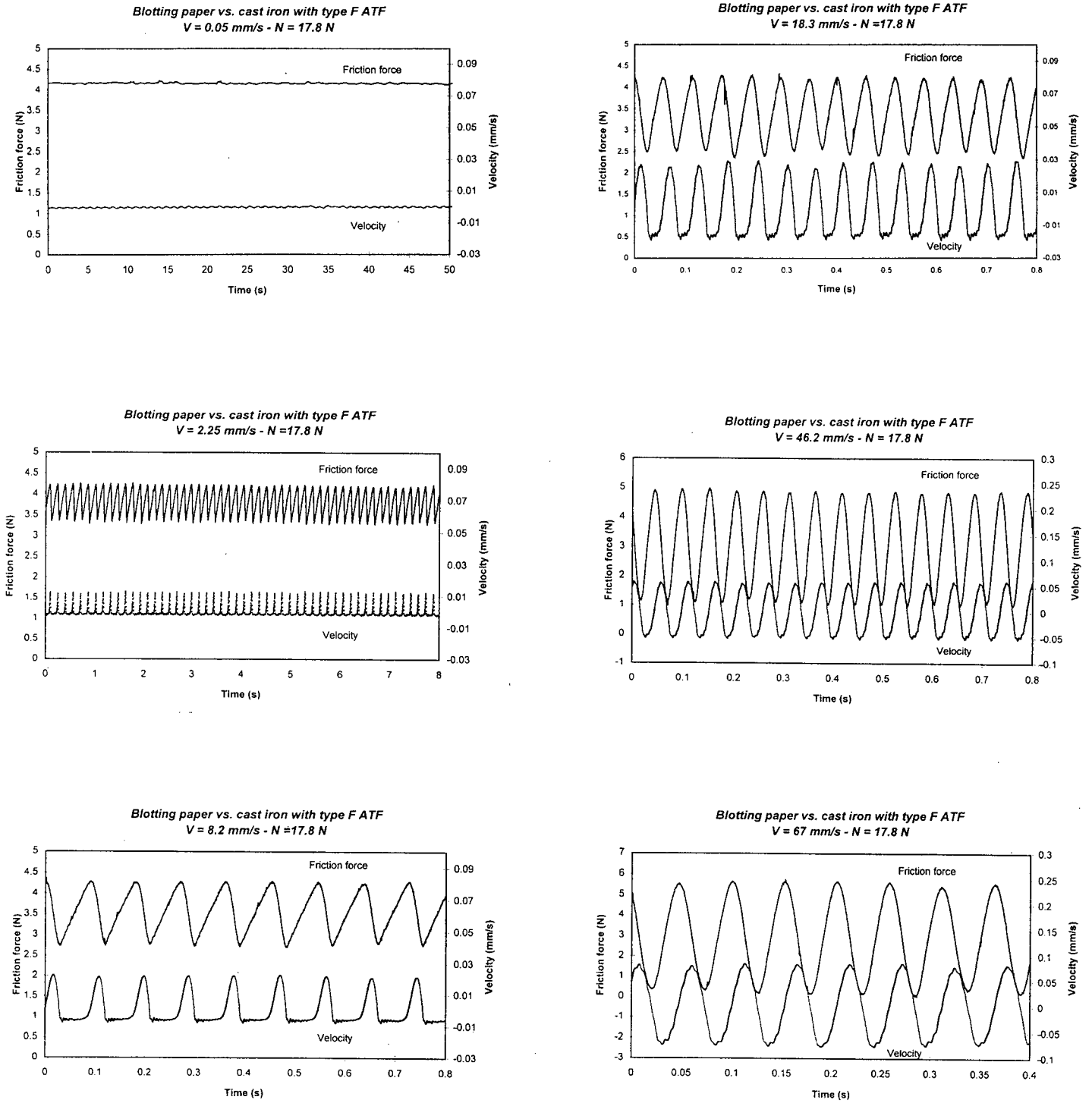


Figure 6.12 Friction vs. time plots at different velocities for type F lubricant

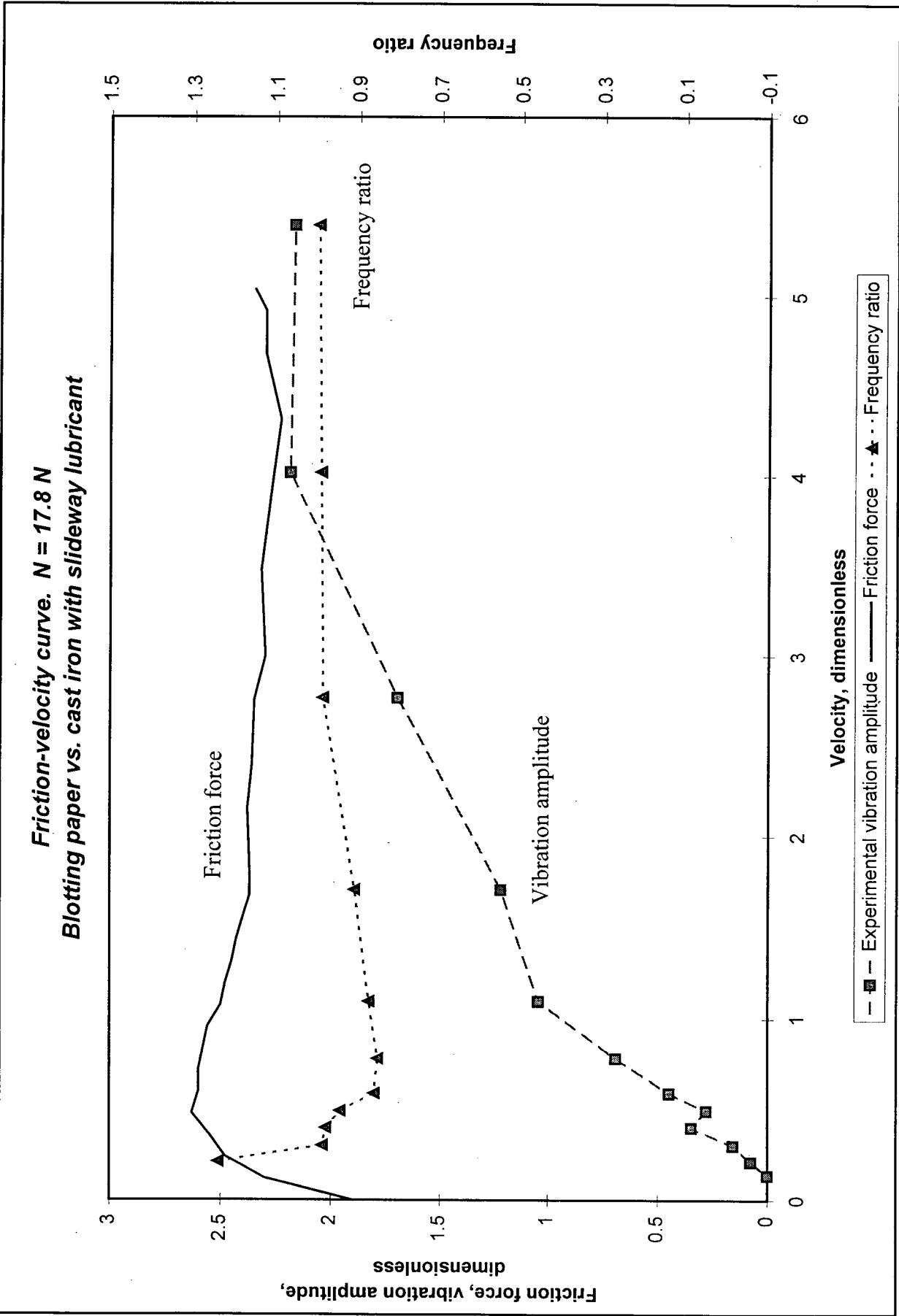


Figure 6.13. F-V curve, amplitude and frequency of experimental vibrations for sideway lubricant

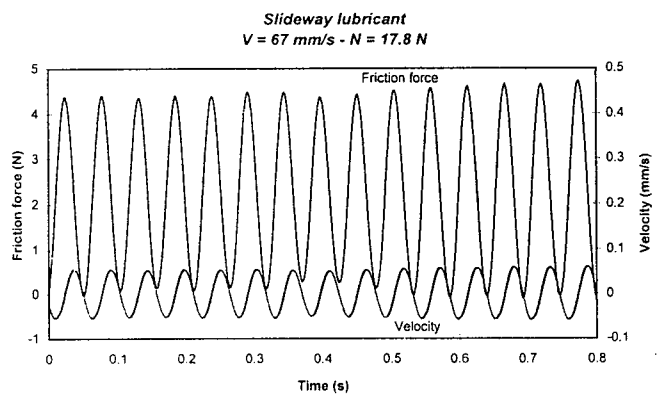
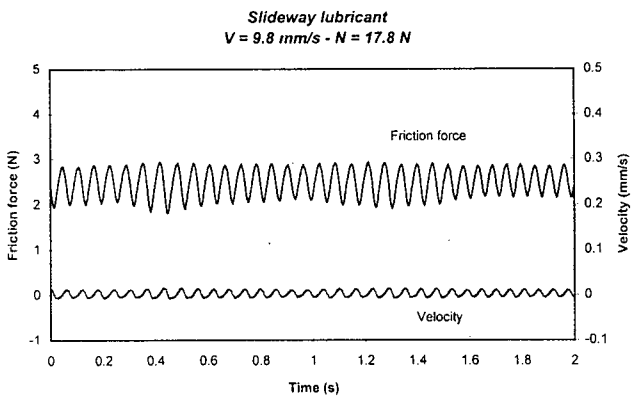
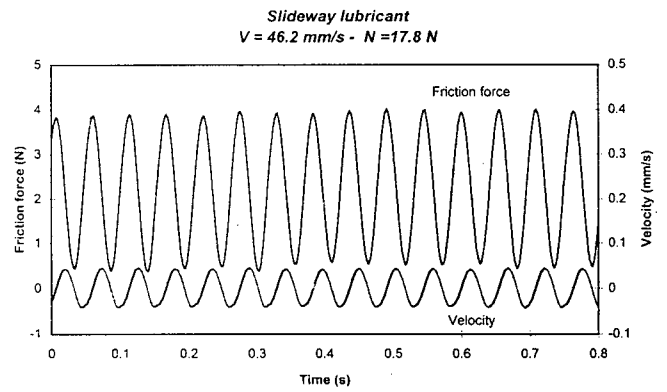
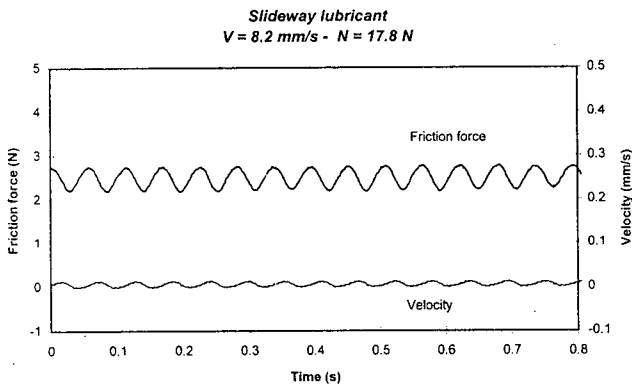
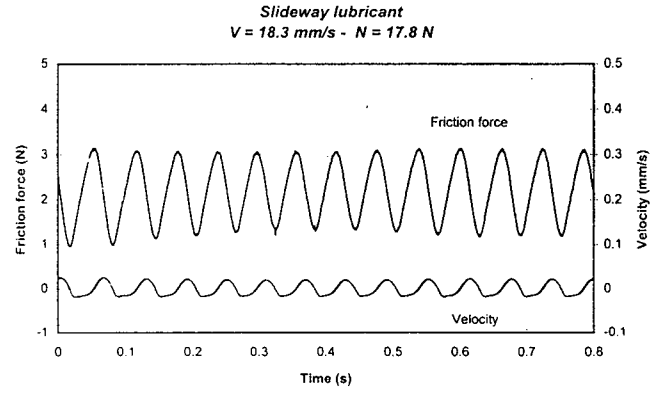
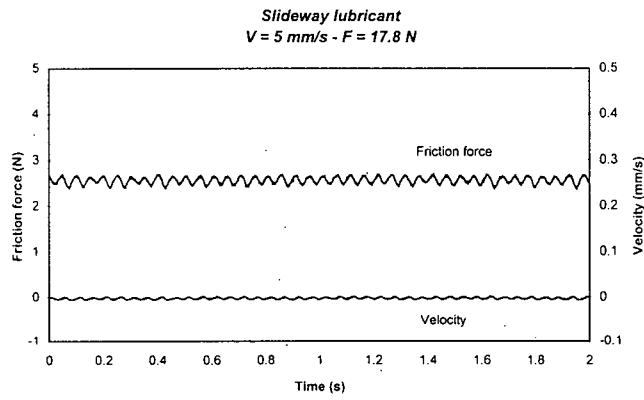
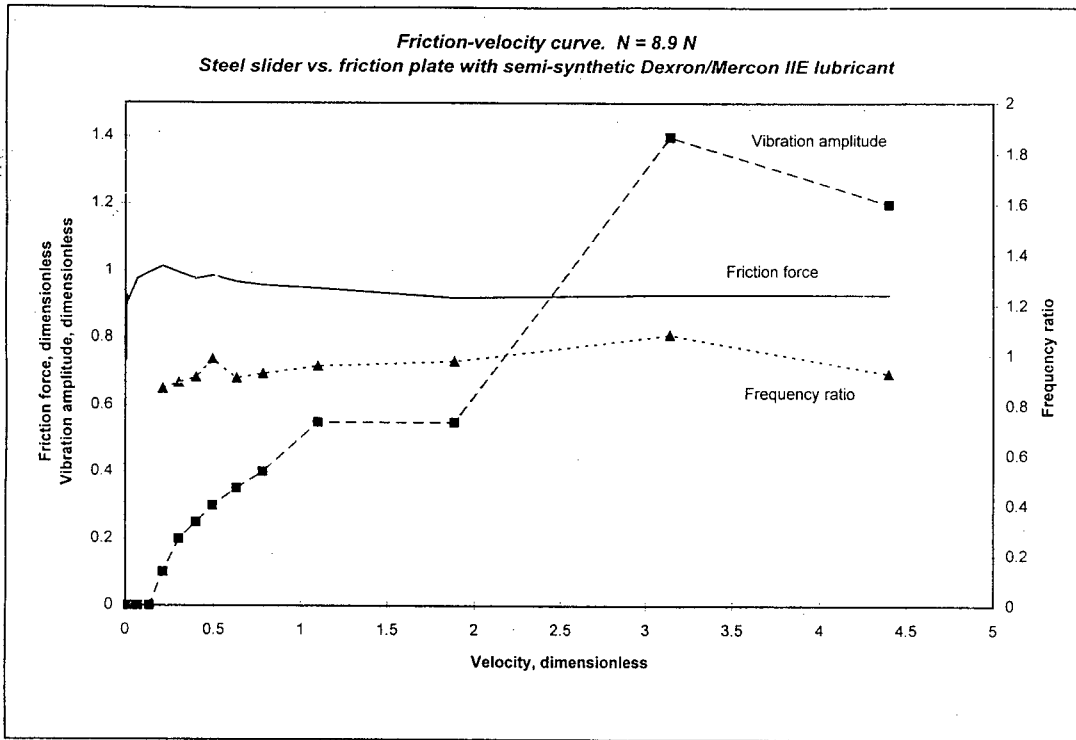
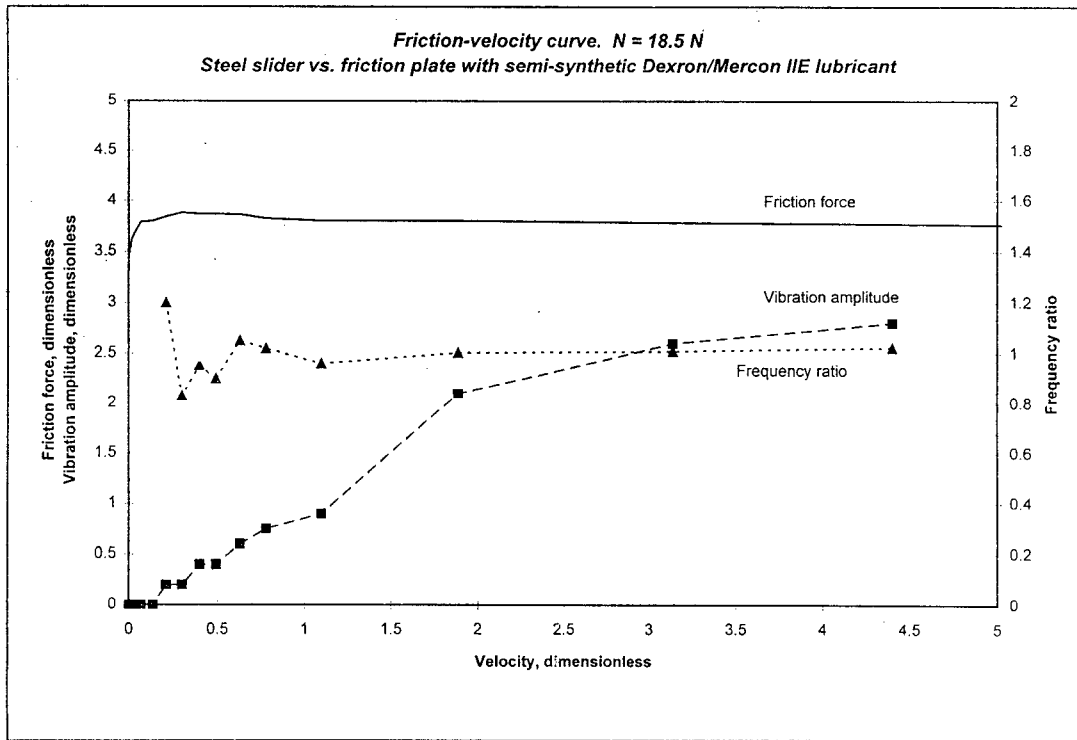


Figure 6.14 Friction vs. time plots at different velocities for slideway lubricant



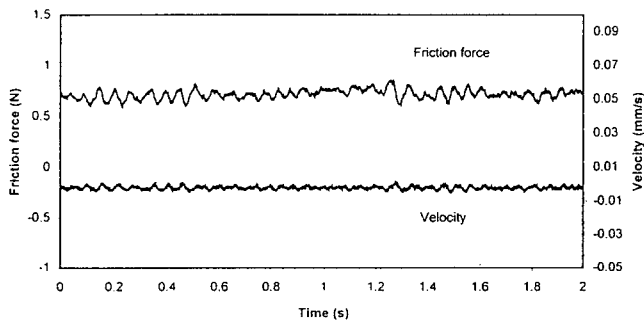
(a) Static normal load: 8.9 N



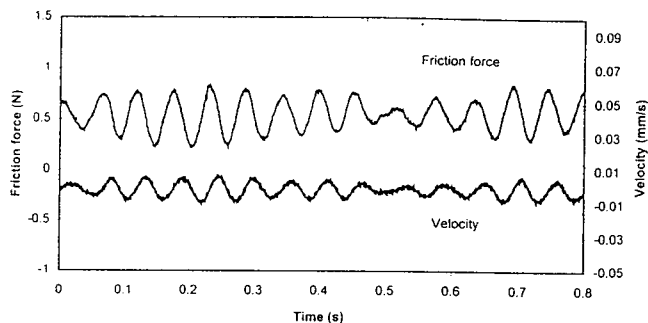
(b) Static normal load: 18.5 N

Figure 6.15 F-V curve, amplitude and frequency of experimental vibrations for friction plate combination

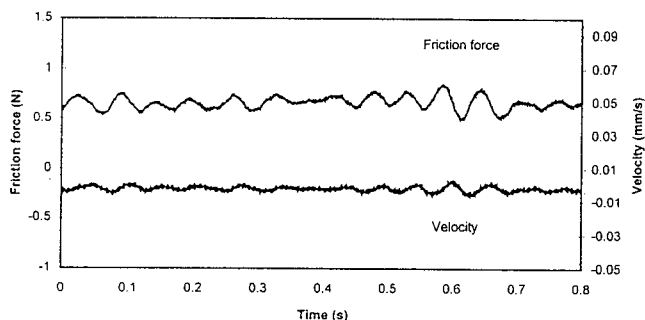
Friction plate vs. steel slider with semi-synthetic Dexron/Mercon IIE
 $V = 5 \text{ mm/s}$. $N = 8.9 \text{ N}$



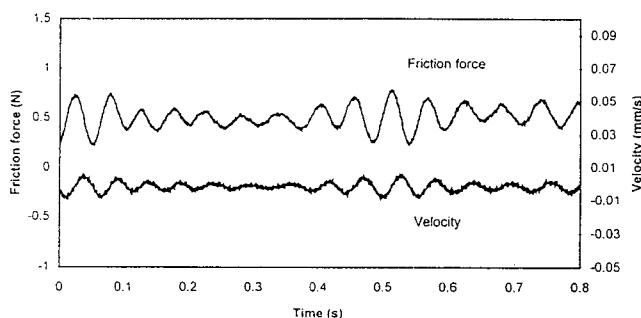
Friction plate vs. steel slider with semi-synthetic Dexron/Mercon IIE
 $V = 18.3 \text{ mm/s}$. $N = 8.9 \text{ N}$



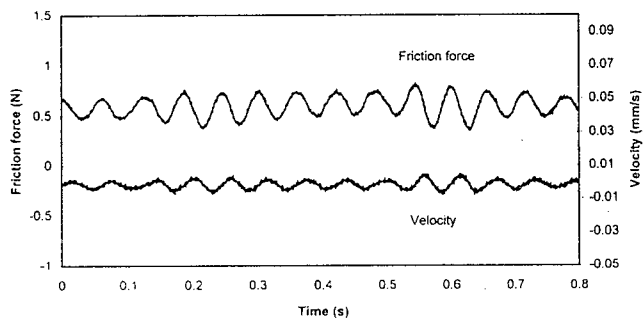
Friction plate vs. steel slider with semi-synthetic Dexron/Mercon IIE
 $V = 8.2 \text{ mm/s}$. $N = 8.9 \text{ N}$



Friction plate vs. steel slider with semi-synthetic Dexron/Mercon IIE
 $V = 31.4 \text{ mm/s}$. $N = 8.9 \text{ N}$



Friction plate vs. steel slider with semi-synthetic Dexron/Mercon IIE
 $V = 10.5 \text{ mm/s}$. $N = 8.9 \text{ N}$



Friction plate vs. steel slider with semi-synthetic Dexron/Mercon IIE
 $V = 73.3 \text{ mm/s}$. $N = 8.9 \text{ N}$

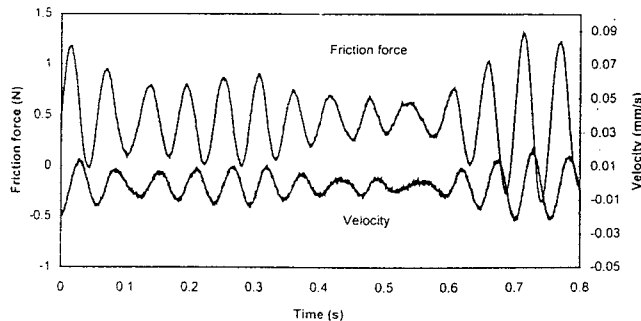


Figure 6.16.

Friction vs. time plots at different velocities for friction plate combination. Static normal load of 8.9 N

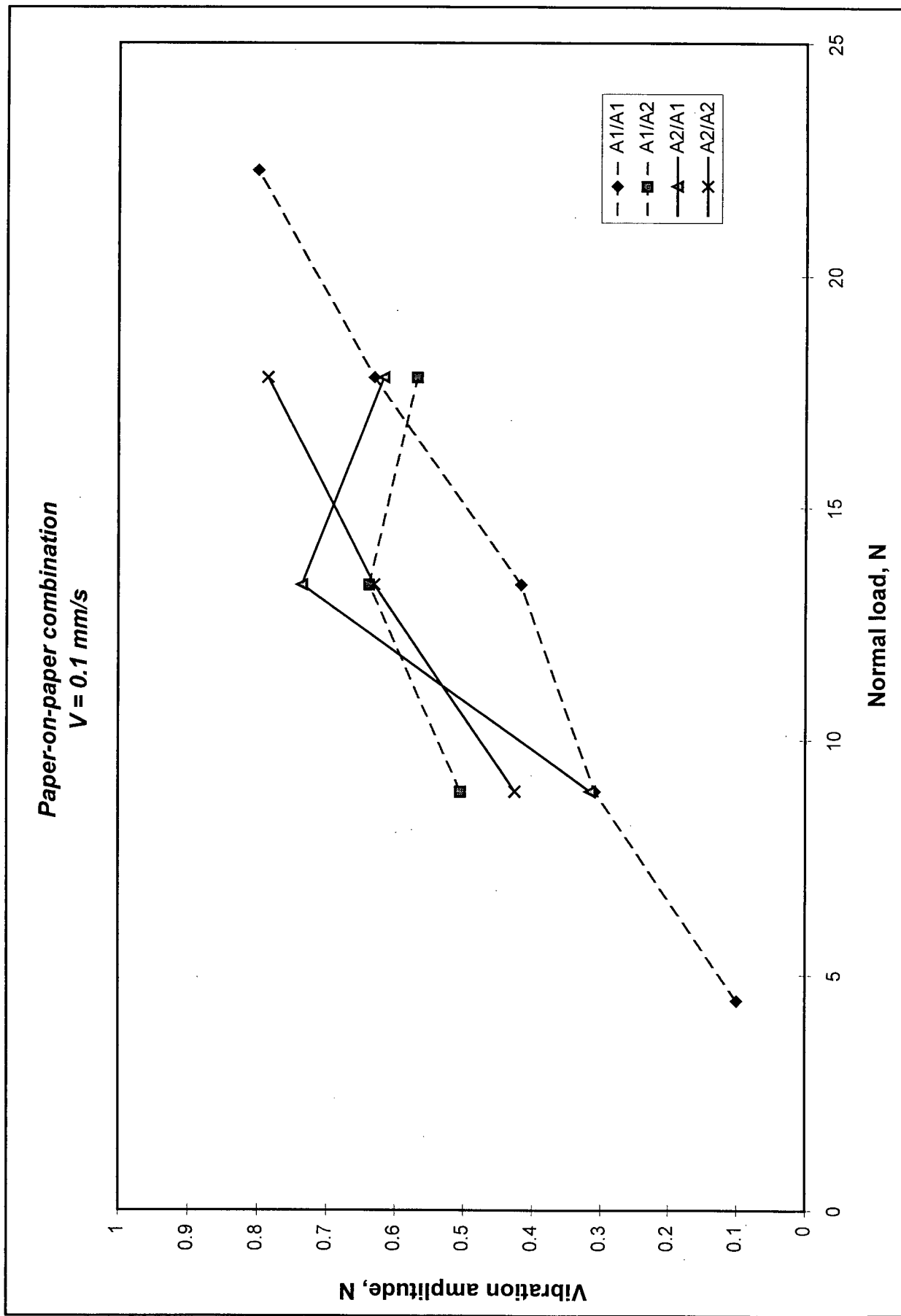


Figure 6.17. Effect of the normal load on the vibration amplitude for the paper-on-paper combinations

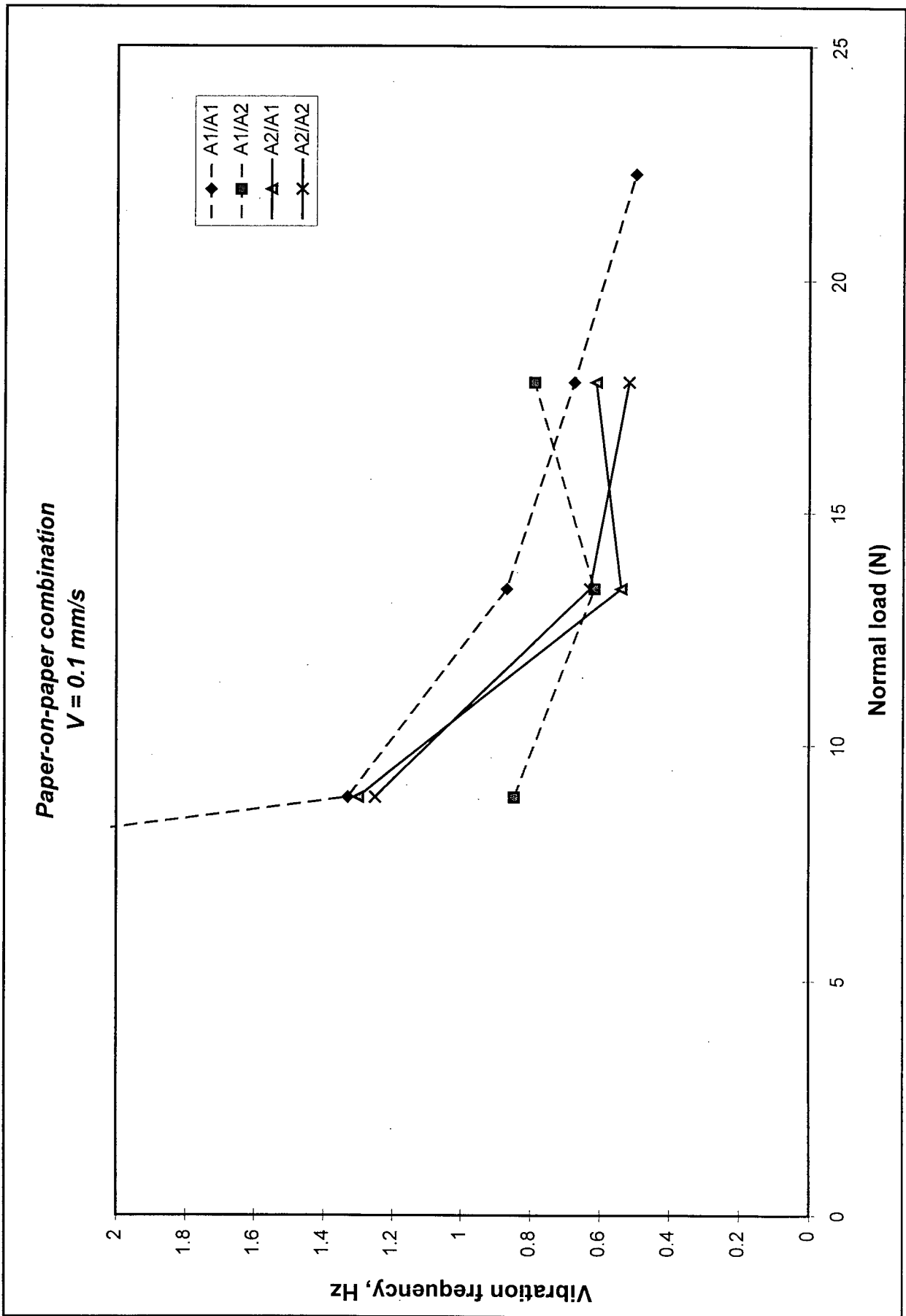


Figure 6.18. Effect of the normal load on the vibration frequency for the paper-on-paper combinations

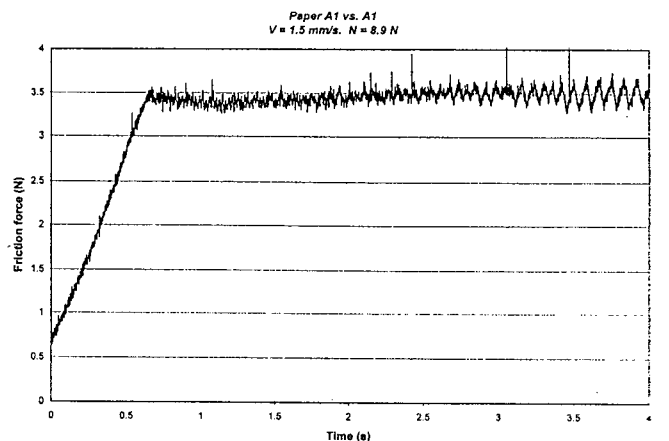
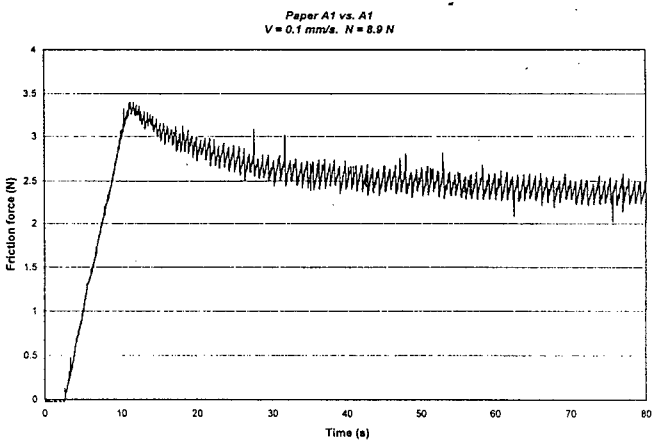
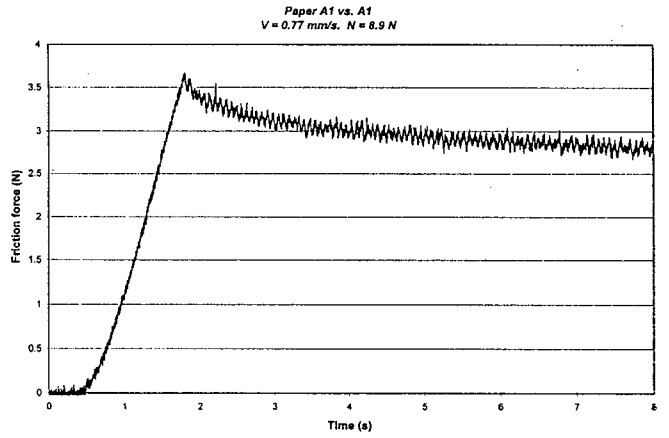
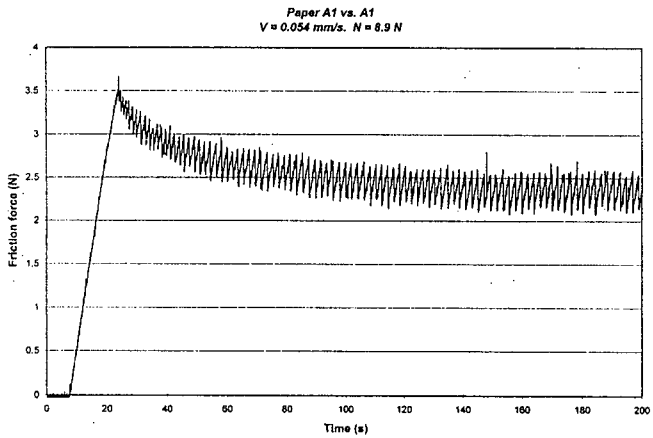
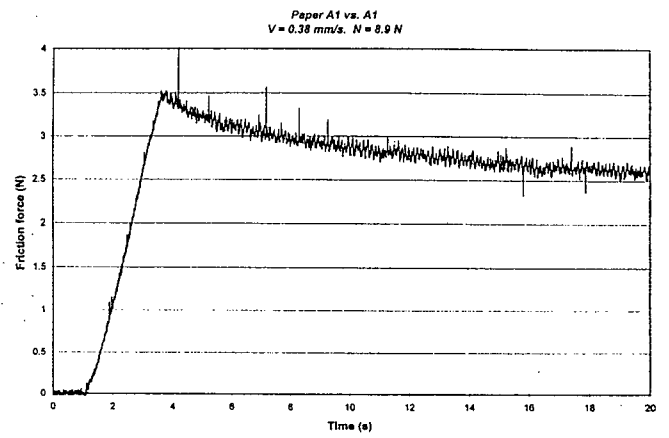
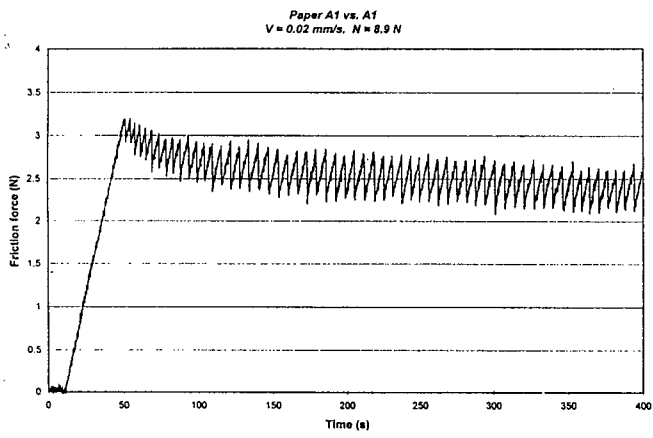


Figure 6.19.(a) Friction vs. time plots at different velocities for same paper-on-paper combination: A₁ vs. A₁

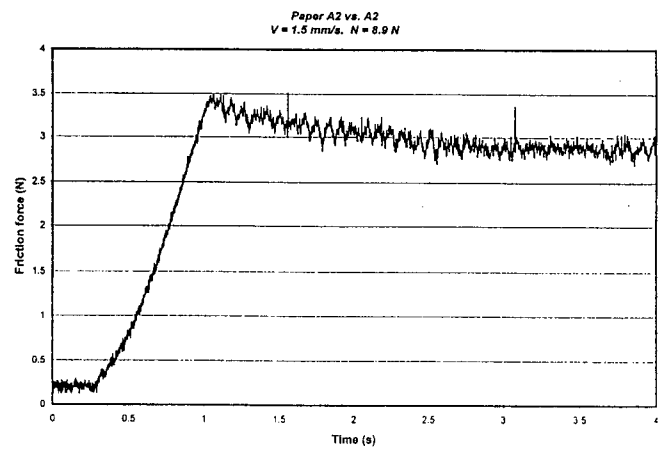
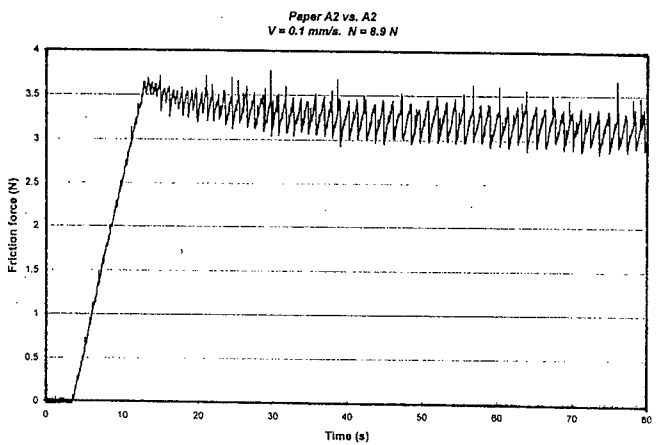
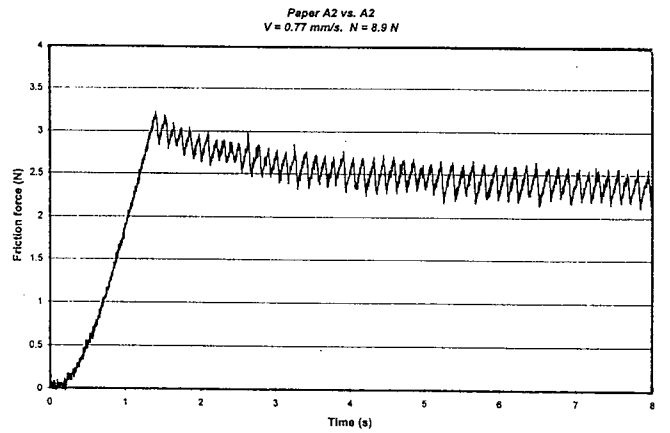
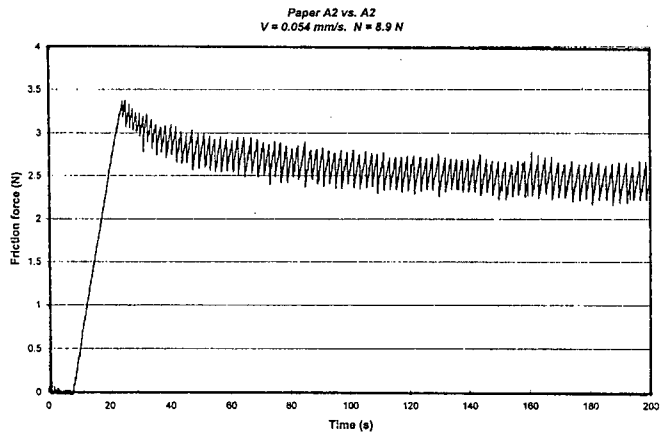
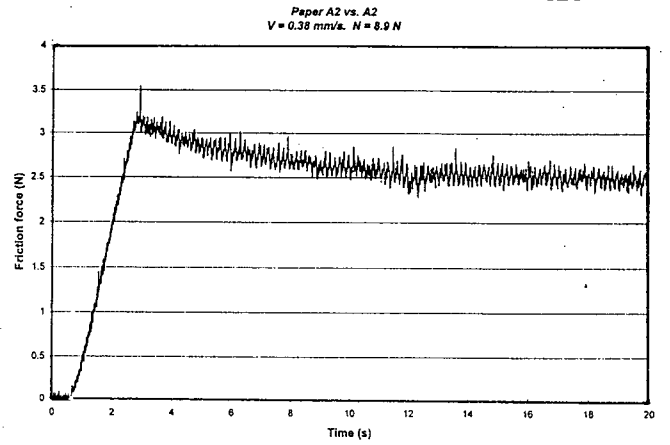
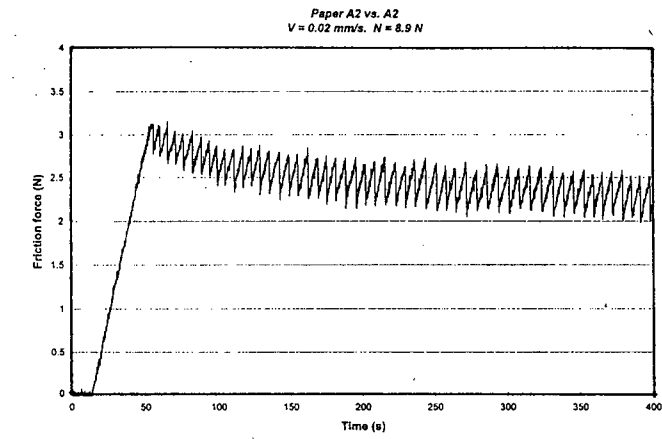


Figure 6.19.(b)

Friction vs. time plots at different velocities for same paper-on-paper combination: A_2 vs. A_2

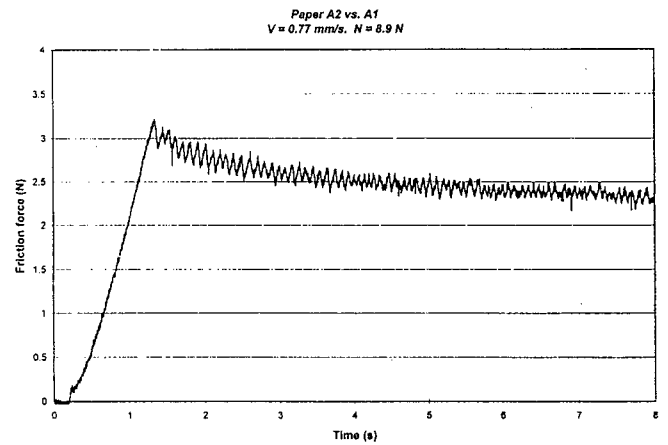
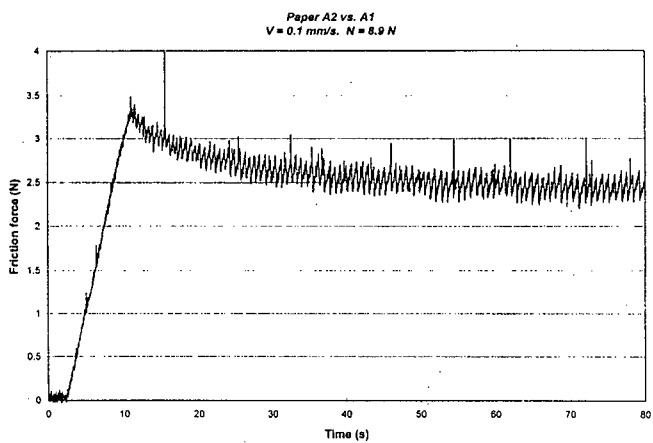
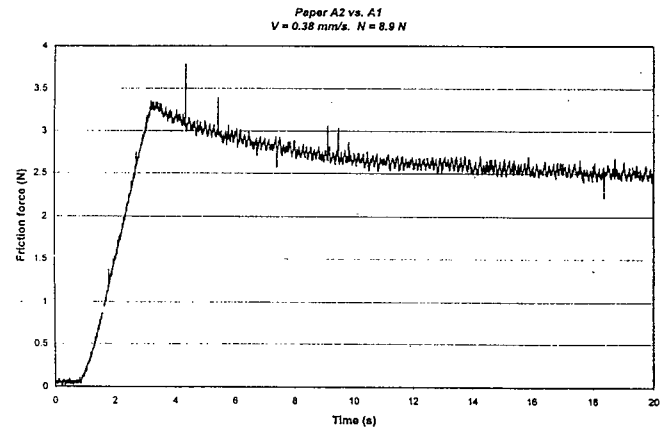
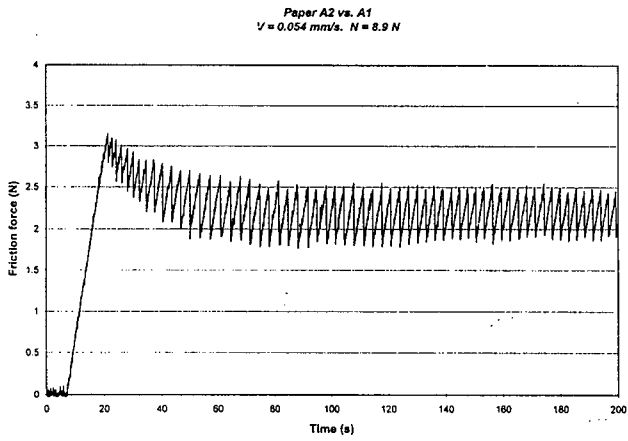
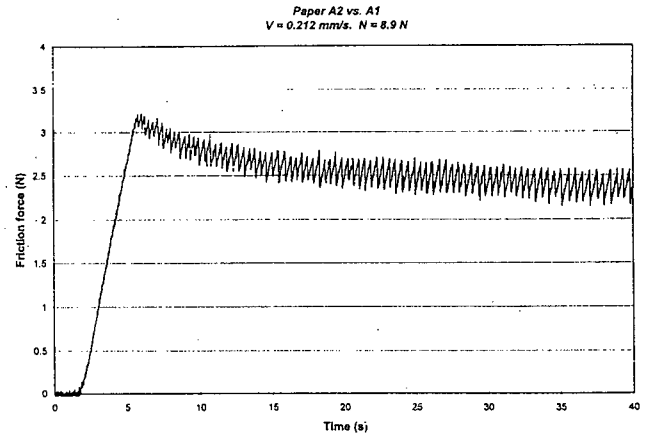
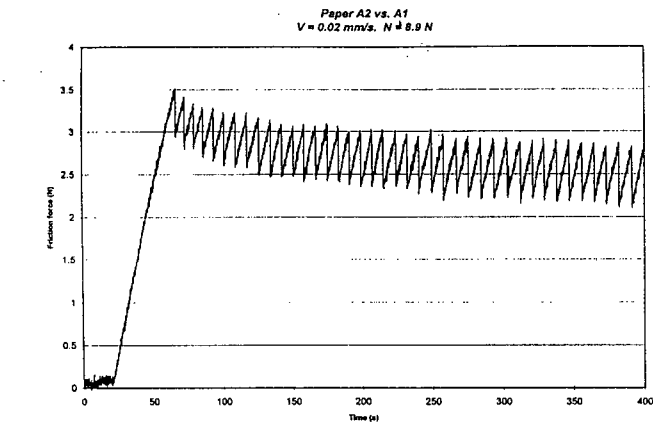


Figure 6.20.(a)

Friction vs. time plots at different velocities for different paper-on-paper combination: A₂ vs. A₁

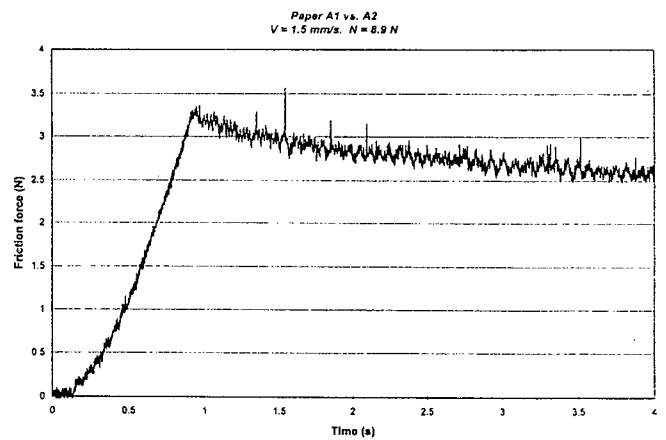
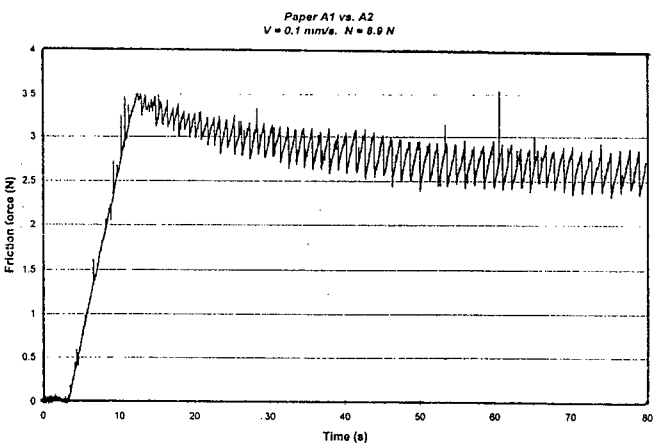
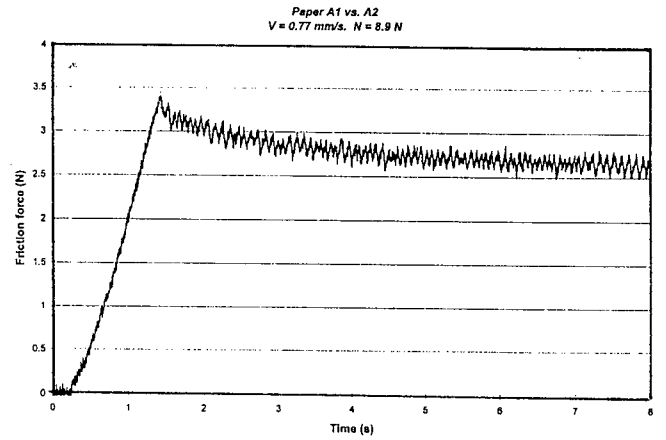
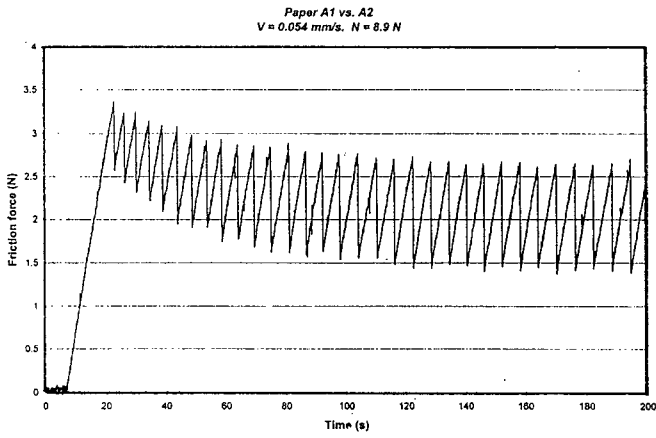
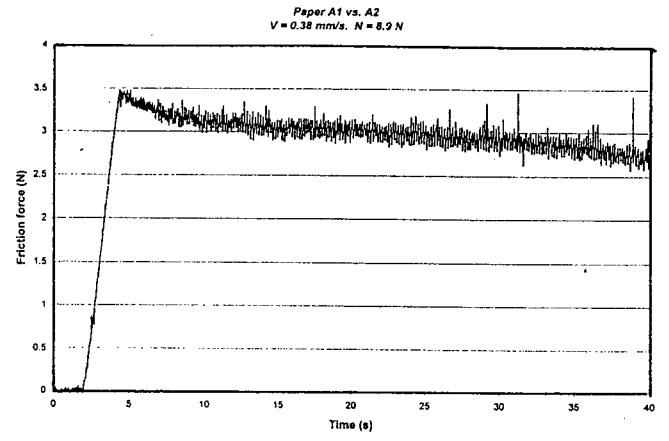
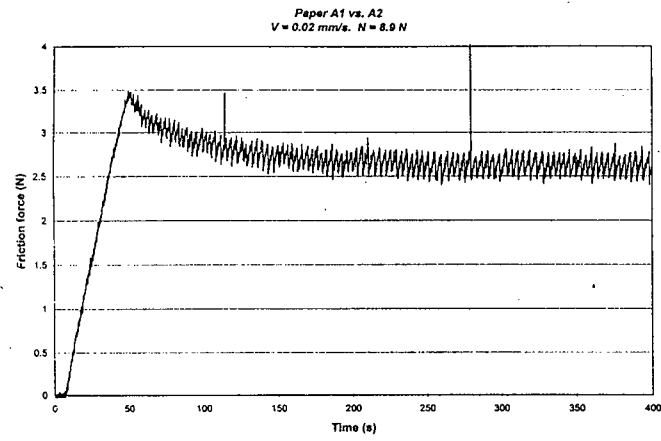


Figure 6.20.(b)

Friction vs. time plots at different velocities for same paper-on-paper combination: A₁ vs. A₂

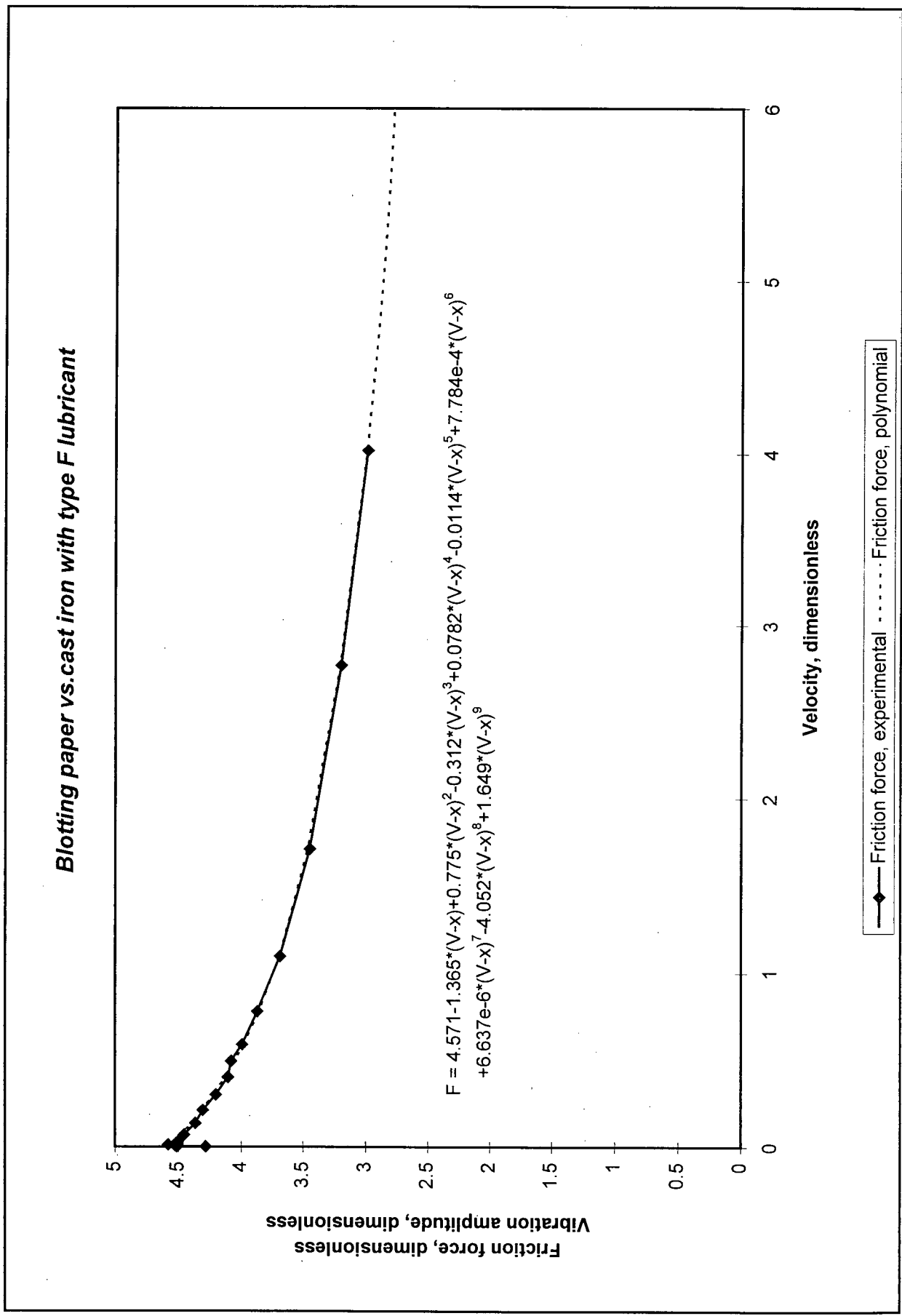


Figure 6.21. Experimental and polynomial fitted F-V curves for blotting paper combination with type F lubricant

Blotting paper vs. cast iron with semi-synthetic Dexron/Mercon IIE lubricant

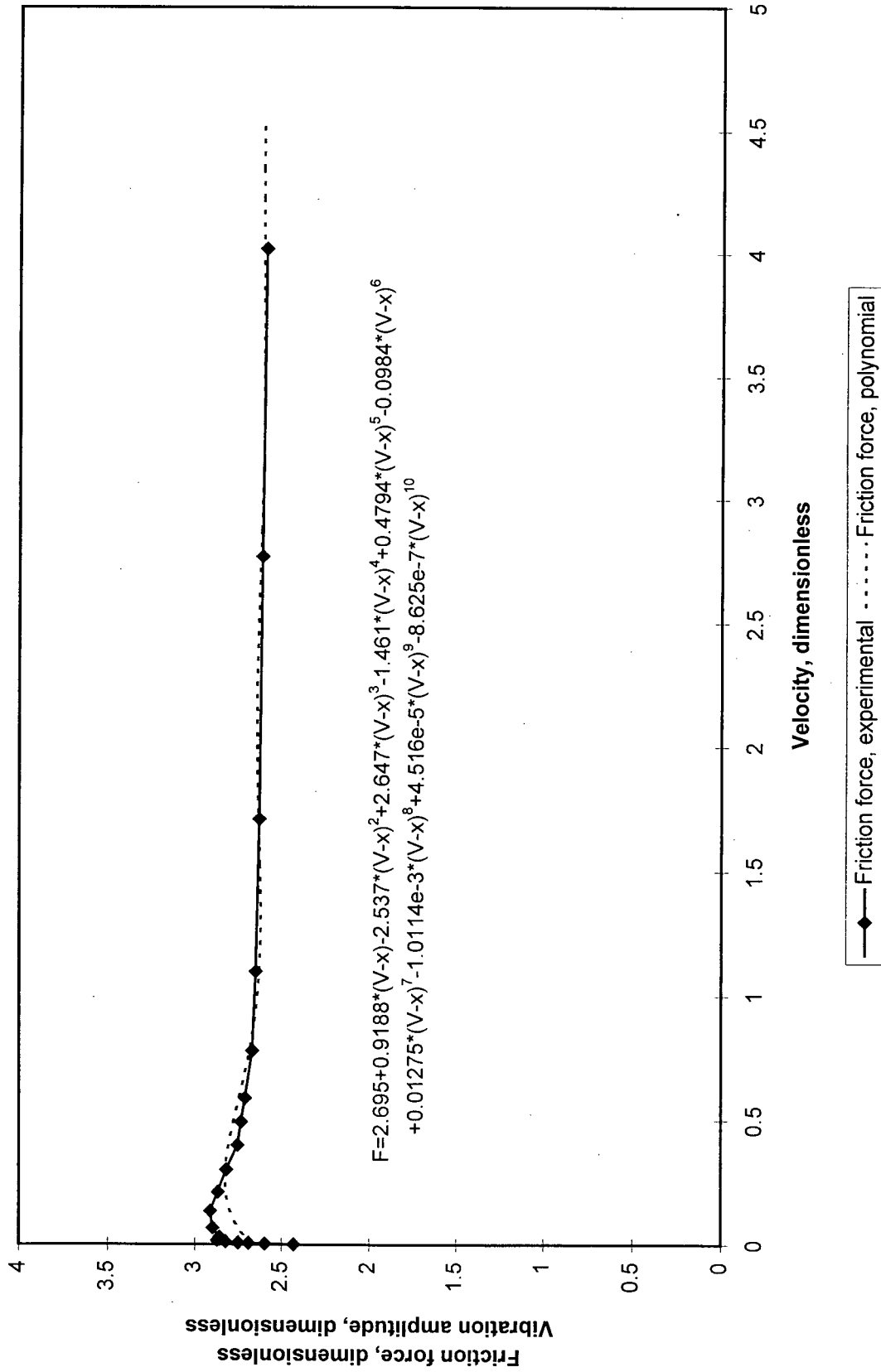


Figure 6.22. Experimental and polynomial fitted F-V curves for blotting paper combination with semi-synthetic Dexron/Mercon IIE lubricant

Blotting paper vs. cast iron with slideway lubricant

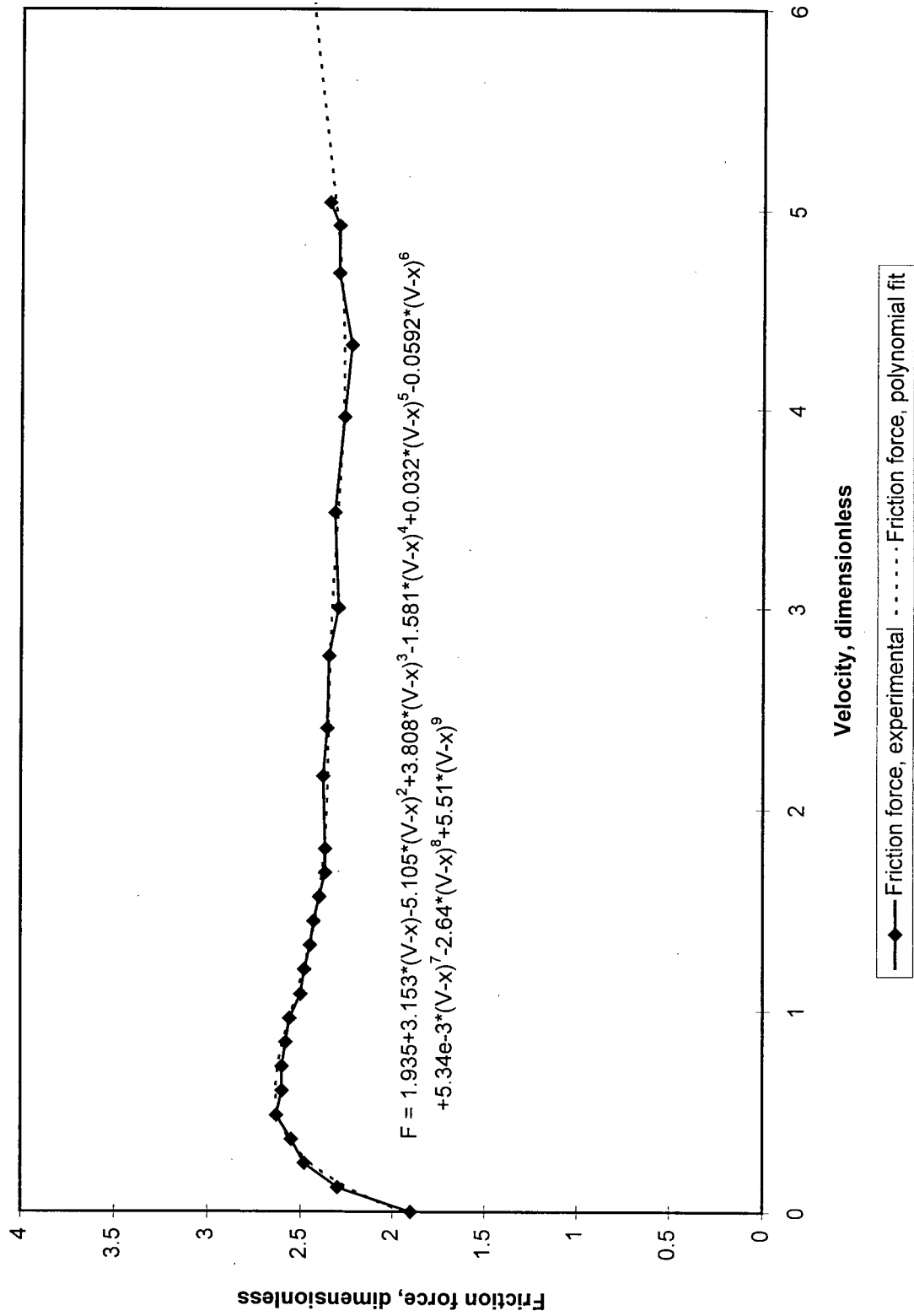


Figure 6.23. Experimental and polynomial fitted F-V curves for blotting paper combination with slideway lubricant

Steel slider vs. friction plate with semi-synthetic Dexron/Mercon IIE lubricant

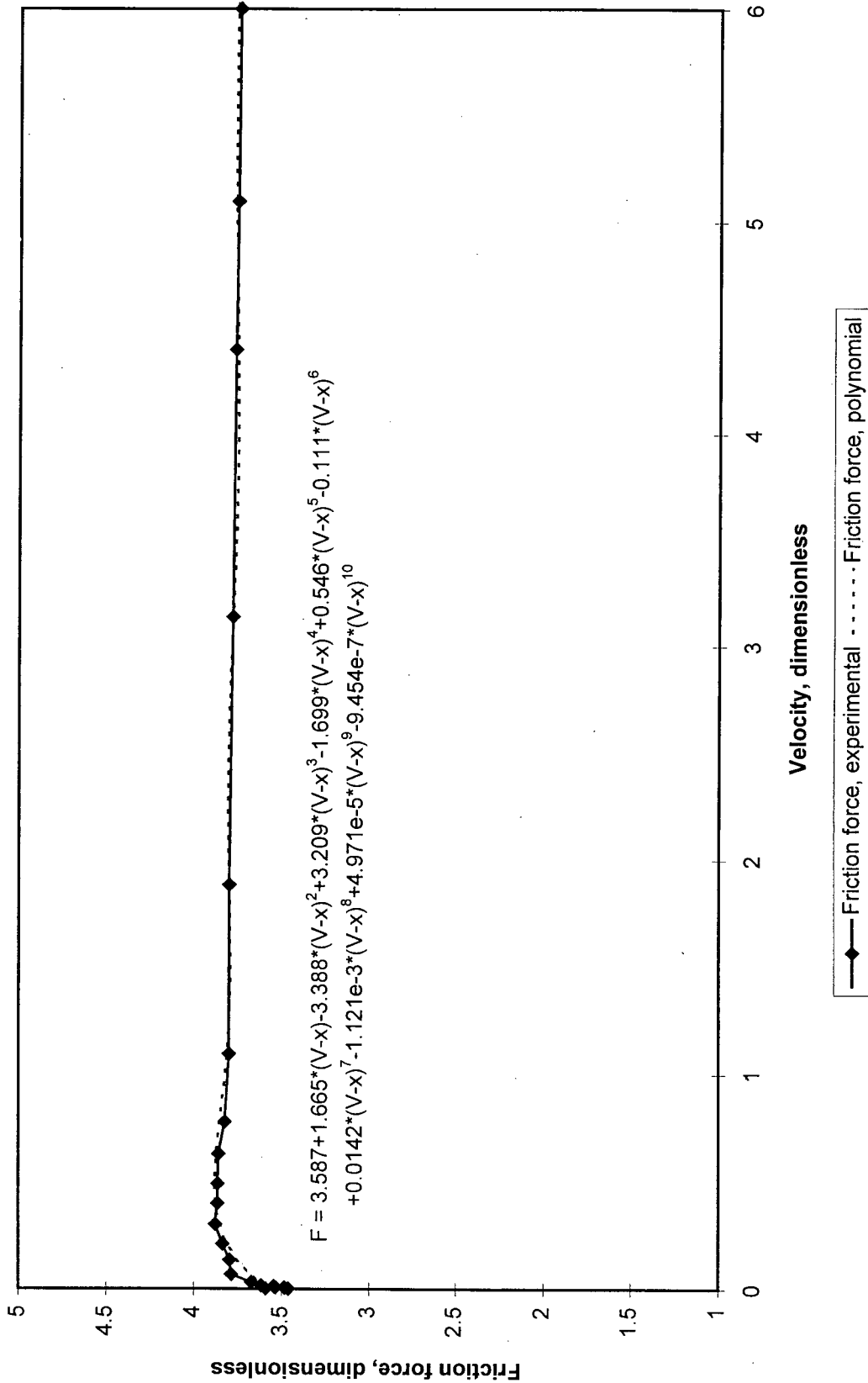


Figure 6.24. Experimental and polynomial fitted F-V curves for friction plate combination with semi-synthetic Dexron/Mercon IIE lubricant

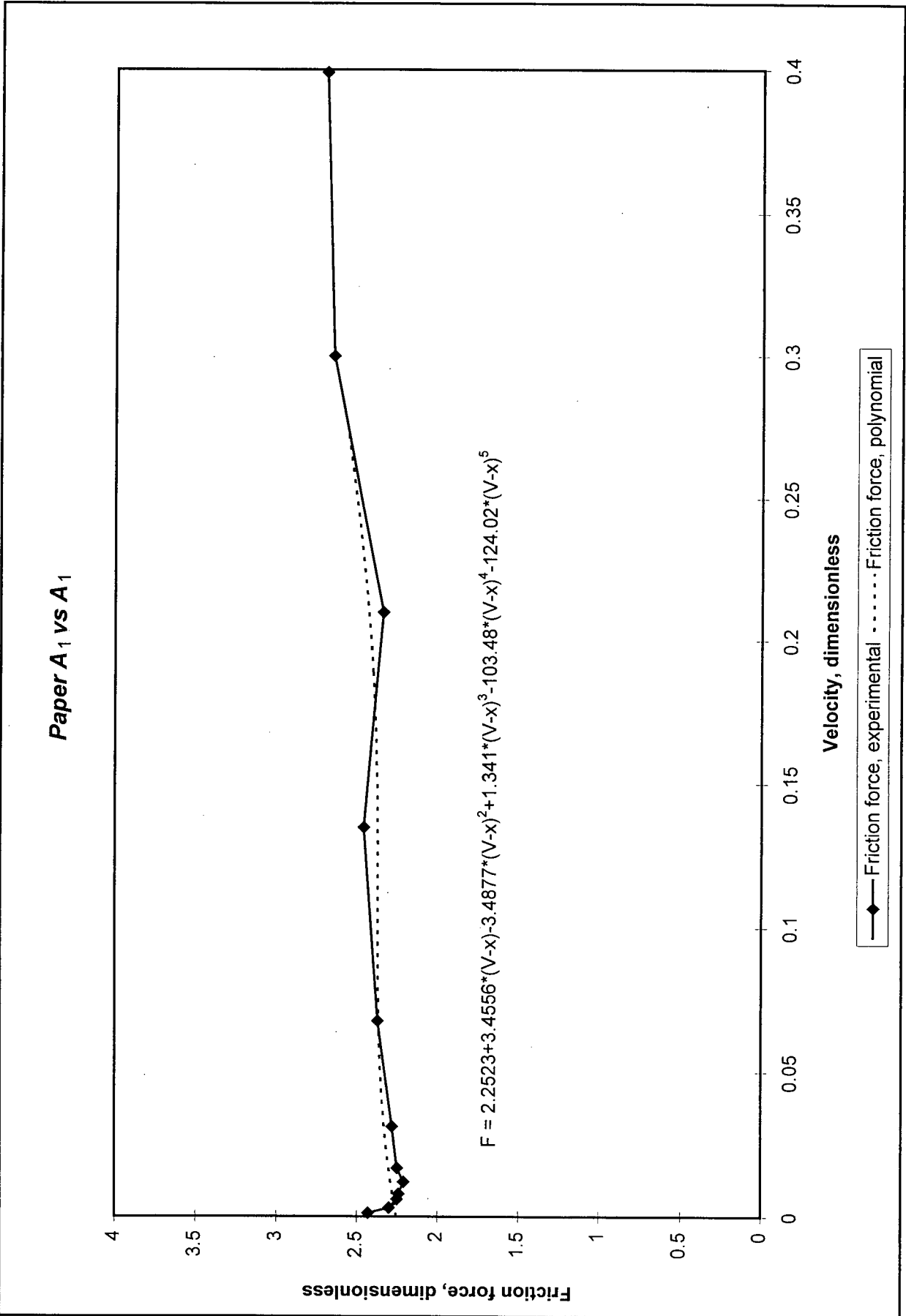


Figure 6.25. Experimental and polynomial fitted F-V curves for A₁ vs. A₁ paper-on-paper combination

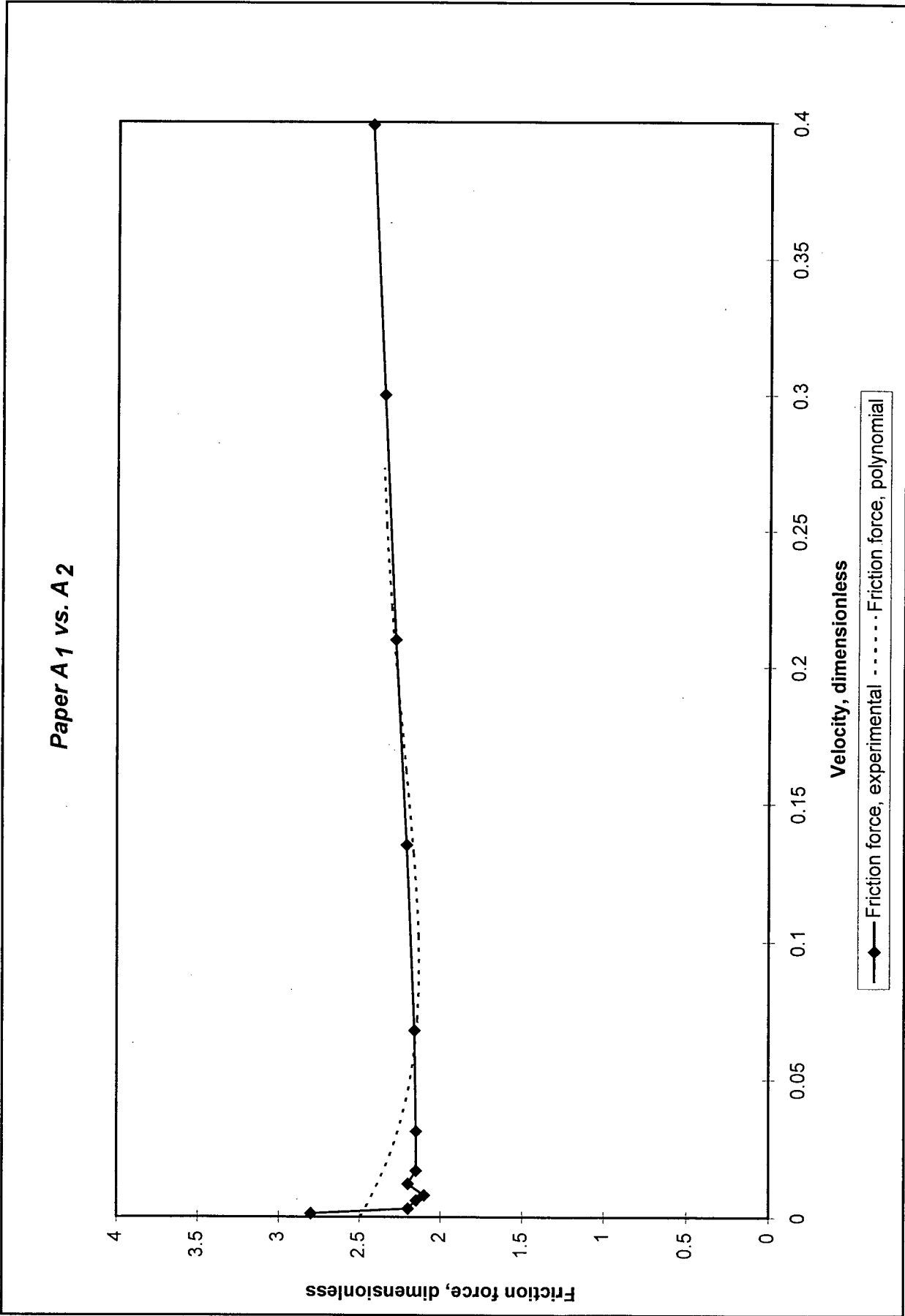


Figure 6.26. Experimental and polynomial fitted F-V curves for A2 vs. A1 paper-on-paper combination

Blotting paper vs. cast iron with semi-synthetic Dexron/Mercon IIE lubricant
Autonomous system

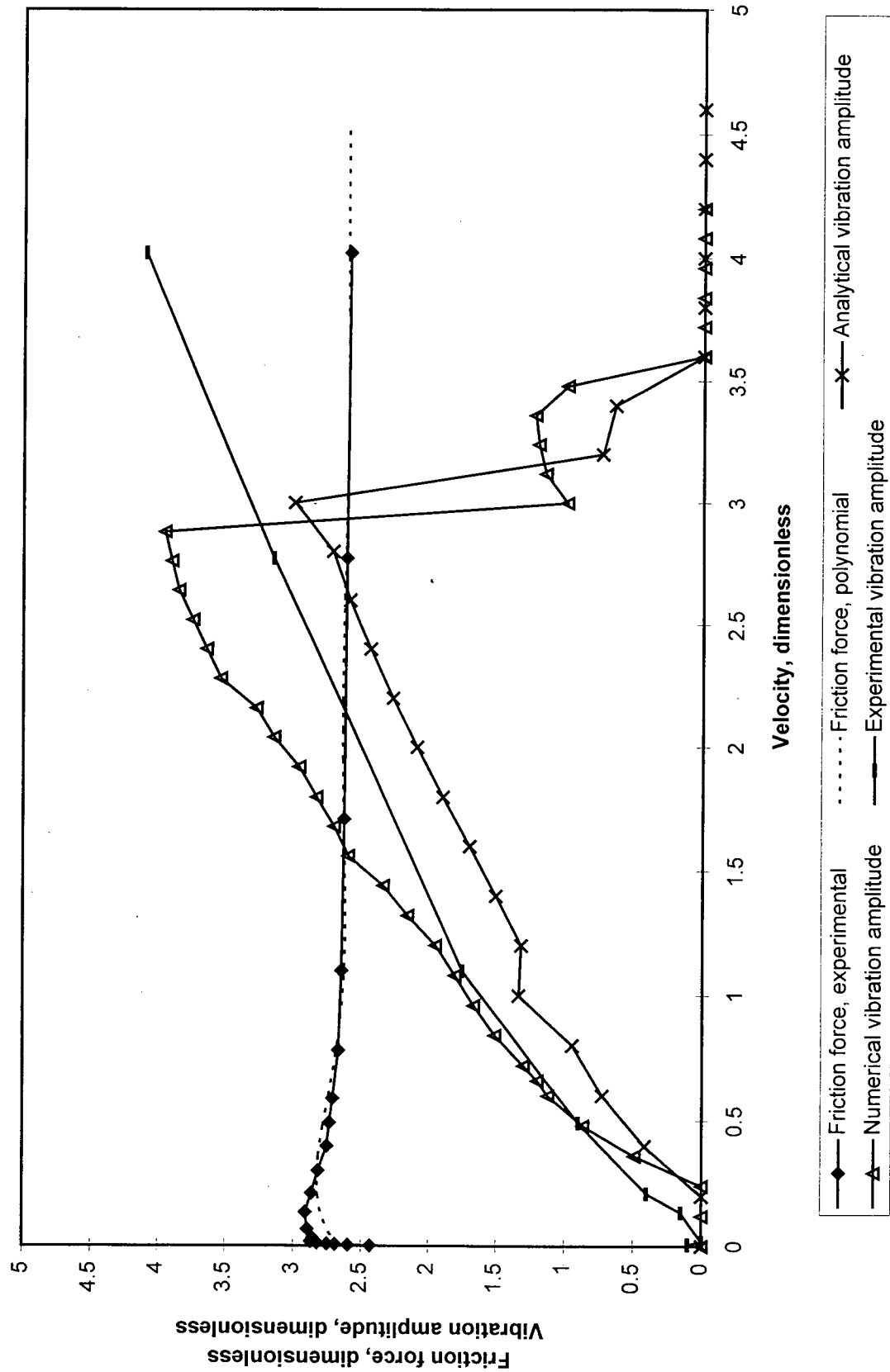


Figure 7.1. Experimental, analytical and numerical vibration amplitudes for blotting paper combination with semi-synthetic Dexron/Mercon IIE

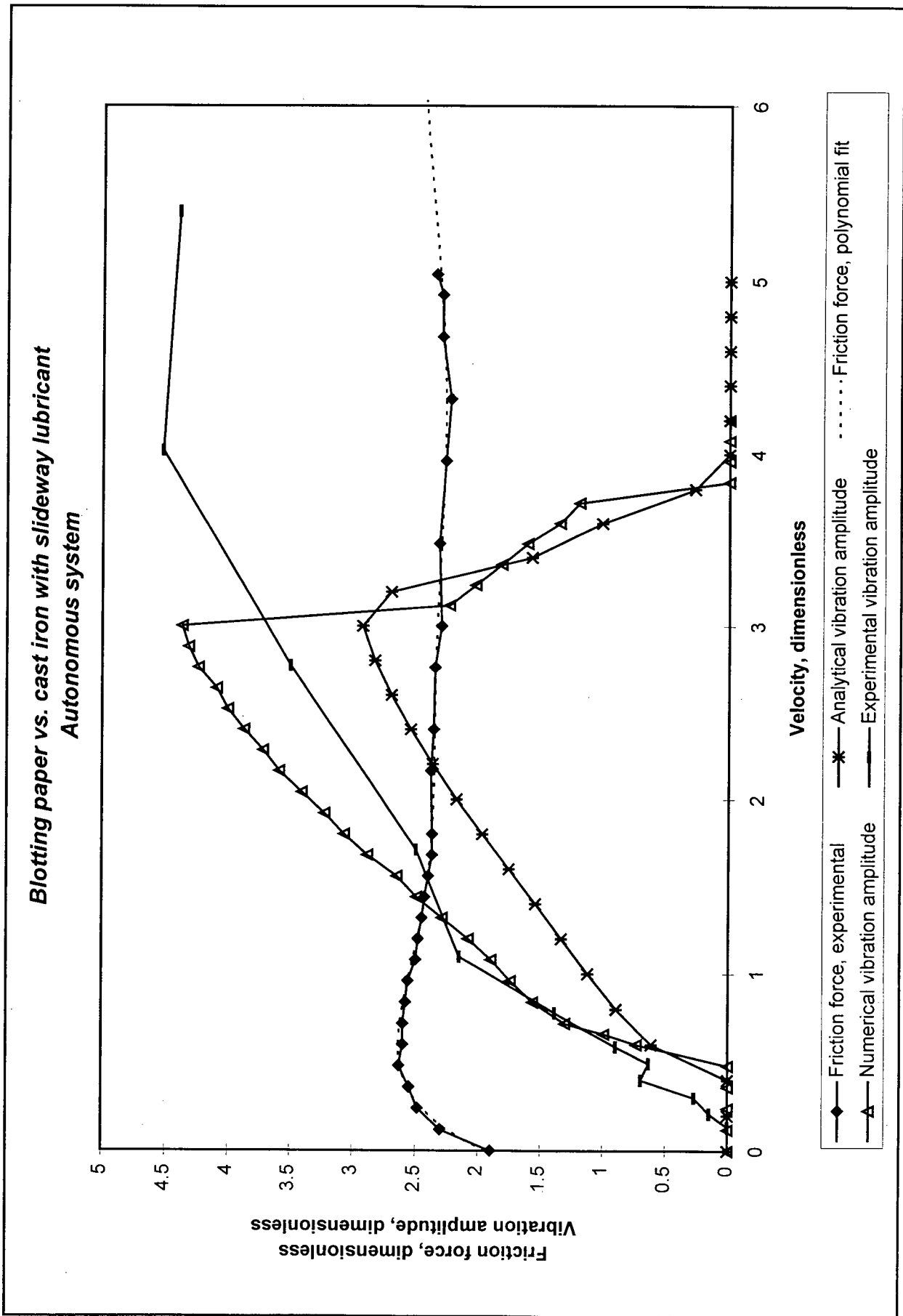


Figure 7.2. Experimental, analytical and numerical vibration amplitudes for blotting paper combination with sideway lubricant

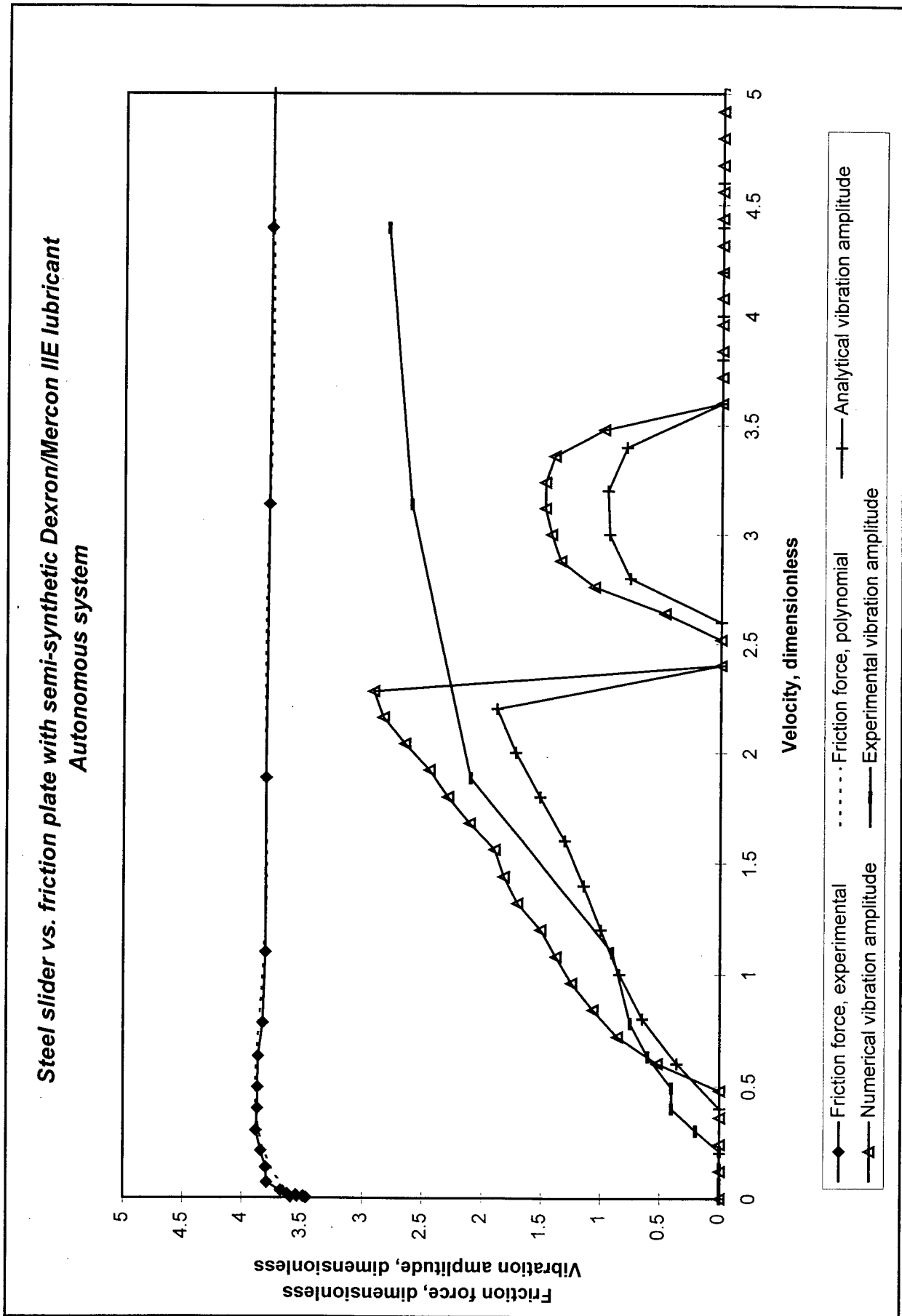


Figure 7.3. Experimental, analytical and numerical vibration amplitudes for friction plate combination with semi-synthetic Dexron/Mercon IIE

Blotting paper vs. cast iron with type F lubricant
Autonomous system

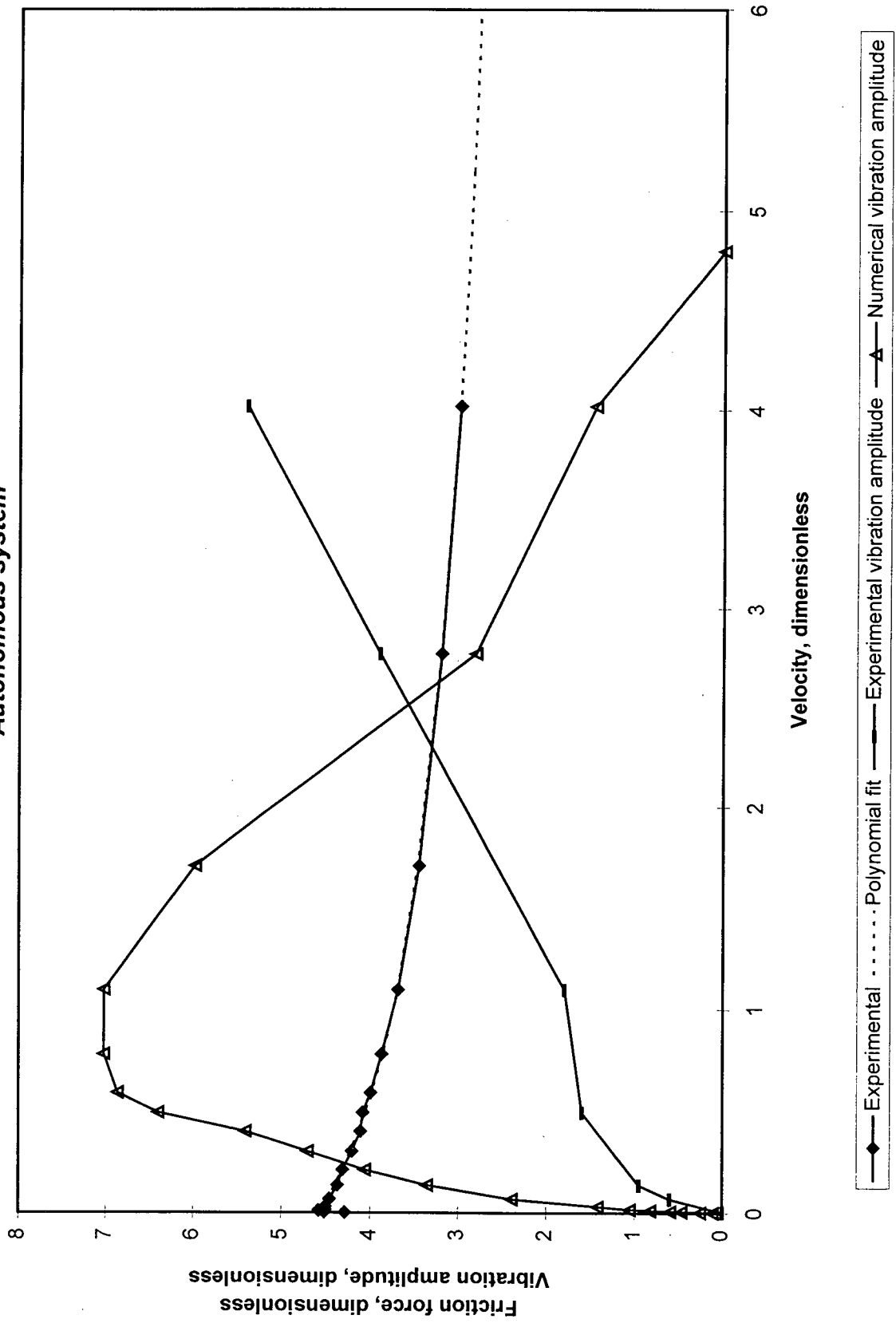


Figure 7.4. Experimental, analytical and numerical vibration amplitudes for blotting paper combination with type F lubricant

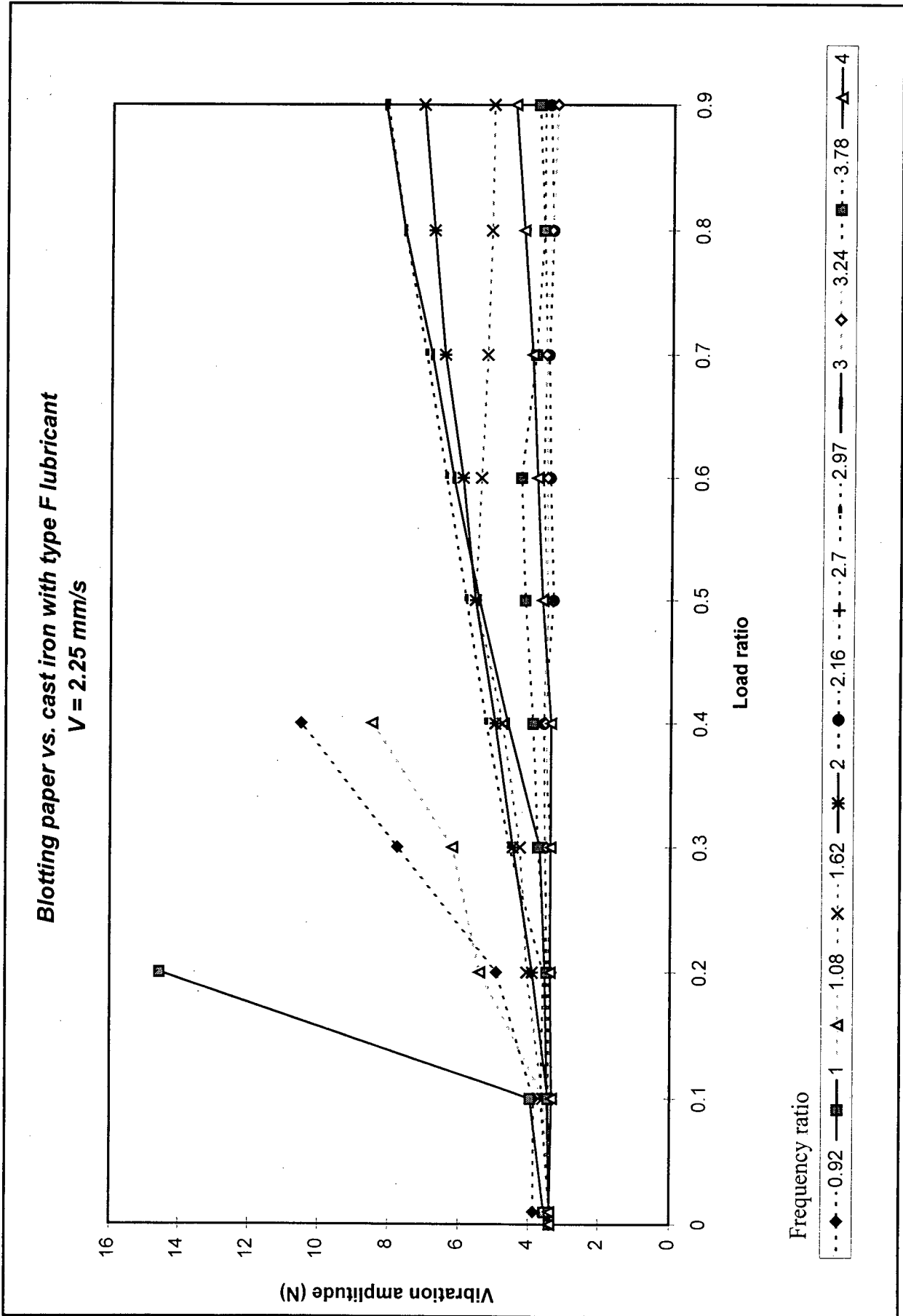
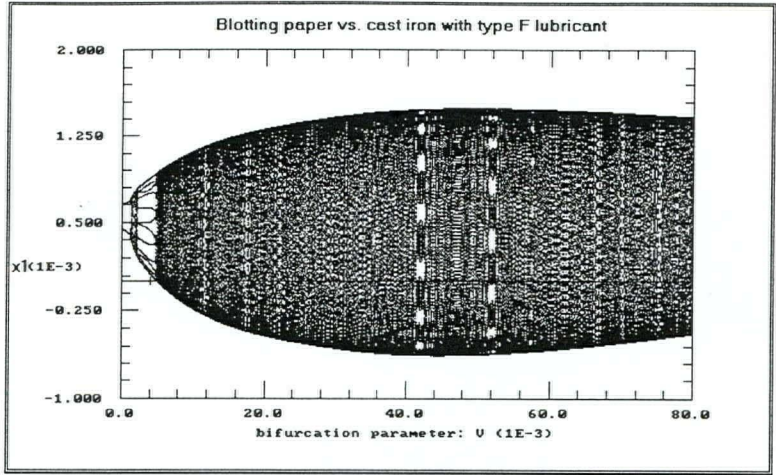
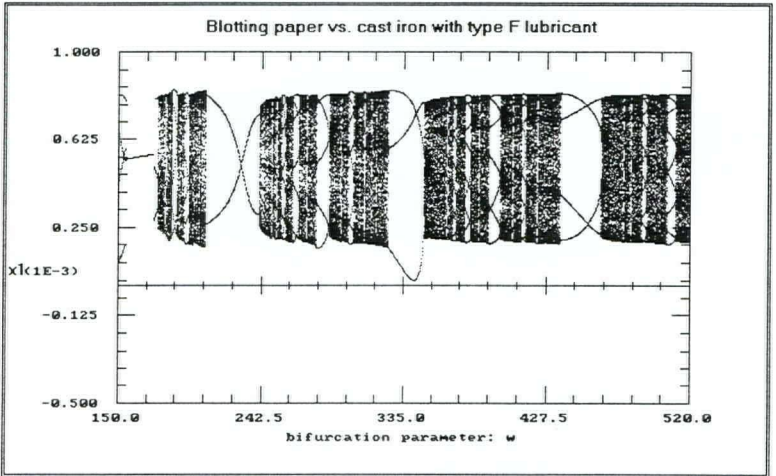


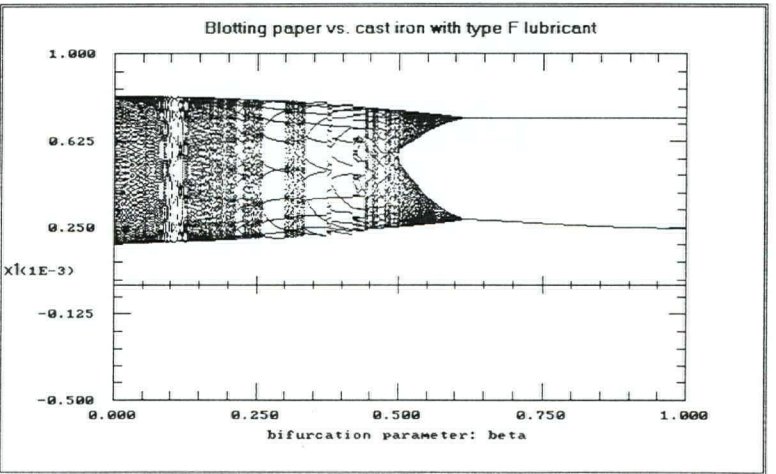
Figure 8.1. Effect of the load and frequency ratios on numerical vibration amplitude.
 Blotting paper combination with type F lubricant



(a) Bifurcation diagram for the parameter V

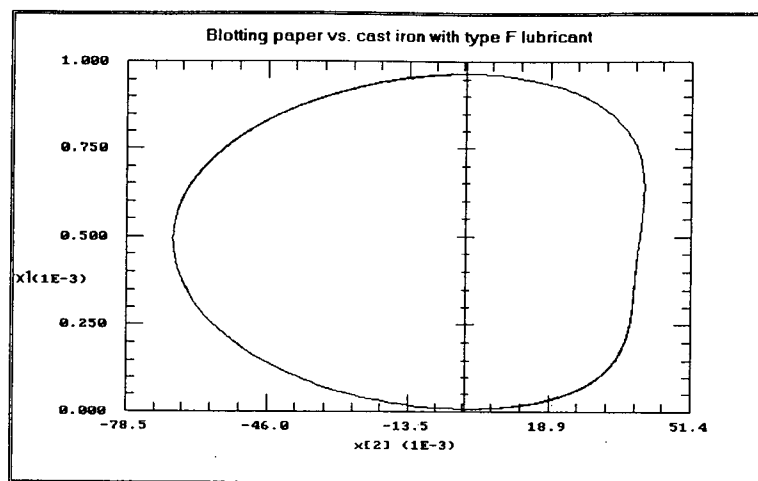


(b) Bifurcation diagram for the parameter α

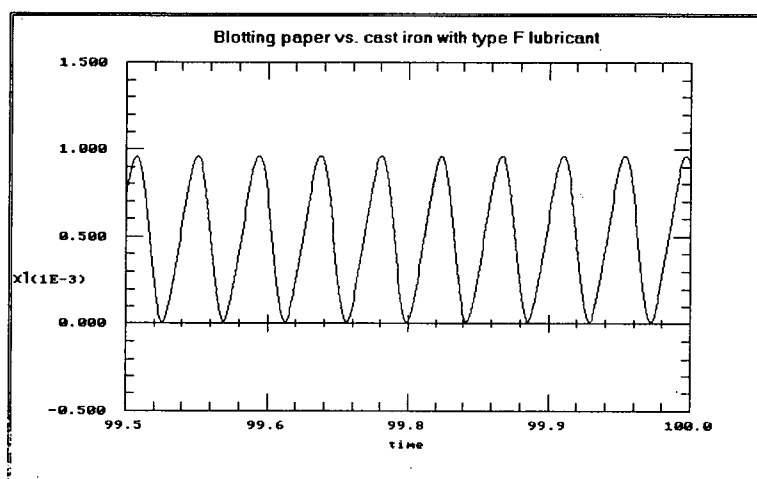


(c) Bifurcation diagram for the parameter β

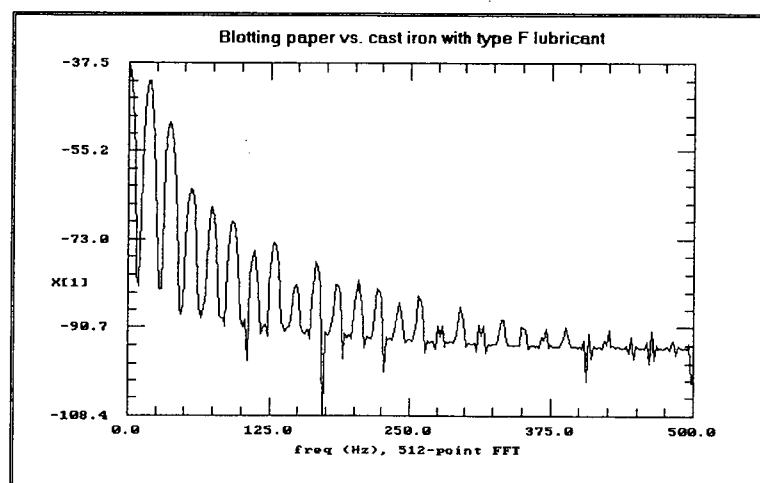
Figure 8.2 Bifurcation diagrams for the type F combination



(a) Phase-plane plot

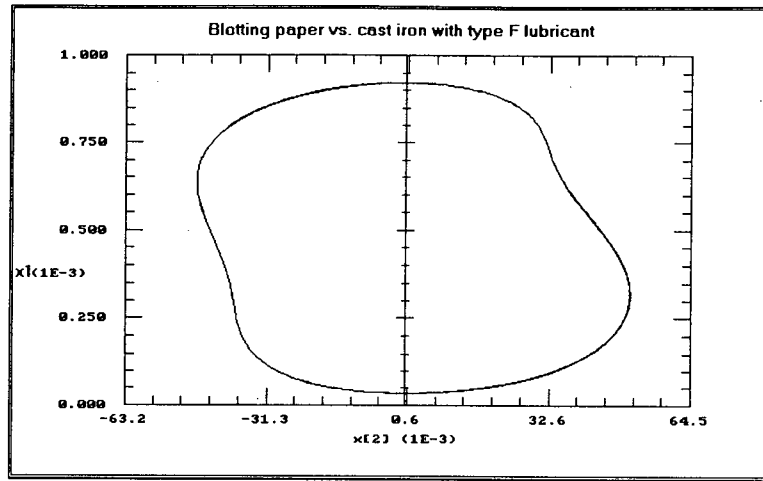


(b) Time series

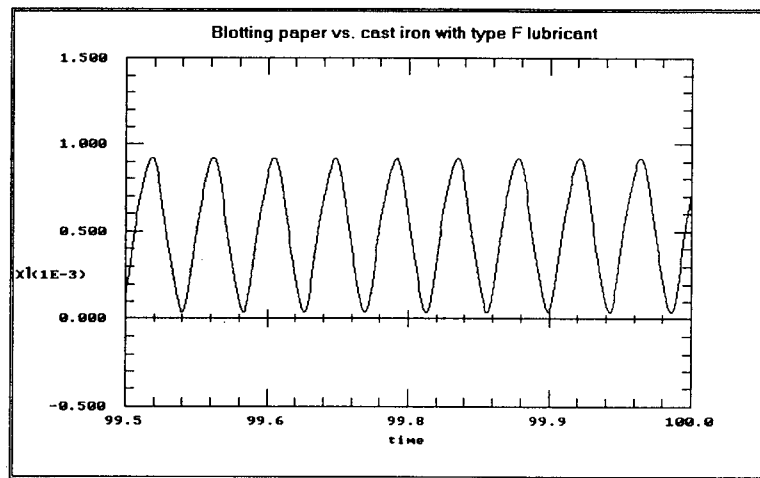


(c) Frequency spectrum

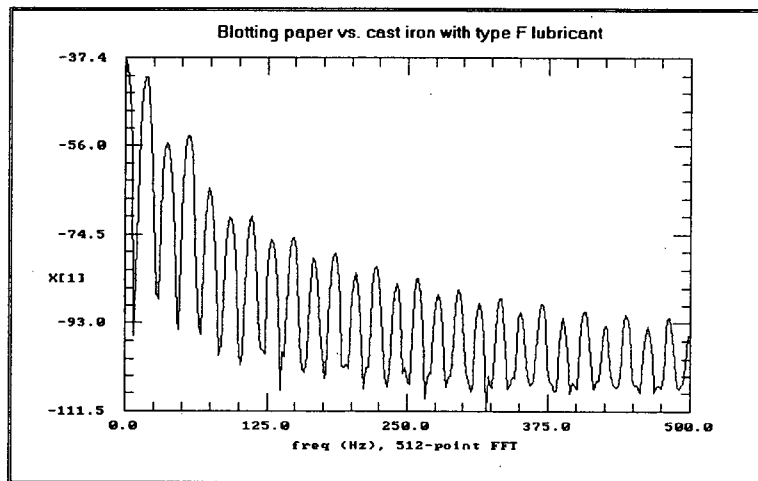
Figure 8.3 Subharmonic entrainment of order 2 with type F lubricant combination



(a) Phase-plane plot

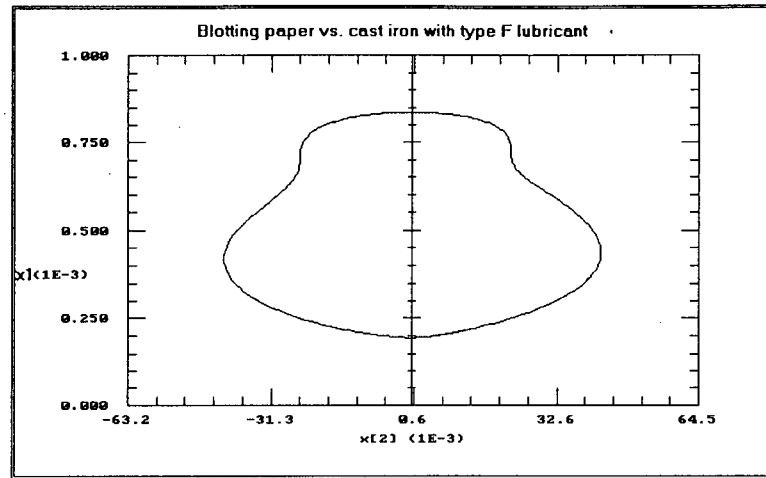


(b) Time series

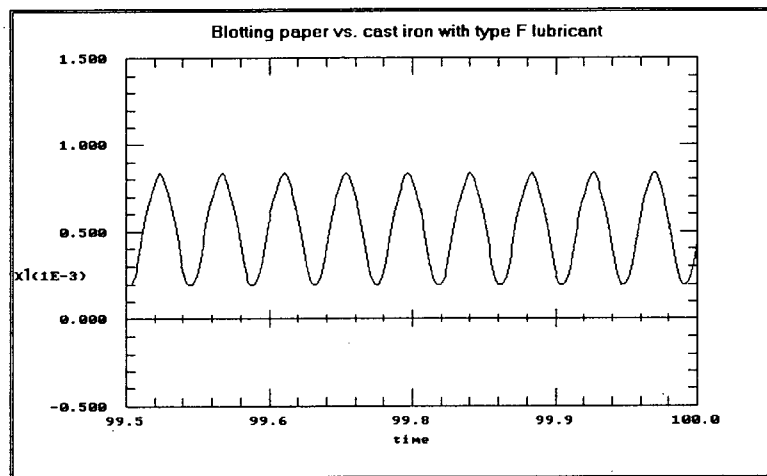


(c) Frequency spectrum

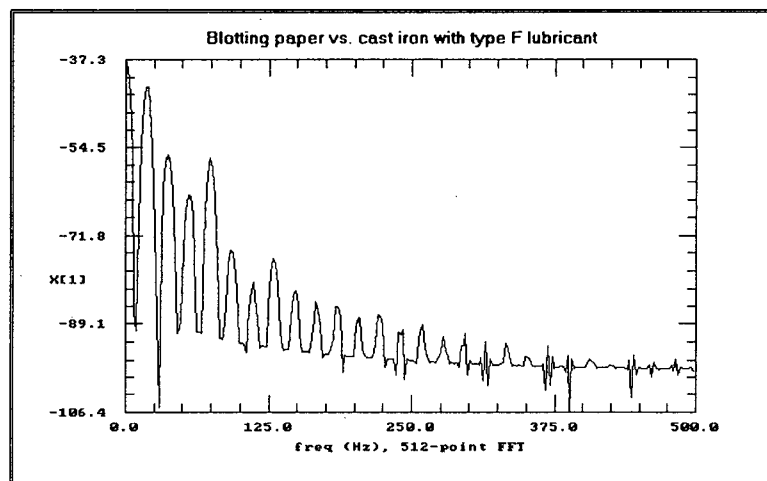
Figure 8.4 Subharmonic entrainment of order 3 with type F lubricant combination



(a) Phase-plane plot

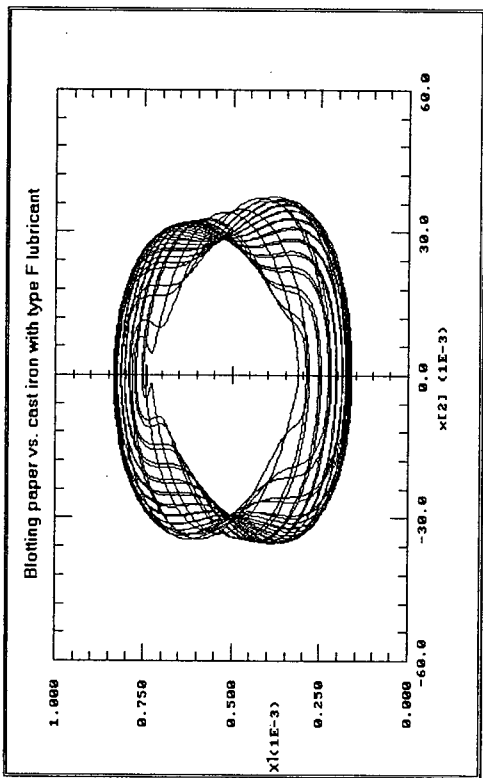


(b) Time series

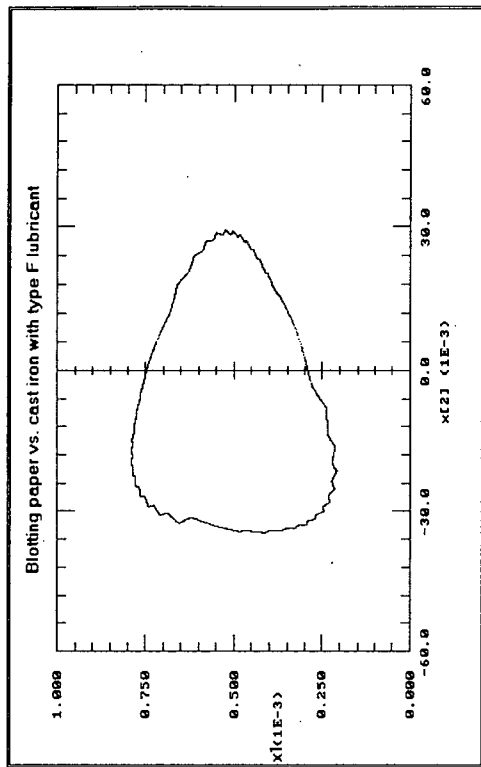


(c) Frequency spectrum

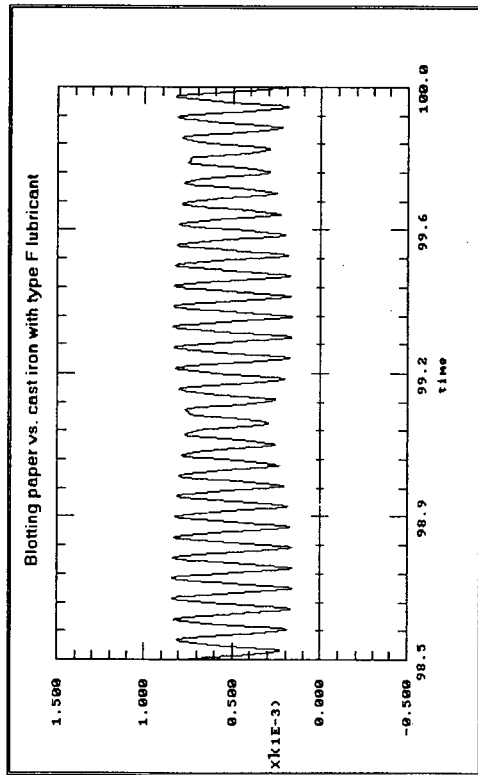
Figure 8.5 Subharmonic entrainment of order 4 with type F lubricant combination



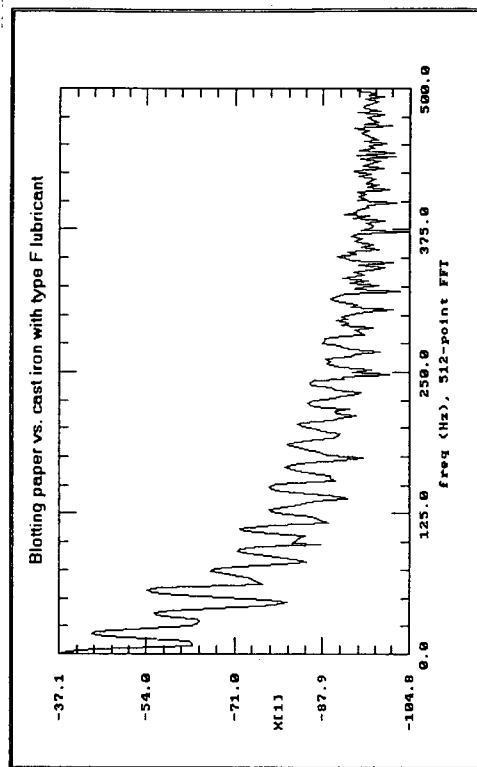
(a) Phase-plane plot



(b) Poincaré section

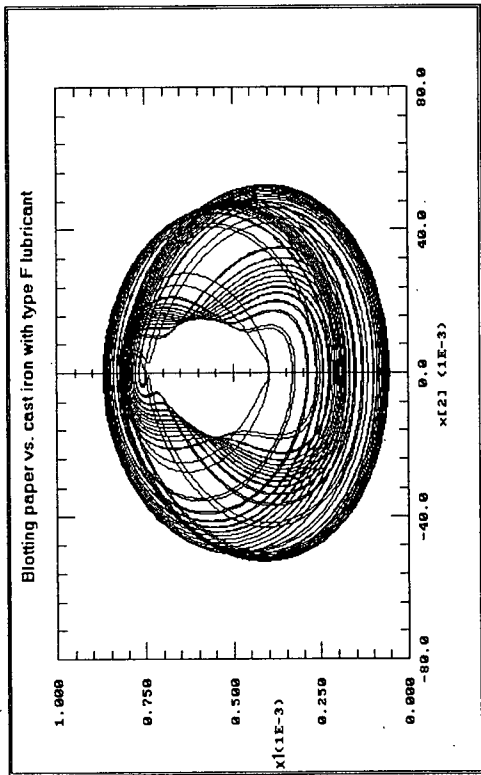


(c) Time series

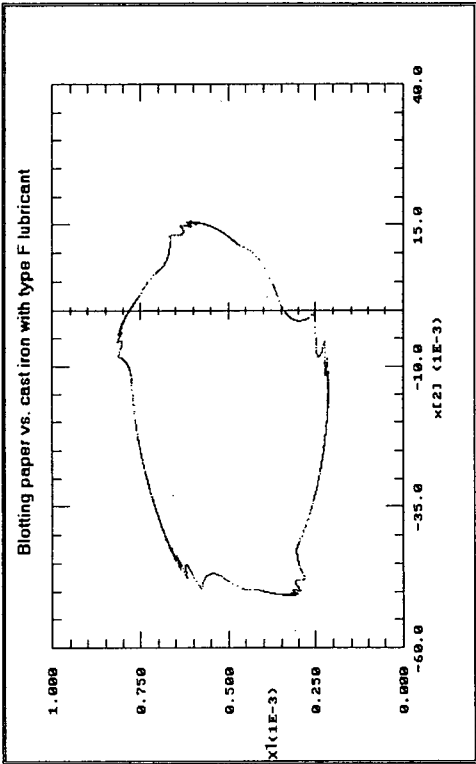


(d) Frequency spectrum

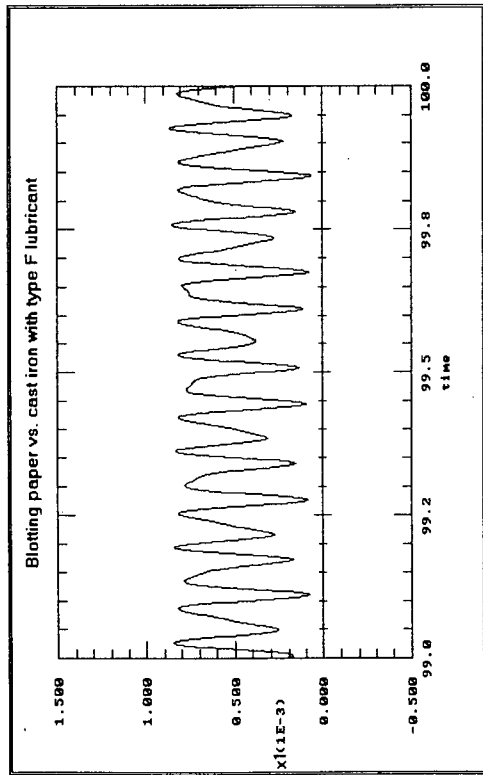
Figure 8.6 Case of chaotic behaviour for the type F lubricant combination



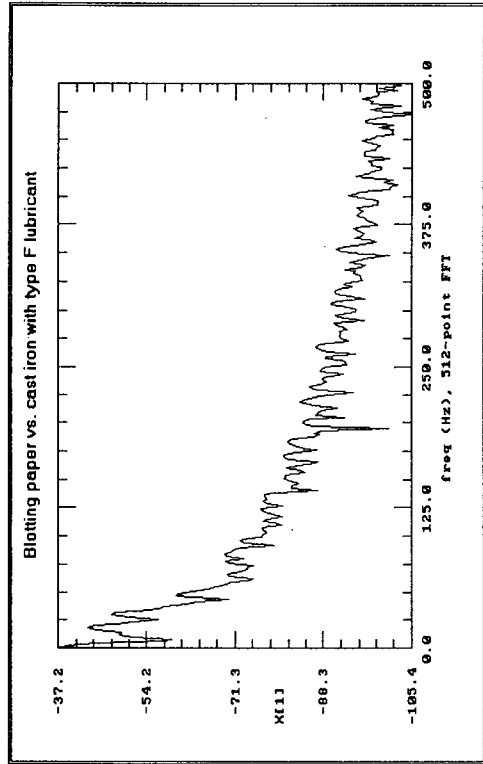
(a) Phase-plane plot



(b) Poincaré section

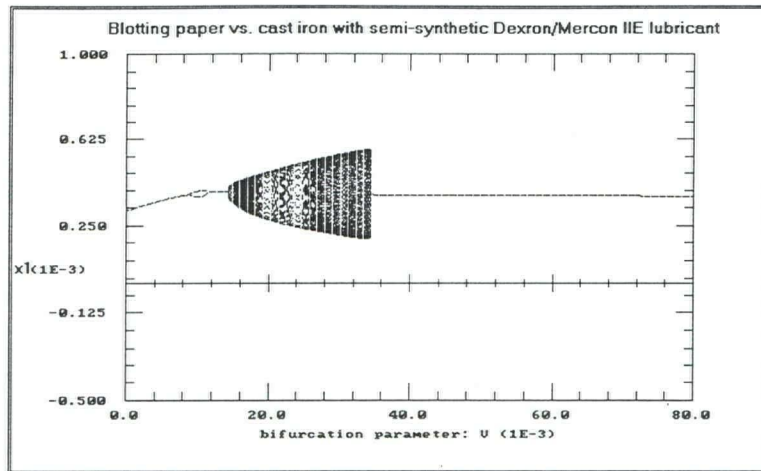


(c) Time series

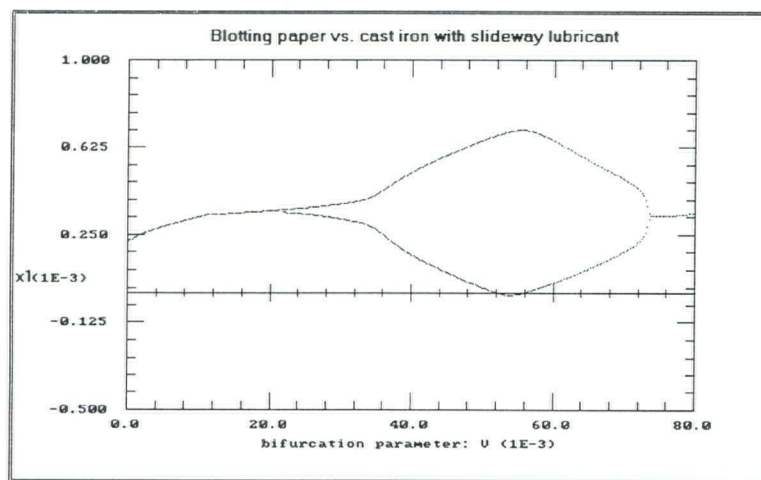


(d) Frequency spectrum

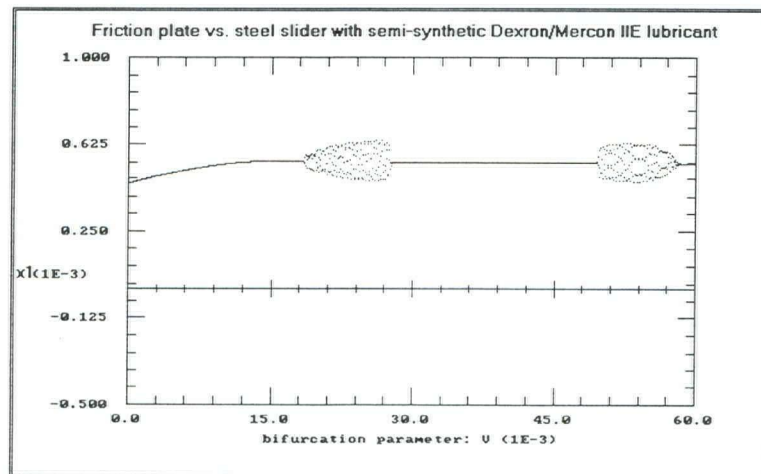
Figure 8.7 Case of chaotic behaviour for the type F lubricant combination



(a) Bifurcation diagram for the blotting paper combination with semi-synthetic Dexron/Mercon IIE lubricant

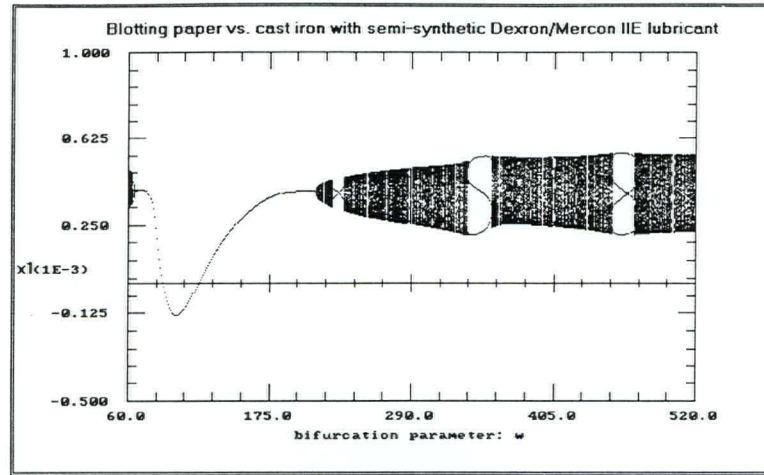


(b) Bifurcation diagram for the blotting paper combination with slideway lubricant

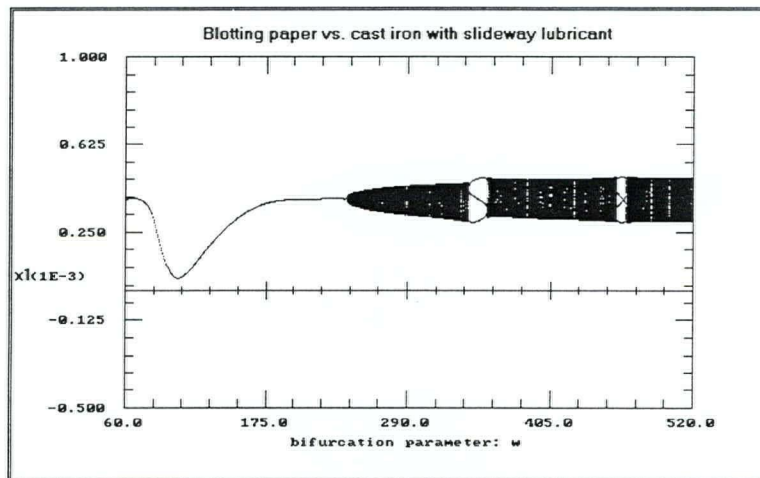


(c) Bifurcation diagram for the friction plate combination with semi-synthetic Dexron/Mercon IIE lubricant

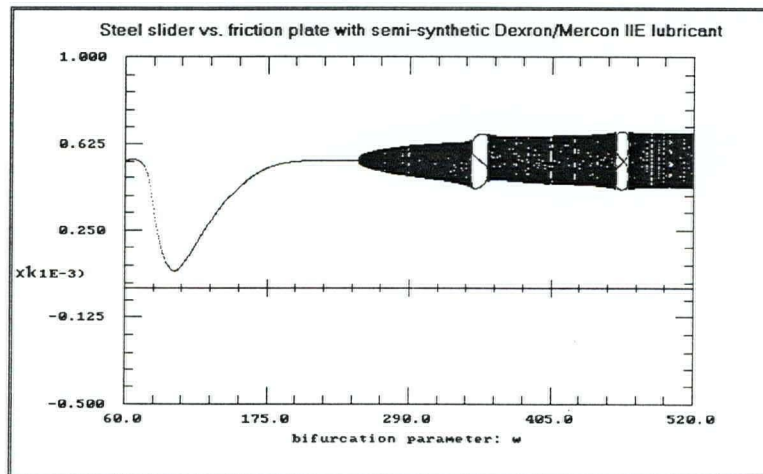
Figure 8.8 Bifurcation diagrams for the parameter V for three combinations



(a) Bifurcation diagram for the blotting paper combination with semi-synthetic Dexron/Mercon IIE lubricant

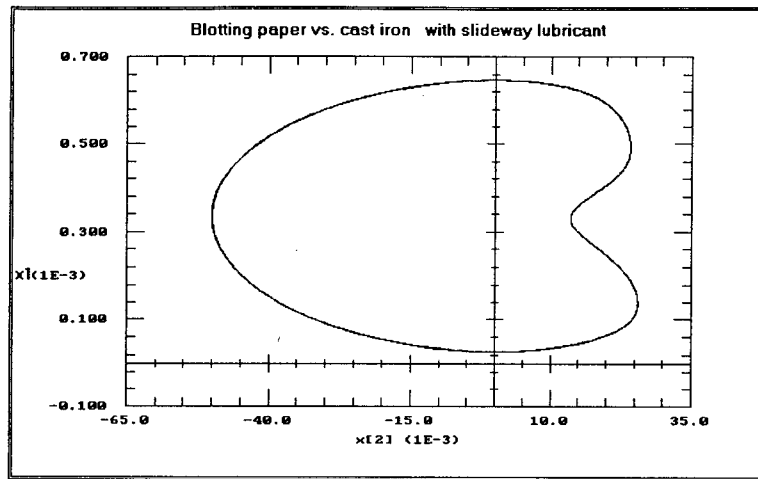


(b) Bifurcation diagram for the blotting paper combination with slideway lubricant

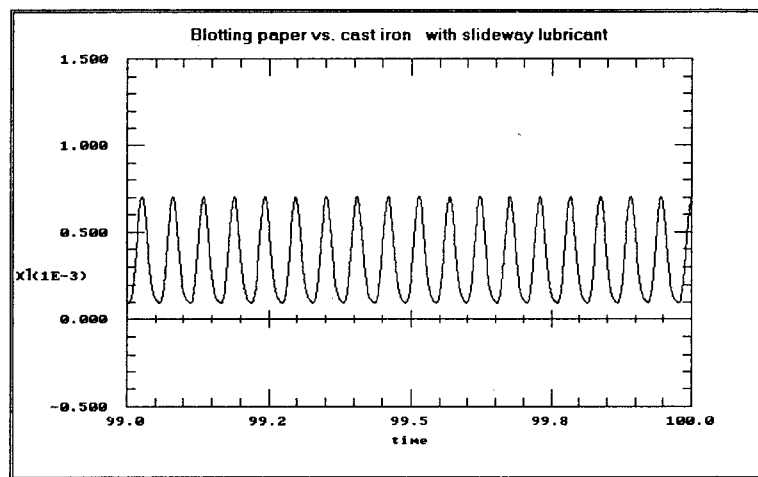


(c) Bifurcation diagram for the friction plate combination with semi-synthetic Dexron/Mercon IIE lubricant

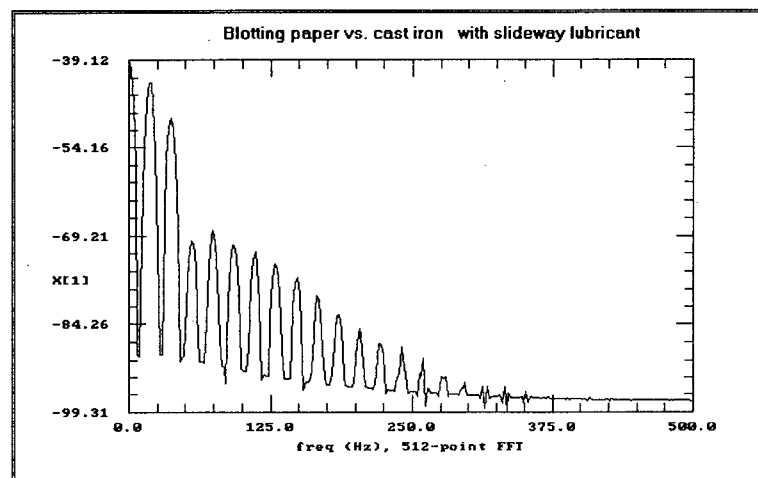
Figure 8.9 Bifurcation diagrams for the parameter α for three combinations



(a) Phase-plane plot

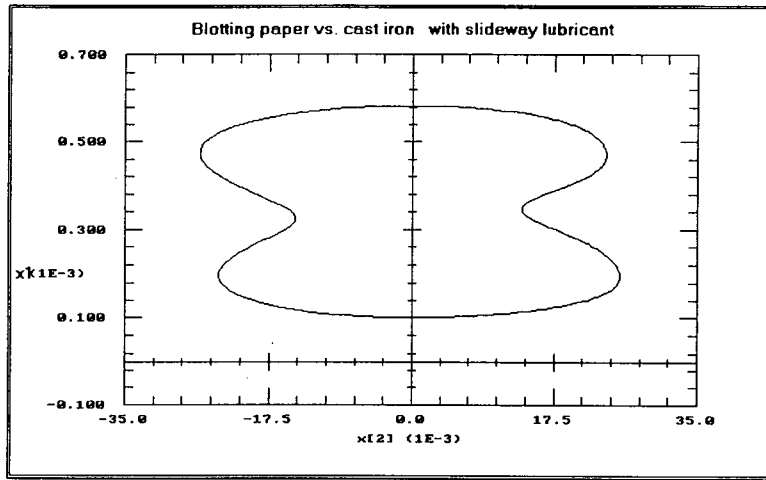


(b) Time series

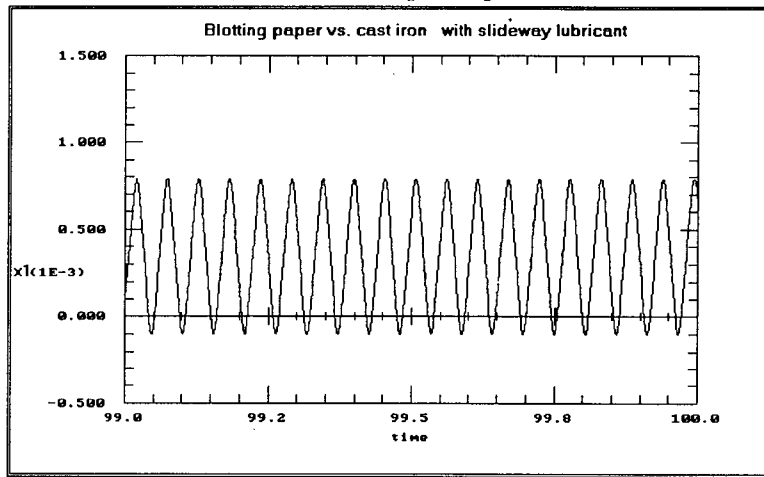


(c) Frequency spectrum

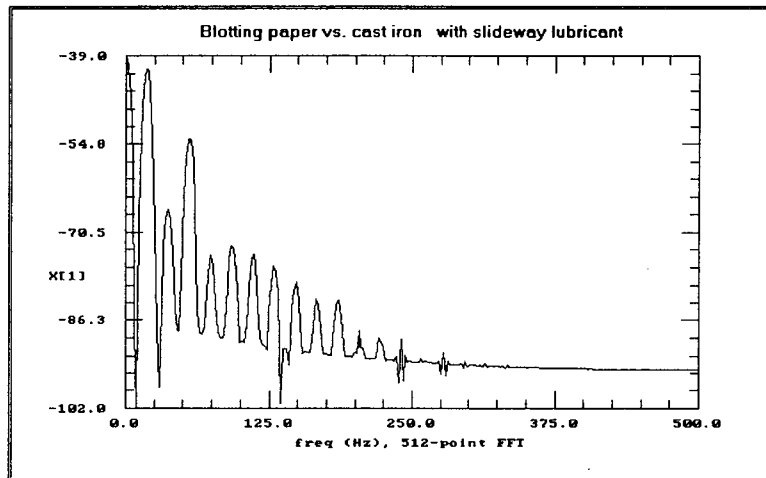
Figure 8.10 Subharmonic entrainment of order 2 with slideway lubricant combination



(a) Phase-plane plot

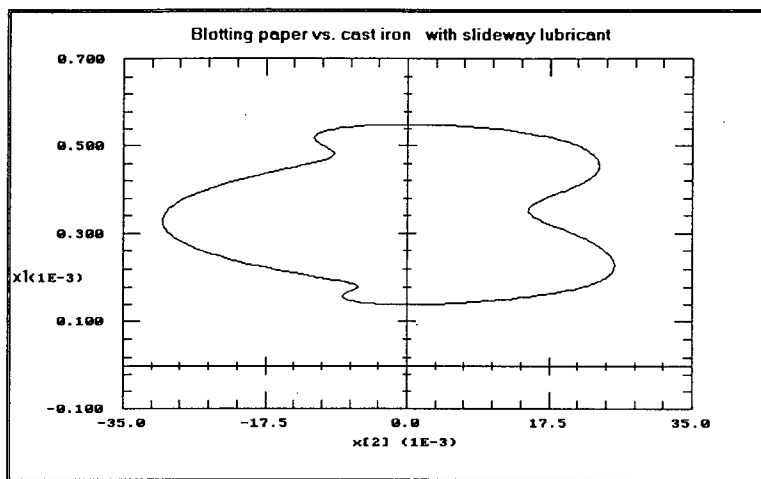


(b) Time series

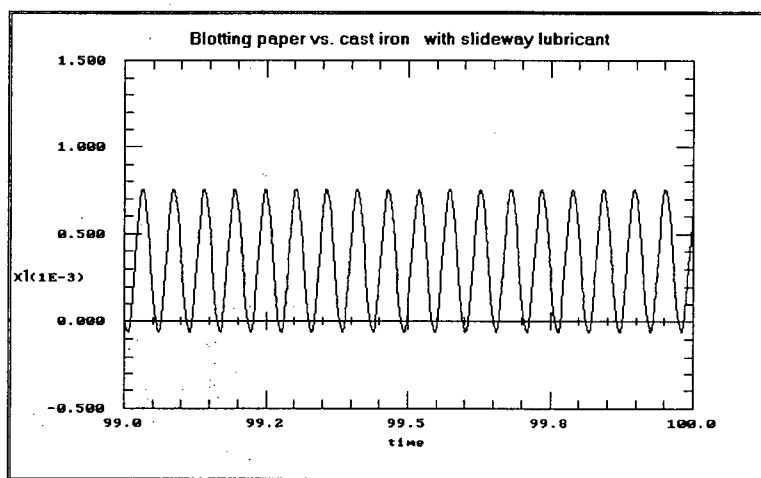


(c) Frequency spectrum

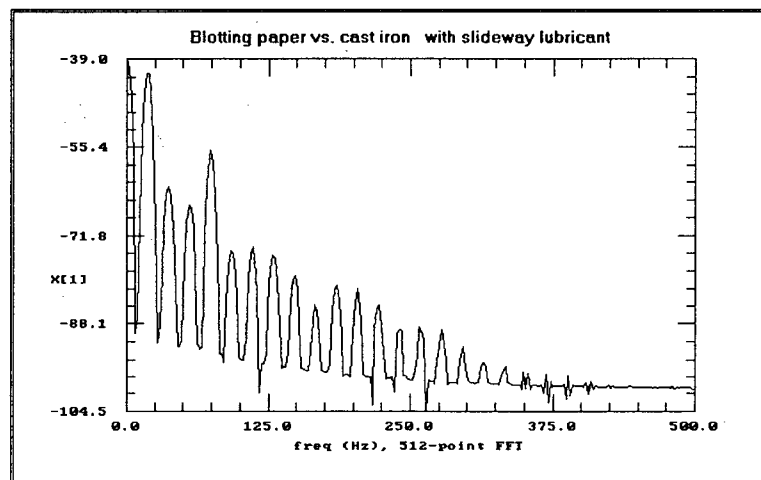
Figure 8.11 Subharmonic entrainment of order 3 with slideway lubricant combination



(a) Phase-plane plot

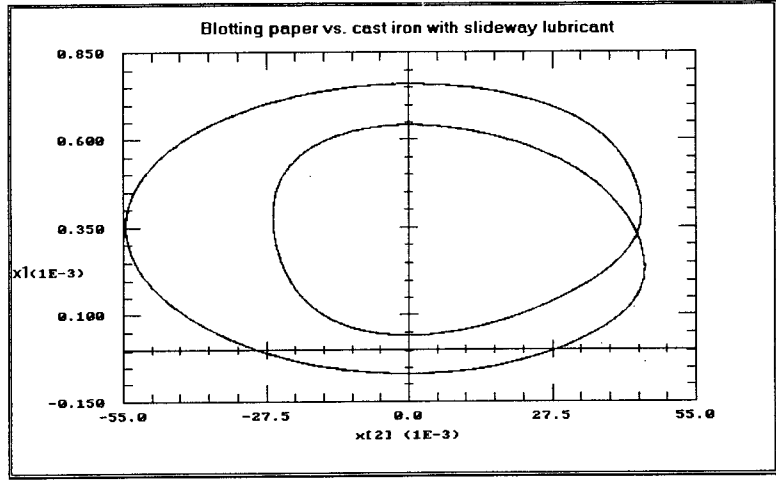


(b) Time series

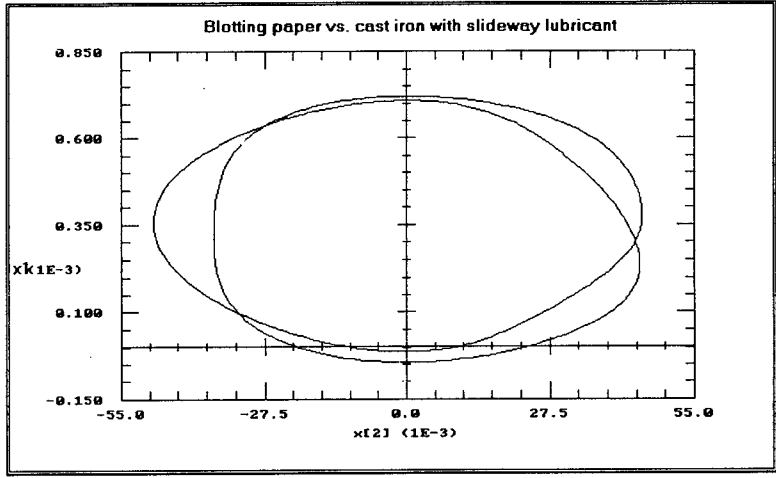


(c) Frequency spectrum

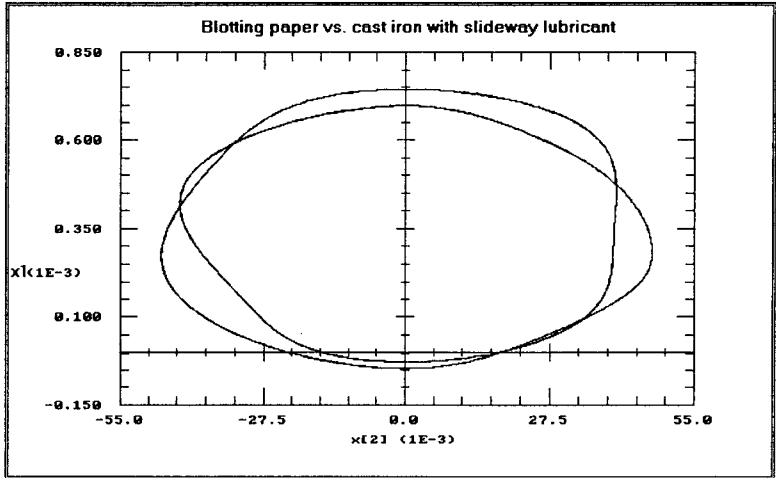
Figure 8.12 Subharmonic entrainment of order 4 with slideway lubricant combination



(a) Phase-plane plot for $\alpha = 1.5$



(b) Phase-plane plot for $\alpha = 2.5$



(c) Phase-plane plot for $\alpha = 3.5$

Figure 8.13 Subharmonic entrainment with slideway lubricant combination

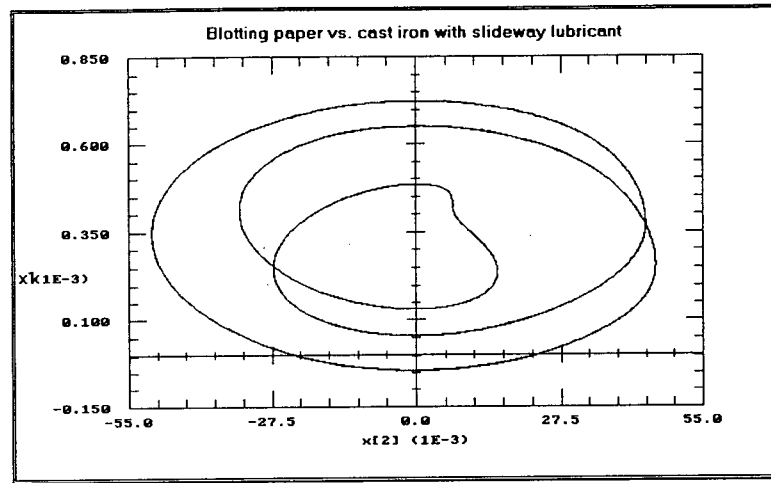
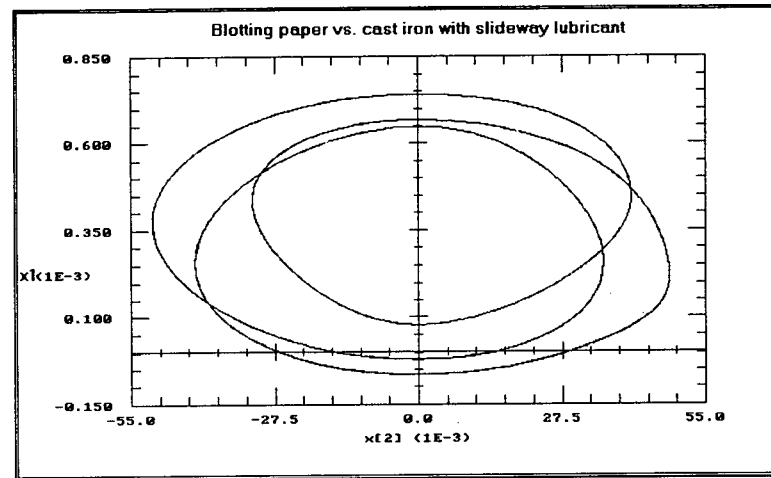
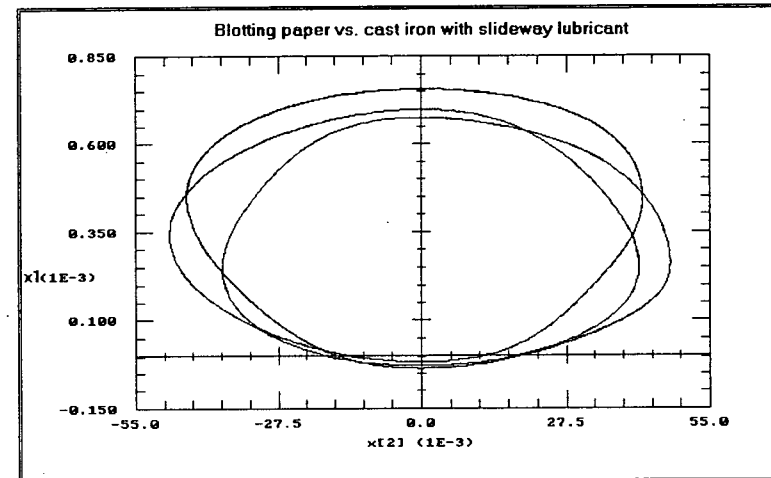
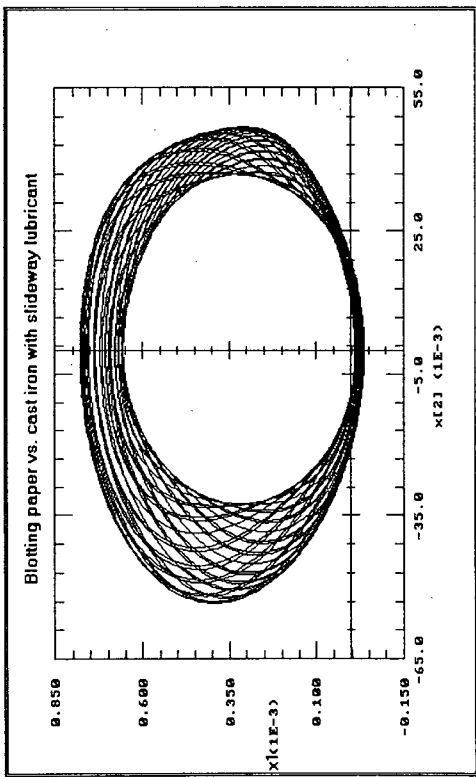
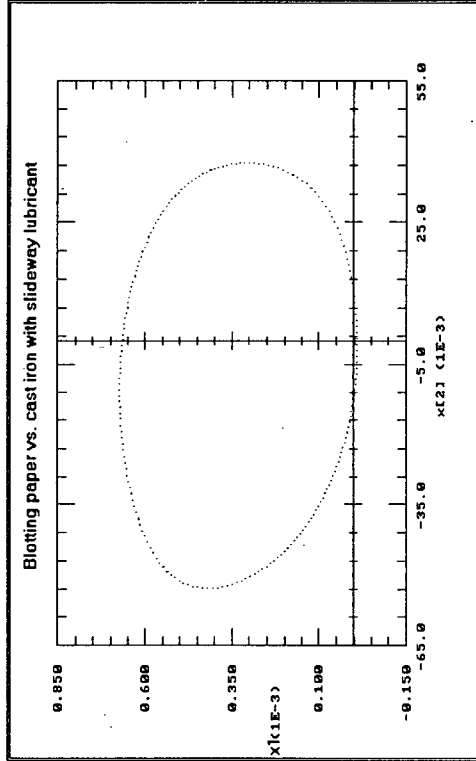
(a) Phase-plane plot for $\alpha = 1.33$ (b) Phase-plane plot for $\alpha = 1.66$ (c) Phase-plane plot for $\alpha = 2.33$

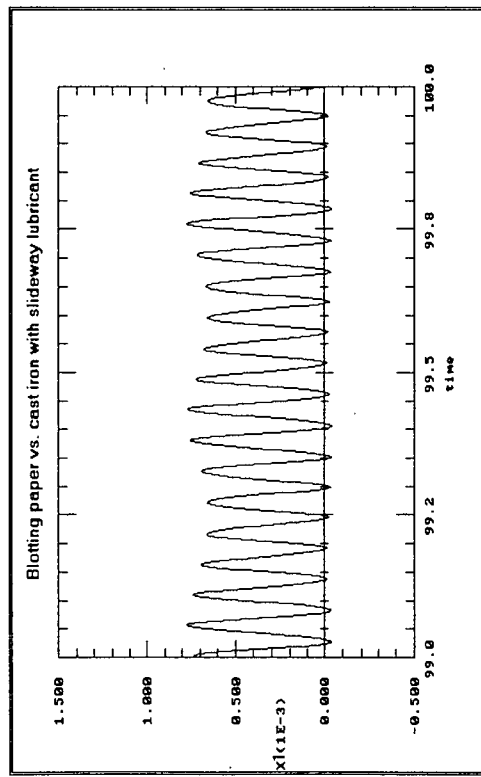
Figure 8.14 Subharmonic entrainment with slideway lubricant combination



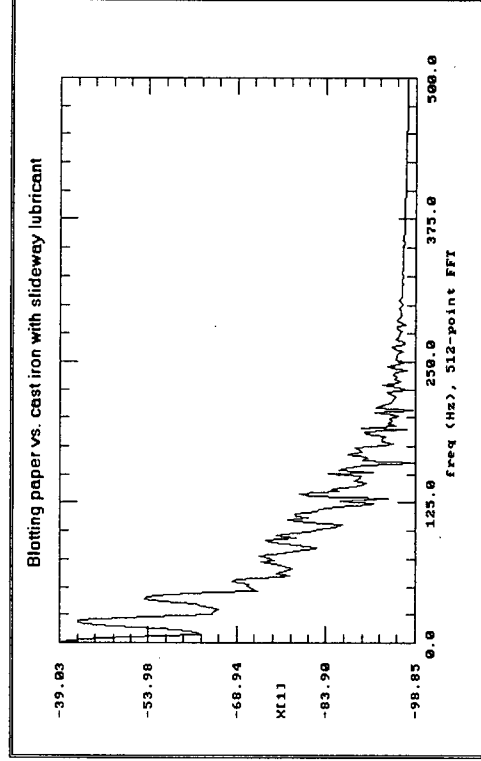
(a) Phase-plane plot



(b) Poincaré section



(c) Time series



(d) Frequency spectrum

Figure 8.15 Case of multiperiodic behaviour for the sideway lubricant combination.

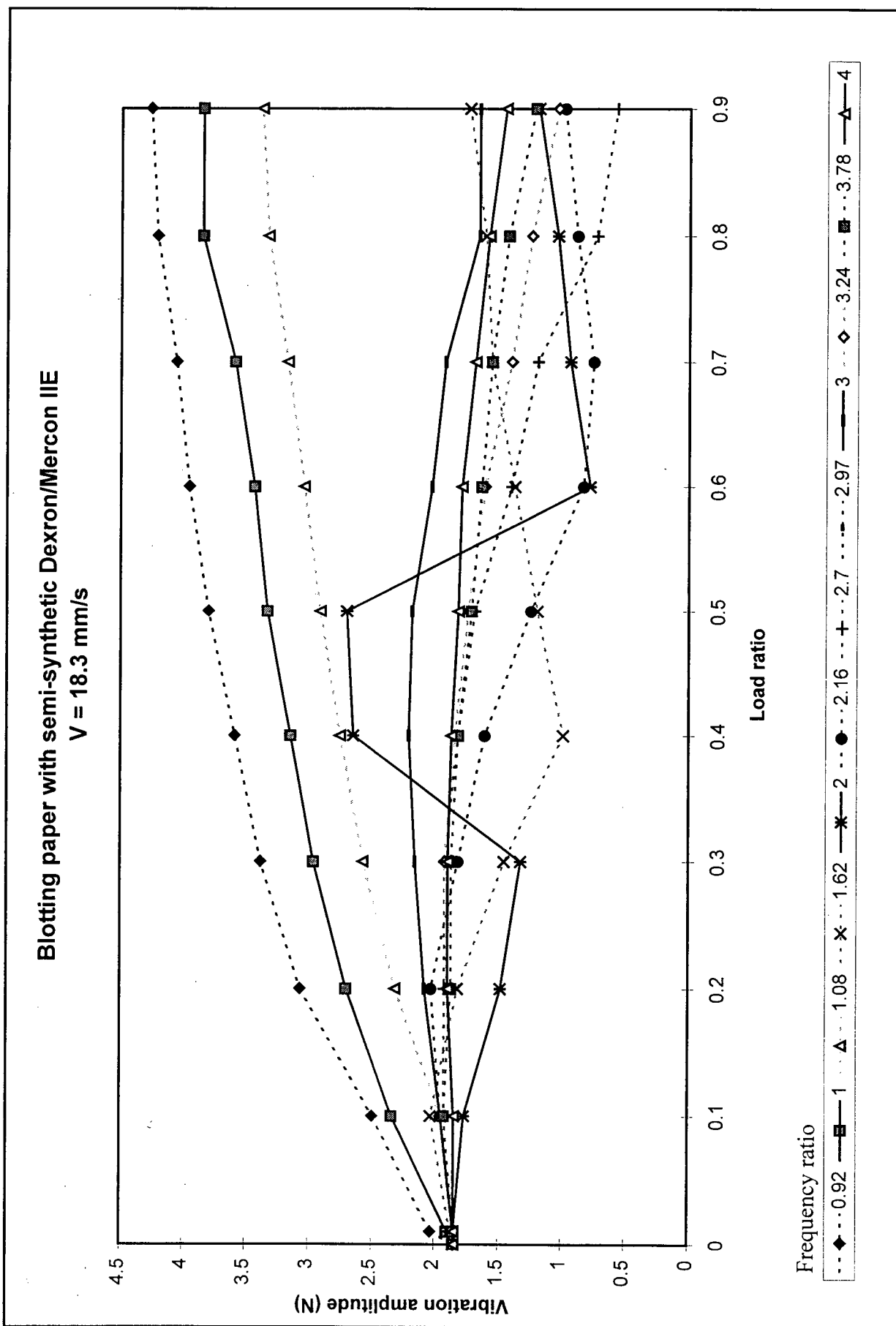


Figure 8.16. Effect of load and frequency ratios on numerical vibration amplitude. Blotting paper combination with semi-synthetic Dexron/Mercon IIE lubricant

Blotting paper vs. cast iron with sideway lubricant
 $V = 46.2 \text{ mm/s}$

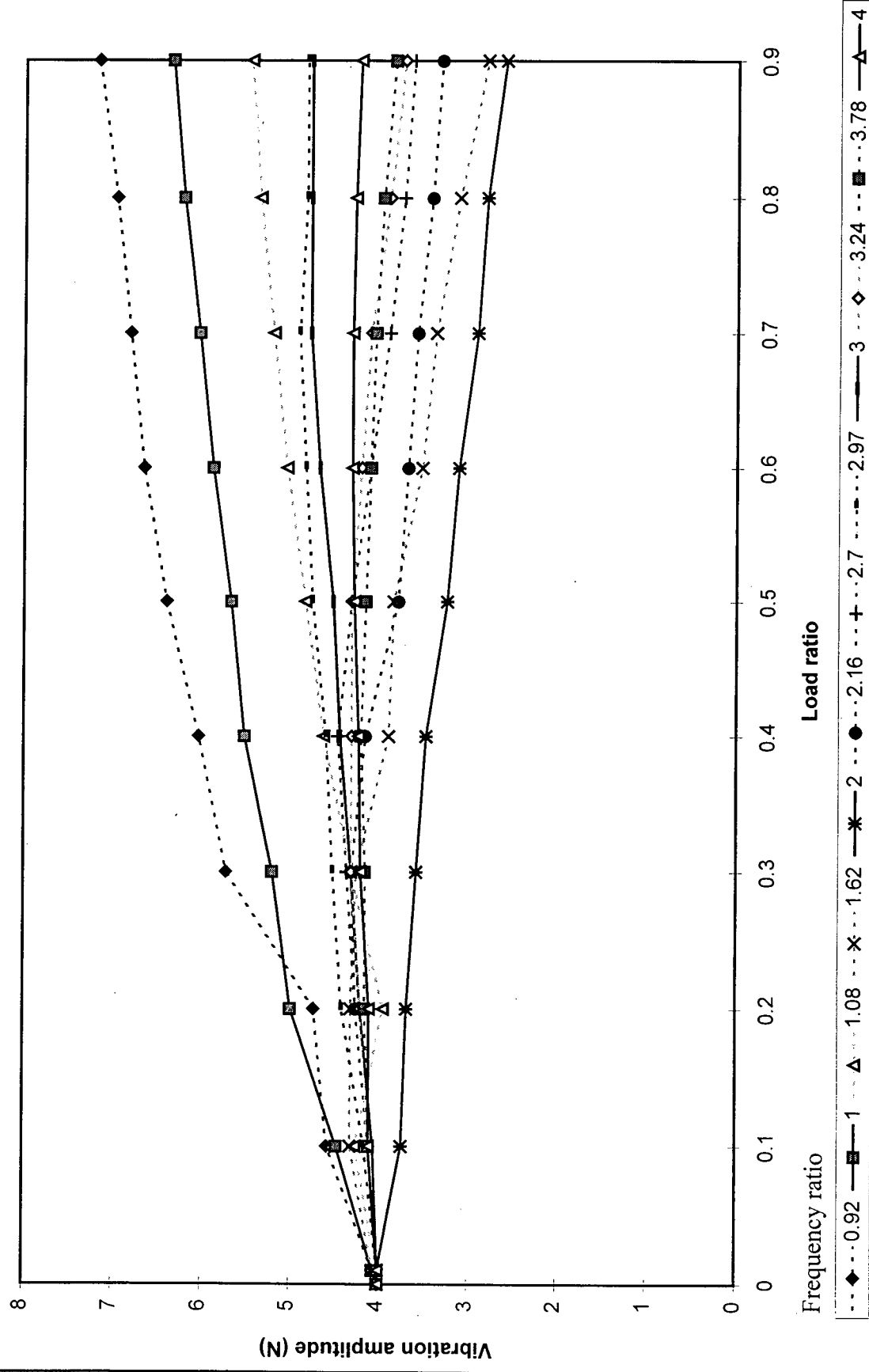
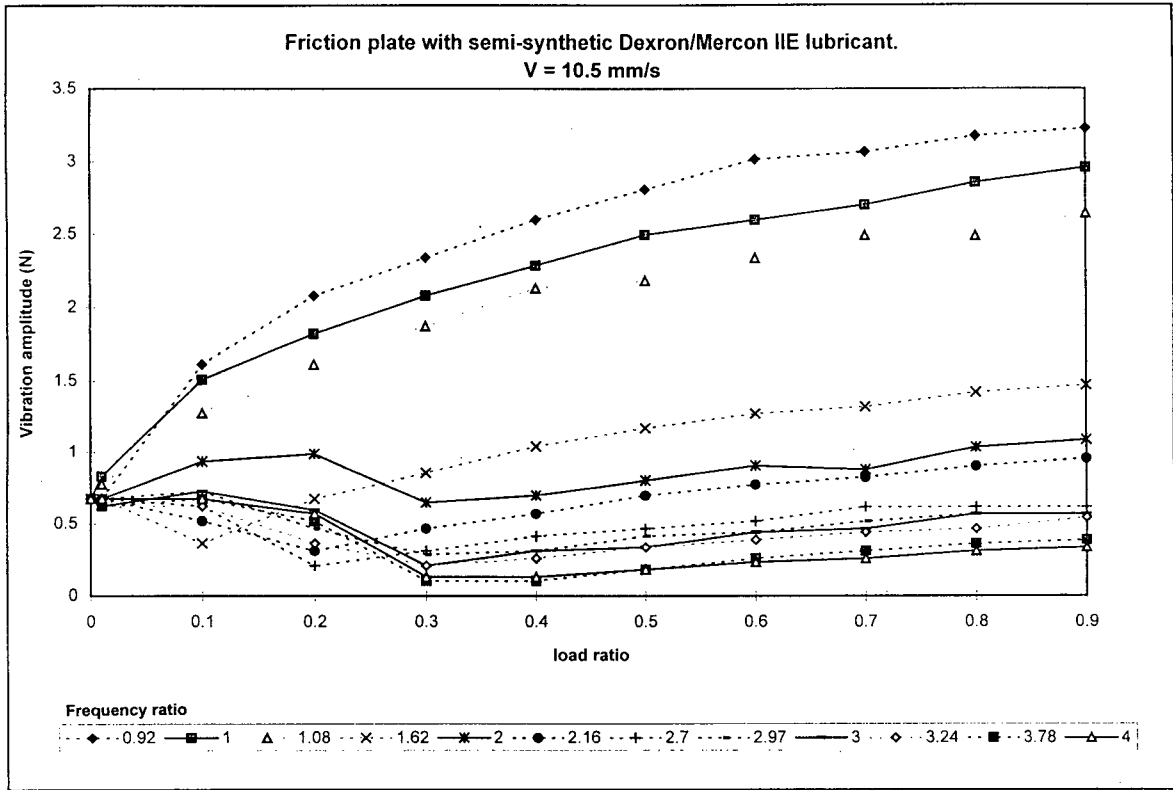
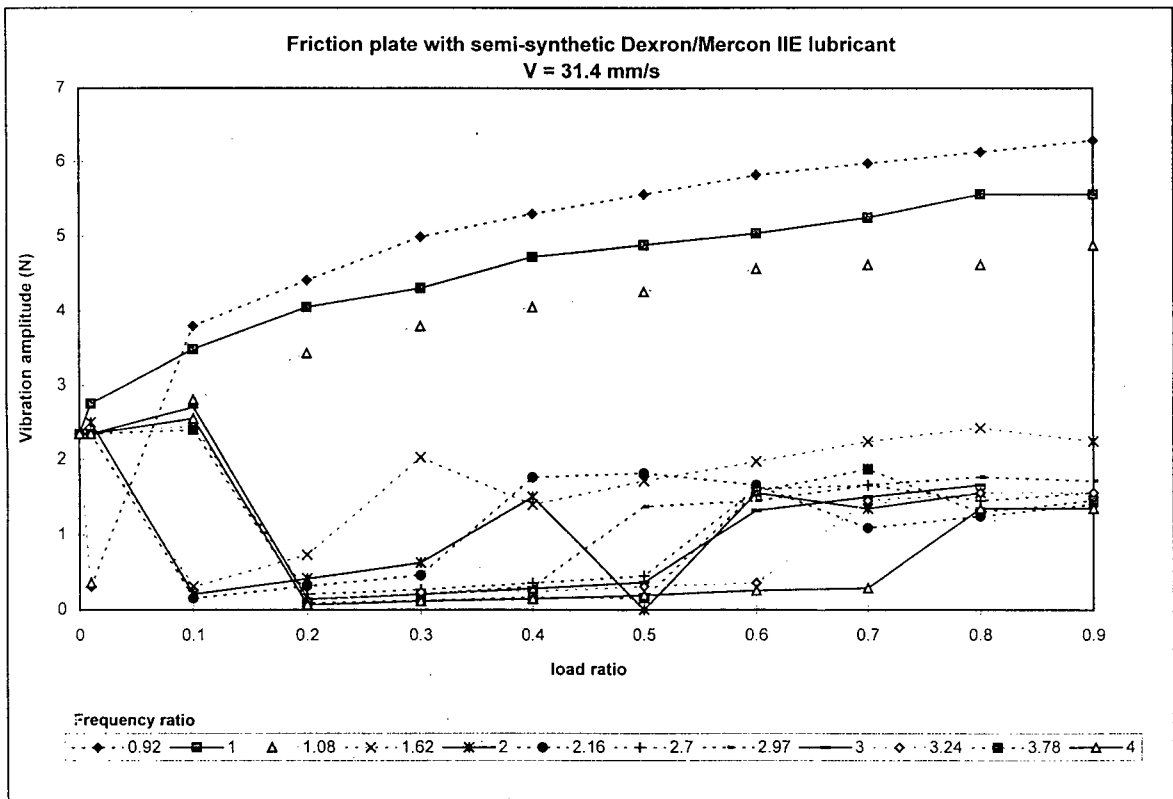


Figure 8.17. Effect of load and frequency ratios on numerical vibration amplitude. Blotting paper combination with sideway lubricant

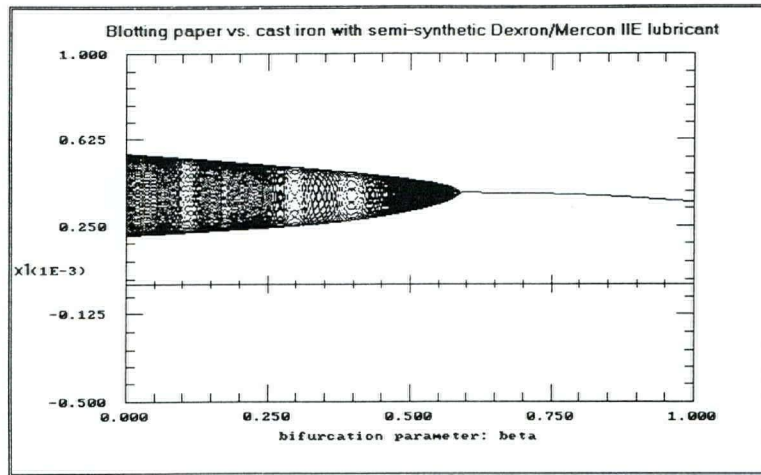


(a) V = 10.5 mm/s

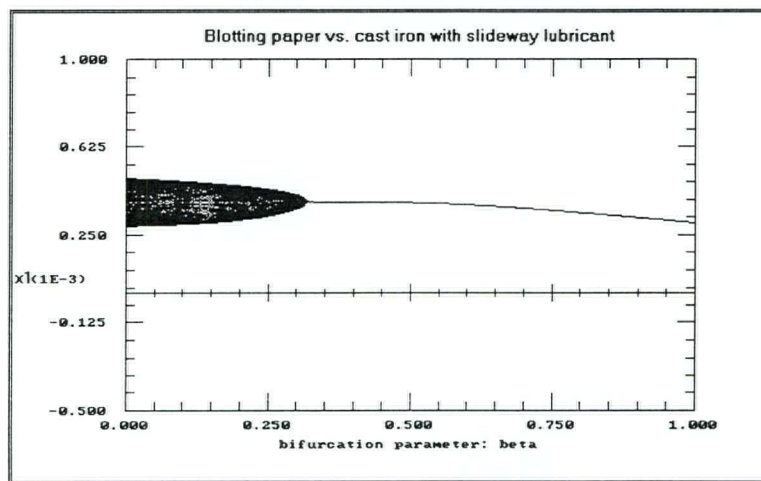


(b) V = 31.4 mm/s

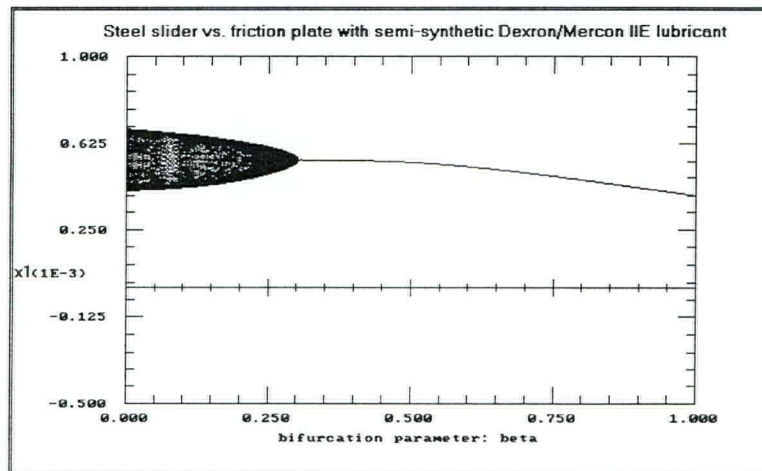
Figure 8.18. Effect of load and frequency ratios on numerical vibration amplitude
Friction plate combination with semi-synthetic Dexron/Mercon IIE lubricant



(a) Bifurcation diagram for the blotting paper combination with semi-synthetic Dexron/Mercon IIE lubricant



(b) Bifurcation diagram for the blotting paper combination with slideway lubricant



(c) Bifurcation diagram for the friction plate combination with semi-synthetic Dexron/Mercon IIE lubricant

Figure 8.19 Bifurcation diagrams for the parameter β for three combinations

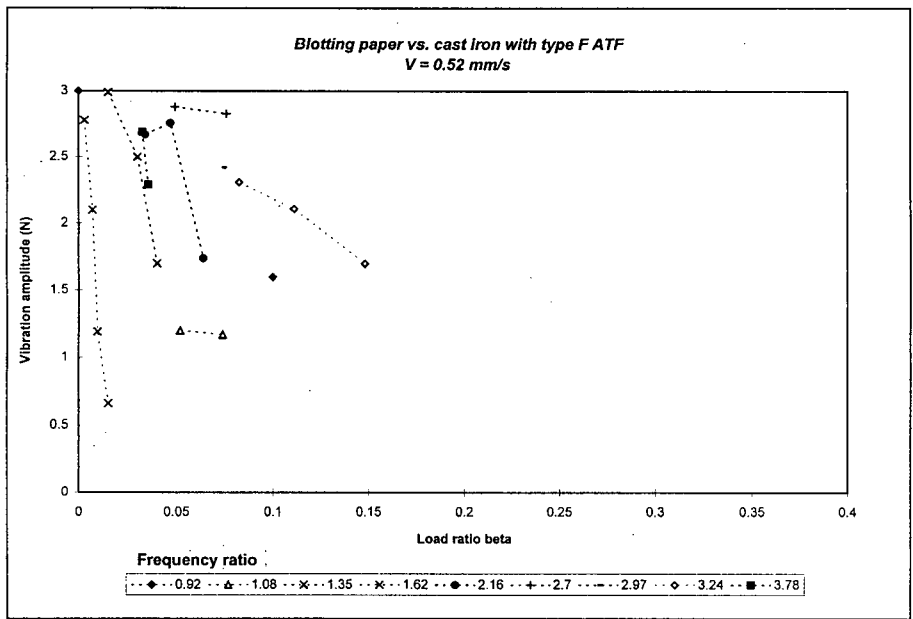


Figure 8.20. Effect of load and frequency ratios on experimental vibration amplitude Blotting paper combination with type F lubricant - V = 0.52 mm/s.

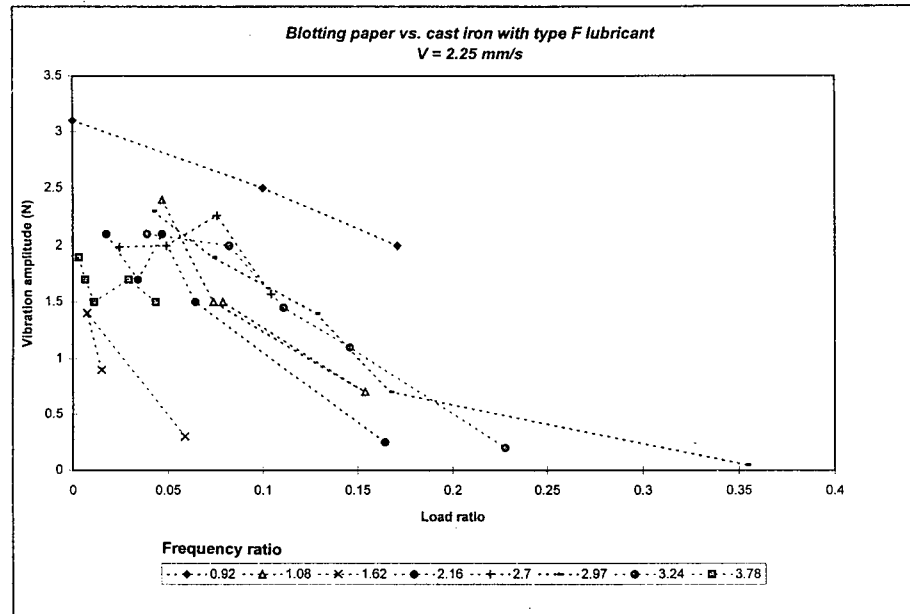


Figure 8.21.(a) Effect of load and frequency ratios on experimental vibration amplitude Blotting paper combination with type F lubricant - $V = 2.25$ mm/s.

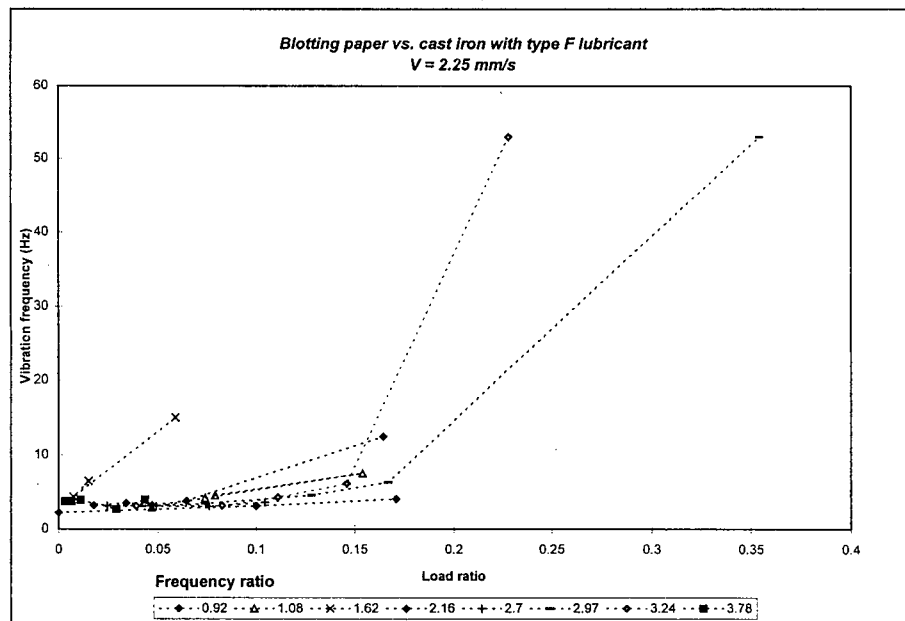


Figure 8.21.(b) Effect of load and frequency ratios on experimental vibration frequency Blotting paper combination with type F lubricant - $V = 2.25$ mm/s.

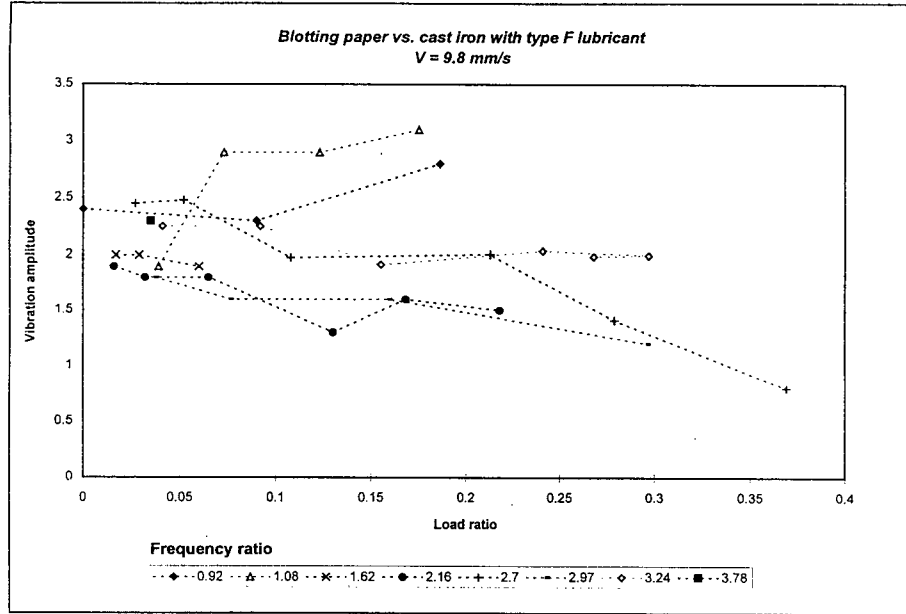


Figure 8.22.(a) Effect of load and frequency ratios on experimental vibration amplitude Blotting paper combination with type F lubricant - V = 9.8 mm/s.

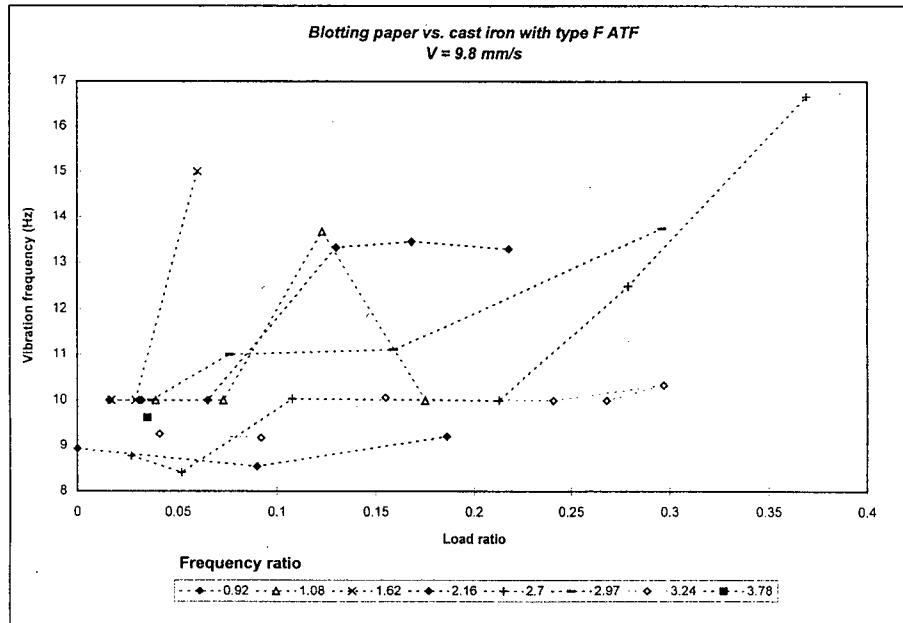


Figure 8.22.(b) Effect of load and frequency ratios on experimental vibration frequency Blotting paper combination with type F lubricant - V = 9.8 mm/s.

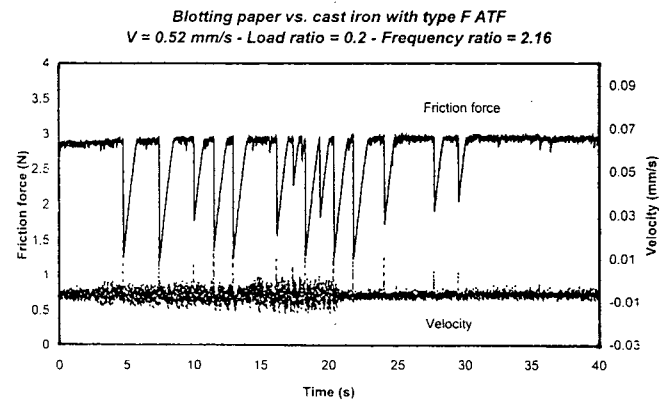
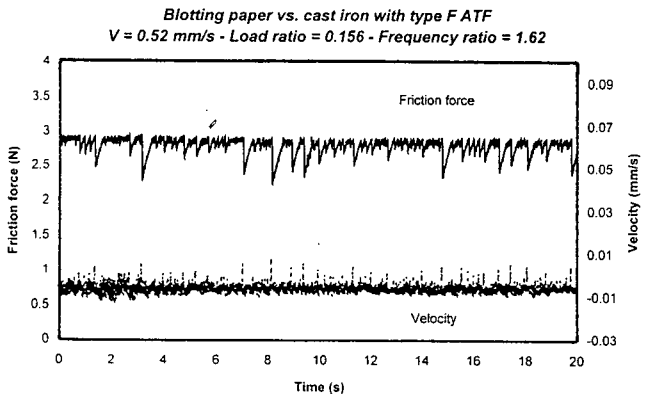
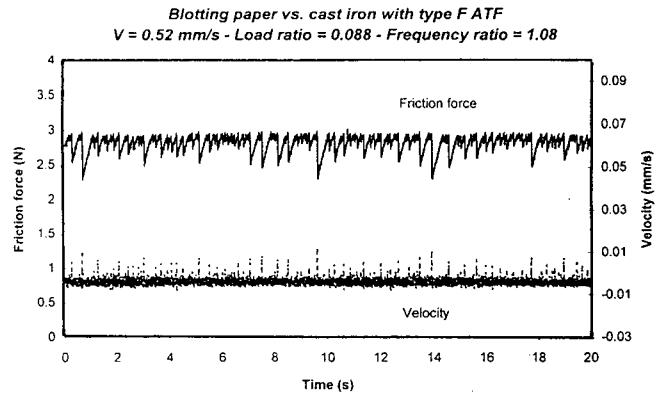
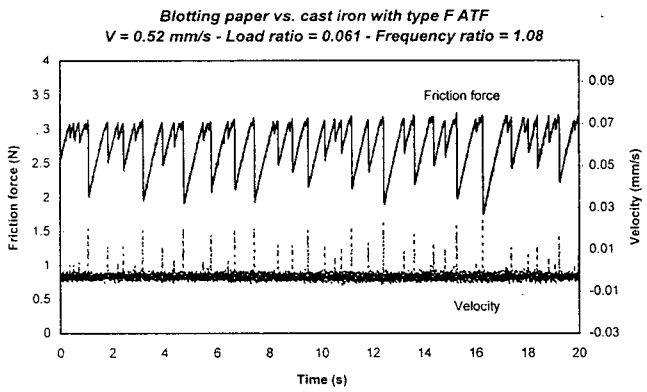
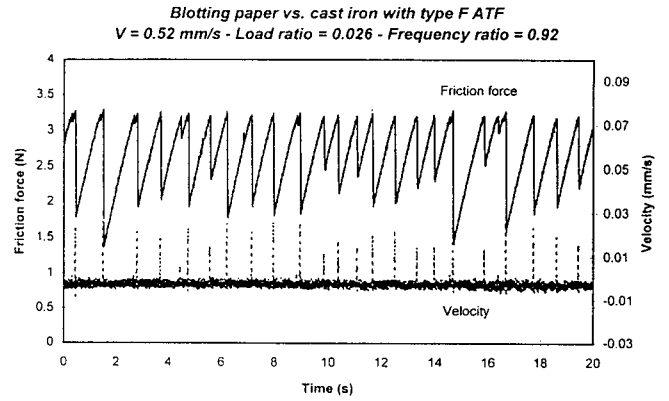
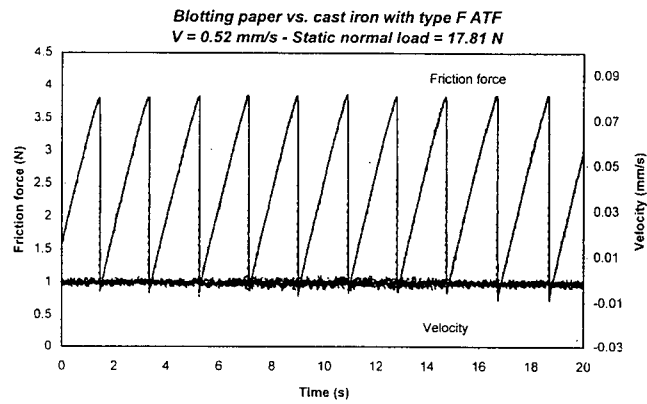


Figure 8.23. Vibration vs. time plots with dynamic loading
 Blotting paper vs. cast iron with type F lubricant. $V = 0.52$ mm/s

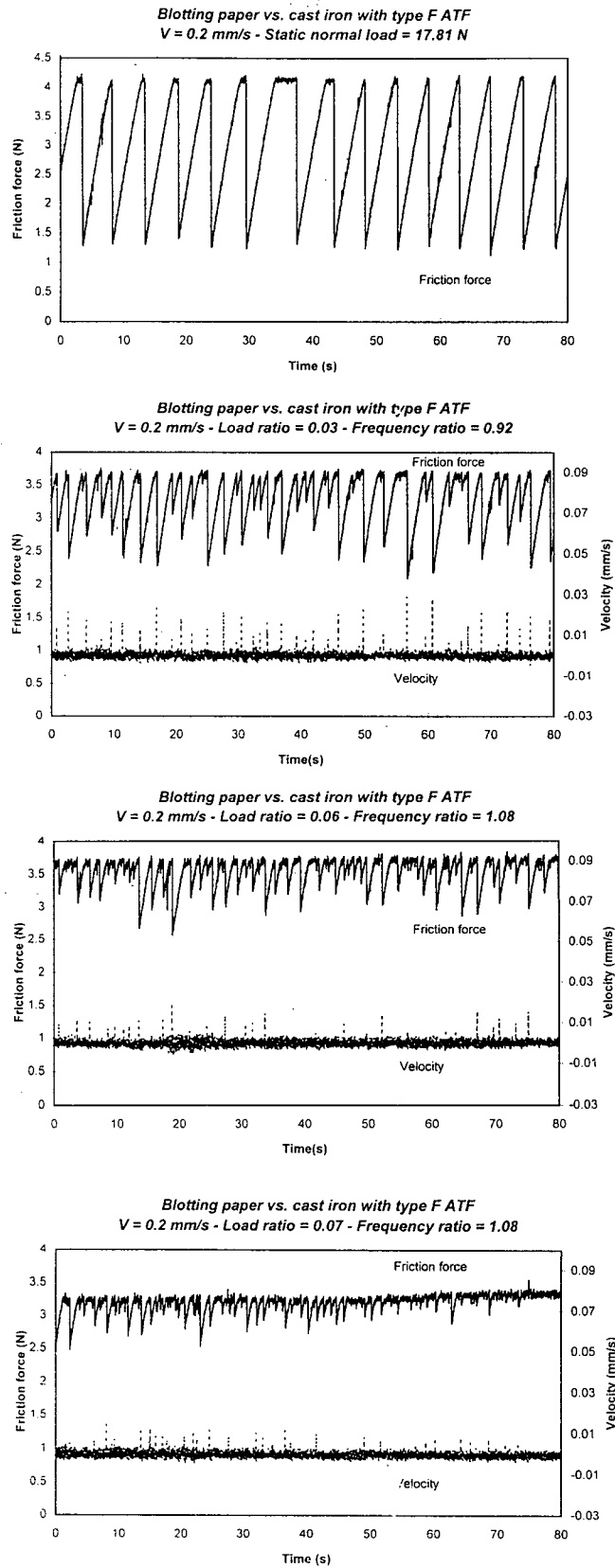


Figure 8.24. Vibration vs. time plots with dynamic loading
Blotting paper vs. cast iron with type F lubricant. $V = 0.2 \text{ mm/s}$

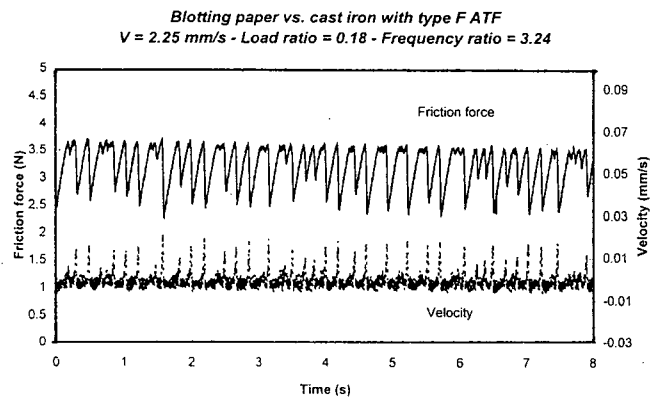
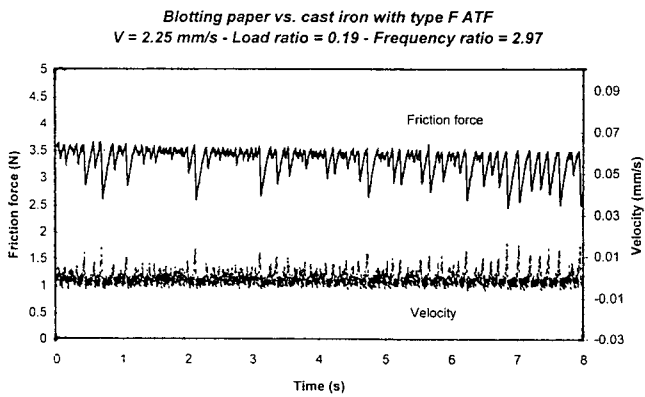
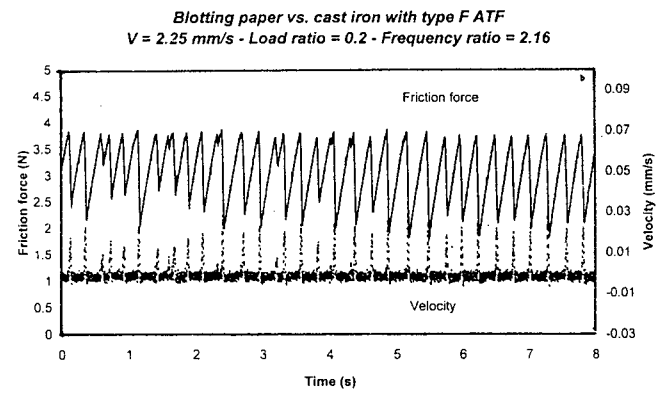
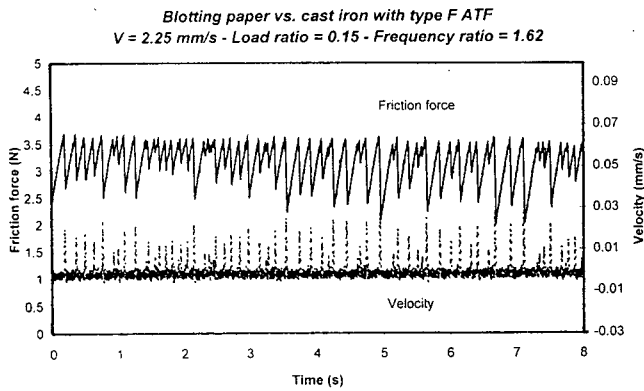
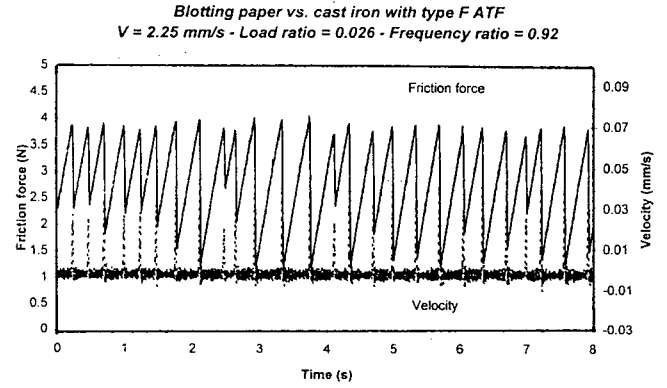
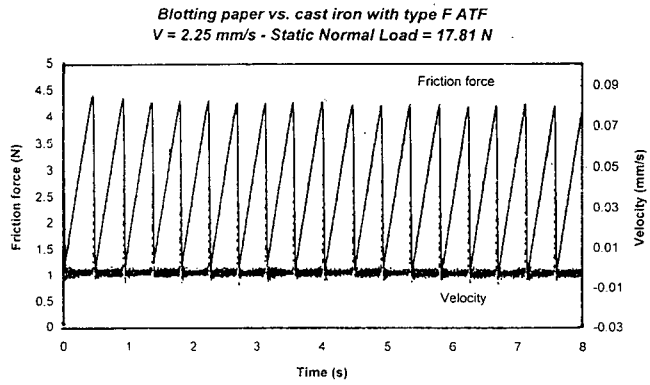
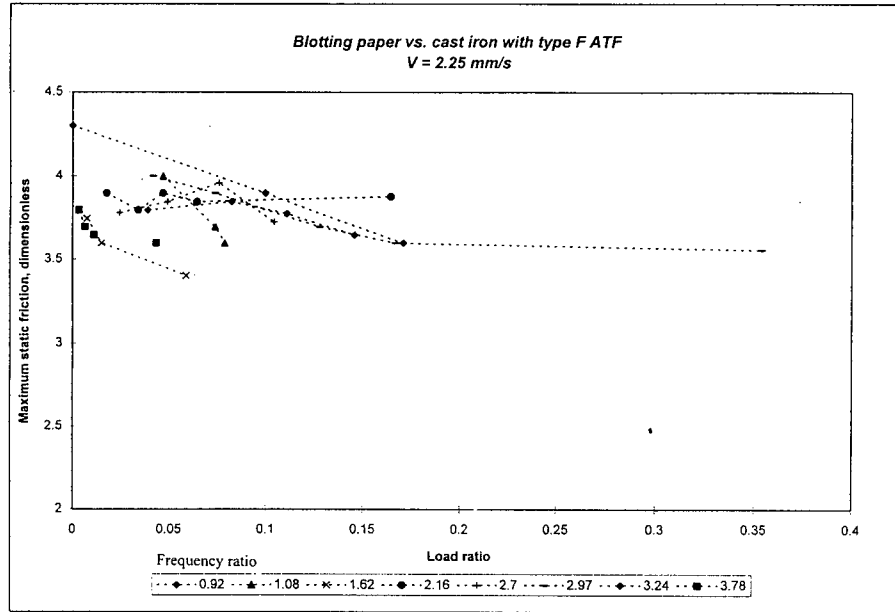
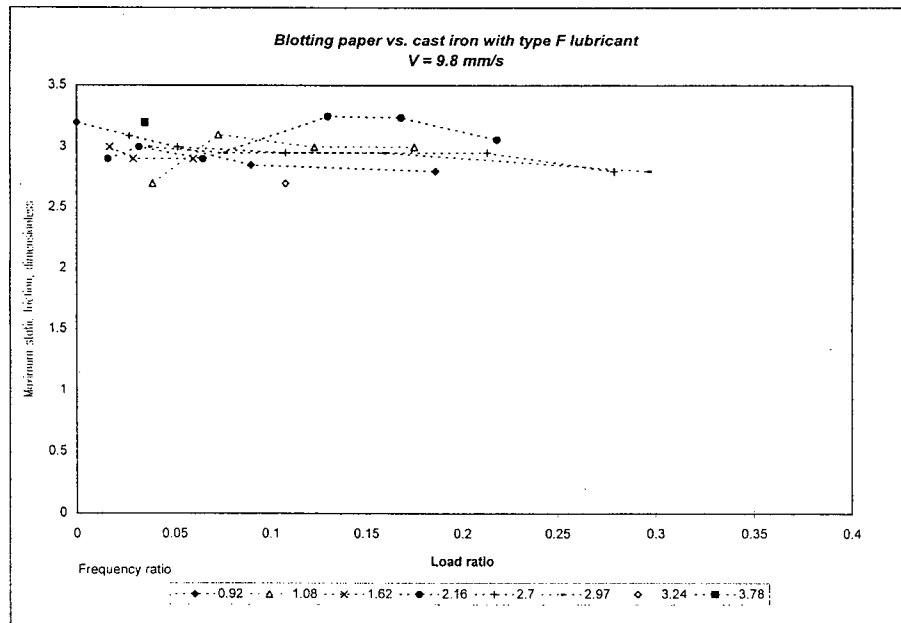


Figure 8.25. Vibration vs. time plots with dynamic loading
 Blotting paper vs. cast iron with type F lubricant. V = 2.25 mm/s

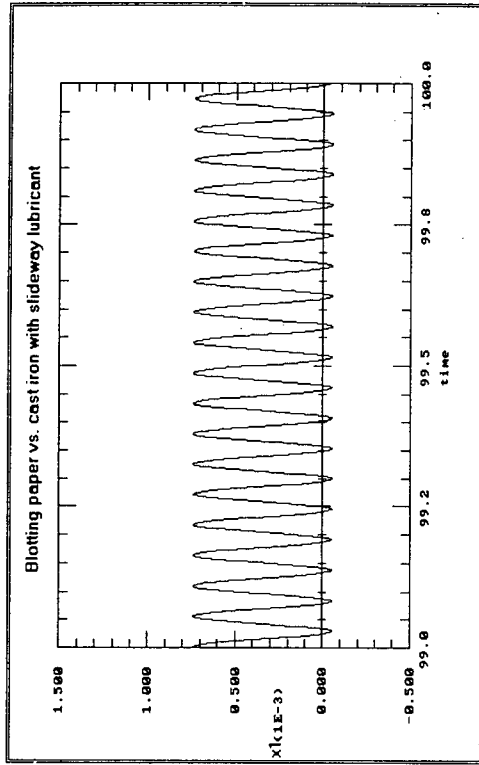
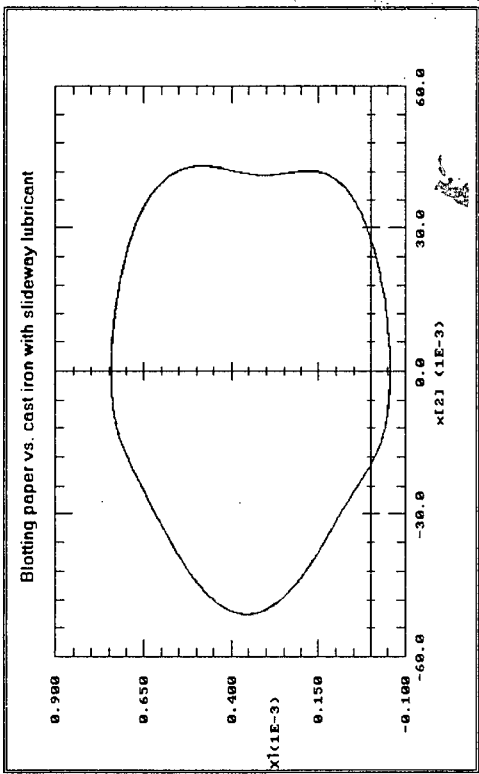


(a) V = 2.25 mm/s

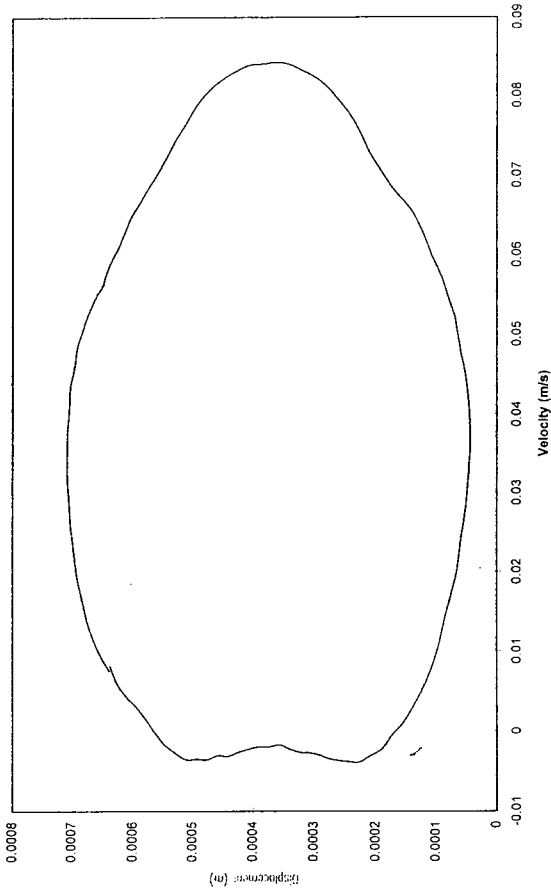


(b) V = 9.8 mm/s

Figure 8.26. Influence of dynamic loading on static friction. Blotting paper with type F lubricant



Blotting paper vs. cast iron with sideway lubricant
 $V = 46.2 \text{ mm/s}$ - Load ratio = 0.464 - Frequency ratio = 4.01



Blotting paper vs. cast iron with sideway lubricant
 $V = 46.2 \text{ mm/s}$ - Load ratio = 0.464 - Frequency ratio = 4.01

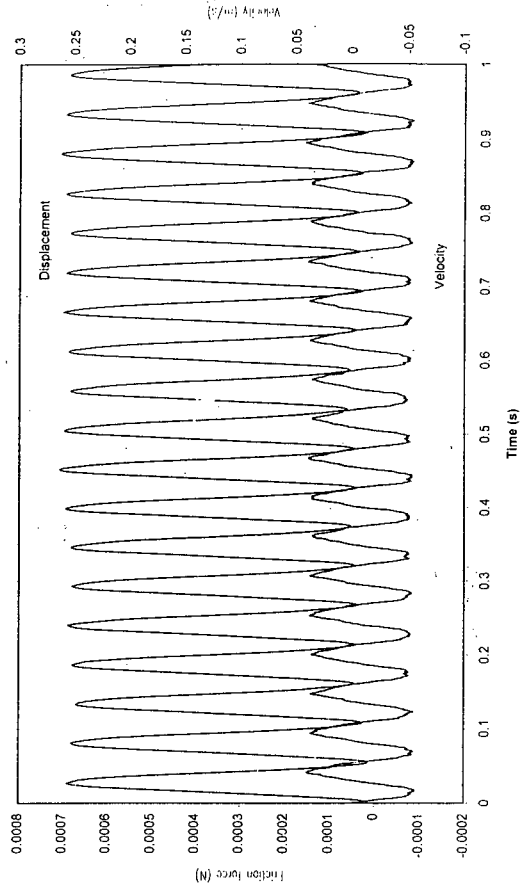


Figure 8.27. Subharmonic entrainment for sideway lubricant combination.
 Comparison between numerical and experimental results

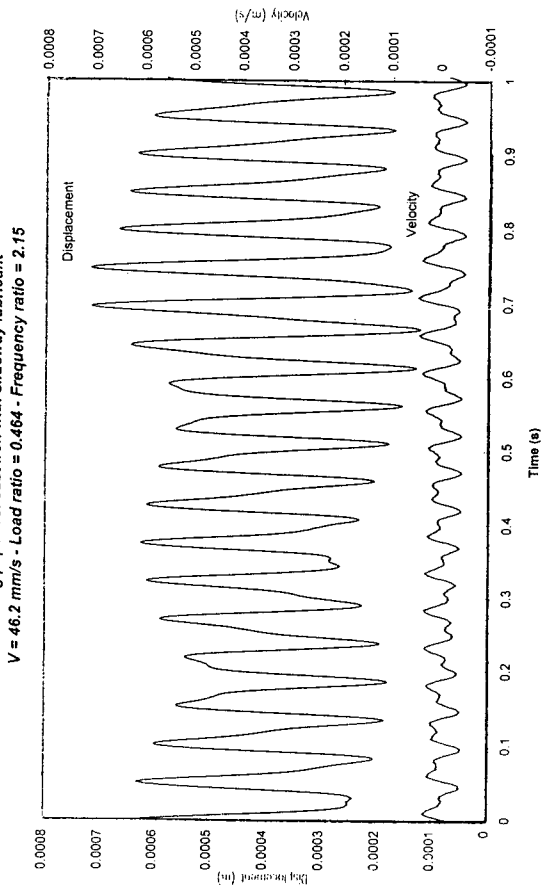
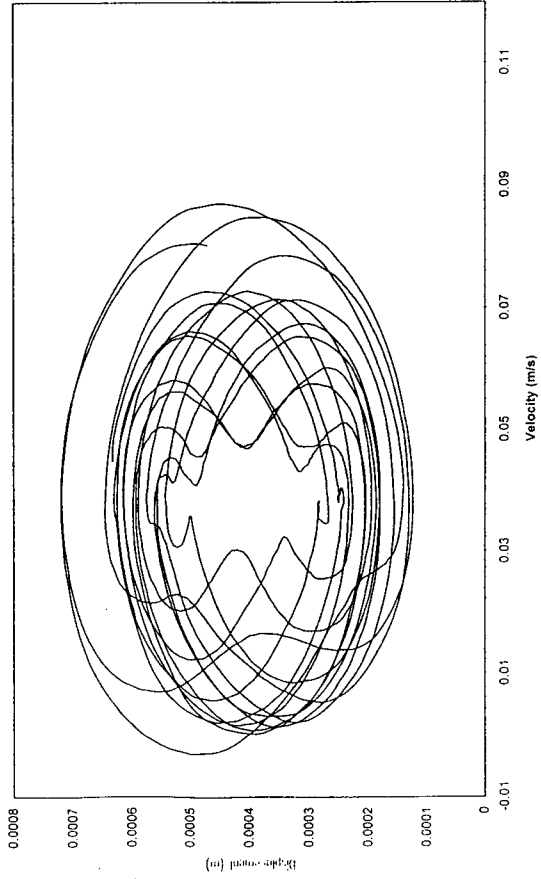
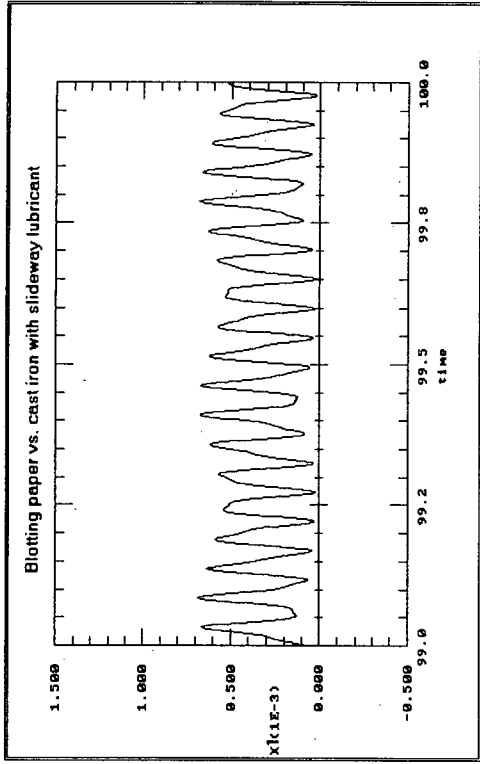
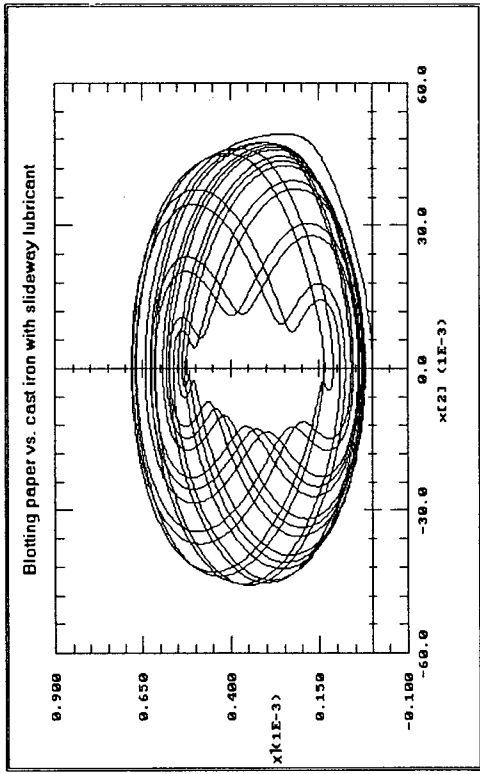


Figure 8.28. Multiperiodic motion for sideway lubricant combination
Comparison between numerical and experimental results

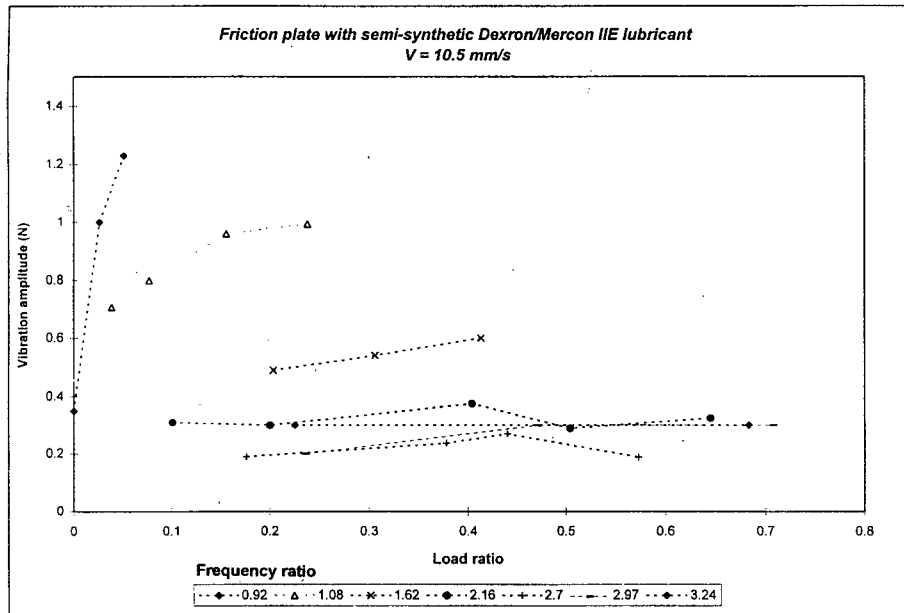


Figure 8.29.(a) Effect of load and frequency ratios on experimental vibration amplitude
Friction plate combination with semi-synthetic Dexron/Mercon IIE - V = 10.5 mm/s.

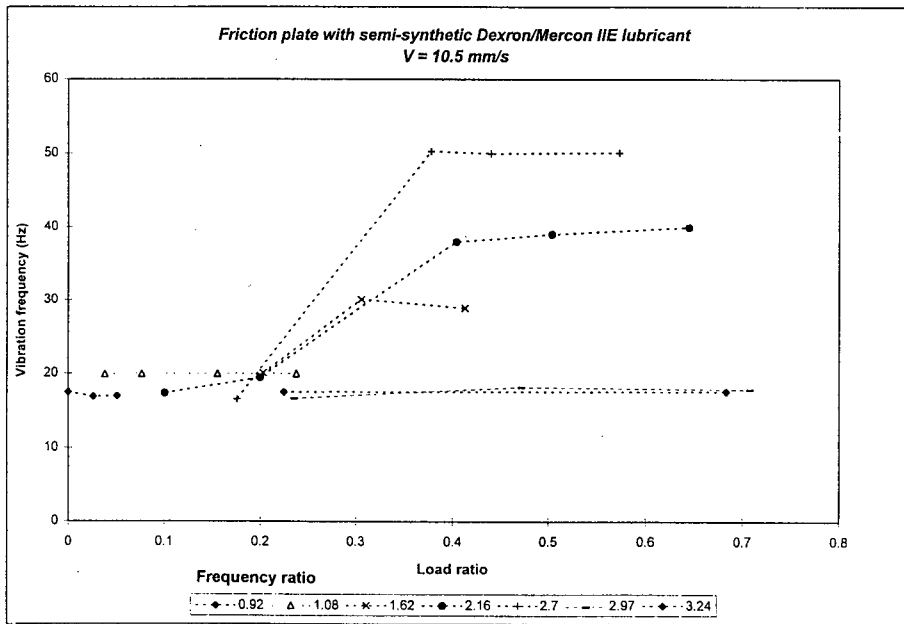


Figure 8.29.(b) Effect of load and frequency ratios on experimental vibration frequency
Friction plate combination with semi-synthetic Dexron/Mercon IIE - V = 10.5 mm/s.

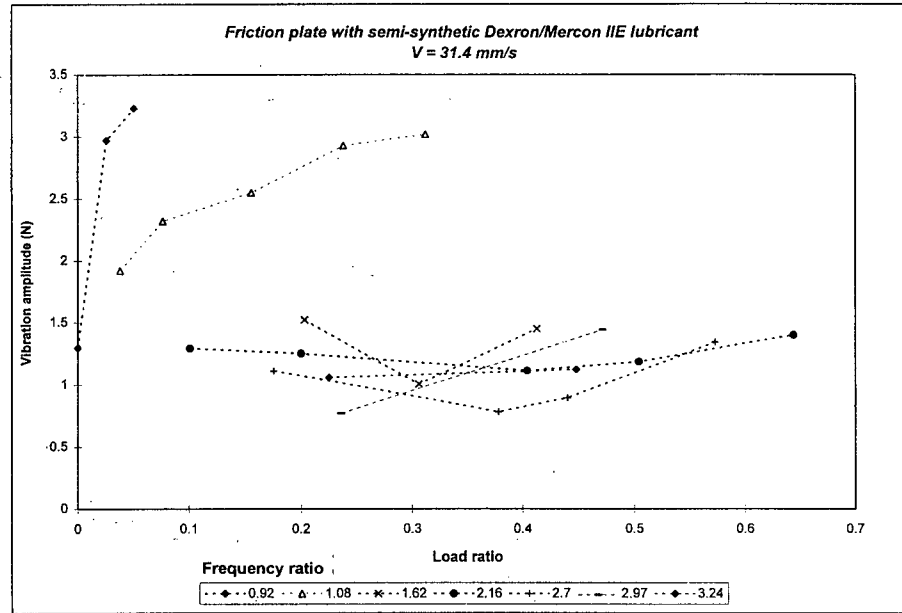


Figure 8.30.(a) Effect of load and frequency ratios on experimental vibration amplitude
Friction plate combination with semi-synthetic Dexron/Mercon IIE - V = 31.4 mm/s.

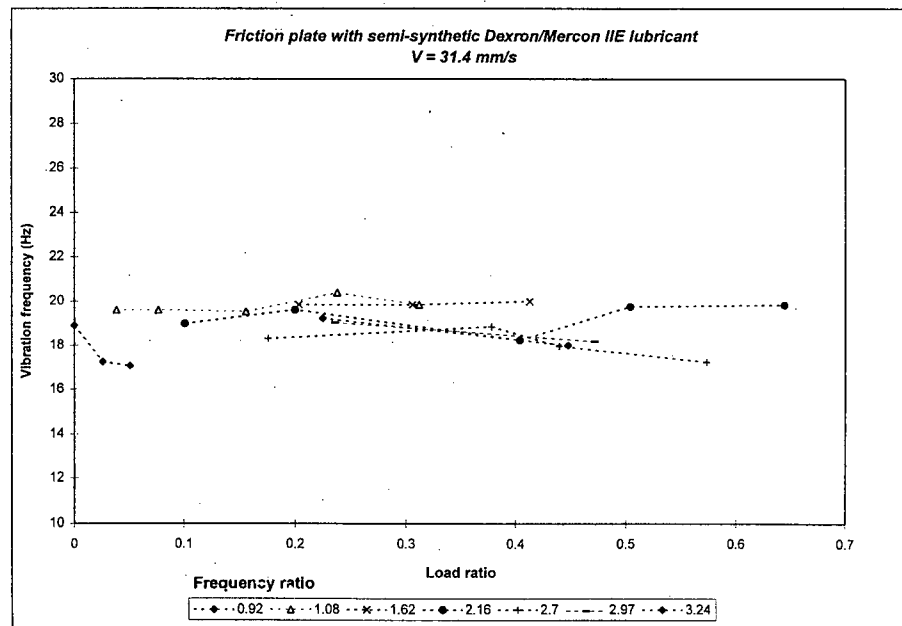
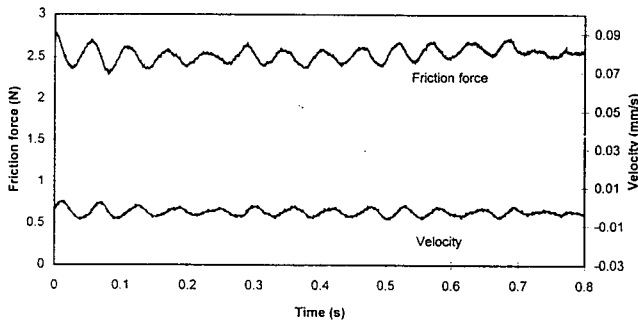
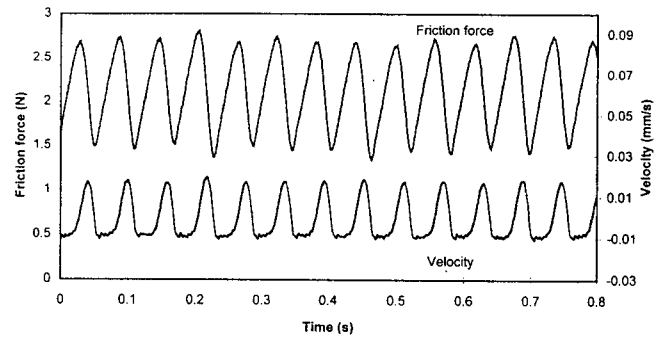


Figure 8.30.(b) Effect of load and frequency ratios on experimental vibration frequency
Friction plate combination with semi-synthetic Dexron/Mercon IIE - V = 31.4 mm/s.

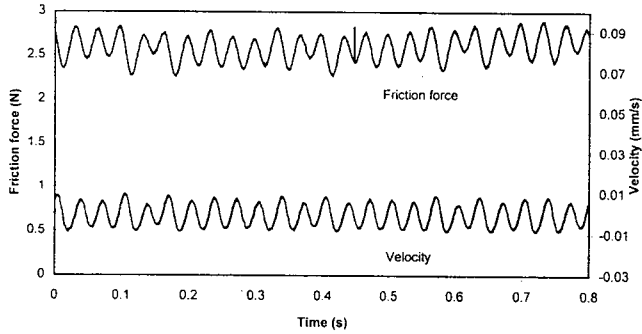
Friction plate vs. steel slider with semi-synthetic Dexron/Mercon IIE
V = 10.5 mm/s. Static normal load.



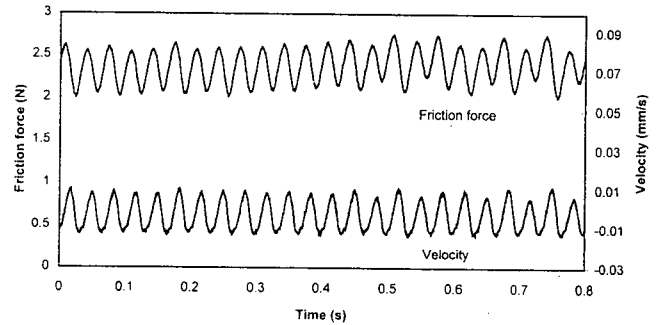
Friction plate vs. steel slider with semi-synthetic Dexron/Mercon IIE
V = 10.5 mm/s. Load ratio = 0.051. Frequency ratio = 0.92



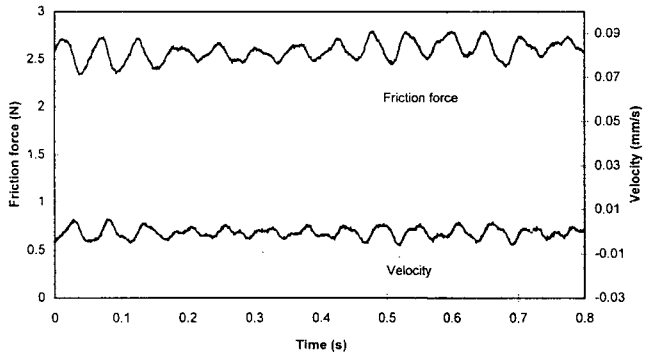
Friction plate vs. steel slider with semi-synthetic Dexron/Mercon IIE
V = 10.5 mm/s. Load ratio = 0.2. Frequency ratio = 1.62



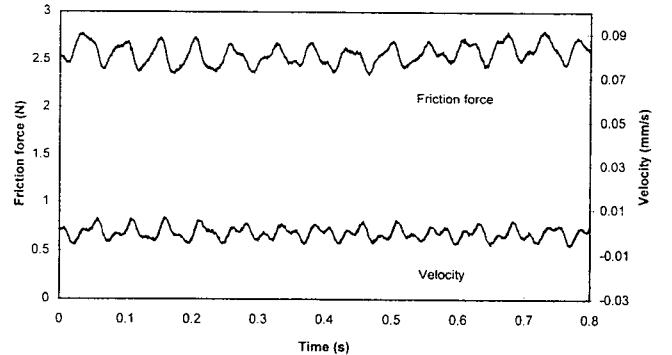
Friction plate vs. steel slider with semi-synthetic Dexron/Mercon IIE
V = 10.5 mm/s. Load ratio = 0.413. Frequency ratio = 1.62



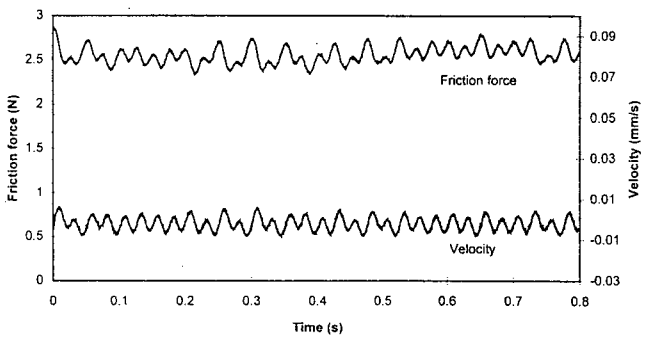
Friction plate vs. steel slider with semi-synthetic Dexron/Mercon IIE
V = 10.5 mm/s. Load ratio = 0.1. Frequency ratio = 2.16



Friction plate vs. steel slider with semi-synthetic Dexron/Mercon IIE
V = 10.5 mm/s. Load ratio = 0.2. Frequency ratio = 2.16



Friction plate vs. steel slider with semi-synthetic Dexron/Mercon IIE
V = 10.5 mm/s. Load ratio = 0.404. Frequency ratio = 2.16



Friction plate vs. steel slider with semi-synthetic Dexron/Mercon IIE
V = 10.5 mm/s. Load ratio = 0.504. Frequency ratio = 2.16

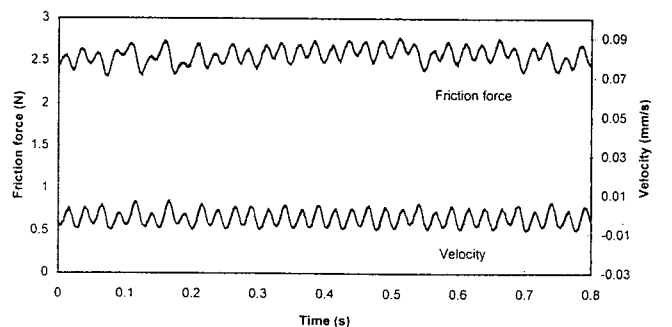
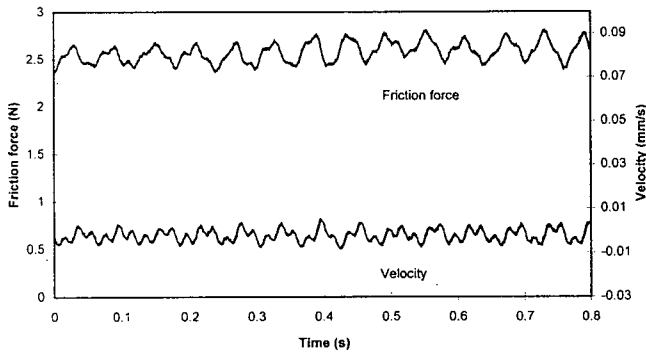
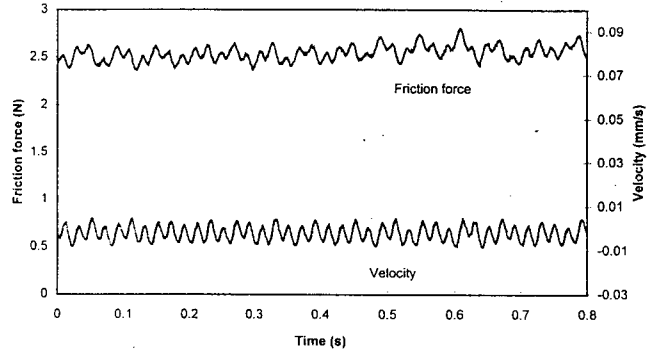


Figure 8.31(a) Vibration vs. time plots with dynamic loading. V = 10.5 mm/s
Friction plate with semi-synthetic Dexron/Mercon IIE lubricant.

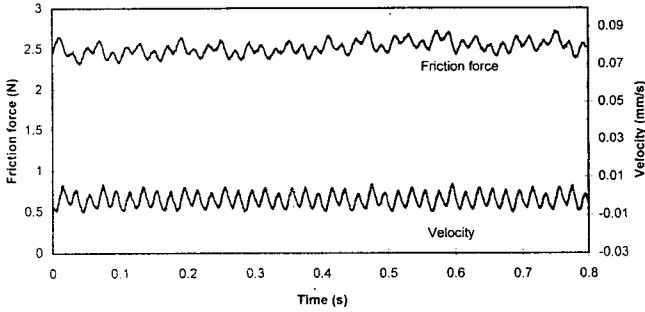
Friction plate vs. steel slider with semi-synthetic Dexron/Mercon IIE
V = 10.5 mm/s. Load ratio = 0.176. Frequency ratio = 2.7



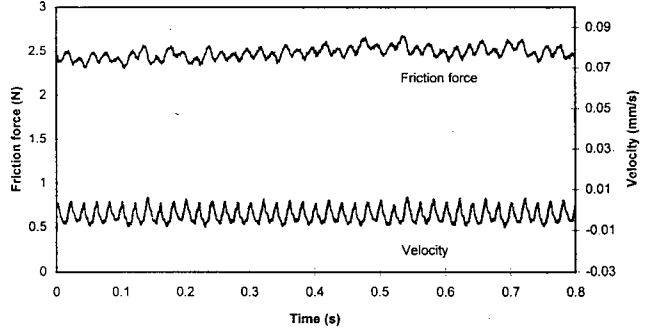
Friction plate vs. steel slider with semi-synthetic Dexron/Mercon IIE
V = 10.5 mm/s. Load ratio = 0.35. Frequency ratio = 2.7



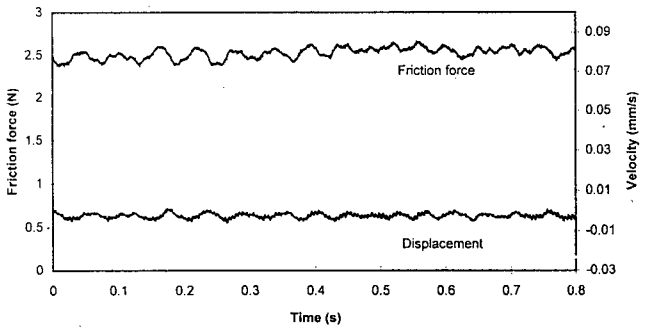
Friction plate vs. steel slider with semi-synthetic Dexron/Mercon IIE
V = 10.5 mm/s. Load ratio = 0.44. Frequency ratio = 2.7



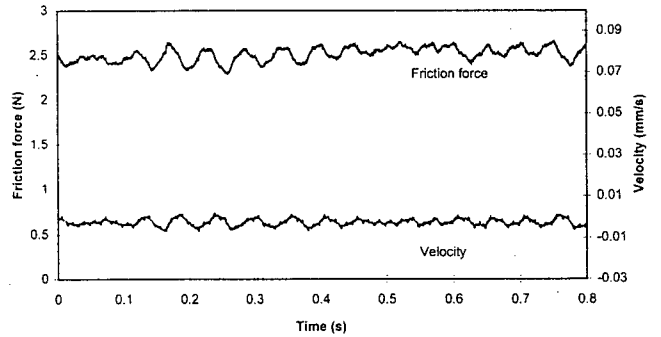
Friction plate vs. steel slider with semi-synthetic Dexron/Mercon IIE
V = 1.05 mm/s. Load ratio = 0.573. Frequency ratio = 2.7



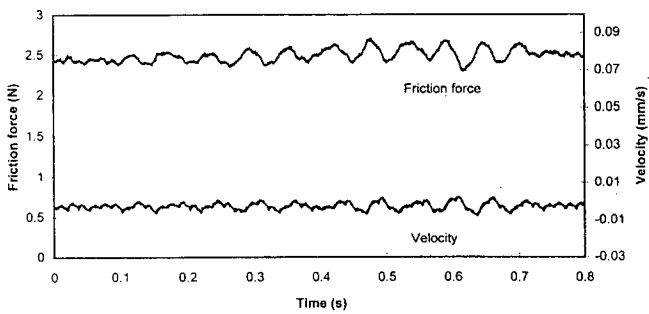
Friction plate vs. steel slider with semi-synthetic Dexron/Mercon IIE
V = 10.5 mm/s. Load ratio = 0.236. Frequency ratio = 2.97



Friction plate vs. steel slider with semi-synthetic Dexron/Mercon IIE
V = 10.5 mm/s. Load ratio = 0.71. Frequency ratio = 2.97



Friction plate vs. steel slider with semi-synthetic Dexron/Mercon IIE
V = 10.5 mm/s. Load ratio = 0.225. Frequency ratio = 3.24



Friction plate vs. steel slider with semi-synthetic Dexron/Mercon IIE
V = 10.5 mm/s. Load ratio = 0.683. Frequency ratio = 3.24

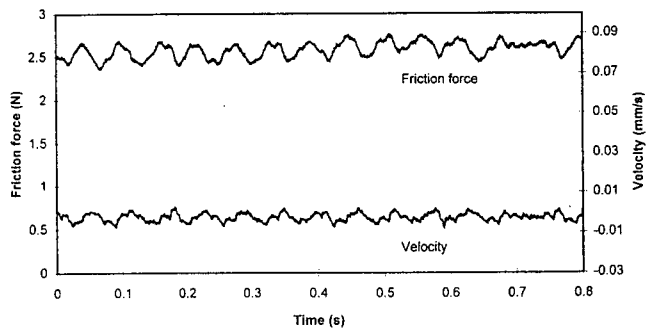
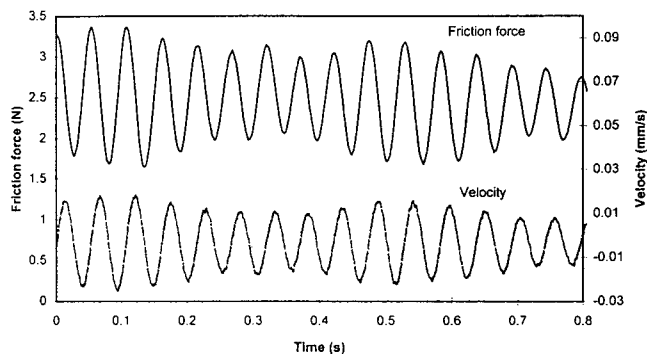
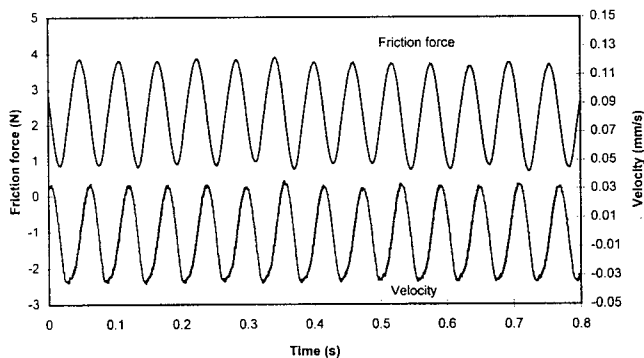


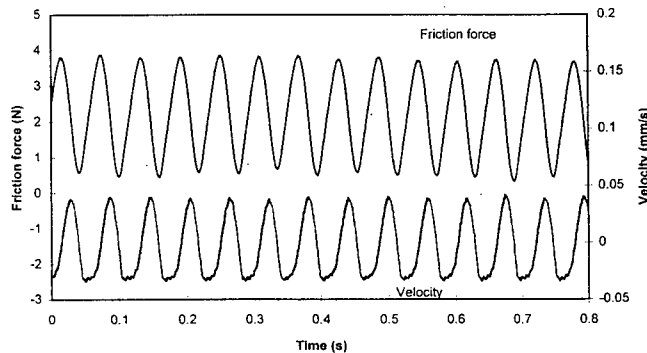
Figure 8.31.(a)(cont.) Vibration vs. time plots with dynamic loading. V = 10.5 mm/s
Friction plate with semi-synthetic Dexron/Mercon IIE lubricant.



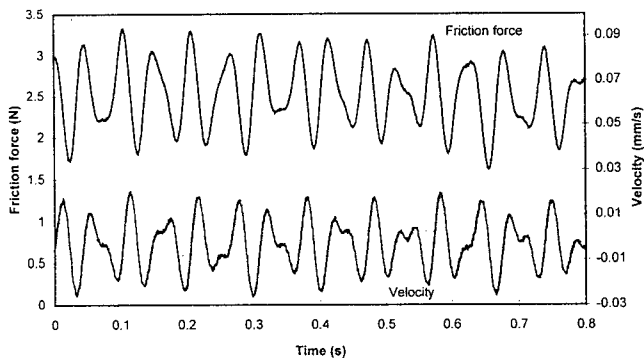
Friction plate vs. steel slider with semi-synthetic Dexron/Mercon IIE
V = 31.4 mm/s. Load ratio = 0.026. Frequency ratio = 0.92



Friction plate vs. steel slider with semi-synthetic Dexron/Mercon IIE
V = 31.4 mm/s. Load ratio = 0.051. Frequency ratio = 0.92



Friction plate vs. steel slider with semi-synthetic Dexron/Mercon IIE
V = 31.4 mm/s. Load ratio = 0.203. Frequency ratio = 1.62



Friction plate vs. steel slider with semi-synthetic Dexron/Mercon IIE
V = 31.4 mm/s. Load ratio = 0.413. Frequency ratio = 1.62

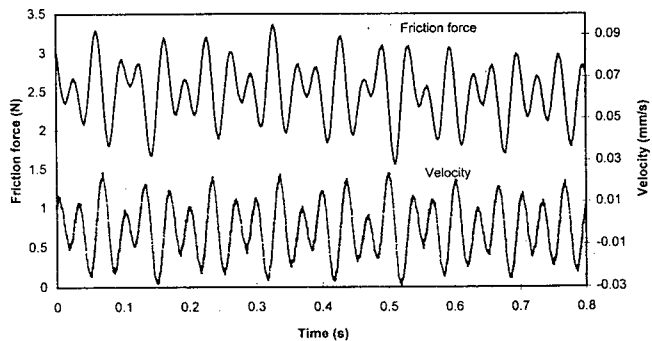
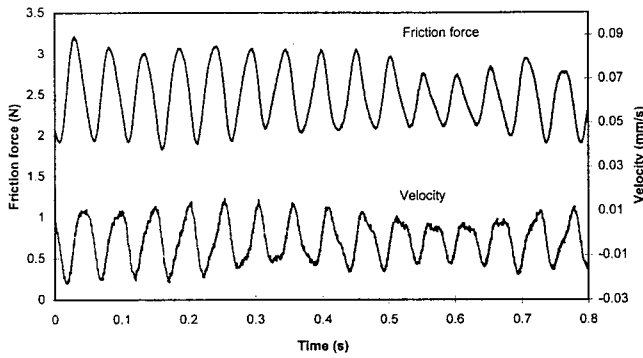


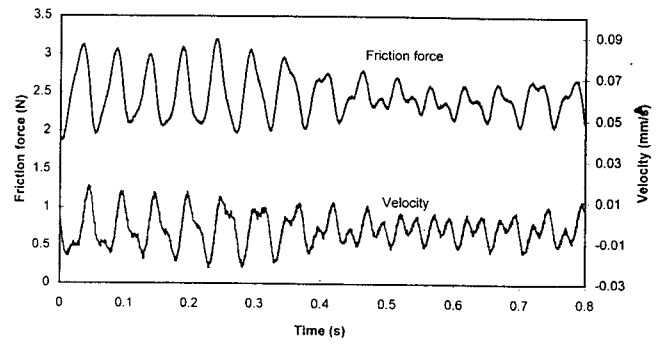
Figure 8.31.(b)

Vibration vs. time plots with dynamic loading. V = 31.4 mm/s
Friction plate with semi-synthetic Dexron/Mercon IIE lubricant.

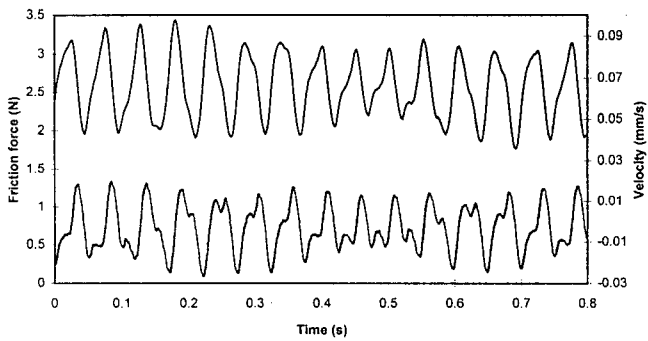
Friction plate vs. steel slider with semi-synthetic Dexron/Mercon IIE
 $V = 31.4 \text{ mm/s}$. Load ratio = 0.3. Frequency ratio = 2.16



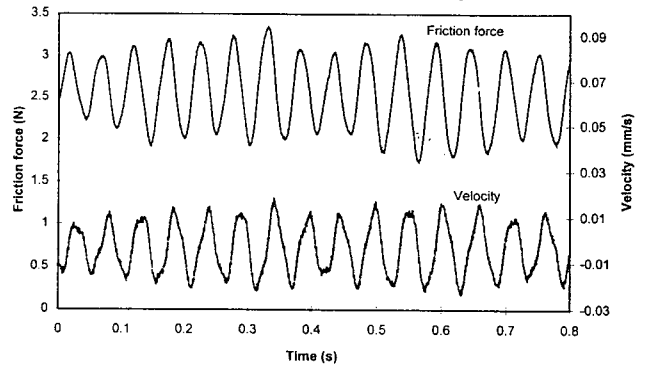
Friction plate vs. steel slider with semi-synthetic Dexron/Mercon IIE
 $V = 31.4 \text{ mm/s}$. Load ratio = 0.504. Frequency ratio = 2.16



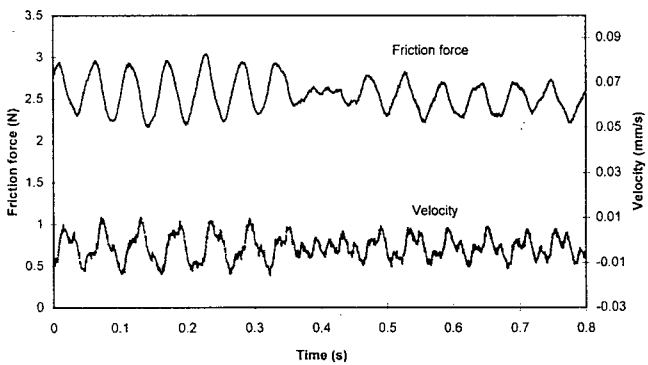
Friction plate vs. steel slider with semi-synthetic Dexron/Mercon IIE
 $V = 31.4 \text{ mm/s}$. Load ratio = 0.645. Frequency ratio = 2.16



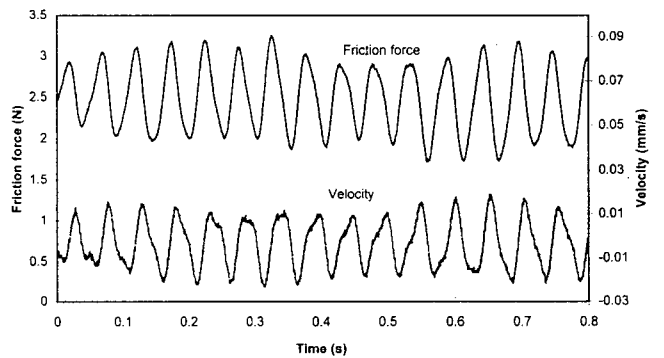
Friction plate vs. steel slider with semi-synthetic Dexron/Mercon IIE
 $V = 31.4 \text{ mm/s}$. Load ratio = 0.176. Frequency ratio = 2.7



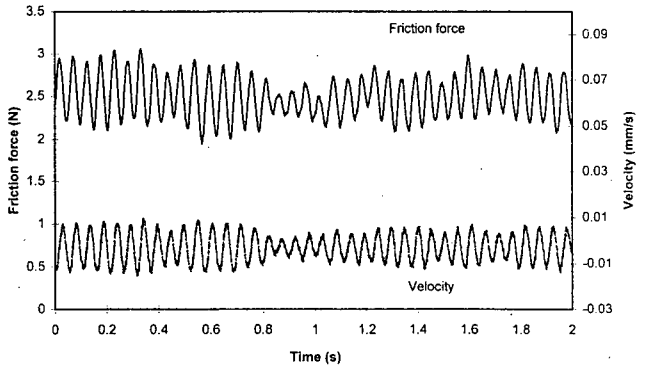
Friction plate vs. steel slider with semi-synthetic Dexron/Mercon IIE
 $V = 31.4 \text{ mm/s}$. Load ratio = 0.35. Frequency ratio = 2.7



Friction plate vs. steel slider with semi-synthetic Dexron/Mercon IIE
 $V = 31.4 \text{ mm/s}$. Load ratio = 0.4. Frequency ratio = 2.16



Friction plate vs. steel slider with semi-synthetic Dexron/Mercon IIE
 $V = 31.4 \text{ mm/s}$. Load ratio = 0.236. Frequency ratio = 2.97



Friction plate vs. steel slider with semi-synthetic Dexron/Mercon IIE
 $V = 31.4 \text{ mm/s}$. Load ratio = 0.225. Frequency ratio = 3.24

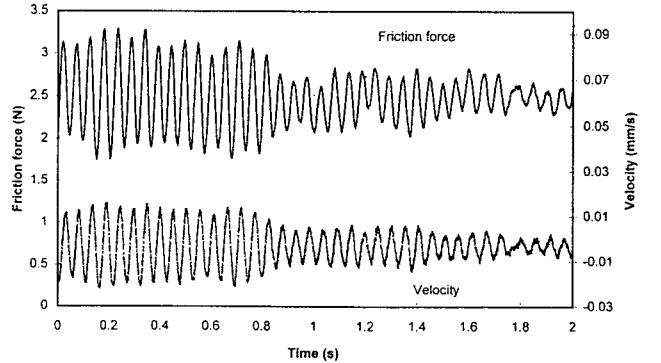


Figure 8.31.(b)(cont.) Vibration vs. time plots with dynamic loading. $V = 31.4 \text{ mm/s}$
 Friction plate with semi-synthetic Dexron/Mercon IIE lubricant